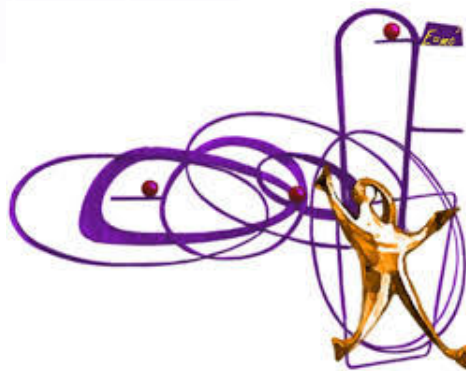# UNIVERSITÀ DEGLI STUDI DI BARI ALDO MORO

DIPARTIMENTO INTERATENEO DI FISICA "M. MERLIN"

DOTTORATO DI RICERCA IN FISICA CICLO XXXIII

Quantum Correlations
from Foundations to Applications

DOTTORANDO:
Dott. Giovanni Scala

(firma del dottorando)

SUPERVISORE (TUTOR):
Ch.mo Prof. Saverio Pascazio

COORDINATORE:
Ch.mo Prof. Giuseppe Iaselli

(firma del Coordinatore)

(firma del Supervisore)

ESAME FINALE 2021

What's up doc? – Lollo Bunny

Contents

Physics is hopefully, simple. Physicist are not. (E. Teller)

I   Part One

II   Part Two

III   Part Three

Impact Statement

Physics breaks into our life since the dawn of time. An impressive example is the advent of the nuclear era. Physics were the balance of the geopolitical equilibrium between the governments across all the world during the wars of last century. To express the crucial role of Physics is enough to think how many technologies (lasers, transistors, imaging methods,...) carried out the knowledge of the atomic structure of the matter. Nowadays, physicists are again involved at the forefront to find out solutions for life-saving drugs discovered through deep analysis of the complex molecules, or diagnostic imaging, or new biomaterials to contrast the climate pollution caused by fossil fuels. Green power batteries for ecological transports. Still, many other breakingthrough discovers to add to this enthusiastic wish list. The way to achieve these target passes through the knowledge of the quantum computation.

Such big goal suited in the foundations of quantum mechanics, although quantum computer is not a new idea, it's only been in recent years that workable technology has begun to catch up to the theory and such prominent applications becomes the engine to deeply investigate what is the nature of quantum reality. The support of applications in addition to the universally exciting questions concerns the true nature of our world would lead us towards fascinating headway.

The most important example is the Bell theorem, it has even been called *"the most profound in science"* (Stapp, 1975). Let us use philosophically the Hanh-Banach theorem, roughly speaking there exists a line which separates an external point from a convex set. The Bell theorem is the line in the sand which separates the noncausal structure of the quantum world from the world as we know it intuitively.Or

> *any local hidden variables theory can ever reproduce all the predictions of quantum mechanics.*

Thus, the feature of quantum mechanics turn out crucial to certify whether numbers are intrinsically random for guarantee stronger cryptographic security, for enhancing bound probability improving communication protocols, for a computational speed-up over classical algorithm and maybe other sensational serendipities.

The results of this thesis, mainly regarding the Quantum Entanglement – a notion originating from the counterintuitive predictions of quantum mechanics about strongly correlated systems – contributes to the understanding of what is the geometry of the quantum states and what are the

resources that justify why such correlations are possible. We also deal with examples on the light–matter interaction, because when two quantum emitters are embedded in a taylored environment the pair can spontaneously relax towards an entangled state. Another example regards the interference effects of the classical chaotic light source recasting phenomena already achieved by entangled photons.

Conclusively, we believe that extending the knowledge on the fundamental concepts is perhaps the highest-impact and the lowest-cost area of basic research which lead to innumerable benefits to society. The reason is simple: since any technology relies on the laws of nature, the better we understand those laws, the more powerful the technologies we can create.

List of Publications and Contributions

- G. Scala, M. D'Angelo, A. Garuccio, S. Pascazio, F. V. Pepe, "Signal-to-noise properties of correlation plenoptic imaging with chaotic light", *Phys. Rev. A* (May 7, 2019) 99, 053808
  `https://doi.org/10.1103/PhysRevA.99.053808`
- G. Sarbicki, G. Scala, D. Chruściński, "A family of multipartite separability criteria based on correlation tensor", *Phys. Rev. A* (January 27, 2020) 101, 012341. `https://doi.org/10.1103/PhysRevA.101.012341`
- G. Sarbicki, G. Scala, D. Chruściński, "Enhanced realignment criterion vs. linear entanglement witnesses", *J. Phys. A: Math. Theor* (October 21, 2020) 53 455302
  `https://doi.org/10.1088/1751-8121/abba46`
- G. Scala, F. V. Pepe, P. Facchi, S. Pascazio, K. Słowik, "Light interaction with extended quantum systems in dispersive media"
  `https://doi.org/10.1088/1367-2630/abd204`
- G. Scala, G. Massaro, M. D'Angelo, A. Garuccio, S. Pascazio, F. V. Pepe, "Signal-to-noise ratio in correlation plenoptic imaging", Proc. SPIE 11347, *Quantum Technologies* (April 14, 2020), 1134713,
  `https://doi.org/10.1117/12.2555701`
- G. Scala, "Two-Level Systems with Broken Inversion Symmetry", *Proceedings* (November 20, 2019), 12, 49,
  `https://doi.org/10.3390/proceedings2019012049`

Preprints

- F. V. Pepe, G. Chilleri, G. Scala, D. Triggiani, Y. Kims, V. Tamma, "Distance sensing with remote double slits" (Nov 10, 2020)
  `https://arxiv.org/abs/2011.05224`
- G. Sarbicki, G. Scala, D. Chruściński, "Detection power of separability criteria based on a correlation tensor: a case study", (submitted to PRA)
  `https://arxiv.org/abs/2012.04359v1`
- G. Scala, F. V. Pepe, K. Słowik, "Asymmetry versus the rotating wave approximation", (private communication, work in progress)

Open Projects

- M. Żukowski, M. Karczewski, G. Scala, A. B. Sainz, *New way of deriving Bell inequalities*, (private communication, work in progress)
- G. Scala, G. Massaro, M. D'Angelo, F. V. Pepe, *Comparison between CPI and CPM*, (private communication, work in progress).
- G. Scala, M. Malitesta, A. Bera, G. Sarbicki, D. Chruściński, *Optimal multipartite linear entanglement witnesses*, (private communication, work in progress)
- G. Scala, G. Sarbicki, D. Chruściński, *Geometrical interpretation of entanglement witnesses and positive maps*, (private communication, work in progress)
- G. Scala, F. V. Pepe, K. Słowik, *The role of the environment on the divergent Green tensor propagator*, (private communication, work in progress)
- G. Scala, F. V. Pepe, G. Massaro, M. D'Angelo, *Turbulence–free in imaging setups* (private communication, work in progress).
- G. Scala, *Phenomenological and canonical derivation of the effective field Hamiltonian,* (private communication, work in progress).
- G. Scala, L. Catani, M. Leifer *Contextuality captures wave-particle duality,* (private communication, work in progress).

An updated list of publications can be found on ArXiV at the following link.

Introduction

Some explorers soars on the sky on the helicopter for recording eruptions from two volcanoes in time and power of emission. The observers notice that when one volcano erupts, the emission form the second volcano happens with a delay, on average, which is larger if its power of emission is lower. Thanks to these measurements the observers can formulate an underground model, obviously not visible from the sky, with some connections between those two volcanoes. Thus, the model reproduces the correlations from the data analysis. Quantum Mechanics is a extremely powerful model to reproduce the correlations between entities, and following the analogy, it perfectly predicts the next eruptions and anything else we can observe from the sky, although the interpretation of the underground model is still under scrutiny.

This thesis is a survey of the main studies and results developed during these years with in common the same ground underpinning devoted to the understanding of the underground model learning knowledge from different branches of theoretical physics. It is divided by three main parts well connected each other, such that each part has an introduction, a detailed analysis based on published papers and at the ends hints for future directions.

1. The first part of the thesis in chapter 1 regards the *Entanglement detection*. In this project we study the problem to distinguish separable and entangled states. The aim of this chapter is to introduce the reader into this profile of research, therefore I chose to explicitly write the most important steps of the calculations in order to have easy reading and fully understanding of the idea behind the birth of a new family of separability criteria both for bipartite and multipartite quantum systems with arbitrary (but finite) dimensions of the corresponding Hilbert spaces. Then, we show that the enhanced (nonlinear) realignment criterion is equivalent to this family of linear criteria based on correlation tensor.

   Moreover, the noncausal structure of the quantum correlations brought to further investigations to develop new methods for deriving Bell's inequalities. One constructs a nonlocal operator that is useful to detect also entanglement. Furthermore, the Contextuality – the leading notion of nonclassicality – is also introduced to capture the wave-particle duality in quantum mechanics in an ontological physical model. This further studies are born to better understand the resources of quantum world, beyond the quantum entanglement and the

nonlocality. Here, an example which shows nonlocality without entanglement [1].

2. The second part of the thesis, in chapter 2 regards the *Light–matter interaction*. This project was born studying a prominent experiment which realize entanglement and the role of the quantum fluctuations of the vacuum in quantum theory which carries on the spontaneous emission of a quantum system. Firstly, we study a two-level quantum system embedded in a dispersive environment and coupled with the electromagnetic field of the vacuum. We expand the theory of light-matter interactions to include the spatial extension of the atomic system, taken into account through its wave–functions, thanks to which we solve the divergence problem related to the Green tensor propagator. In particular, the inclusion of the spatial structure of the atomic system clarifies the role of the asymmetry of atomic states with respect to spatial inversion in these quantities. However, we also provide an alternative solution to overcome the divergence problem by reshaping the susceptibility of the surrounded environment. A further study on the asymmetry of the transition rate is developed in the end of the chapter. Future research should better explain the connection between the phenomenological and canonical derivation of the effective Hamiltonian and derive a many-particle theory.

3. The third part of the thesis, in chapter 3, concerns *Optics with chaotic light* – we will talk about the *Correlation Plenoptic Imaging* (CPI), a novel imaging technique that exploits classical and quantum correlations between intensity fluctuations in two light beams to perform the typical tasks of plenoptic imaging, namely refocusing out-of-focus parts of the scene, extending the depth of field, performing 3D reconstructions. Unless this topic seems far away from the previous two parts, the motivation behind this project has profound fundamental insights as concerns the true nature of light and its correlations. Interestingly, this technique is developed starting from Bell–type coincidence experiments, e.g. Hong-Ou-Mandel and from correlation effects as Hanbury-Brown and Twiss effect (HBT). Keeping in mind the fundamental aspects, we optimize interferometric setups for imaging, such as a CPI microscope. In particular, we will focus on the signal–to–noise ratio of different CPI schemes leading to *Correlation plenoptic Microscope* (CPM), an own protocol for a microscope prototype.

Further developments along this profile of research involve turbulence–free setups to design and build sensitive interferometers that would be helpful in optical observations that require high sensitivity and stability such as gravitational-wave detection. Moreover, we introduce at the end of this chapter a method for remote distance sensing, also based on second-order interferometry through the use of double-slit masks illuminated always by chaotic\thermal light.

Part One

1. Quantum Correlations

"One can, damn it, not reduce the whole of philosophy to a screen with two holes"
(Jørgen Jørgensen)

*S*cience is recognized as a provider of universal and democratic truth, because the system is independent from the role of observer. This paradigm is revisited in quantum mechanics because the knowledge of the system might be part of the system itself. This means that we need to write the apparatus, by which we get knowledge, into the global Hamiltonian. In jargon, the apparatus becomes *entangled* with the system. Then, the concept of *Quantum Entanglement* recognized by Einstein, Podolsky, Rosen and Schrödinger, waited over 70 years to enter in the laboratories as a new real holistic resource of compound quantum systems [2, 3].

After an overview on the theory of quantum entanglement we deeply pay our focus on the derivation of criteria to distinguish separable and entangled states. We provide a novel family of separability criteria, which rests on correlation matrix (tensor). Interestingly, there is a natural generalization to multipartite scenario. In the final sections we give some notion concerns Bell inequalities generalization and an outline on the quantum contextuality, the leading notion of the quantum formalism, and how it is involved in wave–particle dualism of quantum mechanics.

1.1 Prelude to Entanglement

In 1935, Schrödinger realized the "spooky" feature of the quantum mechanical description of Nature written in the well-known EPR paper[2], and he wrote *"This feature implies the existence of global states of composite system which cannot be written as a product of the states of individual subsystems"*.

Einstein, Podosky and Rosen tried to apply such concept which underlines an intrinsic order of statistical relations between subsystems of compound quantum system to ascribe values to physical quantities prior to measurement. They thought the entanglement as the most nonclassical manifestation of quantum theory. But contrary to expectations, in 1964 Bell showed that is just entanglement irrevocably forbids such possibility[4]. He formalized the EPR statement – that quantum description of physical reality is not complete – in terms of local hidden variable LHV

model[4]. The latter assumes that *(i)* exist physical systems with properties regardless of whether they are subjected to an experimental test and regardless of what anyone knows about them ("realism"), *(ii)* negation of action-at-a-distance – whatever action or causality is, it does not happen instantaneously between space-like separated regions ("locality") *(iii)* the setting of local apparatus is own choice and they are independent and not function of the past, of the hidden variables which determine the local results ("free will"). The latter can be formulated as a theorem under the *fin-spin-twin* axiom [5]. Bell proved that the above assumptions impose constraints on statistical correlations in experiments involving bipartite systems in the form of the Bell inequalities. He then showed that the probabilities for the outcomes obtained when suitably measuring some entangled quantum state violate the Bell inequality. In this way entanglement is that feature of quantum formalism which makes impossible to simulate the quantum correlations within any classical formalism. Maintaining only realism as a fundamental concept, Greenberger, Horne and Zeilinger (GHZ) extended Bell inequalities by showing that entanglement of more than two particles leads to a contradiction with hidden variable model for nonstatistical predictions of quantum formalism [6], therefore giving up the concept of locality is not sufficient to be consistent with quantum experiments, unless certain intuitive features of realism are abandoned [7]. Interestingly, in mid-60s, gedanken experiment about quantum entanglement began to scrutinize on laboratory [8, 9] and the first evident violation of Bell inequality was performed by Aspect et al. [10] which paved the way to many kinds of beautiful and precise experimental tests of quantum formalism against the LHV model [11, 12, 13, 14, 15, 16]. All these experiments robustly confirmed the predictions and unveil the curious counterintuitive aspect of the quantum description already mentioned by Schrödinger. He noticed that two-particle EPR state does not admit ascribing individual states to the subsystems implying "entanglement of predictions" for the subsystems. Then he concluded: *"Thus one disposes provisionally (until the entanglement is resolved by actual observation) of only a common description of the two in that space of higher dimension. This is the reason that knowledge of the individual systems can decline to the scantiest, even to zero, while that of the combined system remains continually maximal. Best possible knowledge of a whole does not include best possible knowledge of its parts — and this is what keeps coming back to haunt us"*[3].

Nowadays entanglement theory provides a crucial resource for modern quantum technologies like quantum communication and quantum cryptography with Bell theorem [17, 18, 19], quantum dense coding [20] and quantum teleportation [21, 22].

1.2 Entanglement detection

Since the entanglement has very general structure, it is very fragile to environment and it can be increased only locally, the fundamental tasks to solve are *(i)* how to classify the states of composite quantum systems, and how to detect optimally entanglement theoretically and in laboratory? *(ii)* How to deal with the degradation of entanglement? *(iii)* How to control and quantify entanglement? In the next sections we will focus on the first question, which is of primary importance to test whether a given quantum system is separable or entangled. In the chapter 2 we introduce a system the the aim to answer also to the point *(ii)* and *(iii)*. According to Werner's definition[23] a state of a bipartite system living in $\mathscr{H}_A \otimes \mathscr{H}_B$ represented by a density matrix ρ is separable iff

$$\rho = \sum_{i=1}^{k} p_i \rho_i^A \otimes \rho_i^B, \tag{1.1}$$

where p_i is a probability distribution and ρ_i^A $\left(\rho_i^B\right)$ are density operators of subsystem $A\,(B)$. Werner not only gave accurate definition of separable states (those mixed states that are not entangled), but also noted that there exist entangled states that similarly to separable states, admit LHV model, hence do not violate Bell inequalities. Popescu showed [24] that having system in such state, by

means of local operations and classical communication (LOCC) one can get a new state whose entanglement can be detected by Bell inequalities. It turns out a general technique: once you have a separability criterion via LOCC the entanglement detection can be improved. However, apart the case qubit-qubit and qubit-qutrit, for higher dimensional systems and systems composed of more than two parties the problem is notoriously difficult (actually, it belongs to the class of so called NP-hard problems [25]), although there are many criteria which are not universal, i.e. do not allow to detect all entangled states, but are easily applicable as the PPT criterion [26, 18] and the realignment or computable cross-norm (CCNR) criterion [27, 28, 29]. There are also separability criteria which are nonlinear in the state of the system like for example criteria based on local uncertainty relations (LURs) [30], extensions of realignment criterion [31] or covariance matrix criterion (CMC) [32, 33, 34]. Moreover the most general approach to characterize quantum entanglement uses the notion of *Entanglement Witness (EW)* – an observable which distinguishes a specific entangled state from separable ones – introduced by Terhal [35, 36]. One of the big advantages of entanglement witnesses is that they provide an economic method of detection which does not need the full information about the quantum state. Such information is usually obtained by the full state tomography. Here one uses only the information about the mean value of some observable in a given quantum state. Remarkably, it turns out that any entangled state can be detected by some entanglement witness and hence the knowledge of witnesses enables us to perform full classification of states of composite quantum systems [36, 18, 37, 38]. Interestingly, entanglement witnesses are deeply connected to positive maps in operator algebras, which play an important role both in physics and mathematics providing generalization of *-homomorphisms, Jordan homomorphisms and conditional expectations. In the algebraic approach to quantum physics normalized positive maps define affine mappings between sets of states of C*-algebras [39]. In the following, we describe the space of quantum states with the characterization of entanglement witnesses which will play a central role in the next sections.

1.3 Space of quantum states

Let $\mathscr{H}$ a finite Hilbert space, we denote the linear bounded space

$$\mathscr{B}(\mathscr{H}) = \{A \in \mathscr{M}_n(\mathbb{C}) : \psi \mapsto A\psi\} \tag{1.2}$$

with $\mathscr{M}_n(\mathbb{C})$ is the space of $n \times n$ complex matrices with $n = \dim \mathscr{H}$. This space is endowed with the standard operator norm

$$||A|| = \sup_{\psi \in \mathscr{H}} \frac{||A\psi||_{\mathscr{H}}}{||\psi||_{\mathscr{H}}} \tag{1.3}$$

with $||\psi||_{\mathscr{H}} = \sqrt{\langle \psi | \psi \rangle}$ such that $\langle \psi | \phi \rangle$ denotes the inner product in $\mathscr{H}$. Similar norm can be applied also for $\mathscr{B}(\mathscr{H})$ endowed of the Hilbert–Schmidt inner product $\langle A | B \rangle_{\mathrm{HS}} = \mathrm{Tr}\left(A^\dagger B\right)$. Fixing an orthonormal basis $\{|e_i\rangle\}_{i=1}^n$ in $\mathscr{H}$, then the inner product is "entries-wise"

$$\langle A | B \rangle_{\mathrm{HS}} = \sum_{i=1}^n \langle A e_i | B e_i \rangle = \sum_{i,j=1}^n A_{ij}^* B_{ij} \tag{1.4}$$

and corresponds to a vectorization of a matrix. Hence, this product yield the Hilbert-Schmidt norm

$$||A||_{\mathrm{HS}} = \sqrt{\langle A | A \rangle_{\mathrm{HS}}} = \sqrt{\mathrm{Tr} A^\dagger A}. \tag{1.5}$$

Moreover we can define a third norm in $\mathscr{B}(\mathscr{H})$, which is the trace norm

$$||A||_1 = \mathrm{Tr}|A| = \mathrm{Tr}\sqrt{A^\dagger A}. \tag{1.6}$$

If λ_i's are the eigenvalues of an hermitian matrix A, then $||A||_{\mathrm{HS}} = \sqrt{\sum_i \lambda_i^2}$, and $||A||_1 = \sum_{i=1}^n |\lambda_i|$.

Proposition 1.3.1 The trace norm of a real matrix is equal to maximal Hilbert-Schmidt inner product with an isometry matrix:

$$||A||_1 = \max_{O \in \mathcal{O}(d_A, d_B)} \langle O|A \rangle_{\mathrm{HS}}. \tag{1.7}$$

Proof. Any complex matrix $A \in \mathcal{M}_{\mathbb{C}}(d_1 \times d_2)$ can be written is terms of its *singular value decomposition* (SVD): $A = UDV^\dagger$, where $U \in \mathcal{U}(d_1)$ and $V \in \mathcal{U}(d_2)$ unitary matrices and D is a $d_1 \times d_2$ diagonal positive matrix, i.e.

$$D_{i,j} = \begin{cases} \lambda_i \geq 0 & i = j \leq d, \\ 0 & \text{otherwise.} \end{cases} \tag{1.8}$$

The numbers λ_i are called *singular values* of the matrix A. Since in our case A is real, then U, V are orthogonal and we compute

$$\langle O|A \rangle_{\mathrm{HS}} = \mathrm{Tr}\left(O^T UDV^T\right) = \mathrm{Tr}\left(V^T O^T UD\right) = \mathrm{Tr}\left(\tilde{O}^T D\right) = \sum_i \tilde{O}_{ii} \lambda_i \tag{1.9}$$

where $V^T O^T U = \tilde{O}$ that is also an isometry matrix due to the property of group in $\mathcal{O}(d_1, d_2)$. We are looking for the maximum of the expression and for all $i = 1, \ldots, d$ $\tilde{O}_{ii} \leq 1$, so the bound is reached by a diagonal isometry $\tilde{O}_{ij} = \delta_{ij}$, and $\max \langle O|A \rangle_{\mathrm{HS}} = \sum_i \lambda_i = ||A||_1$. ∎

Corollary 1.3.2 $||A||_1 \geq \mathrm{Tr}A$.

Proof. Let $UDV^T = A$ the SVD, then

$$\mathrm{Tr}A = \mathrm{Tr}UDV^T = \mathrm{Tr}V^T UD = \mathrm{Tr}\tilde{O}D = \sum_i \tilde{O}_{ii} \lambda_i \leq \max_{\tilde{O}} \sum_i \tilde{O}_{ii} \lambda_i = ||A||_1. \tag{1.10}$$

∎

In particular, we are interested in subspace of positive operators in $\mathcal{B}(\mathcal{H})$ denoted $\mathcal{B}_+(\mathcal{H})$, which is not a vector space in $\mathbb{C}$, because $\mathcal{B}_+(\mathcal{H}) = \mathbb{R}_+ \mathcal{B}_+(\mathcal{H}) \oplus \mathbb{R}_+ \mathcal{B}_+(\mathcal{H})$ – a convex cone – where $\mathbb{R}_+$ is the set of positive real number, e.g. $\alpha A + \beta B$. A convex cone is a particular case of a linear cone $(\mathcal{B}_+(\mathcal{H}) = \mathbb{R}_+ \mathcal{B}_+(\mathcal{H}))$, because $\alpha A = \alpha/2A + \alpha/2A$. The section of the convex cone $\mathcal{B}_+(\mathcal{H})$ with unitary trace defines the set of quantum states

$$\mathscr{S}(\mathcal{H}) = \{\rho \in \mathcal{B}_+(\mathcal{H}) : \mathrm{Tr}\rho = 1\}. \tag{1.11}$$

Definition 1.3.1 (Schmidt decomposition, separable state, maximally entangle state, maximally mixed state) Let $\mathcal{H} = \mathcal{H}_A \otimes \mathcal{H}_B$, such that $\dim \mathcal{H}_A = d_A$ and $\dim \mathcal{H}_B = d_B$ finite, with $d = \min(d_A, d_B)$, the *Schmidt decomposition* is always possible for all $|\psi\rangle \in \mathcal{H}$, that is

$$|\psi\rangle = \sum_{k=1}^r \sqrt{p_k} |e_k\rangle \otimes |f_k\rangle, \tag{1.12}$$

where p_k, is a probability distribution, $\{|e_k\rangle\}_{k=1}^{d_A}$ and $\{|f_k\rangle\}_{k=1}^{d_B}$ are orthonormal basis of $\mathcal{H}_A$ and $\mathcal{H}_B$ (for normalized $|\psi\rangle$). The Schmidt rank of $|\psi\rangle$ is $r = \mathrm{SR}(|\psi\rangle) \in [1, d]$. A vector $|\psi\rangle \in \mathcal{H}$ is *separable* $\iff \mathrm{SR}(|\psi\rangle) = 1$, otherwise $|\psi\rangle$ is *entangled*. Notice that for $|\phi\rangle \in \mathcal{H}_A, |\chi\rangle \in \mathcal{H}_B$ a separable state in the Schmidt decomposition is written as $|\psi\rangle = |\phi\rangle \otimes |\chi\rangle$, i.e., the product of the restrictions of $|\psi\rangle$. More generally (for pure and mixed density matrices) the restriction is defined via the partial trace operator. It can be provided invariantly (that is, without reference to

a basis) as follows: it is the unique linear operator such that

$$\text{Tr}_B : \mathscr{B}(\mathscr{H}) \mapsto \mathscr{B}(\mathscr{H}_A), \ \text{Tr}_B(A \otimes B) = \text{Tr}(A)B, \ \forall A \in \mathscr{H}_A, \forall B \in \mathscr{H}_B. \tag{1.13}$$

Vector $\left|\psi_d^+\right\rangle$ is called *maximally entangled* $\Longleftrightarrow$ the restrictions of the corresponding density matrix

$$\rho_d^+ = \left|\psi_d^+\right\rangle \left\langle\psi_d^+\right| = \sum_{ij} E_{ij} \otimes F_{ij}, \quad E_{ij} = |e_i\rangle\langle e_j|, \quad F_{ij} = |f_i\rangle\langle f_j| \tag{1.14}$$

are the maximally mixed states, defined as the completely random density matrix, named proportional to the identity: $\text{Tr}_B |\psi\rangle\langle\psi| = \mathbf{1}/d_A$, $\text{Tr}_A |\psi\rangle\langle\psi| = \mathbf{1}/d_B$. Notice that $\text{SR}\left(\left|\psi_d^+\right\rangle\right) = d$ and from the Schmidt decomposition this is possible only if $\dim\mathscr{H}_A = \dim\mathscr{H}_B = d$, in particular, $p_k = 1/d$ for all k, thus

$$\left|\psi_d^+\right\rangle = \frac{1}{\sqrt{d}} \sum_{k=1}^{d} |e_k\rangle \otimes |f_k\rangle. \tag{1.15}$$

The maximally entangled state (or a maximal Schmidt rank state) enables the famous Choi-Jamiolkowski isomorphism, also known as *Channel-state duality*: notice that $\mathscr{H} = \mathscr{H}_A \otimes \mathscr{H}_B$ and the vector space $\mathscr{B}(\mathscr{H}_B) = \{\Phi : \mathscr{H}_A \mapsto \mathscr{H}_B\}$ have the same finite dimensions, therefore they are isomorphic.

$$\mathfrak{J} : \mathscr{B}_+(\mathscr{H}_B) \mapsto \mathscr{H}$$

$$\Phi \mapsto \mathfrak{J}(\Phi) = \sqrt{d_A}\,(\mathbf{1}\otimes\Phi)\left|\psi_d^+\right\rangle = \sum_{k=1}^{d_A} |e_k\rangle \otimes \Phi|f_k\rangle = |\psi\rangle \tag{1.16}$$

Indeed $\dim\mathscr{B}(\mathscr{H}_B)$ is the cardinality of the basis $\Phi = \sum_{ij} c_{ij}|i\rangle_B\langle j|_A$, for $i = 1, \dots d_A$, $j = 1, \dots d_B$. The inverse map $\mathfrak{J}^{-1}(|\psi\rangle) \mapsto \Phi$ means that for any vector $|\psi\rangle = \sum_{k=1}^{d_A} |e_k\rangle \otimes |y_k\rangle \in \mathscr{H}$ with $|y_k\rangle \in \mathscr{H}_B$, one defines $\Phi|e_k\rangle = |y_k\rangle$. The scalar product $(\cdot, \cdot)$ for the vector space $\mathscr{B}(\mathscr{H}_A, \mathscr{H}_B)$ comes naturally $(\Phi_1, \Phi_2) = \text{Tr}\Phi_1^\dagger\Phi_2$, in particular $(\Phi_1, \Phi_2) = (\mathfrak{J}(\Phi_1), \mathfrak{J}(\Phi_2))$ and the inherited norm shows $||\Phi|| = |||\psi\rangle|| = 1$. It follows that $\text{Rank}(\Phi) = \text{SR}(|\psi\rangle)$. Therefore we can investigate about the Schmidt rank of a vector which does not depend on a basis via the isomorphism $|\psi\rangle = \mathfrak{J}(\Phi)$ that is established upon the basis $\{|e_k\rangle\}$. Beside the definition of separability for vectors states $(\text{SR}(|\psi\rangle) = 1)$ we have also the corresponding definition for the mixed states ρ – the *Schmidt number* $\text{SN}(\rho)$ – given a density matrix ρ we define

$$\text{SN}(\rho) = \min_{\psi_k}\left(\max_k \text{SR}(|\psi_k\rangle)\right), \quad \text{s.t.} \quad \rho = \sum_k |\psi_k\rangle\langle\psi_k| \tag{1.17}$$

with $|\psi_k\rangle$ being (not normalized) vectors of $\mathscr{H}$.

   If $\rho = |\psi\rangle\langle\psi|$, then $\text{SN}(\rho) = \text{SR}(|\psi\rangle)$, therefore we reproduce the analogous definition of Schmidt rank.

(R)   The isomorphism in Eq. 1.16 acts also between positive maps and density matrix

$$\mathfrak{J} : \mathscr{B}_+(\mathscr{H}_B) \mapsto \mathscr{B}(\mathscr{H})$$
$$\Phi \mapsto \mathfrak{J}(\Phi) = d_A\,(\mathbf{1}\otimes\Phi)\rho_d^+ \equiv W \tag{1.18}$$

then $\mathfrak{J}(\Phi) = W$ and $\mathfrak{J}^{-1}(W) = \Phi$, W is also called *Choi's state or matrix*.

Definition 1.3.2 (Family of convex cones for quantum states) Let us define via the Schmidt number the following family of convex cones

$$\mathscr{S}_k = \{\rho \in \mathscr{S}(\mathscr{H}) : \text{SN}(\rho) \leq k\} \tag{1.19}$$

one finds $\mathscr{S}_1 \subseteq \cdots \subseteq \mathscr{S}_d = \mathscr{S}(\mathscr{H})$. Clearly $\mathscr{S}_1$ is the convex subset of separable states and $\mathscr{S}_d/\mathscr{S}_1$ contains all the entangled states.

Let $T : \mathscr{S}(\mathscr{H}_B) \mapsto \mathscr{S}(\mathscr{H}_B)$ the transposition with respect to a basis in $\mathscr{H}_B$. Hence, given $\rho_B \in \mathscr{S}(\mathscr{H}_B)$, then $T(\rho_{Bij}) = \rho_{Bji}$. T is an example of positive map, i.e., $T(\mathscr{S}(\mathscr{H})) \subset \mathscr{S}(\mathscr{H})$. Let $\text{id}_A : \mathscr{H}_A \mapsto \mathscr{H}_A$ be the identity map $\text{id}_A(\rho_A) = \rho_A$ for all $\rho_A \in \mathscr{H}_A$. Then, the definition of the partial transposition is

$$\text{id}_A \otimes T : \mathscr{S}(\mathscr{H}) \mapsto \mathscr{B}(\mathscr{H})$$
$$\phi \otimes \chi \mapsto \phi \otimes \chi^T, \tag{1.20}$$

where $\chi^T = T(\chi)$. Partial transposition is also denoted as $\rho^\Gamma = (\text{id}_A \otimes T)\rho$, and we say that given a quantum state ρ, it is *Positive Partial Transpose* (PPT) iff $\rho^\Gamma \geq 0$, i.e. $\rho^\Gamma \in \mathscr{S}(\mathscr{H})$. Such operation has interpretation as partial time reversal [40].

Proposition 1.3.3 A vector $|\psi\rangle \in \mathscr{H}$ is separable iff $\rho_\psi = |\psi\rangle\langle\psi|$ is PPT.

Proof. if *implication* is trivial. The *only if implication* states that if ρ_ψ is PPT, then it is separable. However, we will prove that $\text{SR}(\psi) = 1 \Longleftrightarrow \exists|\lambda \neq 0$ eigenvalues of ρ_ψ. It follows from the *singular values decomposition* of $\rho_\psi = U\Lambda V^\dagger = \sum_k \lambda_k u_k v_k$ or equivalently from the Schmidt decomposition. We will proof for $\mathbb{C}^3 \otimes \mathbb{C}^3$. There always exist $\{e_i\}_{i=1}^3$ and $\{f_i\}_{i=1}^3$ basis of their relative space such that

$$|\psi\rangle = \lambda_1|e_1, f_1\rangle + \lambda_2|e_2, f_2\rangle + \lambda_3|e_3, f_3\rangle \tag{1.21}$$

is written according its Schmidt decomposition. If two of λ's are vanishing then the Schmidt number is 1 and $|\psi\rangle$ is separable. Hence

$$\rho_\psi = \begin{bmatrix} \lambda_1^2 & \cdot & \cdot & \cdot & \lambda_1\lambda_2 & \cdot & \cdot & \cdot & \lambda_1\lambda_3 \\ \cdot & \cdot & \cdot & \cdot & \cdot & \cdot & \cdot & \cdot & \cdot \\ \cdot & \cdot & \cdot & \cdot & \cdot & \cdot & \cdot & \cdot & \cdot \\ \cdot & \cdot & \cdot & \cdot & \cdot & \cdot & \cdot & \cdot & \cdot \\ \lambda_1\lambda_2 & \cdot & \cdot & \cdot & \lambda_2^2 & \cdot & \cdot & \cdot & \lambda_2\lambda_3 \\ \cdot & \cdot & \cdot & \cdot & \cdot & \cdot & \cdot & \cdot & \cdot \\ \cdot & \cdot & \cdot & \cdot & \cdot & \cdot & \cdot & \cdot & \cdot \\ \lambda_3\lambda_1 & \cdot & \cdot & \cdot & \lambda_2\lambda_3 & \cdot & \cdot & \cdot & \lambda_3^2 \end{bmatrix} \tag{1.22}$$

where the dots replace zeros. The partial transposition is the transposition of each block

$$\rho_\psi^\Gamma = \begin{bmatrix} \lambda_1^2 & \cdot & \cdot & \cdot & \cdot & \cdot & \cdot & \cdot & \cdot \\ \cdot & \cdot & \cdot & \lambda_1\lambda_2 & \cdot & \cdot & \cdot & \cdot & \cdot \\ \cdot & \cdot & \cdot & \cdot & \cdot & \cdot & \lambda_1\lambda_3 & \cdot & \cdot \\ \cdot & \lambda_1\lambda_2 & \cdot & \cdot & \cdot & \cdot & \cdot & \cdot & \cdot \\ \cdot & \cdot & \cdot & \cdot & \lambda_2^2 & \cdot & \cdot & \cdot & \cdot \\ \cdot & \cdot & \cdot & \cdot & \cdot & \cdot & \cdot & \lambda_2\lambda_3 & \cdot \\ \cdot & \cdot & \lambda_3\lambda_1 & \cdot & \cdot & \cdot & \cdot & \cdot & \cdot \\ \cdot & \cdot & \cdot & \cdot & \cdot & \lambda_2\lambda_3 & \cdot & \cdot & \cdot \\ \cdot & \cdot & \cdot & \cdot & \cdot & \cdot & \cdot & \cdot & \lambda_3^2 \end{bmatrix}. \tag{1.23}$$

Studying the positivity of one of the two blue blocks via Sylvester criterion, one finds the eigenvalues $\alpha = 0, \pm \lambda_1 \lambda_2$, the block is negative hence $\rho_\psi^\Gamma < 0$, indeed it is enough to choose as vector $|\phi\rangle = (0, \phi_2, \phi_3, \phi_4, 0, 0, 0, 0, 0)$ to obtain $\langle \phi | \rho_\psi^\Gamma | \phi \rangle = 2\lambda_1 \lambda_2 \phi_2 \phi_4$, which can be negative for a particular choice of ϕ_2, ϕ_4. It implies that $\lambda_1 \lambda_2 \neq 0$ iff $\rho_\psi^\Gamma < 0$. The generalization is proven analogously. ∎

Equivalently the rank of either of reduced density matrices ρ_A and ρ_B is equal to 1, or there is single nonzero Schmidt coefficient. Thus for bipartite pure states it is elementary to decide whether the state is separable or not by the diagonalization of its reduced density matrix. On the other hand, the most interesting and unsolved fully characterization of the entangled states regards mixed states which are the quantum states present in the laboratory because of the decoherence and the multipartite scenario. As we have already mentioned, there exist many criteria to detect entanglement which are only necessary condition for the separability, and one of the most powerful is the partial transposition, also known as *Peres-Horodecki criterion* (or PPT criterion).

> **Theorem 1.3.4** If $\rho \in \mathscr{S}(\mathscr{H})$ is separable $\implies \rho$ is PPT.

Therefore a NPT (not PPT) state is necessary entangled. This means there exists PPT entangled state, unless the dimension $d_A d_B \leq 6$, where the sufficient condition holds. Therefore, the open problem in entanglement theory for bipartite system becomes the characterization of the family of PPT entangled states. Let us define

$$\mathscr{S}_k^l = \mathscr{S}^l \cap \mathscr{S}_k,$$
$$\mathscr{S}^l := (\mathrm{id}_A \otimes T)\, \mathscr{S}_l = \left\{ \rho \in \mathscr{S} : \mathrm{SN}(\rho) \leq l,\ \rho^\Gamma \geq 0 \right\} \tag{1.24}$$

$\mathscr{S}_k^l$ is the convex cone of PPT state ρ such that $\mathrm{SN}(\rho^\Gamma) \leq l$ and $\mathrm{SN}(\rho) \leq k$. One has

$$\mathscr{S}_{\mathrm{SEP}} = \mathscr{S}_1^1 \subseteq \mathscr{S}_2^2 \subseteq \cdots \subseteq \mathscr{S}_d^d = \mathscr{S}_{\mathrm{PPT}} \subset \mathscr{S}(\mathscr{H}). \tag{1.25}$$

It is worth to notice that a set of PPT states is convex, but the set of PPT entangled state is not. If one would attack the problem of entanglement detection via the characterization of PPT hierarchy could explore PPT entangled state via the *range criterion*[37], which provides a tool to construct edge density matrices. This is just the starting point to characterize PPT entangled state. In conclusion, the state of the art is that, PPT criterion might provide an immediate response to the problem, but not for any mixed state. In the following, we do not pursue this direction. We will introduce the tool of the entanglement witness showing how it can be use to check whether a given mixed state ρ is separable or not. We shall restrict subsequent analysis to the case of finite dimensions. The set of all separable states defined in this way is convex, compact and invariant under the product unitary operations $U_A \otimes U_B$. Moreover the separability property is preserved under so called (stochastic) separable operations (see [18] Sec. XI.B).

1.4 Entanglement witnesses and positive maps

("Be careful from quantum channels: they are completely positive!" Coronavirus time)

Entanglement witnesses analyses the problem of separability in quantum entanglement theory from the geometrical point of view: the convex sets can be described by hyperplanes. This translates into observables that completely characterize separable states and allow to detect entanglement physically via Hanh-Banach theorem, as follows

> **Theorem 1.4.1** Let $\mathscr{S}_1^1$ and $\mathscr{S}/\mathscr{S}_1^1$ disjoint subset, and $\mathscr{S}_1^1$ is a convex set, then there exists a
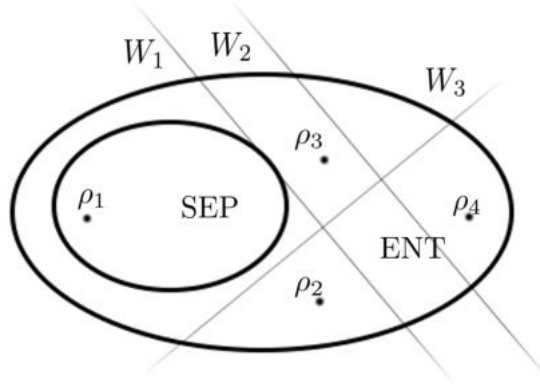
Figure 1.1: The set of quantum states is pictorially divided by the separable states and the quantum states. The line represents hyperplane corresponding to the entanglement witness W_i for $i = 1, 2, 3$ which split the set of the quantum states into two disjoint subset. All states on one side of the hyperplane or belonging to it (in particular all separable states) provide nonnegative mean value of the witness, while those located to the other side are entangled states detected by the witness. For instance $\mathrm{Tr}W_1\rho_i \geq 0$, $i = 1, 2$ and $\mathrm{Tr}W_1\rho_j < 0$, $i = 3, 4$; $\mathrm{Tr}W_2\rho_i \geq 0$, $i = 1, 2, 3$ and $\mathrm{Tr}W_2\rho_4 < 0$; $\mathrm{Tr}W_3\rho_i \geq 0$, $i = 1, 3$ and $\mathrm{Tr}W_3\rho_j < 0$, $i = 2, 4$. To give a rough idea, W_1 is tangent to the set of separability states, and it is called *optimal*.

> bounded functional $f_W : \rho \mapsto \mathrm{Tr}W\rho$ separating the two sets.

This is a generalization of the fact that, in real Euclidean space, there always exists an affine subspace which separates a given point outside from a given convex set. The affine subspace manifests itself as the functional f_W, or as an operator W, because the dual space of the Banach space of trace-class operators is isomorphic to the set of bounded operators via Riesz lemma. In the present context, the family of separable states $\mathscr{S}_1^1$ is a convex set in the space of trace class operators $\mathscr{S}(\mathscr{H})$. If ρ is an entangled state (thus lying outside the convex set), then by theorem above, there is such operator W separating ρ from the separable states. We call W an *Entanglement Witness*. Notice, there is more than one hyperplane separating a closed convex set from a point lying outside of it, so for an entangled state might be more than one entanglement witness (see figure 1.1). To give a rough idea, W_1 in figure 1.1 is tangent to the set of separability states, and it is called *optimal*. Optimal witnesses will be discussed in detail later on. Formally, given any entangled state ρ_{ent} there exist an Hermitian operator W such that $\mathrm{Tr}W\rho_{\mathrm{ent}} < 0$ and for all separable states ρ_{sep} yields to $\mathrm{Tr}W\rho_{\mathrm{sep}} \geq 0$. Let

$$\mathscr{W} = \left\{ W \in \mathscr{B}(\mathscr{H}) : W = W^\dagger, \ \langle \psi \otimes \varphi | W \psi \otimes \varphi \rangle \geq 0 \quad \forall \psi, \varphi \in \mathscr{H}_A, \mathscr{H}_B \right\} \tag{1.26}$$

the set of Hermitian block-positive (positive for product states) operator in $\mathscr{H}$. It defines a convex cone in $\mathscr{B}(\mathscr{H})$, and obviously $W \in \mathscr{W}$ iff $\forall \rho \in \mathscr{S}_1$, then $\mathrm{Tr}W\rho \geq 0$. Let $\left\{ |e_i\rangle_{i=1}^{d_A} \right\}$ an orthonormal basis of $\mathscr{H}_A$, any operator $W \in \mathscr{B}(\mathscr{H})$ may be represented in the following block form

$$W = \sum_{i,j=1}^{d_A} E_{ij} \otimes W_{ij}, \qquad W_{ij} \in \mathscr{B}(\mathscr{H}_B), E_{ij=} |e_i\rangle \langle e_j| \tag{1.27}$$

that is a matrix $d_A \times d_A$ with matrix elements (blocks) being operators $W_{ij} \in \mathscr{B}(\mathscr{H}_B)$. Moreover, if W is block-positive one has

$$\langle e_i \otimes \phi | W | e_i \otimes \phi \rangle = \langle \phi | W_{ij} | \phi \rangle \geq 0, \tag{1.28}$$

and diagonal blocks W_{ii} are positive operators. Clearly if W is positive, then W is also block-positive, but we say that W is an EW iff it is block-positive but not positive, i.e. $W \in \mathscr{W} / \mathscr{B}_+ (\mathscr{H})$. However one can also obtain $W_{ij} = \Phi \left(|e_i\rangle \langle e_j| \right)$, where $\Phi \in \mathscr{B} \left(\mathscr{H}_A, \mathscr{H}_B \right)$ maps density states from $\mathscr{H}_A$ to $\mathscr{H}_B$. We have

$$W = d_A \left[\mathrm{id}_A \otimes \Phi \right] \rho_{d_A}^+, \qquad \rho_{d_A}^+ = \left| \psi_{d_A}^+ \right\rangle \left\langle \psi_{d_A}^+ \right|. \tag{1.29}$$

This way establishes a correspondence between linear maps $\Phi \in \mathscr{B} \left(\mathscr{H}_A, \mathscr{H}_B \right)$ and Choi-matrix $W \in \mathscr{B} \left(\mathscr{H} \right)$ as 1.3. It should be stress that this correspondence depends upon the basis $\{ |e\rangle_i \}_{i=1}^{d_A}$. The inverse relation is

$$\Phi \left(\rho_A \right) = \mathrm{Tr}_A \left[\left(\rho_A^T \otimes \mathbf{1}_B \right) W \right], \quad \forall \rho_A \in \mathscr{B}_+ \left(\mathscr{H}_A \right). \tag{1.30}$$

Proof. Let $\rho_A = \sum_{ij} p_{ij} E_{ij}$, then

$$\Phi \left(\rho_A \right) = \sum_{ij} p_{ij} \Phi \left(E_{ij} \right) = \sum_{ij} p_{ij} W_{ij}. \tag{1.31}$$

On the other hand

$$\mathrm{Tr}_A \left[\left(\rho_A^T \otimes \mathbf{1}_B \right) W \right] = \mathrm{Tr}_A \left[\left(\sum_{ij} p_{ij} E_{ji} \otimes \mathbf{1}_B \right) \sum_{i',j'} E_{i'j'} \otimes W_{i'j'} \right]$$

$$= \mathrm{Tr}_A \left[\sum_{ij,i'j'} p_{ij} \delta_{ii'} E_{jj'} \otimes W_{i'j'} \right]$$

$$= \sum_{k,ij,i'j'} p_{ij} \delta_{ii'} \delta_{kj} \delta_{kj'} W_{i'j'} = \sum_{ij} p_{ij} W_{ij}. \tag{1.32}$$

Notice the flexibility of the transposition. that can be applied on the states, as we have done or on the blocks W_{ij}. ∎

> **Definition 1.4.1** Positive map – a map $\Phi \in \mathscr{B} \left(\mathscr{H}_B \right)$ is positive iff $\forall \rho \in \mathscr{S} \left(\mathscr{H}_B \right) : \Phi_i \left(\rho \right) \in \mathscr{S} \left(\mathscr{H}_B \right)$. Then $\Phi \in \mathscr{B}_+ \left(\mathscr{H}_B \right)$

> **Definition 1.4.2** Completely Positive map – a positive map $\Phi \in \mathscr{B}_+ \left(\mathscr{H}_B \right)$ is completely positive iff $\mathrm{id}_A \otimes \Phi \in \mathscr{B}_+ \left(\mathscr{H}_A \otimes \mathscr{H}_B \right)$.

This above relation becomes crucial if Φ_1 and Φ_2 are positive maps, (e.g. id_A and T). Then

$$\Phi_1 \otimes \Phi_2 : \mathscr{B} \left(\mathscr{H}_A \otimes \mathscr{H}_B \right) \mapsto \mathscr{B} \left(\mathscr{H}_A \otimes \mathscr{H}_B \right) \tag{1.33}$$

needs not be positive (clearly $\Phi_1 \otimes \Phi_2$ is positive if Φ_1 and Φ_2 are both completely positive), therefore we will use maps to detect entanglement which are positive but not completely positive. We have a criterion for positive map

Proposition 1.4.2 A quantum state $\rho \in \mathscr{S} \left(\mathscr{H}_A \otimes \mathscr{H}_A \right)$ is separable iff for all maps $\Phi \in \mathscr{B}_+ \left(\mathscr{H}_B \right)$

$$\left[\mathrm{id}_A \otimes \Phi \right] \rho \geq 0. \tag{1.34}$$

Proof. ($\Longrightarrow$) Indeed if ρ is separable $\rho = \sum_{i=1}^k p_i \rho_i^A \otimes \sigma_i^A$, then $\forall \Phi$ positive map $\in \mathscr{B}_+ \left(\mathscr{H}_B \right)$, we get

$$\mathrm{Tr} \left(\left[\mathrm{id}_A \otimes \Phi \right] \left(\rho \right) \right) = \sum_{i=1}^k p_i \mathrm{Tr} \left(\rho_i^A \right) \mathrm{Tr} \left[\Phi \left(\sigma_i^A \right) \right] \geq 0. \tag{1.35}$$

($\Longleftarrow$) Conversely, if $[\mathrm{id}_A \otimes \Phi]\rho \geq 0$, then for arbitrary $|\psi\rangle = \sum_{i\mu} p_{i\mu} |i,\mu\rangle$ results

$$\langle\psi|\,[\mathrm{id}_A \otimes \Phi]\,\rho\,|\psi\rangle = \sum_{i\mu}\sum_{jv} p_{i\mu} p_{jv}^* \,\langle j,v|\,[\mathrm{id}_A \otimes \Phi]\,\rho\,|i,\mu\rangle \geq 0.$$

In particular for $v = j$, $\mu = i$ and $p_{ii} = 1/\sqrt{d}$ we get $\mathrm{Tr}\left(\rho_A^+ [\mathrm{id}_A \otimes \Phi](\rho)\right) \geq 0$. Now denote by $\Phi^\#$ the dual map

$$\mathrm{Tr}\left[\Phi^\#(A)B\right] := \mathrm{Tr}\left[A\Phi(B)\right]. \tag{1.36}$$

Notice, that $\Phi^\#$ is positive iff Φ is positive. Then

$$\mathrm{Tr}\left(\rho_A^+ [\mathrm{id}_A \otimes \Phi](\rho)\right) = \mathrm{Tr}\left(\rho\,[\mathrm{id}_A \otimes \Phi^\#]\,(\rho_A^+)\right) \geq 0. \tag{1.37}$$

Via Choi-Jamilkowski isomorphism $W = [\mathrm{id}_A \otimes \Phi^\#]\rho_{d_A}^+$ is block-positive and hence $\mathrm{Tr}W\rho \geq 0$ which implies that ρ is separable. Actually, $[\mathrm{id}_A \otimes \Phi]\rho \in \mathscr{S}\left(\mathscr{H}_A \otimes \mathscr{H}_A\right)$ for all trace-preserving positive map $\Phi \in \mathscr{B}\left(\mathscr{H}_B\right)$. Choi-Jamiołkowski isomorphism linked the EW W in $\mathscr{B}\left(\mathscr{H}\right)$ and positive but non-completely positive maps Φ in $\mathscr{B}\left(\mathscr{H}_B\right)$. The very important observation is that while the condition $\mathrm{Tr}W\rho_{\mathrm{sep}} \geq 0$ as a whole is equivalent to $(\mathrm{id}_A \otimes \Phi)\rho_{\mathrm{sep}} \geq 0$, a particular witness is not equivalent to a positive map associated via isomorphism: the map proves a stronger condition [37, 18]. ∎

■ **Example 1.1** Consider the transposition map T and the EW F called *flip* (or *swap*) operator

$$F(\phi \otimes \xi) = \xi \otimes \phi \tag{1.38}$$

form the Choi-Jamilkowski isomorphism the flip EW is related to the transposition map which exactly applies the PPT criterion,

$$F = (\mathrm{id}_A \otimes T)\rho_d^+. \tag{1.39}$$

It is well known that an isotropic state

$$\rho_p = \frac{p}{d^2}\mathbf{1}_d \otimes \mathbf{1}_d + (1-p)\rho_d^+ \tag{1.40}$$

is separable iff it is PPT which is equivalent to $p \geq \frac{d}{d+1}$. Hence the map T detects all entangled isotropic states. On the other hand, the mean value of corresponding witness F is

$$\mathrm{Tr}(F\rho_p) = \frac{p}{d^2}\mathrm{Tr}F + (1-p)\mathrm{Tr}\left(F\rho_d^+\right) = \frac{p}{d^2} + (1-p) > 0 \tag{1.41}$$

and any isotropic state is detected by F.

In the following, given a separability criterion, we will use a canonical way to assign an entanglement witness that detects $\rho \in \mathscr{S}\left(\mathscr{H}\right)$. Since $[\mathrm{id}_A \otimes \Lambda]\rho < 0$ this operator has at least one negative eigenvalue $([\mathrm{id}_A \otimes \Lambda]\rho)|\psi\rangle = \lambda|\psi\rangle$, with $\lambda < 0$ and $|\psi\rangle \in \mathscr{H}_A \otimes \mathscr{H}_A$ is an entangled vector. Observe that $W = [\mathrm{id}_A \otimes \Lambda^\#]|\psi\rangle\langle\psi|$ is an EW such that $\mathrm{Tr}W\rho < 0$, in fact

$$\mathrm{Tr}(W\rho) = \mathrm{Tr}\left([\mathrm{id}_A \otimes \Lambda^\#]|\psi\rangle\langle\psi|\rho\right) = \mathrm{Tr}\left(|\psi\rangle\langle\psi|[\mathrm{id}_A \otimes \Lambda]\rho\right) = \lambda\||\psi\rangle\|^2 < 0. \tag{1.42}$$

In the next we will refer to the isomorphism up to a transposition of a basis, the duality of the map and a multiplicative constant to have a more light notation and only where it will be strictly important we will specify. ∎

1.5 Construction of separability criteria, witness and map

The transposition map $\Phi(\rho) = \rho^T$ carries the notion of the indecomposability and the PPT criterion with its related witness, the flip operator $F = d_A (\text{id}_A \otimes T) \rho_d^+$. On the other hand, we analyze other separability criteria based on correlation matrix (or correlation tensor) with the aim to detect PPT entangled states. In the following we present a natural procedure to derive a criterion from a positive map and its EW, and viceversa. We choose to introduce the bipartite case of equal dimensions to better understand the key idea and then the generalization to different dimensions of the relative Hilbert spaces.

1.5.1 Kossakowski criterion – Equal dimension

Definition 1.5.1 From the map to the criterion – given a state $\rho \in \mathscr{S}\left(\mathbb{C}^d\right)$ in a subsystem, we choose $G_0 = \mathbf{1}_d / d$ and orthonormal traceless hermitian operators $\{G_\alpha\}_{\alpha=1}^{d-1}$, such that ρ is decomposed separating the traceless part as follows

$$\rho = \frac{1}{d} \mathbf{1}_d + \sum_{\alpha=1}^{d^2-1} \text{Tr}\left(G_\alpha \rho\right) G_\alpha. \tag{1.43}$$

This decomposition and the idea of Fig. 1.2 defines the *Kossakowski map*, a trace and positive preserving map $\Phi_O^K \in \mathscr{L}_+\left(\mathscr{H}_A\right)$ related to an orthonormal matrix $O \in \mathscr{O}\left(d^2 - 1\right)$

$$\Phi_O^K(\rho) = \frac{1}{d} \mathbf{1}_d + \frac{1}{d-1} \sum_{\alpha=1}^{d^2-1} \sum_{\beta=1}^{d^2-1} O^{\alpha\beta} G_\beta \text{Tr}\left(G_\alpha \rho\right). \tag{1.44}$$

In Fig. 1.2 we pictorially represent how the Kossakowski map acts on the quantum states for the endomorfic case which explain the shrink factor $\vec{r}_{\text{circ}} / \vec{r}_{\text{insc}} = 1/(d-1)$. Basically, the set of quantum state is represented by the convex triangle in light-gray, and rotating by the matrix O around the maximally mixed state $\mathbf{1}_d / d$ some state goes out the triangle, therefore we shrink the triangle into the smaller dark gray triangle to guarantee a positive and trace preserving map Φ_O^K. The shrink factor is the ratio $\vec{r}_{\text{circ}} / \vec{r}_{\text{insc}}$ such that $\vec{r}_{\text{circ}}$ defines the greatest distance between a quantum state and the maximally mixed,

$$\vec{r}_{\text{circ}} = \max_{\rho \in \mathscr{S}(\mathbb{C}^d)} ||\mathbf{1}_d / d - \rho||_{\text{HS}} = \max_{\{\lambda_i\} \in \Lambda} \sqrt{\sum_i (1/d - \lambda_i)^2}$$

$$= \sqrt{-\frac{1}{d} + \max_{\{\lambda_i\} \in \Lambda} \sum_i \lambda_i^2} = \sqrt{1 - \frac{1}{d}},$$

because $\Lambda = \left\{ \{\lambda\}_{i=1}^d \text{ eigenvalues of } \rho \, | \, \sum_i \lambda_i = 1, \lambda_i \geq 0 \right\}$. On the other hand, $\vec{r}_{\text{insc}}$ define the closest quantum state which "touches" the bound of positive operators, therefore now the minimum must be found into $\Lambda_0 = \left\{ \{\lambda\}_{i=1}^d \text{ eigenvalues of } \rho \, | \, \sum_i \lambda_i = 1, \lambda_i \geq 0, \exists | \lambda_j = 0 \right\}$.

$$\vec{r}_{\text{insc}} = \min_{\rho \in \mathscr{S}(\mathbb{C}^d)} ||\mathbf{1}_d / d - \rho||_{\text{HS}} = \min_{\{\lambda_i\} \in \Lambda_0} \sqrt{\sum_i (1/d - \lambda_i)^2}.$$

We applied the Lagrange multiplier method such that

$$\partial_{\lambda_i} \left(-\frac{1}{d} + \sum_{i=1}^{d-1} \lambda_i^2 + \mu \sum_{i=1}^{d-1} \lambda_i \right) = 0. \tag{1.45}$$

It implies that all λ_i for $i = 1, \ldots, d-1$ are the same, therefore $\lambda = 1/(d-1)$ and

$$\vec{r}_{\mathrm{insc}} = \sqrt{\frac{1}{d(d-1)}}. \tag{1.46}$$

Notice that if there exists two eigenvalues equal to zero, then $\vec{r}_{insc} = 2/d(d-2)$ which is greater than Eq. 1.46. Iteratively, this argument explain also $\vec{r}_{circ}$.
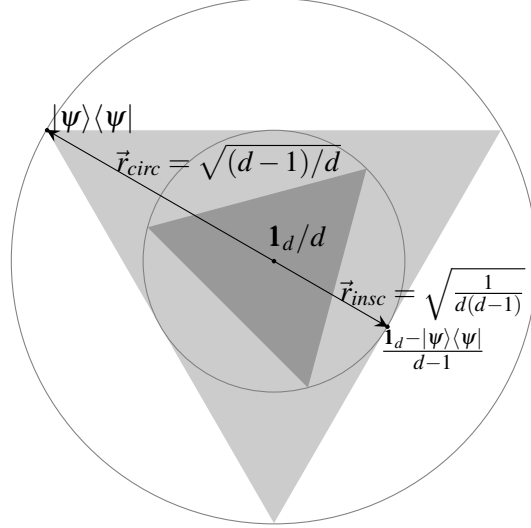
Figure 1.2: Kossakowski map – The convex set of quantum states is rotated by the isometry matrix O and to guarantee that any state does not go out the gray triangle, the factor $1/(d-1)$ shrinks the triangle into the smaller dark gray triangle providing a positive and trace preserving map $\Phi_O^K \in \mathcal{L}_+(\mathcal{H}_A)$.

Proposition 1.5.1 An EW family related to the above map via the Jamiołkowski isomorphism $W_O^K = (\mathrm{id}_A \otimes \Phi_O^K) \rho_d^+$ (up to an irrelevant multiplication constant) is

$$W_O^K = \frac{\mathbf{1}_{\mathrm{d}}}{d} \otimes \frac{\mathbf{1}_{\mathrm{d}}}{d} + \frac{1}{d-1} \sum_{\alpha=1}^{d^2-1} \sum_{\beta=1}^{d^2-1} O^{\alpha\beta} (G_\alpha)^T \otimes G_\beta. \tag{1.47}$$

Proof. We use Eq. 1.43 on the maximally mixed state

$$\rho_d^+ = \frac{1}{d} \sum_{i=1}^{d} \sum_{j=1}^{d} |i\rangle\langle j| \otimes |i\rangle\langle j| = \frac{1}{d} \sum_{i=1}^{d} \sum_{j=1}^{d} |i\rangle\langle j| \otimes \left(\delta_{ij} \frac{\mathbf{1}_B}{d} + \sum_{\alpha=1}^{d^2-1} \mathrm{Tr}\,(G_\alpha |i\rangle\langle j|)\, G_\alpha \right). \tag{1.48}$$

Therefore Φ_O^K shrinks and rotates the state $|i\rangle\langle j|$

$$\Phi_O^K(|i\rangle\langle j|) = \left(\delta_{ij} \frac{\mathbf{1}_{\mathrm{d_B}}}{d} + \frac{1}{d-1} \sum_{\beta=1}^{d^2-1} \sum_{\alpha=1}^{d^2-1} O^{\alpha\beta} \mathrm{Tr}\,(G_\alpha |i\rangle\langle j|)\, G_\alpha \right). \tag{1.49}$$

Now, Eq. 1.49 yields

$$W_O^K = \frac{1}{d} \left(I \otimes \Phi_O^K \right) \sum_{i=1}^{d} \sum_{j=1}^{d} |ii\rangle\langle jj|$$

$$= \frac{1}{d} \sum_{ij} |i\rangle\langle j| \otimes \left(\frac{1}{d} \mathbf{1}_d \delta_{ij} + \frac{1}{d-1} \sum_{\alpha=1}^{d^2-1} \sum_{\beta=1}^{d^2-1} O^{\alpha\beta} G_\beta \langle j|G_\alpha|i\rangle \right)$$

$$= \frac{\mathbf{1}_d}{d} \otimes \frac{\mathbf{1}_d}{d} + \frac{1}{d(d-1)} \sum_{\alpha=1}^{d^2-1} \sum_{\beta=1}^{d^2-1} \sum_{ij} |i\rangle\langle j| \langle j|G_\alpha|i\rangle \otimes O^{\alpha\beta} G_\beta \tag{1.50}$$

$$= \frac{\mathbf{1}_d}{d} \otimes \frac{\mathbf{1}_d}{d} + \frac{1}{d(d-1)} \sum_{\alpha=1}^{d^2-1} \sum_{\beta=1}^{d^2-1} O^{\alpha\beta} (G_\alpha)^T \otimes G_\beta. \tag{1.51}$$

The multiplicative constant is irrelevant because is always possible to normalize the EW W_O^K. ∎

The expected value in a bipartite state $\rho \in \mathscr{S} \left(\mathbb{C}^d \otimes \mathbb{C}^d \right)$ of W_O^K is

$$\mathrm{Tr}(W_O^K \rho) = \frac{1}{d^2} + \frac{1}{d(d-1)} \sum_{\alpha=1}^{d^2-1} \sum_{\beta=1}^{d^2-1} O^{\alpha\beta} \mathrm{Tr} \left(\rho G_\alpha^T \otimes G_\beta \right)$$

$$= \frac{1}{d^2} + \frac{1}{d(d-1)} \sum_{\alpha=1}^{d^2-1} \sum_{\beta=1}^{d^2-1} O^{\alpha\beta} C_{\alpha\beta} = \frac{1}{d^2} + \frac{1}{d(d-1)} \langle O|C\rangle_{HS}. \tag{1.52}$$

We defined $C_{\alpha\beta} = \mathrm{Tr} \left(\rho G_\alpha^T \otimes G_\beta \right)$ the entries of the matrix $C \in \mathscr{M}_{d^2-1}(\mathbb{R})$, know as *tensor correlator*. Entanglement of the state ρ is not detected by the above family of states (a necessary separability condition), if $\mathrm{Tr} W_O^K \rho \geq 0$, named

$$\frac{1}{d} + \frac{1}{d-1} \min_{O \in O(d^2-1)} \langle O|C\rangle_{HS} \geq 0. \tag{1.53}$$

Let $C = UDV^T$ for a diagonal matrix D and orthogonal matrices U, V (singular value decomposition). Then $\langle O^T|C\rangle_{HS} = \langle U^T O V|D\rangle_{HS}$ and the condition (1.53) will take the following form

$$\frac{1}{d} + \frac{1}{d-1} \min_{O \in O(d^2-1)} \langle O|D\rangle_{HS} = \frac{1}{d} + \frac{1}{d-1} \min_{O \in O(d^2-1)} \sum_{\alpha=1}^{d^2-1} O^{\alpha\alpha} D_{\alpha\alpha} \geq 0. \tag{1.54}$$

A diagonal element of an orthogonal matrix is bounded from below by -1 and all the bound are saturated for the matrix $O = -\mathbf{1}_d$. The above condition will be

$$\frac{1}{d} - \frac{1}{d-1} \sum_{\alpha=1}^{d^2-1} D_{\alpha\alpha} \geq 0. \tag{1.55}$$

Elements of diagonal matrix D are singular values of the matrix C, hence one can write down the above condition as

$$||C||_{tr} \leq \frac{d-1}{d}. \tag{1.56}$$

The Kossakowski map realized in Eq. 1.56 the Di Vincente's criterion[41][1].

---

[1]We obtained the criterion in Eq. 1.56 and only after a bibliographic research we realized it was already found by de Vincente, therefore we suggest the following: the De Vincente criterion with its related Kossakowski map.

1.5.2 Cross Computation Norm or Realignmnet criterion

From the criterion to the map – Consider a bipartite system living in $\mathbb{C}^{d_A} \otimes \mathbb{C}^{d_B}$ with dimensions d_A and d_B, respectively (in what follows we assume $d_A \leq d_B$). Let G_α^A and G_β^B denote arbitrary orthonormal basis in $\mathscr{S}\left(\mathbb{C}^{d_A}\right)$ and $\mathscr{S}\left(\mathbb{C}^{d_B}\right)$, that is, the $\langle G_\mu^A | G_\nu^A \rangle_{HS} = \delta_{\mu\nu}$, and the same for G_β^B. Now, given a bipartite state ρ

$$\rho = \sum_{\alpha=0}^{d_A^2-1} \sum_{\beta=0}^{d_B^2-1} \widetilde{C}_{\alpha\beta} \left(G_\alpha^A\right)^T \otimes G_\beta^B \tag{1.57}$$

one defines the following correlation matrix

$$\widetilde{C}_{\alpha\beta} = \left\langle \left(G_\alpha^A\right)^T \otimes G_\beta^B \right\rangle_\rho = \mathrm{Tr}\left(\rho \left(G_\alpha^A\right)^T \otimes G_\beta^B\right). \tag{1.58}$$

> **Theorem 1.5.2** If ρ is separable, then the Cross Computation Norm or Realignmnet (CCNR) criterion gives the following bound for the trace norm of $\widetilde{C}$:
>
> $$\|\widetilde{C}\|_{\mathrm{tr}} \leq 1. \tag{1.59}$$

Proposition 1.5.3 The satisfying the CCNR criterion is equivalent to the family of entanglement witnesses parametrised by $O \in \mathscr{O}\left(d_A^2 \times d_B^2\right)$ having $\mathrm{Tr}W_O = 1$

$$W_O^R = \frac{\mathbf{1}_{d_A}}{d_A} \otimes \frac{\mathbf{1}_{d_B}}{d_B} + \frac{1}{d_A d_B} \sum_{\alpha=0}^{d_A^2-1} \sum_{\beta=0}^{d_B^2-1} O^{\alpha\beta} \left(G_\alpha^A\right)^T \otimes G_\beta^B. \tag{1.60}$$

Proof. The norm $\|\widetilde{C}\|_{\mathrm{tr}}$ does not depend upon the particular orthonormal basis G_α^A and G_β^B. Using 1.3.1

$$1 - \|\widetilde{C}\|_{\mathrm{tr}} = 1 - \max_{O\in O(d^2)} \langle O|\widetilde{C}\rangle_{HS} = 1 + \min_{O\in\mathscr{O}(d_A,d_B)} \sum_{\alpha,\beta=0}^{d^2-1} O^{\alpha\beta} \widetilde{C}_{\alpha\beta}$$

$$= \mathrm{Tr}\rho + \min_{O\in\mathscr{O}(d_A,d_B)} \sum_{\alpha=0}^{d_A^2-1} \sum_{\beta=0}^{d_B^2-1} O^{\alpha\beta} \mathrm{Tr}\left(\rho \left(G_\alpha^A\right)^T \otimes G_\beta^B\right)$$

$$= \min_{O\in\mathscr{O}(d_A,d_B)} \mathrm{Tr}\left(\rho \left(\mathbf{1}_{d_A} \otimes \mathbf{1}_{d_B} + \sum_{\alpha=0}^{d_A^2-1} \sum_{\beta=0}^{d_B^2-1} O^{\alpha\beta} \left(G_\alpha^A\right)^T \otimes G_\beta^B\right)\right) \geq 0. \tag{1.61}$$

then, the normalization ends the proof.   ∎

> **R**   The normalization of a witness does not affect its powerful entanglement detection. This trick will be interestingly used in the section 1.12.

> **R**   Given an orthonormal matrix $O \in \mathscr{O}(n)$ it is defined by $n(n-1)/2$ independent parameters. In the above case O is defined by $d_A^2 d_B^2 \left(d_A^2 d_B^2 - 1\right)/2$ independent entries, which corresponds to the cardinality of EW family W_O at fixed basis G_α^A and G_β^B.

Proposition 1.5.4 The family of trace preserving and positive map $\Phi_O^R \in \mathscr{B}_+(\mathscr{H}_A)$ related to the above EW family via the Jamiołkowski isomorphism 1.30 is

$$\Phi_O^R(\rho_A) = d_A \mathrm{Tr}_A\left[(\rho_A^T \otimes \mathbf{1}_{d_B}) W_O\right] = \frac{\mathbf{1}_{d_B}}{d_B} + \frac{1}{d_B} \sum_{\alpha=0}^{d_A^2-1} \sum_{\beta=0}^{d_B^2-1} O^{\alpha\beta} \mathrm{Tr}_A\left(\rho_A G_\alpha^A\right) G_\beta^B. \tag{1.62}$$

Notice, the decomposition of ρ in term of the G_α^A's transposed is cancel with the transposition on ρ_A. Moreover, the CCNR criterion can be also equivalently defined via the realignment operation. Let $\left\{|i\rangle_{i=1}^{d_A}\right\}$ and $\left\{|\mu\rangle_{\mu=1}^{d_B}\right\}$ basis respectively of $\mathscr{H}_A$ and $\mathscr{H}_B$, a state $\rho \in \mathscr{S}(\mathscr{H})$ is

$$\rho = \sum_{i,j=1}^{d_A} \sum_{a,b=1}^{d_B} \rho_{ia;jb} |i\rangle\langle j| \otimes |a\rangle\langle b|, \qquad \text{then } [\mathscr{R}(\rho)]_{ij;\mu\nu} := \rho_{i\mu;j\nu}.$$

In another words, introducing a vectorization of an operator $A = \sum_{i,j} A_{ij} |i\rangle\langle j|$ via $|A\rangle\rangle = \sum_{i,j} A_{ij} |i\rangle \otimes |j\rangle$ one has $\mathscr{R}(A \otimes B) = |A\rangle\rangle\langle\langle B^*|$, where the complex conjugation is taken w.r.t. the basis used for the vectorization, e. g.

$$|A\rangle\rangle = \begin{pmatrix} a_{11} \\ a_{12} \\ a_{21} \\ a_{22} \end{pmatrix}, |B\rangle\rangle = \begin{pmatrix} b_{11} \\ b_{12} \\ b_{21} \\ b_{22} \end{pmatrix} \tag{1.63}$$

$$\mathscr{R}(A \otimes B) = \begin{pmatrix} a_{11} \\ a_{12} \\ a_{21} \\ a_{22} \end{pmatrix} \begin{pmatrix} b_{11} & b_{12} & b_{21} & b_{22} \end{pmatrix}. \tag{1.64}$$

In jargon, we say that the realignment operation transforms *blocks to rows* of a matrix, namely in the easiest example one has

$$\begin{pmatrix} \rho_{00,00} & \rho_{00,01} & \rho_{01,00} & \rho_{01,01} \\ \rho_{00,10} & \rho_{00,11} & \rho_{01,10} & \rho_{01,11} \\ \rho_{10,00} & \rho_{10,01} & \rho_{11,00} & \rho_{11,01} \\ \rho_{10,10} & \rho_{10,11} & \rho_{11,10} & \rho_{11,11} \end{pmatrix} \xrightarrow{\mathscr{R}} \begin{pmatrix} \rho_{00,00} & \rho_{00,01} & \rho_{00,10} & \rho_{00,11} \\ \rho_{01,00} & \rho_{01,01} & \rho_{01,10} & \rho_{01,11} \\ \rho_{10,00} & \rho_{10,01} & \rho_{10,10} & \rho_{10,11} \\ \rho_{11,00} & \rho_{11,01} & \rho_{11,10} & \rho_{11,11} \end{pmatrix}. \tag{1.65}$$

A reformulation of Th. 1.5.2 follows[29].

Theorem 1.5.5 if ρ is separable, then

$$\|\mathscr{R}(\rho)\|_1 \le 1. \tag{1.66}$$

Proposition 1.5.6 The maps related to CCNR in Eq. 1.62 detect at least all the states that Kossakowski maps in Eq. 1.44 detect for $d_A = d_B = d$. (When it happens we will say that such criterion is "stronger" that the other.)

Proof. We will prove that the Kossakowski map is a special case of CCNR map, therefore explores less states – Let us take a particular basis consisting of hermitian operators such that $G_0^A = \mathbf{1}_{d_A}/\sqrt{d_A}$ and $G_0^B = \mathbf{1}_{d_B}/\sqrt{d_B}$ (we call it canonical basis). It is clear that G_α^A and G_β^B are traceless for $\alpha, \beta > 0$.

We decompose the map 1.62 as follows

$$\Phi_O^R(\rho) = \frac{\mathbf{1}_d}{d} + \frac{1}{d}\sum_{\alpha,\beta=1}^{d^2-1} O^{\alpha\beta}\mathrm{Tr}(\rho G_\alpha)G_\beta$$

$$+ \frac{\mathbf{1}_d}{\sqrt{d}^3}\sum_{\alpha=1}^{d^2}\mathrm{Tr}\left(O^{\alpha 0}G_\alpha\rho\right) + \frac{1}{\sqrt{d}^3}\sum_{\beta=1}^{d^2} O^{0\beta}G_\beta + \frac{O^{00}}{d^2}\mathbf{1}_d. \tag{1.67}$$

Now let us restrict ourselves to a coset (not a subgroup) of orthogonal matrices of a form

$$O = \left[\begin{array}{c|c} -1 & \vec{0}^T \\ \hline \vec{0} & O_{d^2-1} \end{array}\right]. \tag{1.68}$$

For such orthogonal matrices the maps become

$$\Phi_O^R(\rho) = \frac{\mathbf{1}_d}{d} + \frac{1}{d}\sum_{\alpha,\beta=1}^{d^2-1} O^{\alpha\beta}G_\beta\mathrm{Tr}(\rho G_\alpha) - \frac{\mathbf{1}_d}{d^2}$$

$$= \frac{d-1}{d}\left(\frac{\mathbf{1}_d}{d} + \frac{1}{d-1}\sum_{\alpha,\beta=1}^{d^2-1} O^{\alpha\beta}G_\beta\mathrm{Tr}(\rho G_\alpha)\right) = \frac{d-1}{d}\Phi_O^K(\rho). \tag{1.69}$$

Hence such maps related to CCNR are equal (up to a factor) to Kossakowski maps Φ_O^K in Eq. 1.44. Therefore the realignment criterion is stronger than the criterion arising from Kossakowski maps of Eq. 1.56 for bipartite system the same dimension. Notice that the correlation tensor $\widetilde{C}$ as concerns CCNR criterion is related to the correlator tensor C of Kossakowski criterion as follows

$$\widetilde{C} = \left[\begin{array}{c|c} \frac{1}{d} & \frac{1}{\sqrt{d}}\vec{r}_B^T \\ \hline \frac{1}{\sqrt{d}}\vec{r}_A & C \end{array}\right]. \tag{1.70}$$

∎

1.5.3   Kossakowski criterion – Unequal dimensions

The above Kossakowski maps let to detect entanglement in systems with equal dimensions of subsystems. For different dimensions of subsystems, let $\mathbb{C}^{d_A} \otimes \mathbb{C}^{d_B}$ be the Hilbert space with fix $d_A \leq d_B$. Let $\{G_\alpha^A\}_{\alpha=0}^{d_A-1}$ and $\{G_\alpha^B\}_{\alpha=0}^{d_B-1}$ the orthonormal *canonical* basis of $\mathscr{B}(\mathbb{C}^{d_A})$ and $\mathscr{B}(\mathbb{C}^{d_B})$ respectively such that $G_0^A = \mathbf{1}_{d_A}/d_A$ and $G_0^B = \mathbf{1}_{d_B}/d_B$. Any d_A^2 subspace of $\mathscr{B}(\mathbb{C}^{d_B})$ can be obtained as a rotation by an $O_B \in O(d_A^2 - 1)$ (preserving the identity) of the space V_I spanned by the first d_A^2 G_α^A's. We will denote it by V_{O_B}. A set of states in $\mathscr{B}(\mathbb{C}^{d_B})$ contains an inscribed ball of the radius $1/\sqrt{d_B(d_B-1)}$ centered in the maximally mixed state. A set of states in V_{O_B} is a section of the set of all states by a subspace V_{O_B} containing the identity. This section contains $d_A^2 - 1$ dimensional ball of the radius $1/\sqrt{d_B(d_B-1)}$ around the projector onto V_{O_B} (with trace normalized to 1). A Kossakowski map $\Phi_O^K(O_A, O_B)$ rotates the traceless part of its argument by O_A, scales it then by $\sqrt{d_A}/\sqrt{(d_A-1)d_B(d_B-1)}$, embeds in V_I and rotates by O_B:

$$\Phi_O^K(O_A, O_B) : \rho \mapsto \frac{1}{d_B}\mathbf{1}_{d_B} + \sqrt{\frac{d_A}{(d_A-1)d_B(d_B-1)}}\sum_{\gamma=1}^{d_B^2-1}\sum_{\beta=1}^{d_A^2-1}\sum_{\alpha=1}^{d_A^2-1} G_\gamma O_B^{\gamma\beta} O_A^{\beta\alpha}\mathrm{Tr}(F_\alpha\rho). \tag{1.71}$$

One can see, that pair of rotation matrices O_A and O_B can be replaced by an $(d_B^2-1)\times(d_A^2-1)$ isometric matrix O

$$\Phi_O^K : \rho \mapsto \frac{1}{d_B}\mathbf{1}_{d_B} + \sqrt{\frac{d_A}{(d_A-1)d_B(d_B-1)}}\sum_{\beta=1}^{d_B^2-1}\sum_{\alpha=1}^{d_A^2-1} G_\beta O^{\beta\alpha}\mathrm{Tr}(F_\alpha\rho). \tag{1.72}$$

Proceeding, one can find the related entanglement witness

$$W_O^K = \mathfrak{J}(\Phi_O^K) = \frac{1}{d_A}(\mathbf{1}_{d_A} \otimes \Phi_O^K) \sum_{i,j=0}^{d_A-1} |ii\rangle\langle jj|$$

$$= \frac{\mathbf{1}_{d_A}}{d_A} \otimes \frac{\mathbf{1}_{d_B}}{d_B} + \frac{1}{\sqrt{d_A d_B (d_A-1)(d_B-1)}} \sum_{\beta=1}^{d_B^2-1} \sum_{\alpha=1}^{d_A^2-1} \sum_{i,j=0}^{d_A-1} |i\rangle\langle j|\langle j|G_\alpha^A|i\rangle \otimes O^{\beta\alpha} G_\beta^B$$

$$= \frac{\mathbf{1}_{d_A}}{d_A} \otimes \frac{\mathbf{1}_{d_B}}{d_B} + \frac{1}{\sqrt{d_A d_B (d_A-1)(d_B-1)}} \sum_{\beta=1}^{d_B^2-1} \sum_{\alpha=1}^{d_A^2-1} O^{\beta\alpha} (G_\alpha^A)^T \otimes G_\beta^B.$$

Positive expected value for all the witnesses from the above family yields to the condition

$$||C||_{\mathrm{Tr}} \leq \sqrt{\frac{(d_A-1)(d_B-1)}{d_A d_B}}, \tag{1.73}$$

in analogy with Eq. 1.51.

Comparison with CCNR

Let us decompose the sum in (1.62) as follows

$$\Phi_O^R(\rho) = \frac{\mathbf{1}_{d_B}}{d_B} + \frac{1}{d_B} \sum_{\alpha=0}^{d_A^2-1} \sum_{\beta=0}^{d_B^2-1} O^{\alpha\beta} \mathrm{Tr}_A (\rho_A G_\alpha^A) G_\beta^B.$$

$$= \frac{\mathbf{1}_{d_B}}{d_B} + \frac{1}{d_B} \sum_{\alpha=1}^{d_A^2-1} \sum_{\beta=1}^{d_B^2-1} O^{\alpha\beta} \mathrm{Tr}_A (\rho_A G_\alpha^A) G_\beta^B + \frac{O^{00}}{d_B} \mathrm{Tr}_A (\rho_A G_0^A) G_0^B$$

$$+ \frac{1}{d_B} \sum_{\beta=0}^{d_B^2-1} O^{0\beta} \mathrm{Tr}_A (\rho_A G_0^A) G_\beta^B + \frac{1}{d_B} \sum_{\alpha=0}^{d_A^2-1} O^{\alpha 0} \mathrm{Tr}_A (\rho_A G_\alpha^A) G_0^B$$

$$= \frac{\mathbf{1}_{d_B}}{d_B} + \frac{1}{d_B} \sum_{\alpha=1}^{d_A^2-1} \sum_{\beta=1}^{d_B^2-1} O^{\alpha\beta} \mathrm{Tr}_A (\rho_A G_\alpha^A) G_\beta^B + \frac{O^{00}}{d_B \sqrt{d_A d_B}} \mathbf{1}_{d_B} \tag{1.74}$$

$$+ \frac{1}{d_B \sqrt{d_A}} \sum_{\beta=0}^{d_B^2-1} O^{0\beta} G_\beta^B + \frac{1}{d_B \sqrt{d_B}} \sum_{\alpha=0}^{d_A^2-1} O^{\alpha 0} \mathrm{Tr}_A (\rho_A G_\alpha^A) \mathbf{1}_{d_B}. \tag{1.75}$$

Now let us restrict ourselves to isometry matrices of a form

$$O = \left[\begin{array}{c|c} -1 & \vec{0}^T \\ \hline \vec{0} & \tilde{O} \end{array} \right], \qquad \tilde{O} \in \mathcal{O}(d_A^2-1, d_B^2-1). \tag{1.76}$$

For such orthogonal matrices the maps (1.74) take a form

$$\Phi_O^R(\rho) = \left(\frac{1}{d_B} - \frac{1}{d_B \sqrt{d_A d_B}} \right) \mathbf{1}_{d_B} + \frac{1}{d_B} \sum_{\alpha=1}^{d_A^2-1} \sum_{\beta=1}^{d_B^2-1} O^{\alpha\beta} \mathrm{Tr}_A (\rho_A G_\alpha^A) G_\beta^B$$

$$= \sqrt{\frac{(d_A-1)(d_B-1)}{d_A d_B}} \left(\frac{\sqrt{d_A d_B} - 1}{\sqrt{(d_A-1)(d_B-1)}} \frac{\mathbf{1}_{d_B}}{d_B} + \right. \tag{1.77}$$

$$\left. \frac{\sqrt{d_A}}{\sqrt{(d_A-1)} d_B (d_B-1)} \sum_{\alpha=1}^{d_A^2-1} \sum_{\beta=1}^{d_B^2-1} O^{\alpha\beta} \mathrm{Tr}_A (\rho_A G_\alpha^A) G_\beta^B \right). \tag{1.78}$$

One can easily check that the following inequality holds

$$\frac{\sqrt{d_1 d_2} - 1}{\sqrt{(d_1 - 1)(d_2 - 1)}} \geq 1, \tag{1.79}$$

with equality only for $d_1 = d_2$. If the dimensions of subsystems are equal, the above maps $\Phi_O^R(\rho)$ are equal (up to a factor) to Kossakowski maps Φ_O^K in Eq. 1.72. It implies, that in the case of equal subsystems the realignment criterion is stronger than de Vincente criterion arising from Kossakowski maps. If the dimensions are not equal, the maps (1.78) are proportional to Kossakowski maps in Eq. (1.72) with an amount of white noise added, hence they cannot be optimal [42] and the Kossakowski maps detect more entangled states than (1.78). There is still a possibility, that non-optimality of the maps (1.78) is compensated by other maps (which do not preserve the trace) in realignment criterion. In section 1.9 we show that in the case of unequal dimensions the de Vincente criterion can be indeed stronger than CCNR criterion. This comparison will include also another criterion that we are presenting in the following section.

1.5.4 Entanglement SIC–POVMs criterion

In a recent paper [43] authors proposed an interesting separability criterion based on symmetric informationally complete positive operator valued measure (SIC POVM). Recall, that a family of d^2 rank-1 operators $\Pi_i = \frac{1}{d}|\psi_i\rangle\langle\psi_i|$ in d-dimensional Hilbert space defines SIC POVM iff

$$|\langle \psi_i | \psi_j \rangle|^2 = \frac{d\delta_{ij} + 1}{d + 1} \ , \ \sum_{i=1}^{d^2} \Pi_i = \mathbf{1}_d. \tag{1.80}$$

There is a conjecture (1999) by Zauner that SIC POVM exists for any d [44] (see also [45]). So far these objects have been found for several dimensions (see [46] and [47] for the recent progress). It is, therefore, clear that the result of [43] was restricted to specific dimensions only. Here we show that this criterion is universal (valid for any d_A and d_B). Moreover, it belongs to our class (1.109) with $(x, y) = (\sqrt{d_A + 1}, \sqrt{d_B + 1})$ as we will see in the next section 1.6. The separability criterion (so called ESIC criterion) derived in [43] states that

> **Theorem 1.5.7** if ρ is separable, then
>
> $$\|P\|_{\mathrm{tr}} \leq \frac{2}{\sqrt{d_A(d_A + 1)d_B(d_B + 1)}}, \tag{1.81}$$
>
> here $P_{\alpha\beta} = \left\langle \left(\Pi_\alpha^A\right)^T \otimes \Pi_\beta^B \right\rangle$, and Π_α^A and Π_β^B are elements of SIC POVMs in $\mathscr{H}_A$ and $\mathscr{H}_B$, respectively.

Proof. Given a SIC POVM $\{\Pi_\alpha\}_{\alpha=1}^{d^2}$ of a quantum state $\rho_A \in \mathscr{S}(\mathscr{H}_A)$, with $\dim \mathscr{H}_A = d_A$ can be restored as follows

$$\rho = d(d + 1) \sum_{i=1}^{d^2} p_i \Pi_i - \mathbf{1}_d \tag{1.82}$$

where $p_i = \mathrm{Tr}\rho\Pi_i$, is the probability to get the $i-$th outcome and $\sum_i p_i = 1$. The trace of the square of Eq. 1.82 yields

$$\sum_{i=1}^{d^2} |p_i|^2 = \frac{1 + \mathrm{Tr}\rho^2}{d(d + 1)} \leq \frac{2}{d(d + 1)}, \tag{1.83}$$

because $\mathrm{Tr}\rho^2 \in [0,1]$. Now, $\rho = \sigma^A \otimes \sigma^B$ is a product state, then using SVD $\mathscr{P}_{ij} = p_i^A p_j^B$, and as an application on the state appear as

$$\mathscr{P}\left(\sigma^A \otimes \sigma^B\right) = |p^A\rangle\langle p^B| = ||\vec{p}_A|| \cdot ||\vec{p}_B^T|| \, |u^A\rangle\langle u^B| \tag{1.84}$$

with $|u^A\rangle$ and $|u^B\rangle$ normalize vector. Hence

$$||\mathscr{P}\left(\sigma^A \otimes \sigma^B\right)||_{\mathrm{tr}} = ||\vec{p}_A|| \cdot ||\vec{p}_B^T|| \leq \sqrt{\frac{2}{d_A(d_A+1)}}\sqrt{\frac{2}{d_B(d_B+1)}}. \tag{1.85}$$

From the triangle inequality follows that for any separable state

$$\left|\left|\mathscr{P}\left(\sum_i p_i \sigma_i^A \otimes \sigma_i^B\right)\right|\right|_{\mathrm{tr}} \leq \sum_i p_i ||\mathscr{P}\left(\sigma_i^A \otimes \sigma_i^B\right)||_{\mathrm{tr}} \leq \frac{2}{\sqrt{d_A(d_A+1)}\sqrt{d_B(d_B+1)}}. \tag{1.86}$$

because $\sum_i p_i = 1$.   ∎

Proposition 1.5.8 One can rewrite the ESIC criterion to find a family of entanglement witnesses parametrized by $O \in \mathscr{O}(d_A^2 \times d_B^2)$

$$W_O^E = \mathbf{1}_{d_A} \otimes \mathbf{1}_{d_B} + \frac{\sqrt{d_A(d_A+1)d_B(d_B+1)}}{2}\sum_{\alpha=0}^{d_A^2-1}\sum_{\beta=0}^{d_B^2-1} O^{\alpha\beta}\left(\Pi_\alpha^A\right)^T \otimes \Pi_\beta^B. \tag{1.87}$$

Proof. from the criterion in Eq. 1.81

$$\frac{\sqrt{d_A(d_A+1)d_B(d_B+1)}}{2}||\mathscr{P}||_{\mathrm{Tr}} \leq 1$$

$$\frac{\sqrt{d_A(d_A+1)d_B(d_B+1)}}{2}\max_{O\in\mathscr{O}(d_A^2,d_B^2)}\mathrm{Tr}\left(\rho\sum_{\alpha\beta}O^{\alpha\beta}\left(\Pi_\alpha^A\right)^T\otimes\Pi_\beta^B\right) \leq \mathrm{Tr}\left(\rho\mathbf{1}_{d_A}\otimes\mathbf{1}_{d_B}\right)$$

$$\min_{O\in\mathscr{O}(d_A^2,d_B^2)}\mathrm{Tr}\left[\rho\left(\mathbf{1}_{d_A}\otimes\mathbf{1}_{d_B} + \frac{\sqrt{d_A(d_A+1)d_B(d_B+1)}}{2}\sum_{\alpha\beta}O^{\alpha\beta}\left(\Pi_\alpha^A\right)^T\otimes\Pi_\beta^B\right)\right] \geq 0$$

in this case the Π's are not traceless thus the normalization is pointless.   ∎

Proposition 1.5.9 The maps associated to ESIC using the isomorphism $\Phi_O^E = j^{-1}\left(W_O^E\right) = d_A\mathrm{Tr}_A\left[\left(\rho^T \otimes \mathbf{1}_{d_B}\right)W\right]$ is

$$\Phi_O^E(\rho) = d_A\mathbf{1} + d_A\frac{\sqrt{d_A(d_A+1)d_B(d_B+1)}}{2}\sum_{\alpha\beta}O^{\alpha\beta}\mathrm{Tr}\left(\rho\Pi_\alpha^A\right)\Pi_\beta^B. \tag{1.88}$$

It is pedagogical to obtain the map before the EW as in the following proposition.

Proposition 1.5.10 Given O^{kl} an orthogonal matrix satisfying $\sum_k O^{kl} = 1$ and ρ a density state, then Φ is a trace-preserving positive map following defined

$$\Phi(\rho) = \frac{1}{d-1}\left(2\mathbf{1}\mathrm{Tr}\rho - \frac{d+1}{d}\sum_{k,l=1}^{d^2}O^{kl}\Pi_k\mathrm{Tr}(\Pi_l\rho)\right). \tag{1.89}$$

Proof. To prove it, we use the following well known result. Let ρ be hermitian operator such that $\text{Tr}\rho = 1$. If $\text{Tr}\rho^2 \leq \frac{1}{d-1}$, then $\rho \geq 0$. Let P be a rank-1 projector (pure state). One has

$$
\begin{aligned}
\text{Tr}[\Phi(P)]^2 &= \frac{1}{(d-1)^2}\left\{ 4d - 4\frac{d-1}{d}\sum_{k,l=1}^{d^2} O^{kl}\text{Tr}(\Pi_l P) \right. \\
&\quad + \left. \left(\frac{d-1}{d}\right)^2 \sum_{k,l=1}^{d^2} O^{kl}\text{Tr}(\Pi_l P)\sum_{m,n=1}^{d^2} O^{mn}\text{Tr}(\Pi_n P)\text{Tr}(\Pi_k \Pi_m) \right\} \\
&= \frac{1}{(d-1)^2}\left\{ 4d - 4\frac{d-1}{d}d + \left(\frac{d-1}{d}\right)^2\left(\frac{2d^2}{(d+1)^2} + \frac{d^2(d+1)}{(d+1)^2}\right) \right\} \\
&= \frac{1}{d-1}.
\end{aligned}
\tag{1.90}
$$

which ends the proof. In Eq.(1.90) we used Eq. 1.80 and the following property of SIC POVM

$$
\sum_k [\text{Tr}(\Pi_k P)]^2 = \frac{2d}{d+1}.
$$

This map gives rise to the following entanglement witness (up to normalization)

$$
W = 2\mathbf{1} \otimes \mathbf{1} - \frac{d+1}{d}\sum_{k,l=1}^{d^2} O^{kl}\Pi_k \otimes \Pi_l^{\text{T}}.
\tag{1.91}
$$

∎

(R) It was conjectured in [43] that ESIC criterion is stronger than CCNR criterion. This conjecture is supported by several examples and numerical analysis (cf. [43]). In the section **??** we analytically demonstrate the validity only for a symmetric and positive tensor correlator, generalize the conjecture and show some numerical analysis.

Proposition 1.5.11 Let us observe that if Π_α define SIC–POVM in d-dimension Hilbert space, then

$$
G_\alpha^{(\mp)} := \sqrt{d(d+1)}\,\Pi_\alpha - \frac{\sqrt{d+1}\mp 1}{\sqrt{d^3}}\,\mathbf{1}_d,
\tag{1.92}
$$

defines on orthonormal basis in $\mathscr{B}(\mathscr{H})$, that is, $\left\langle G_\alpha^{(\mp)}|G_\beta^{(\mp)}\right\rangle_{\text{HS}} = \delta_{\alpha\beta}$. Note, that this is not a canonical basis. Indeed, $G_0^{(\mp)}$ is not proportional to $\mathbf{1}_d$. However, it enjoys the following properties

$$
\text{Tr}\,G_\alpha^{(\mp)} = \pm\frac{1}{\sqrt{d}}\ ,\quad \sum_\alpha G_\alpha^{(\mp)} = \pm\sqrt{d}\,\mathbf{1}_d.
\tag{1.93}
$$

Proof. Impose $G_\alpha = c_1\Pi_\alpha + c_2\mathbf{1}_d$ such that $\text{Tr}G_\alpha G_\beta = \delta_{\alpha\beta}$, we solved the system in term of c_1 and c_2

$$
\begin{cases}
c_1 = \sqrt{d(d+1)} \\
d^2 c_2 + 2\sqrt{d(d+1)}c_2 + 1 = 0
\end{cases}
\tag{1.94}
$$

which ends to proof. To prove Eq. 1.93 one use $\text{Tr}\Pi_\alpha = 1/d$ and the POVM property $\sum_{\alpha=1}^{d^2}\Pi_\alpha = \mathbf{1}_d$. ∎

In what follows, we take $G_\alpha := G_\alpha^{(-)}$ (but the final result applies for $G_\alpha^{(+)}$ as well) and reformulate ESIC criterion (1.81) in terms of the correlation matrix $\widetilde{C}_{\alpha\beta}$ for $\alpha = 0\ldots d_A^2 - 1$ and $\beta = 0\ldots d_B^2 - 1$ as follows

Theorem 1.5.12 if ρ is separable, then

$$\|A\widetilde{C}B\|_{\text{tr}} \leq 2. \tag{1.95}$$

with

$$\sqrt{d_A(d_A+1)d_B(d_B+1)}\,P = A\widetilde{C}B, \tag{1.96}$$

where $\widetilde{C}_{\alpha\beta} = \left\langle G_\alpha^A \otimes G_\beta^B \right\rangle_\rho$ is a correlation matrix defined in terms of $G_\alpha = G_\alpha^{(-)}$, and

$$\begin{aligned}
A &= \mathbf{1}_A \otimes \mathbf{1}_A + a\,\mathbb{J}_A \otimes \mathbb{J}_A, \\
B &= \mathbf{1}_B \otimes \mathbf{1}_B + b\,\mathbb{J}_B \otimes \mathbb{J}_B,
\end{aligned} \tag{1.97}$$

where $\mathbb{J}_A$ is $d_A \times d_A$ matrix such that $[\mathbb{J}_A]_{ij} = 1$ (and similarly for $\mathbb{J}_B$). Finally

$$a = \frac{\sqrt{d_A+1}-1}{d_A^2} \ , \quad b = \frac{\sqrt{d_B+1}-1}{d_B^2}. \tag{1.98}$$

It should be stressed that here $\widetilde{C}_{\alpha\beta}$ is not written in the canonical basis. However we can compare it in the section 1.9 using the unitary invariance of the trace norm.

Proof. Using 1.92 and 1.93 the mean value of the state ρ from Eq. 1.87 is

$$\begin{aligned}
\text{Tr}\rho W_O^E = 1 + \frac{1}{2}\sum_{\alpha=0}^{d_A^2-1}\sum_{\beta=0}^{d_B^2-1} O^{\alpha\beta} \\
\text{Tr}\rho\left((G_\alpha^A)^T + \frac{\sqrt{d_A+1}\mp 1}{\sqrt{d_A}^3}\mathbf{1}_{d_A}\right) \otimes \left(G_\beta^B + \frac{\sqrt{d_B+1}\mp 1}{\sqrt{d_B}^3}\mathbf{1}_{d_B}\right)
\end{aligned} \tag{1.99}$$

and by the definition of $\widetilde{C}_{\alpha\beta}$ and notice from 1.93 that $\sqrt{d_B}\text{Tr}\rho G_\alpha^A \otimes \mathbf{1}_{d_B} = \pm\sum_\gamma \widetilde{C}_{\alpha\gamma}$

$$\begin{aligned}
\text{Tr}\rho W_O &= 1 + \frac{1}{2}\sum_{\alpha=0}^{d_A^2-1}\sum_{\beta=0}^{d_B^2-1} O^{\alpha\beta}\left(\widetilde{C}_{\alpha\beta} + \frac{\pm\sqrt{d_A+1}-1}{d_A^2}\sum_{\gamma=0}^{d_A^2-1}\widetilde{C}_{\gamma\beta}\right. \\
&\left. + \frac{\pm\sqrt{d_B+1}-1}{d_B^2}\sum_{\delta=0}^{d_B^2-1}\widetilde{C}_{\alpha\delta} + \frac{\pm\sqrt{d_A+1}-1}{d_A^2}\cdot\frac{\pm\sqrt{d_B+1}-1}{d_B^2}\sum_{\gamma=0}^{d_A^2-1}\sum_{\delta=0}^{d_B^2-1}\widetilde{C}_{\gamma\delta}\right) \\
&= 1 + \frac{1}{2}\sum_{\alpha=0}^{d_A^2-1}\sum_{\beta=0}^{d_B^2-1} O^{\alpha\beta}\left[(\mathbf{1}_{d_A}\otimes\mathbf{1}_{d_A} + a_\pm\mathbb{J}_A\otimes\mathbb{J}_A)\widetilde{C}(\mathbf{1}_{d_B}\otimes\mathbf{1}_{d_B} + b_\pm\mathbb{J}_B\otimes\mathbb{J}_B)\right]_{\alpha\beta} \\
&\stackrel{\text{def}}{=} 1 + \frac{1}{2}\sum_{\alpha=0}^{d_A^2-1}\sum_{\beta=0}^{d_B^2-1} O^{\alpha\beta}\left(A\widetilde{C}B\right)_{\alpha\beta} \geq 0.
\end{aligned} \tag{1.100}$$

In particular, it holds for the minimum of O

$$\begin{aligned}
1 + \frac{1}{2}\min_O \sum_{\alpha=0}^{d_A^2-1}\sum_{\beta=0}^{d_B^2-1} O^{\alpha\beta}\left(A\widetilde{C}B\right)_{\alpha\beta} &= 1 - \frac{1}{2}\max_O \sum_{\alpha=0}^{d_A^2-1}\sum_{\beta=0}^{d_B^2-1} O^{\alpha\beta}\left(A\widetilde{C}B\right)_{\alpha\beta} \\
&= 1 - \frac{1}{2}\|A\widetilde{C}B\|_{\text{Tr}} \geq 0.
\end{aligned} \tag{1.101}$$

∎

The block form (1.70) of the matrix $\widetilde{C}$ in the canonical basis is

$$A\widetilde{C}B = \left[\begin{array}{c|c} \sqrt{\frac{d_A+1}{d_A}}\sqrt{\frac{d_B+1}{d_B}} & \sqrt{\frac{d_A+1}{d_A}}\vec{r}_B^T \\ \hline \sqrt{\frac{d_B+1}{d_B}}\vec{r}_A & C \end{array} \right]. \tag{1.102}$$

R Observe, that it is enough to have the covariance matrix $\widetilde{C}$ to check the ESIC criterion - no explicit form of the SIC POVM is necessary!

In the appendix we analyse the conjecture of 1.5.4 using particular SIC–POVMs generated via the fiducial vectors [48] under the *Weyl displacement operator*[49, 50].
Summarizing, the three criteria: Kossakowski's, realignment and ESIC criterion can be written in an unified form

$$||C||_{\mathrm{Tr}} \leq \sqrt{\frac{d_1-1}{d_1}}\sqrt{\frac{d_2-1}{d_2}} \tag{1.103}$$

$$||\widetilde{C}||_{\mathrm{Tr}} = \left\| \left[\begin{array}{c|c} \frac{1}{\sqrt{d_A d_B}} & \frac{1}{\sqrt{d_A}}\vec{r}_B^T \\ \hline \frac{1}{\sqrt{d_B}}\vec{r}_A & C \end{array} \right] \right\|_{\mathrm{Tr}} \leq 1 \tag{1.104}$$

$$||A\widetilde{C}B||_{\mathrm{Tr}} = \left\| \left[\begin{array}{c|c} \sqrt{\frac{d_A+1}{d_A}}\sqrt{\frac{d_B+1}{d_B}} & \sqrt{\frac{d_A+1}{d_A}}\vec{r}_B^T \\ \hline \sqrt{\frac{d_B+1}{d_B}}\vec{r}_A & C \end{array} \right] \right\|_{\mathrm{Tr}} \leq 2 \tag{1.105}$$

The formulas (1.103-1.105) suggest the existence of one criterion generalizing all the tree considered. In the canonical basis, we have

$$||\mathrm{diag}\{x\sqrt{d_1+1},1,\ldots,1\}C^{\mathrm{can}}\mathrm{diag}\{y\sqrt{d_2+1},1,\ldots,1\}||_{\mathrm{Tr}} \leq f_{d_1,d_2}(x,y). \tag{1.106}$$

The three criteria arise from the three values of the f_{d_1,d_2} function: $f_{d_1,d_2}(0,0) = \sqrt{1-1/d_1}\sqrt{1-1/d_2}$, $f_{d_1,d_2}(1,1) = 1$, $f_{d_1,d_2}(\sqrt{d_1+1},\sqrt{d_2+1}) = 2$. More known values of this function will lead to new separability criteria as we are going to construct. Once it is constructed, then we will show its powerful for the isotropic states.

1.6 A novel unifying family of separability criteria

The construction of a unification of several bipartite separability criteria is based on correlation matrix (or correlation tensor). In this category one finds Di Vicente criterion (dV) [41], CCNRseparability criterion, the criterion derived in [51] and the recent criterion based on SIC POMVs (ESIC) [43]. This new criterion in general is not stronger that correlation matrix criterion (CMC), however we provide an example of PPT state which is not detected by filtered CMC [32, 33] (LFCMC) but is detected by the new one. Our result is then generalized to multipartite scenario. We stress that the new criteria are linear in the density operator and hence may be used to construct new classes of entanglement witness and positive maps. In fact with a proper limit procedure we will obtain an extremely relevant equivalence between our criterion an the enhanced realignment criterion [52, 53].
Consider a bipartite system living in $\mathscr{H}_A \otimes \mathscr{H}_B$ with dimensions d_A and d_B, respectively (in what follows we assume $d_A \leq d_B$). Let us take a particular basis consisting of Hermitian operators such that $G_0^A = \mathbf{1}_{d_A}/\sqrt{d_A}$ and $G_0^B = \mathbf{1}_{d_B}/\sqrt{d_B}$ (canonical basis). It is clear that G_α^A and G_β^B are traceless for $\alpha, \beta > 0$. The canonical basis gives rise the following generalized Bloch representation

$$\rho = \frac{\mathbf{1}_{d_A}}{d_A} \otimes \frac{\mathbf{1}_{d_B}}{d_B} + \sum_{i>0} r_i^A G_i^A \otimes \frac{\mathbf{1}_{d_B}}{d_B} + \sum_{j>0} r_j^B \frac{\mathbf{1}_{d_A}}{d_A} \otimes G_j^B$$

$$+ \sum_{i,j>0} t_{ij} G_i^A \otimes G_j^B = \sum_{\alpha=0}^{d_A^2-1} \sum_{\beta=0}^{d_B^2-1} C_{\alpha\beta}^{\mathrm{can}} G_\alpha^A \otimes G_\beta^B, \tag{1.107}$$

where r_i^A and r_j^B are generalized Bloch vectors $r_i^A = \mathrm{Tr}\left(\rho G_\alpha^A \otimes \mathbf{1}_{d_B}\right) = \mathrm{Tr}\rho_A G_\alpha^A$ (analogously for r_i^B) corresponding to reduces states ρ_A and ρ_B, respectively, and t_{ij} is the usual correlation tensor, that is, one finds for the reduces states

$$\rho_A = \mathrm{Tr}_B \rho = \frac{\mathbf{1}_{d_A}}{d_A} + \sum_{i>0} r_i^A G_i^A, \qquad \rho_B = \mathrm{Tr}_A \rho = \frac{\mathbf{1}_{d_B}}{d_B} + \sum_{j>0} r_j^B G_j^B.$$

We denote $C_{\alpha\beta}$ defined by the canonical basis by $C_{\alpha\beta}^{\mathrm{can}}$ as in Eq. 1.58. Clearly $\|C^{\mathrm{can}}\|_1 = \|C\|_1$. Let us introduce two square diagonal matrices:

$$D_x^A = \mathrm{diag}\{x, 1, \ldots, 1\}, \qquad D_y^B = \mathrm{diag}\{y, 1, \ldots, 1\}. \tag{1.108}$$

where D_x^A is $d_A^2 \times d_A^2$ and D_y^B is $d_B^2 \times d_B^2$, and the real parameters $x, y \geq 0$.

> **Theorem 1.6.1** If ρ is separable, then

$$\|D_x^A C^{\mathrm{can}} D_y^B\|_1 \leq \mathcal{N}_A(x)\mathcal{N}_B(y), \tag{1.109}$$

where

$$\mathcal{N}_A(x) = \sqrt{\frac{d_A - 1 + x^2}{d_A}}, \qquad \mathcal{N}_B(y) = \sqrt{\frac{d_B - 1 + y^2}{d_B}}, \tag{1.110}$$

for arbitrary $x, y \geq 0$. In the following we will call it *XY-criterion*.

Proof. Separability implies that ρ is a convex combination of product states and hence (due to the triangle inequality for the norm) it is enough to check (1.109) for a product state $\rho_A \otimes \rho_B$. One finds for the correlation matrix

$$(C^{\mathrm{can}})_{\alpha\beta} = R_\alpha^A R_\beta^B,$$

where $R_0^A = 1/\sqrt{d_A}$, $R_i^A = r_i^A$ $(i \geq 1)$, and similarly for R_β^B. It implies $\|C^{\mathrm{can}}\|_1 = |R^A||R^B|$, where $|R^A|^2 = \frac{1}{d_A} + |\mathbf{r}^A|^2$ (and the same for R^B). Let us observe that

$$(D_x^A C^{\mathrm{can}} D_y^B)_{\alpha\beta} = (R_x^A)_\alpha (R_y^B)_\beta,$$

with $R_x^A = (x/\sqrt{d_A}, \mathbf{r}^A)$ and $R_y^B = (y/\sqrt{d_B}, \mathbf{r}^B)$. It implies

$$\|D_x^A C^{\mathrm{can}} D_y^B\|_1 = \sqrt{\frac{x^2}{d_A} + |\mathbf{r}^A|^2} \sqrt{\frac{y^2}{d_B} + |\mathbf{r}^B|^2}. \tag{1.111}$$

Finally, positivity of ρ_A and ρ_B requires that

$$\mathrm{Tr}\rho_A^2 \leq 1 \, , \quad \mathrm{Tr}\rho_B^2 \leq 1 \, ,$$

which imply that the corresponding Bloch vectors $\mathbf{r}^A$ and $\mathbf{r}^B$ satisfy

$$|\mathbf{r}^A|^2 \leq \frac{d_A - 1}{d_A} \, , \quad |\mathbf{r}^B|^2 \leq \frac{d_B - 1}{d_B},$$

and hence formula (1.109) easily follows. Clearly $(x,y) = (1,1)$ reproduces CCNR criterion. Interestingly, $(x,y) = (0,0)$ reproduces separability criterion derived by de Vicente [41] and equivalent to Kossakowski criterion. We had proven in 1.5.6 that If $d_A = d_B$, then CCNR criterion is stronger than dV criterion. However, for bipartite states ρ such that $\rho_A = \mathbf{1}_{d_A}/d_A$ and $\rho_B = \mathbf{1}_{d_B}/d_B$, dV criterion is stronger than CCNR if $d_A \neq d_B$, and they are equivalent if $d_A = d_B$ [41]. Interestingly, we found another example of such criterion in [51]. After suitable renormalization the result of [51] corresponds to $(x,y) = (\sqrt{2/d_A}, \sqrt{2/d_B})$. Also the criterion in 1.81 belongs to the family of XY–criterion. It should be stressed that here $C_{\alpha\beta}$ in 1.95 is not a canonical matrix and hence (1.95) cannot be immediately related to (1.109). Note, however, that due to the fact that the trace norm is unitarily invariant one has   ∎

$$\|ACB\|_{\mathrm{Tr}} = \|UAU^\dagger(UCV^\dagger)VBV^\dagger\|_{\mathrm{Tr}},$$

for arbitrary unitary matrices U and V. Taking U and V such that they diagonalize A and B, respectively, one obtains

$$\|ACB\|_{\mathrm{Tr}} = \|D_x^A C^{\mathrm{can}} D_y^B\|_{\mathrm{Tr}},$$

with $(x,y) = (\sqrt{d_A + 1}, \sqrt{d_B + 1})$ and using the invariance of the trace norm with respect to the unitary operators U and V. It proves that the original assumption about the existence of two SIC POVMs $\{\Pi_\alpha^A\}$ and $\{\Pi_\beta^B\}$ is not essential and the ESIC criterion universally holds for arbitrary d_A and d_B.

Moreover, the covariance matrix criterion (CMC) [32, 33] supplemented by the procedure of local filtering (LFCMC) turned out to be very powerful criterion. Interestingly, for $d_A \leq d_B$ (but $d_B - d_A$ is not to big, cf. [33]) this criterion is equivalent to (supplemented by a local filtering) dV criterion [41]. Now, in our case if $\mathbf{r}^A = 0$ and $\mathbf{r}^B = 0$, one finds

$$\|D_x^A C^{\mathrm{can}} D_y^B\|_{\mathrm{Tr}} = \frac{xy}{\sqrt{d_A d_B}} + \|D_0^A C^{\mathrm{can}} D_0^B\|_{\mathrm{Tr}},$$

and hence one may wonder whether is it possible to obtain a stronger result than dV criterion. One easily finds that the function $\mathcal{N}_A(x)\mathcal{N}_B(y) - \frac{xy}{\sqrt{d_A d_B}}$ realizes minimum for $x\sqrt{d_B - 1} = y\sqrt{d_A - 1}$ which reproduces dV [41]. Hence, it proves that within a class of states with maximally mixed marginals (and $d_B - d_A$ is not too big) dV condition is the strongest one. In Fig.1.3 is summarized this discussion.

1.6.1   Witnesses and map of XY-criterion

As the previous section, we derive from the XY–criterion its witnesses and maps, starting from Eq. 1.109
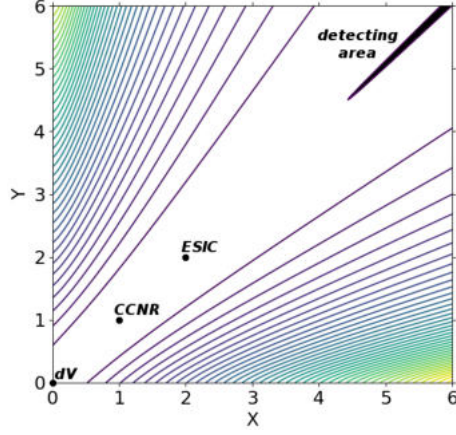
Figure 1.3: Contour levels of the function $f(x,y) = \mathcal{N}_A(x)\mathcal{N}_B(y) - \|D_x^A C^{\mathrm{can}} D_y^B\|_{\mathrm{Tr}}$. In the *detecting area* $f(x,y) < 0$, since the state is detected according to our criterion (1.109) with parameters (x,y) as in Eq. (1.110). Three characteristic points on the xy plane which restore well-known criteria: $(0,0) - \mathrm{dV}$; $(1,1) - \mathrm{CCNR}$, and $(2,2) - \mathrm{ESIC}$.

$$
\begin{aligned}
0 \leq & \mathcal{N}_A(x)\mathcal{N}(y) - \|D_x^A C^{\mathrm{can}} D_y^B\|_{\mathrm{Tr}} \\
= & \mathcal{N}_A(x)\mathcal{N}(y)\,\mathrm{Tr}(\rho\mathbf{1}_{d_A} \otimes \mathbf{1}_{d_B}) - \max_{O \in \mathscr{O}(d_A^2, d_B^2)} \langle O|D_x^A C^{\mathrm{can}} D_y^B \rangle_{HS} \\
= & \mathcal{N}_A(x)\mathcal{N}(y)\,\mathrm{Tr}(\rho\mathbf{1}_{d_A} \otimes \mathbf{1}_{d_B}) + \min_{O \in \mathscr{O}(d_A^2, d_B^2)} \langle O|D_x^A C^{\mathrm{can}} D_y^B \rangle_{HS}.
\end{aligned}
\tag{1.112}
$$

Therefore for an arbitrary isometry O

$$
\mathrm{Tr}(W_O^{xy}\rho) \geq 0,
\tag{1.113}
$$

where

$$
W_O^{xy} = \mathcal{N}_A(x)\mathcal{N}(y)\,\mathbf{1}_{d_A} \otimes \mathbf{1}_{d_B} + \sum_{\alpha,\beta} \widetilde{O}_{\alpha\beta} G_\alpha^A \otimes G_\beta^B
\tag{1.114}
$$

and the "deformed" isometry $\widetilde{O}^{\alpha\beta}$ reads

$$
\widetilde{O}^{\alpha\beta} = (D_x^A)_{\alpha\alpha} O^{\alpha\beta} (D_y^B)_{\beta\beta}.
\tag{1.115}
$$

Finally, W_O^{xy} has the following structure

$$
W_O^{xy} = \sum_{\alpha,\beta} w^{\alpha\beta} G_\alpha^A \otimes G_\beta^B
\tag{1.116}
$$

with

$$
w^{00} = \sqrt{(d_A - 1 + x^2)(d_B - 1 + y^2)} + xy O^{00},
$$

and

(a) Positivity of *XY-maps* (endomorphic case).

(b) Positivity of *CCNR-maps*
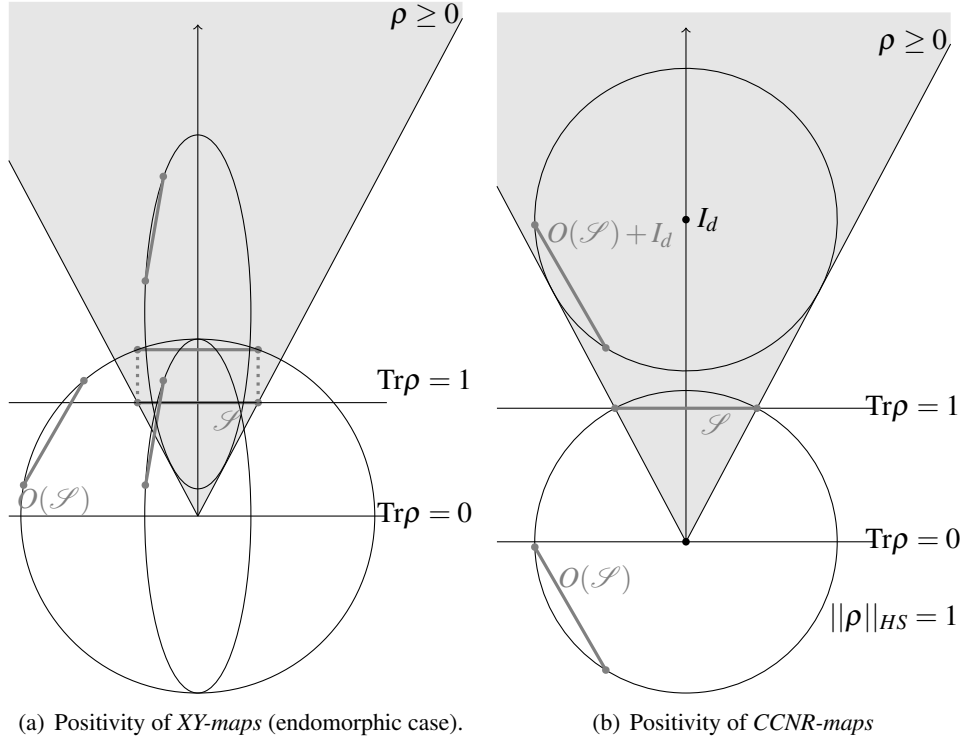
Figure 1.4: (Endomorphic case). The set of states $\mathscr{S}$ is the intersection of the cone of positive operators and the hypersurface $\text{Tr}\rho = 1$. In (1.4(a)) the first action on the states comes from $D^A_{x_{00}} = x$ as a shift towards up (or down) for $x > 1$ ($1 > x > 0$). Then it rotate by an orthogonal matrix O which does not preserve positivity, but then $D^B_{y_{00}} = y$ stretch the sphere in an ellipsoid and adding a minimal amount (optimality) of $\mathbf{1}_d$, the whole ellipsoid $||\rho||_{HS} = 1$ become a subset of the cone, hence all states restoring the positive preserving behavior of the map. In (1.4(b)) a rotation by an arbitrary orthogonal matrix O does not preserve positivity, but after adding $\mathbf{1}_d$, the whole ball $||\rho||_{HS} = 1$ become a subset of the cone, hence all states are mapped to positive operators.

$$w^{0\beta} = \frac{x}{\sqrt{d_A}} O^{0\beta} \quad , \quad w^{\alpha 0} = \frac{y}{\sqrt{d_B}} O^{\alpha 0} \quad , \quad w^{\alpha\beta} = O^{\alpha\beta}$$

for $\alpha, \beta > 0$. This way one obtains a big class of witnesses parameterized by $d_A^2 \times d_B^2$ isometry O and two nonnegative parameters x, y. If we consider W_O^{xy} the *Choi-Jamiołkowski's state* via isomorphism we have

$$\Phi_O(\rho) = d_A \mathscr{N}_A(x) \mathscr{N}(y) \text{id}_B + d_A \sum_{\alpha,\beta} O^{\alpha\beta} D^A_{x_{\alpha\alpha}} D^B_{y_{\beta\beta}} \left(\text{Tr}_A \rho^T G_\alpha^A \right) G_\beta^B. \tag{1.117}$$

In Fig. 1.4 we present a pictorial representation of the action of *XY-maps* and the well-known realignment criterion in an endomorphic case.

Interestingly in Ref.[52] we show an example of PPT state which is not detected by filtered CMC but is detected by our *XY-criteiron*. Apart of the PPT criterion, in the hierarchy of separability criteria based on correlator tensor one of the strongest criterion comes from a generalization of CCNR, known as *enhanced realignment criterion*. We compare it with our XY–criterion via the powerful tool of the EW. Follows

> **Theorem 1.6.2** The enhanced (nonlinear) realignment criterion is equivalent to the family of linear XY–criteria based on correlation tensor.

An appropriate limiting procedure on the EW releted to XY–criteria is proposed which leads to a novel class of witnesses. These witnesses are as powerful as the enhanced realignment criterion.

1.7 Enhanced realignment criterion vs. linear entanglement witnesses

Interestingly, CCNR criterion 1.5.5 was further generalized in [31] as follows

> **Theorem 1.7.1** if ρ is separable, then
>
> $$\|\mathscr{R}(\rho - \rho_A \otimes \rho_B)\|_1 \leq \sqrt{1 - \mathrm{Tr}\rho_A^2}\sqrt{1 - \mathrm{Tr}\rho_B^2}, \qquad (1.118)$$
>
> where $\rho_A = \mathrm{Tr}_B\rho$ and $\rho_B = \mathrm{Tr}_A\rho$ are local states in A and B subsystems, respectively. This is called Enhanced realignment criterion.

Enhanced realignment criterion (1.118) turns out to be the strongest effectively computable simplification of Correlation Matrix Criterion[32, 54] (see also [33] for the unifying approach). It was further analyzed in [55, 56].

Interestingly, the enhanced criterion (1.118) is equivalent to the following family of nonlinear (quadratic) witnesses [57]

$$\begin{aligned}
W(\rho) =& \mathrm{Tr}\left(\left(\mathbf{1}_{d_A} \otimes \mathbf{1}_{d_B} - \sum_{\mu=0}^{d^2-1} G_\mu^A \otimes G_\mu^B\right)\rho\right), \\
& - \frac{1}{2}\left(\mathrm{Tr}\left(\left(\sum_{\alpha=0}^{d_A^2-1} G_\alpha^A \otimes \mathbf{1}_{d_B} + \sum_{\beta=0}^{d_B^2-1} \mathbf{1}_{d_A} \otimes G_\beta^B\right)\rho\right)\right)^2
\end{aligned} \qquad (1.119)$$

with G_α^A and G_β^B being local orthonormal basis for A and B systems, respectively, and as usual $d = \min\{d_A, d_B\}$. The expectation value minimal among this family for a state ρ reads [58]

$$\mathscr{F}(\rho) = 1 - \|T\|_1 - \frac{1}{2}(\mathrm{Tr}\rho_A^2 + \mathrm{Tr}\rho_B^2), \qquad (1.120)$$

where $\|T\|_1$ stands for the trace norm of $d_A^2 \times d_B^2$ matrix

$$T_{\alpha\beta} = \mathrm{Tr}([\rho - \rho_A \otimes \rho_B]G_\alpha^A \otimes G_\beta^B). \qquad (1.121)$$

Now we want to proof the theorem 1.6.2. Let us start from the first implication

> **Theorem 1.7.2** enhanced CCNR (1.118) is equivalent to the whole family of criteria (1.109).

Proof. ($\longmapsto$) *A state ρ satisfying the enhanced CCNR criterion (1.118) satisfies (1.109) for all values of parameters $x, y \geq 0$.*

Let us note that the correlation matrix C for a product state is of rank one:

$$C(\rho_A \otimes \rho_B) = \begin{bmatrix} \frac{1}{\sqrt{d_A}} \\ \mathbf{r}_A \end{bmatrix} \begin{bmatrix} \frac{1}{\sqrt{d_B}} & | & \mathbf{r}_B^T \end{bmatrix}, \qquad (1.122)$$

being a product of one-particle correlation matrices. In (1.122) $\mathbf{r}_A$ and $\mathbf{r}_B$ are Bloch vectors corresponding to ρ_A and ρ_B, respectively, that is,

$$\rho_A = \frac{1}{d_A}\mathbf{1}_{d_A} + \sum_{\alpha>0} (\mathbf{r}_A)_\alpha G_\alpha^A,$$

and similarly for $\mathbf{r}_B$. One has

$$C(\rho) = \left[\begin{array}{c|c} \frac{1}{\sqrt{d_A d_B}} & \frac{1}{\sqrt{d_A}}\mathbf{r}_B^T \\ \hline \frac{1}{\sqrt{d_B}}\mathbf{r}_A & \mathbf{C} \end{array} \right] = \left[\begin{array}{c} \frac{1}{\sqrt{d_A}} \\ \mathbf{r}_A \end{array} \right] \left[\begin{array}{c|c} \frac{1}{\sqrt{d_B}} & \mathbf{r}_B^T \end{array} \right] + C(\rho - \rho_A \otimes \rho_B), \tag{1.123}$$

and hence

$$D_x^A C(\rho) D_y^B = \left[\begin{array}{c} \frac{x}{\sqrt{d_A}} \\ \mathbf{r}_A \end{array} \right] \left[\begin{array}{c|c} \frac{y}{\sqrt{d_B}} & \mathbf{r}_B^T \end{array} \right] + C(\rho - \rho_A \otimes \rho_B). \tag{1.124}$$

Let us observe that

$$\mathrm{Tr}\rho_A^2 = \frac{1}{d_A} + |\mathbf{r}_A|^2, \quad \mathrm{Tr}\rho_B^2 = \frac{1}{d_B} + |\mathbf{r}_B|^2. \tag{1.125}$$

Assume now, that the enhanced realignment criterion (1.118) is satisfied for a state ρ. Due to triangle inequality for the trace norm and the decomposition (1.124) one has:

$$\|D_x^A C(\rho) D_y^B\|_1 \leq \sqrt{\frac{x^2}{d_A} + |\mathbf{r}_A|^2}\sqrt{\frac{y^2}{d_B} + |\mathbf{r}_B|^2} + \|C(\rho - \rho_A \otimes \rho_B)\|_1 \tag{1.126}$$

$$\leq \sqrt{\frac{x^2}{d_A} + |\mathbf{r}_A|^2}\sqrt{\frac{y^2}{d_B} + |\mathbf{r}_B|^2} + \sqrt{1 - \frac{1}{d_A} - |\mathbf{r}_A|^2}\sqrt{1 - \frac{1}{d_B} - |\mathbf{r}_B|^2}.$$

Finally, using the following property

$$\sqrt{a}\sqrt{b} + \sqrt{c}\sqrt{d} \leq \sqrt{a+c}\sqrt{b+d}$$

which holds for any non-negative a, b, c, d, one gets

$$\|D_x^A C(\rho) D_y^B\|_1 \leq \mathcal{N}_A(x)\mathcal{N}_B(y). \tag{1.127}$$

$$\blacksquare$$

Now, we prove the converse, i.e. the violation of the necessary condition for the separability. The witness (1.114) can be rewritten as

$$W = a(x,y)G_0^A \otimes G_0^B + xG_0^A \otimes \sum_{\beta>0} O^{0\beta}G_\beta^B + y\sum_{\alpha>0} O^{\alpha 0}G_\alpha^A \otimes G_0^B + \sum_{\alpha,\beta>0} O^{\alpha\beta}G_\alpha^A \otimes G_\beta^B \tag{1.128}$$

where

$$a(x,y) = \sqrt{d_A - 1 + x^2}\sqrt{d_B - 1 + y^2} + xy\, O^{00}. \tag{1.129}$$

In the following we want to find the limit for $x, y \to \infty$. We introduce the polar coordinates

$$x = r\cos\theta, \qquad y = r\sin\theta \tag{1.130}$$

with $\theta \in [0, \pi/2]$, and assume that $O^{\alpha\beta}$ does not depend on (x, y) the limit $r \to \infty$ exists iff $O^{00} = -1$, and $O^{\alpha 0} = O^{0\beta} = 0$ for $\alpha, \beta > 0$, that is, $O^{\alpha\beta}$ has the following structure

$$O = \left[\begin{array}{c|c} -1 & \mathbf{0}^T \\ \hline \mathbf{0} & \mathbf{O} \end{array} \right], \tag{1.131}$$

where $\mathbf{O}$ is a $(d_A^2 - 1) \times (d_B^2 - 1)$ real isometry matrix, as in 1.68. It gives rise to the following limiting formula

$$W^\infty = a(\theta) G_0^A \otimes G_0^B + \sum_{\alpha, \beta > 0} O^{\alpha\beta} G_\alpha^A \otimes G_\beta^B \tag{1.132}$$

with

$$a(\theta) = \frac{1}{2} \left((d_B - 1) \cot\theta + (d_A - 1) \tan\theta \right). \tag{1.133}$$

Finally, minimizing $a(\theta)$ w.r.t. θ one finds

$$a_{\min} = \sqrt{(d_A - 1)(d_B - 1)}, \tag{1.134}$$

which reproduces EW corresponding to de Vicente criterion [41]. But, to get more refined limit let us assume that $O^{\alpha\beta}$ can depend on (x, y). The only way to guarantee the existence of the limit $r \to \infty$ is to assume the following asymptotics for the matrix elements of an isometry $O^{\alpha\beta}$

$$O^{00} = -\sqrt{1 - \frac{\eta^2}{r^2}} + O(r^{-2}) \tag{1.135}$$

together with

$$O^{0\beta} = \frac{\eta}{r} v^\beta + O(r^{-2}), \qquad O^{\alpha 0} = \frac{\eta}{r} u^\alpha + O(r^{-2}), \tag{1.136}$$

for $\alpha, \beta > 0$, where $\mathbf{u} \in \mathbb{R}^{d_A^2 - 1}$ and $\mathbf{v} \in \mathbb{R}^{d_B^2 - 1}$. One finds in the limit $r \to \infty$

$$W^\infty = b(\theta, \eta) G_0^A \otimes G_0^B + \sum_{\alpha, \beta > 0} O^{\alpha\beta} G_\alpha^A \otimes G_\beta^B$$
$$+ \eta \left(\cos\theta G_0^A \otimes \sum_{\beta > 0} v^\beta G_\beta^B + \sin\theta \sum_{\alpha > 0} u^\alpha G_\alpha^A \otimes G_0^B \right), \tag{1.137}$$

with

$$b(\theta, \eta) = \frac{1}{2} \left((d_B - 1) \cot\theta + (d_A - 1) \tan\theta + \eta^2 \sin\theta \cos\theta \right). \tag{1.138}$$

The isometry $O^{\alpha\beta}$ has the following asymptotic structure (up to leading powers of $1/r$)

$$O^{\alpha\beta}(r) = \left[\begin{array}{c|c} -\sqrt{1 - \frac{\eta^2}{r^2}} & \frac{\eta}{r} \mathbf{v}^T \\ \hline \frac{\eta}{r} \mathbf{u} & \sqrt{1 - \frac{\eta^2}{r^2}} \mathbf{O} \end{array} \right], \tag{1.139}$$

where $\mathbf{O}$ is a $(d_A^2 - 1) \times (d_B^2 - 1)$ real matrix and $\eta > 0$.

Formula (1.114) may be rewritten as follows One proof the lemma in the limit $r \to \infty$ .Now, the isometry condition for $O^{\alpha\beta}$ imply that $\mathbf{O}\mathbf{O}^T$ and $\mathbf{O}^T\mathbf{O}$ are $\min\{d_A^2, d_B^2\}$–dimensional projectors and hence $|\mathbf{u}| = |\mathbf{v}| = 1$, together with the following constraint for $\mathbf{u}$ and $\mathbf{v}$

$$\mathbf{u} = \mathbf{O}\mathbf{v}. \tag{1.140}$$

Summarizing, the asymptotic witness W^∞ is characterized by an isometry $\mathbf{O}$, two normalized vectors satisfying (1.140), an angle $\theta \in [0, \pi/2]$, and an arbitrary real parameter $\eta \geq 0$. Actually, one can assume that $\eta \geq 0$ since η always multiplies $\mathbf{u}$ and $\mathbf{v}$. Note, that in the limit $\eta \to 0$ one recovers again a witness corresponding to de Vicente criterion [41].

(R) Note, that if one replaces an isometry $O^{\alpha\beta}$ by an arbitrary real matrix $M^{\alpha\beta}$ such that $\|M\| \leq 1$, then one can essentially repeat all the steps of the proof and finds

$$W^\infty = b(\theta, \eta)G_0^A \otimes G_0^B + \sum_{\alpha, \beta > 0} \mathbf{M}^{\alpha\beta} G_\alpha^A \otimes G_\beta^B + \cos\theta G_0^A \otimes \sum_{\beta > 0} v^\beta G_\beta^B + \sin\theta \sum_{\alpha > 0} u^\alpha G_\alpha^A \otimes G_0^B,$$
(1.141)

where $\mathbf{u} = \mathbf{M}\mathbf{v}$, and $\mathbf{M}^{\alpha\beta} := M^{\alpha\beta}$ for $\alpha, \beta > 0$. Note, that $\mathbf{u}$ and $\mathbf{v}$ are no longer normalized.

Theorem 1.7.3 ($\Longleftarrow$)*An entangled state detected by the enhanced CCNR criterion (1.118) is also detected by the criterion (1.109) for some values of parameters (x, y).*

Proof. Let us consider an arbitrary state ρ in $\mathbb{C}^{d_A} \otimes \mathbb{C}^{d_B}$

$$\rho = \frac{1}{d_A d_B}\mathbf{1}_{d_A} \otimes \mathbf{1}_{d_B} + \widetilde{\rho},$$
(1.142)

where the traceless part $\widetilde{\rho}$ reads

$$\widetilde{\rho} = \frac{1}{d_A}\mathbf{1}_{d_A} \otimes \widetilde{\rho}_B + \widetilde{\rho}_A \otimes \frac{1}{d_B}\mathbf{1}_{d_B} + \sum_{\alpha, \beta > 0} C_{\alpha\beta} G_\alpha^A \otimes G_\beta^B$$
(1.143)

with

$$\widetilde{\rho}_A = \sum_{\alpha > 0} (\mathbf{r}_A)_\alpha G_\alpha^A, \qquad \widetilde{\rho}_B = \sum_{\beta > 0} (\mathbf{r}_B)_\beta G_\beta^B.$$
(1.144)

Defining $\mathbf{C}_{\alpha\beta} = C_{\alpha\beta}$ for $\alpha, \beta > 0$ one finds

$$\text{Tr}(W^\infty \rho) = \frac{b(\theta, \eta)}{\sqrt{d_A d_B}} + \langle \mathbf{O}|\mathbf{C}\rangle + \eta \left(\frac{\cos\theta}{\sqrt{d_A}}\langle \mathbf{r}_B|\mathbf{v}\rangle + \frac{\sin\theta}{\sqrt{d_B}}\langle \mathbf{r}_A|\mathbf{u}\rangle \right)$$

$$= \frac{b(\theta, \eta)}{\sqrt{d_A d_B}} + \langle \mathbf{O}|\mathbf{C}\rangle + \eta \langle \frac{\cos\theta}{\sqrt{d_A}}\mathbf{r}_B + \frac{\sin\theta}{\sqrt{d_B}}\mathbf{O}^T\mathbf{r}_A|\mathbf{v}\rangle.$$
(1.145)

■

Lemma 1.7.4 For a given bipartite state ρ there exists $\mathbf{u}$, $\mathbf{v}$, η, and isometry $\mathbf{O}$ such that the corresponding witness W^∞ satisfies

$$\text{Tr}(W^\infty \rho) = \sqrt{(1 - \text{Tr}\rho_A^2)(1 - \text{Tr}\rho_B^2)} - \|\mathcal{R}(\rho - \rho_A \otimes \rho_B)\|_1,$$
(1.146)

and this is the minimal value of $\text{Tr}(W^\infty \rho)$ for a given state ρ.

Proof. observe that to minimize $\text{Tr}(W^\infty \rho)$ the unit vector $\mathbf{v}$ has to be antiparallel to $\frac{\eta \cos\theta}{\sqrt{d_A}}\mathbf{r}_B + \frac{\eta \sin\theta}{\sqrt{d_B}}\mathbf{O}^T\mathbf{r}_A$, where we used $\mathbf{u} = \mathbf{O}\mathbf{v}$. The third addend in (1.145) becomes then $-\eta \left| \frac{\cos\theta}{\sqrt{d_A}}\mathbf{r}_B + \frac{\sin\theta}{\sqrt{d_B}}\mathbf{O}^T\mathbf{r}_A \right|$. Let us perform now minimization w.r.t. parameter η. One easily finds

$$\eta_{\min} = \left| \frac{\cos\theta}{\sqrt{d_A}}\mathbf{r}_B + \frac{\sin\theta}{\sqrt{d_B}}\mathbf{O}^T\mathbf{r}_A \right| \frac{\sqrt{d_A d_B}}{\sin\theta\cos\theta},$$
(1.147)

and hence for these particular parameters the value of $\text{Tr}(W^\infty \rho)$ reads

$$
\begin{aligned}
\text{Tr}(W^\infty \rho) =& \frac{(d_B-1)\cot\theta + (d_A-1)\tan\theta}{2\sqrt{d_A d_B}} + \langle \boldsymbol{O}|\boldsymbol{C}\rangle - \left| \frac{\cos\theta}{\sqrt{d_A}}\mathbf{r}_B + \frac{\sin\theta}{\sqrt{d_B}}\mathbf{O}^T\mathbf{r}_A \right|^2 \frac{\sqrt{d_A d_B}}{2\sin\theta\cos\theta} \\
=& \frac{(d_B-1)\cot\theta + (d_A-1)\tan\theta}{2\sqrt{d_A d_B}} - \sqrt{d_A d_B}\left(\frac{\cot\theta}{2d_A}|\mathbf{r}_B|^2 + \frac{\tan\theta}{2d_B}|\mathbf{r}_A|^2 \right) \\
& + \langle \boldsymbol{O}|\boldsymbol{C}\rangle + \langle \mathbf{r}_B|\mathbf{O}^T\mathbf{r}_A\rangle \\
=& \frac{1}{2\sqrt{d_A d_B}}\left(\cot\theta\left(d_B - 1 - d_B|\mathbf{r}_B|^2\right) + \tan\theta\left(d_A - 1 - d_A|\mathbf{r}_A|^2\right)\right) + \langle \boldsymbol{O}|\boldsymbol{C} - \mathbf{r}_A\mathbf{r}_B^T\rangle.
\end{aligned}
$$

Finally, using the following identities from Eq. (1.125)

$$
1 - \text{Tr}\rho_A^2 = \frac{1}{d_A}\left(d_A - 1 - d_A|\mathbf{r}_A|^2\right), \qquad 1 - \text{Tr}\rho_B^2 = \frac{1}{d_B}\left(d_B - 1 - d_B|\mathbf{r}_B|^2\right),
$$

one finds

$$
\text{Tr}(W^\infty \rho) = \frac{d_B(1 - \text{Tr}\rho_B^2)\cot\theta + d_A(1 - \text{Tr}\rho_A^2)\tan\theta}{2\sqrt{d_A d_B}} + \langle \boldsymbol{O}|\boldsymbol{T}\rangle, \tag{1.148}
$$

where $\mathbf{T}_{\alpha\beta} = T_{\alpha\beta}$ (from Eq. (1.121)) for $\alpha, \beta > 0$, that is,

$$
\mathbf{T}_{\alpha\beta} = \mathbf{C}_{\alpha\beta} - (\mathbf{r}_A)_\alpha (\mathbf{r}_B)_\beta.
$$

The last step is the minimization w.r.t. θ and the isometry $\mathbf{O}$. One finds for the optimal θ

$$
\tan\theta_{\min} = \sqrt{\frac{d_B(1 - \text{Tr}\rho_B^2)}{d_A(1 - \text{Tr}\rho_A^2)}} \tag{1.149}
$$

and

$$
\min_{\mathbf{O}}\langle \mathbf{O}|\mathbf{T}\rangle = -\max_{\mathbf{O}}\langle \mathbf{O}|\mathbf{T}\rangle = -\|\mathbf{T}\|_1, \tag{1.150}
$$

and hence noting that $\langle \mathbf{O}|\mathbf{T}\rangle = \langle O|T\rangle$ one finally arrives at (1.146). Clearly, if ρ is detected by the enhanced CCNR criterion, then due to the theorem one can find a witness W^∞ detecting ρ as well. While the witness W^∞ is realised as a limit of witnesses W (1.128), there exist witnesses W detecting the state for large enough x and y, which ends the proof. ∎

Interestingly, our analysis enables one to construct a witness for an entangled state detected by (1.118). Indeed, observe that $T_{00} = T_{0\beta} = T_{\alpha 0} = 0$ and hence the entire information of T is encoded into $\mathbf{T}$. Now, consider a singular value decomposition

$$
\mathbf{T} = \mathbf{O}_1\mathbf{D}\mathbf{O}_2^T,
$$

with $\mathbf{O}_1$ and $\mathbf{O}_2$ orthogonal matrices and let $\mathbf{O} := \mathbf{O}_1\mathbf{O}_2^T$. The corresponding angle θ is defined in (1.149) and the parameter η is defined in (1.147). Finally, a unit vector $\mathbf{v}$ reads

$$
\mathbf{v} = -\frac{\frac{\cos\theta}{\sqrt{d_A}}\mathbf{r}_B + \frac{\sin\theta}{\sqrt{d_B}}\mathbf{O}^T\mathbf{r}_A}{\left|\frac{\cos\theta}{\sqrt{d_A}}\mathbf{r}_B + \frac{\sin\theta}{\sqrt{d_B}}\mathbf{O}^T\mathbf{r}_A\right|}, \tag{1.151}
$$

and it is fully determined by $\mathbf{r}_A, \mathbf{r}_B$, the isometry $\mathbf{O}$, and the angle θ. In the following section we provide a graphical representation of such equivalence for a particular family of isotropic quantum states.

1.8 Powerful detection of XY- criterion

In this following we illustrate the detection power of the aforementioned criteria: CCNR criteiron, Di Vincente's criterion, the criterion in [51] and ESIC, on several well known examples of quantum states. In particular, in the next section is discussed the detection power of above criteria for the family of isotropic states.

This new criterion, *XY-criterion,* in general is not stronger that CMC, but we provide the following example of PPT state which is not detected by filtered CMC [32, 33] (LFCMC) but is detected by the *XY-criterion*.
In [28], Rudolph constructed an example of two qubit state which is entangled (and hence NPT) but it is not detected by CCNR criterion. It turns out that such state is always detected by our criterion for sufficiently big x and y. However, contrary to CMC it does not detect all NTP qubit-qubit states.

Proof. Consider a qubit-qubit density operator

$$\rho = \frac{1}{2}\begin{pmatrix} 1+r & 0 & 0 & t \\ 0 & 0 & 0 & 0 \\ 0 & 0 & s-r & 0 \\ t & 0 & 0 & 1-s \end{pmatrix}, \tag{1.152}$$

where the real parameter $\{r,s,t\}$ are taken such that $\rho \geq 0$. This state is NPT (entangled) iff $|t| > 0$. One finds for the correlation matrix

$$C^{\text{can}} = \frac{1}{2}\begin{pmatrix} 1 & 0 & 0 & r \\ 0 & t & 0 & 0 \\ 0 & 0 & -t & 0 \\ s & 0 & 0 & 1+r-s \end{pmatrix}, \tag{1.153}$$

and hence $\|C^{\text{can}}\|_{\text{tr}} = |t| + \sqrt{g_+(r,s)} + \sqrt{g_-(r,s)}$ [28], with

$$g_\pm(r,s) = \frac{1}{4}\left(r^2 - rs + r + s^2 - s + 1 \pm \sqrt{(r^2+s^2)(r^2 - 2(r+1)s + 2r + s^2 + 2)}\right) \tag{1.154}$$

For $t = 0, s = \frac{1}{2} = -r$, $\|C^{\text{can}}\|_{\text{tr}}$ reaches the global minimum equal to $1/\sqrt{2}$ and in general $\|C^{\text{can}}\|_{\text{tr}} \leq 1$ even if $|t| > 0$. Now, using our criterion one finds

$$D_x^A C^{\text{can}} D_y^B = \frac{1}{2}\begin{pmatrix} xy & 0 & 0 & xr \\ 0 & t & 0 & 0 \\ 0 & 0 & -t & 0 \\ ys & 0 & 0 & 1+r-s \end{pmatrix}, \tag{1.155}$$

and hence for a separable (PPT) state

$$\|D_x^A C^{\text{can}} D_y^B\|_{\text{tr}} = |t| + f(x,y;r,s),$$

$$f(x,y,r,s) = \sqrt{\lambda_+(x,y;r,s)} + \sqrt{\lambda_-(x,y;r,s)},$$

$$(1+r-s)^2 = (1+r^2+s^2+2r-2s-2rs) \tag{1.156}$$

$$\lambda_\pm(x,y;r,s) = \frac{1}{8}\Bigg((1+r-s)^2 + r^2x^2 + s^2y^2 + x^2y^2$$

$$-\sqrt{((1+r-s)^2 + r^2x^2 + s^2y^2 + x^2y^2)^2 - 4(r+1)^2(s-1)^2 x^2y^2}\Bigg). \tag{1.157}$$

and $\lambda_{\pm}(1,1;r,s) = g_{\pm}(r,s)$. Note, that in the limit $x,y \to \infty$

$$\lambda_+(x,y;r,s) \to \frac{x^2 y^2}{4}, \quad \lambda_-(x,y;r,s) \to 0, \quad f(x,y;r,s) \to \frac{xy}{2},$$

and hence for PPT (separable) state our criterion requires

$$|t| + f(x,y;r,s) \le \sqrt{\frac{1+x^2}{2}} \sqrt{\frac{1+y^2}{2}},$$

gives in the limit $x,y \to \infty$ the condition $|t| \le 0$ which recovers PPT condition for (1.152). ∎

As second example, let us consider two one-parameter families of two-qutrit states constructed from unextendable product basis (UPB) [59, 60]. The first family contains states of the form $\rho_p^{PP} = p\rho^{PP} + (1-p)\mathbf{1}_3 \otimes \mathbf{1}_3/9$, where ρ^{PP} is a bound entangled state constructed by use of the Pentagon Pyramid (PP) construction. The second family contains states of the form $\rho_p^{Ti} = p\rho^{Ti} + (1-p)\mathbf{1}_3 \otimes \mathbf{1}_3/9$, where ρ^{Ti} is a bound entangled state constructed by use of the Tiles (Ti) construction. We compare detection thresholds in this families w.r. to dV, CCNR, ESIC, and LFCMC criterion:

	dV	CCNR	ESIC	LFCMC
PP	.9371	.8785	.8739	.8639
Ti	.9493	.8897	.8845	.8722

whereas our criterion detects entanglement in the PP family for $p \ge 0.8721$ ($x = y = 4059.7$) and in Ti family for $p \ge 0.8822$ ($x = y = 2442.1$). Our criterion detects more than linear criteria (dV, CCNR and ESIC) but less than non-linear LFCMC.

Now, we provide an example of a qutrit-qutrit state which is detected neither by CCNR nor by ESIC but it is detected by (1.109). Consider a chessboard state [61] defined in terms of four orthogonal vectors in $\mathbb{C}^3 \otimes \mathbb{C}^3$:

$$|V_1\rangle = |m,0,s;0,n,0;0,0,0\rangle$$
$$|V_2\rangle = |0,a,0;b,0,c;0,0,0\rangle$$
$$|V_3\rangle = |n^*,0,0;0,-m^*,0;t,0,0\rangle$$
$$|V_4\rangle = |0,-b^*,0;a^*,0,0;0,d,0\rangle$$

giving rise to $\rho = \mathcal{N} \sum_i |V_i\rangle\langle V_i|$, with $\mathcal{N}$ being a normalization factor. Let us consider the mixture with white noise $\rho_p = p\rho + (1-p)\mathbf{1}_3 \otimes \mathbf{1}_3/9$. It is shown in the following that by taking a suitable parameters, we may construct a PPT state ρ_p that is detected neither by CCNR nor by ESIC, nor by filter CMC [43] but it is detected by (1.109) for $(x,y) = (5.5,5.9)$ (cf. the Figure 1.3).

Proof. Taking the following parameters [61]

$$a = 0.3346 \qquad\qquad b = -0.1090 \qquad\qquad c = -0.6456$$
$$d = 0.8560 \qquad\qquad m = 0.4690 \qquad\qquad n = -0.3161$$
$$s = -1.0178 \qquad\qquad t = -0.6085 \qquad\qquad p = 0.8062$$

one obtains the following PPT density matrix (whose entanglement is not detected by realignment,

CMC criterion and ESIC criterion), ρ_p is

$$
\begin{bmatrix}
0.0964 & 0 & -0.1118 & 0 & 0 & 0 & 0.0450 & 0 & 0 \\
0 & 0.0505 & 0 & 0 & 0 & -0.0506 & 0 & -0.0218 & 0 \\
-0.1118 & 0 & 0.2641 & 0 & 0.0753 & 0 & 0 & 0 & 0 \\
0 & 0 & 0 & 0.0505 & 0 & 0.0165 & 0 & -0.0671 & 0 \\
0 & 0 & 0.0753 & 0 & 0.0964 & 0 & 0.0668 & 0 & 0 \\
0 & -0.0506 & 0 & 0.0165 & 0 & 0.1191 & 0 & 0 & 0 \\
0.0450 & 0 & 0 & 0 & 0.0668 & 0 & 0.1082 & 0 & 0 \\
0 & -0.0218 & 0 & -0.0671 & 0 & 0 & 0 & 0.1931 & 0 \\
0 & 0 & 0 & 0 & 0 & 0 & 0 & 0 & 0.0215
\end{bmatrix}.
$$

$$\tag{1.158}$$

We calculate the quantity:

$$
\sqrt{\frac{2+x^2}{3}}\sqrt{\frac{2+y^2}{3}} - \|D_x^A C^{\mathrm{can}} D_y^B\|_{\mathrm{tr}}
\tag{1.159}
$$

for $(x,y) = (5.8, 5.9)$. It should be nonegative for separable states. We get $\approx -5.45 \times 10^{-5}$ and hence we detect entanglement in the state. On the other hand performing a local filtering of ρ_p:

$$
\rho_{\mathrm{LF}} = \frac{A \otimes B\rho_p A^\dagger \otimes B^\dagger}{\mathrm{Tr}(A \otimes B\rho_p A^\dagger \otimes B^\dagger)}
\tag{1.160}
$$

with operators:

$$
A = \begin{bmatrix}
1.2970 & 0 & -0.0770 \\
0 & 1.4374 & 0 \\
-0.0892 & 0. & 1.2698
\end{bmatrix}, \quad
B = \begin{bmatrix}
0.9171 & 0 & 0.1126 \\
0 & 0.7412 & 0 \\
0.1126 & 0 & 0.6961
\end{bmatrix}
\tag{1.161}
$$

one obtains a state ρ_{LF} with maximally mixed partial traces, $\rho_{\mathrm{LF}}$is

$$
\begin{bmatrix}
0.0962 & 0 & -0.0717 & 0 & 0.0067 & 0 & 0.0466 & 0 & 0.0113 \\
0 & 0.0497 & 0 & -0.0028 & 0 & -0.0480 & 0 & -0.0334 & 0 \\
-0.0717 & 0 & 0.1878 & 0 & 0.0718 & 0 & 0.0113 & 0 & -0.0131 \\
0 & -0.0028 & 0 & 0.0980 & 0 & 0.0522 & 0 & -0.0827 & 0 \\
0.0067 & 0 & 0.0718 & 0 & 0.1095 & 0 & 0.0821 & 0 & 0.0052 \\
0 & -0.0480 & 0 & 0.0522 & 0 & 0.1259 & 0 & -0.0069 & 0 \\
0.0466 & 0 & 0.0113 & 0 & 0.0821 & 0 & 0.1391 & 0 & 0.0194 \\
0 & -0.0334 & 0 & -0.0827 & 0 & -0.0069 & 0 & 0.1740 & 0 \\
0.0113 & 0 & -0.0131 & 0 & 0.0052 & 0 & 0.0194 & 0 & 0.0198
\end{bmatrix}.
$$

$$\tag{1.162}$$

Calculating quantity:

$$
\sqrt{\frac{2}{3}}\sqrt{\frac{2}{3}} - \|D_0^A C^{\mathrm{can}} D_0^B\|_{\mathrm{tr}}
\tag{1.163}
$$

one gets $\approx 5.41 \times 10^{-3}$, hence the state is not detected by the Covariance Matrix Criterion after local filtering making its partial traces maximally mixed.   ∎

1.9 Entanglement detection for bipartite isotropic states

The purpose of this section is to analyze this criterion for isotropic states with unequal dimensions of the subsystems

$$\rho_p = \frac{1-p}{d_1 d_2} \sum_{i=0}^{d_1-1} \sum_{j=0}^{d_2-1} |e_i\rangle\langle e_i| \otimes |f_j\rangle\langle f_j| + \frac{p}{d_1} \sum_{i,j=0}^{d_1-1} |e_i\rangle\langle e_j| \otimes |f_i\rangle\langle f_j|, \tag{1.164}$$

such that $\{|e_i\rangle\}_{i=0}^{d_1-1}$ and $\{|f_i\rangle\}_{i=0}^{d_2-1}$ are standard basis respectively for the Hilbert spaces $\mathbb{C}^{d_1}$ and $\mathbb{C}^{d_2}$ (we will assume $d_1 \leq d_2$). Let us perform the realignment operation on ρ_p, i.e. $|e_i\rangle\langle e_j| \otimes |f_k\rangle\langle f_l| \mapsto |e_i \otimes e_j\rangle\langle f_k \otimes f_l|$. In other words, introducing a vectorization of an operator as in Eq. 1.63. The resulting matrix $\mathscr{R}(\rho_p)$ is the correlation tensor $C(\rho_p)$ for a choice of bases: $\{|e_i\rangle\langle e_j|\}_{i,j=0}^{d_1-1} \subset \mathscr{B}(\mathbb{C}^{d_1})$ and $\{|f_i\rangle\langle f_j|\}_{i,j=0}^{d_2-1} \subset \mathscr{B}(\mathbb{C}^{d_2})$. These bases are orthonormal, but not hermitian, hence the matrix C can have complex entries, but its singular values and trace norm are the same as the case we choose hermitian orthonormal bases. Then

$$\begin{aligned}
C = \mathscr{R}(\rho_p) &= (1-p)\frac{1}{d_1 d_2} \sum_{i=0}^{d_1-1} \sum_{j=0}^{d_2-1} |e_{ii}\rangle\langle f_{jj}| + p\frac{1}{d_1} \sum_{i,j=0}^{d_1-1} |e_{ij}\rangle\langle f_{ij}| \\
&= (1-p)\left|\frac{\mathbf{1}_{d_1}}{d_1}\right\rangle\left\langle\frac{\mathbf{1}_{d_2}}{d_2}\right| + \frac{p}{d_1}\mathbf{1}_{d_1^2}.
\end{aligned} \tag{1.165}$$

To recast $D_x^{(1)}, D_y^{(2)}$ in the not hermitian basis we sandwich the above matrix with $\left(\mathbf{1}_{d_1^2} + \frac{x-1}{d_1}|\mathbf{1}_{d_1}\rangle\langle\mathbf{1}_{d_1}|\right)$ and $\left(\mathbf{1}_{d_2^2} + \frac{y-1}{d_2}|\mathbf{1}_{d_2}\rangle\langle\mathbf{1}_{d_2}|\right)$. In other words, $D_x^{(1)}$ is obtained replacing the first entry 1 with x using the projector $|\mathbf{1}_{d_1}\rangle\langle\mathbf{1}_{d_1}|$. Analogously for $D_y^{(2)}$. Then matrix C_{xy} follows

$$\begin{aligned}
C_{xy} &= \left(\mathbf{1}_{d_1} \otimes \mathbf{1}_{d_1} + \frac{x-1}{d_1}|\mathbf{1}_{d_1}\rangle\langle\mathbf{1}_{d_1}|\right) \\
&\quad \times \left((1-p)\left|\frac{\mathbf{1}_{d_1}}{d_1}\right\rangle\left\langle\frac{\mathbf{1}_{d_2}}{d_2}\right| + \frac{p}{d_1}\sum_{i,j=1}^{d_1}|e_i \otimes e_j\rangle\langle f_i \otimes f_j|\right)\left(\mathbf{1}_{d_2} \otimes \mathbf{1}_{d_2} + \frac{y-1}{d_2}|\mathbf{1}_{d_2}\rangle\langle\mathbf{1}_{d_2}|\right) \\
&= \frac{(y-p)x}{d_1 d_2}|\mathbf{1}_{d_1}\rangle\langle\mathbf{1}_{d_2}| + \frac{p}{d_1}\sum_{i,j=1}^{d_1}|e_i \otimes e_j\rangle\langle f_i \otimes f_j| + p\frac{(x-1)}{d_1^2}\sum_{i,j=1}^{d_1}|e_i \otimes e_i\rangle\langle f_j \otimes f_j|.
\end{aligned} \tag{1.166}$$

In a more compact notion we can rewrite as

$$\begin{aligned}
C_{xy} &= \left(\mathbf{1}_{d_1^2} + \frac{x-1}{d_1}|\mathbf{1}_{d_1}\rangle\langle\mathbf{1}_{d_1}|\right)\left(\frac{1-p}{d_1 d_2}|\mathbf{1}_{d_1}\rangle\langle\mathbf{1}_{d_2}| + \frac{p}{d_1}\mathbf{1}_{d_1^2}\right)\left(\mathbf{1}_{d_2^2} + \frac{y-1}{d_2}|\mathbf{1}_{d_2}\rangle\langle\mathbf{1}_{d_2}|\right) \\
&= \frac{(y-p)x}{d_1 d_2}|\mathbf{1}_{d_1}\rangle\langle\mathbf{1}_{d_2}| + \frac{p}{d_1}\mathbf{1}_{d_1^2} + p\frac{(x-1)}{d_1^2}|\mathbf{1}_{d_1}\rangle\langle\mathbf{1}_{d_1}|.
\end{aligned}$$

To better clarify this point, we demote the matrix as vectors as in Eq.1.63(here we change notation, the vectorized matrix $|A\rangle\rangle \equiv |A\rangle$). More specifically, $|\mathbf{1}_{d_k}\rangle : \mathbb{C}^{d_k} \mapsto \mathbb{C}^{d_k}$ (acting on vectors $|\psi\rangle \in \mathbb{C}^{d_k}$) has the decomposition $\left(|\mathbf{1}_{d_k}\rangle = \sum_{i=1}^{d_k}|E_{ii}\rangle = \sum_{i=1}^{d_k}|i\rangle\langle i|\right)$ and $\mathbf{1}_{d_k^2} : \mathscr{B}(\mathbb{C}^{d_k})$ (acting on operators in $\mathscr{B}(\mathbb{C}^{d_k})$) has the decomposition $\mathbf{1}_{d_1^2} = \sum_{i,j=1}^{d_1}|E_{ij}\rangle\langle E_{ij}|$. We calculate $||C_{xy}||_{\text{Tr}}$ as the sum of square roots of eigenvalues of $C_{xy}C_{xy}^\dagger$, yielding

$$C_{xy}C_{xy}^\dagger = \left(\frac{x^2(y^2-p^2)}{d_1^2 d_2} + \frac{p^2(x^2-1)}{d_1^3}\right)|\mathbf{1}_{d_1}\rangle\langle\mathbf{1}_{d_1}| + \frac{p^2}{d_1^2}\mathbf{1}_{d_1^2}.$$

Now, since $|\mathbf{1}_{d_1}\rangle\langle\mathbf{1}_{d_1}|$ commutes with $\mathbf{1}_{d_1^2}$, they share the same set of eigenvectors, therefore the spectrum σ (expressed with the geometric multiplicity of the eigenvalues) is

$$\sigma\left(C_{xy}C_{xy}^\dagger\right) = \left(d_1^2 - 1\right) \times \left\{\frac{p^2}{d_1^2}\right\} \cup \left\{\frac{x^2}{d_1 d_2}\left(y^2 + p^2\frac{d_2 - d_1}{d_1}\right)\right\}. \tag{1.167}$$

Finally, we have that separability of an isotropic state with unequal dimension ρ_p implies

$$\|C_{xy}\|_{\mathrm{Tr}} = \frac{d_1^2 - 1}{d_1}p + \frac{x}{\sqrt{d_1 d_2}}\sqrt{y^2 + p^2\frac{d_2 - d_1}{d_1}} \leq \sqrt{\frac{d_1 - 1}{d_1} + \frac{x^2}{d_1}}\sqrt{\frac{d_2 - 1}{d_2} + \frac{y^2}{d_2}}. \tag{1.168}$$

We will denote by $p_{xy} \equiv p_{d_1,d_2}(x,y)$ (for a lighter notation) the value of p such that the equality holds. One can observe the inequality in (1.168) becomes linear for $x = 0$, $y = 0$ or $d_1 = d_2$. As special case of Eq. (1.168) for $x = y$ and $d_1 = d_2 = d$ the separability of ρ_p implies

$$p < \frac{1}{d+1}. \tag{1.169}$$

In the following, we are interested to unequal dimension of the subsystems. In particular, the analysis of all the aforementioned criteria rise up choosing $x, y = 0$, $x, y = 1$, $x = \sqrt{2/d_1}, y = \sqrt{2/d_2}$ and $x = \sqrt{d_1 + 1}, y = \sqrt{d_2 + 1}$ to get the criteria Di Vicente, realignment, Fei and ESIC. Therefore Eq.(1.168) for isotropic states respectively becomes

$$p\frac{d_1^2 - 1}{d_1} \leq \sqrt{\frac{d_1 - 1}{d_1}}\sqrt{\frac{d_2 - 1}{d_2}}, \tag{1.170}$$

$$\frac{d_1^2 - 1}{d_1}p + \frac{1}{\sqrt{d_1 d_2}}\sqrt{1 + p^2\left(\frac{d_2}{d_1} - 1\right)} \leq 1, \tag{1.171}$$

$$\frac{d_2\left(d_1^2 - 1\right)p + \sqrt{4 + 2p^2\left(\frac{d_2}{d_1} - 1\right)d_2}}{\sqrt{d_1^2 - d_1 + 2}\sqrt{d_2^2 - d_2 + 2}} \leq 1, \tag{1.172}$$

$$\frac{d_1^2 - 1}{d_1}p + \sqrt{\frac{d_1 + 1}{d_1 d_2}}\sqrt{d_2 + 1 + p^2\left(\frac{d_2}{d_1} - 1\right)} \leq 2. \tag{1.173}$$

We can rewrite the criterion on Eq. (1.168) in the following way to highlight the contribution that improve the entanglement detection. If the state ρ_p is separable, then

$$0 \geq \frac{d_1^2 - 1}{d_1}p + \frac{x}{\sqrt{d_1 d_2}}\sqrt{y^2 + p^2\frac{d_2 - d_1}{d_1}} - \mathcal{N}_{x,d_1}\mathcal{N}_{y,d_2} \tag{1.174}$$

$$0 \geq \frac{d_1^2 - 1}{d_1}p - \mathcal{N}_{x,d_1}\mathcal{N}_{y,d_2}. \tag{1.175}$$

Notice that Eq.(1.175) defines a weaker criterion than Eq.(1.174) because the second term is always positive. The threshold of Eq. (1.175) is

$$p_0 = \frac{d_1}{d_1^2 - 1}\mathcal{N}_{x,d_1}\mathcal{N}_{y,d_2}. \tag{1.176}$$

Then, if $p > p_0$ this inequality is enough to detect the entanglement of the state under consideration, namely, the right hand side of Eq.(1.175) is strictly positive ($p_0 > 0$) and criterion have already

detected the entanglement. Otherwise we can tight the inequality to have more chance to detect entanglement with the second term of Eq.1.174 and proceed with the calculation

$$-\frac{x}{\sqrt{d_1 d_2}}\sqrt{y^2 + p^2 \frac{d_2 - d_1}{d_1}} \geq \frac{d_1^2 - 1}{d_1}p - \mathcal{N}_{x,d_1}\mathcal{N}_{y,d_2}. \tag{1.177}$$

Under the assumption that we do not detect entanglement with the weaker condition (1.175), both the terms of the inequality are negative, hence we can square and inverse the inequality:

$$\mathcal{F}(p) = \left(\frac{d_1^2 - 1}{d_1}p - \mathcal{N}_{x,d_1}\mathcal{N}_{y,d_2}\right)^2 - \frac{x^2}{d_1 d_2}\left(y^2 + p^2 \frac{d_2 - d_1}{d_1}\right)$$
$$= a_{d_1,d_2}(x)\, p^2 + b_{d_1,d_2}(x,y)\, p + c_{d_1,d_2}(x,y) \geq 0, \tag{1.178}$$

where

$$a \equiv a_{d_1,d_2}(x) = \frac{\left(d_1^2 - 1\right)^2}{d_1^2} - x^2 \frac{d_2 - d_1}{d_1^2 d_2}, \tag{1.179}$$

$$b \equiv b_{d_1,d_2}(x,y) = -2\frac{d_1^2 - 1}{d_1}\mathcal{N}_{x,d_1}\mathcal{N}_{y,d_2}, \tag{1.180}$$

$$c \equiv c_{d_1,d_2}(x,y) = \left(\mathcal{N}_{x,d_1}\mathcal{N}_{y,d_2}\right)^2 - \frac{x^2 y^2}{d_1 d_2}. \tag{1.181}$$

A direct calculation shows always $\Delta = b^2 - 4ac \geq 0$. Let $p_{\pm} = \frac{-b \pm \sqrt{\Delta}}{2a}$ be the roots of $\mathcal{F}(p)$. Notice, that $\mathcal{F}(p_0) \leq 0$ (equality only for $x = 0$), $c \geq 0$, $b < 0$. Hence Vieta's formulas implies

1. $a > 0 \Longrightarrow p_{xy}^{(+)} > p_0 > p_{xy}^{(-)} > 0$
2. $a < 0 \Longrightarrow p_0 > p_{xy}^{(-)} > 0 > p_{xy}^{(+)}$.

In both cases the solution of the inequality reads as $p \in [0, p_-]$ and due to the continuity of $\mathcal{F}$ the limit formula for $a = 0$ agrees with the solution of the linear inequality. Resuming, we have proven the following theorem.

Theorem 1.9.1 If an isotropic state ρ_p defined as in Eq. (1.164) is separable, then $p \leq p_{xy}$, namel

$$p_{xy} = \Gamma\frac{\sqrt{(1 + \tilde{x})(1 + \tilde{y})} - \sqrt{\tilde{x}((1 + \gamma)\tilde{y} + \gamma\tilde{x} + \gamma)}}{1 - \gamma\tilde{x}} \tag{1.182}$$

with

$$\tilde{x} = \frac{x^2}{d_1 - 1}, \quad \tilde{y} = \frac{y^2}{d_2 - 1}, \quad \gamma = \frac{(d_2 - d_1)}{d_2(d_1 - 1)(d_1 + 1)^2}, \quad \Gamma = \frac{d_1}{d_1^2 - 1}\frac{\sqrt{d_1 - 1}\sqrt{d_2 - 1}}{\sqrt{d_1 d_2}}. \tag{1.183}$$

for arbitrary $x, y \geq 0$.

In particular, we have the following thresholds for de Vicente criterion ($x = y = 0$), for realignment

criterion $x = y = 1$ and for ESIC criterion ($x = \sqrt{d_1 + 1}$, $y = \sqrt{d_2 + 1}$), respectively:

$$p_{dV} = \frac{d_1}{d_1^2 - 1} \frac{\sqrt{d_1 - 1}\sqrt{d_2 - 1}}{\sqrt{d_1 d_2}} \tag{1.184}$$

$$p_R = \frac{(d_1^2 - 1)d_2 - \sqrt{d_1^3 d_2 - 3d_1 d_2 + d_2^2 + 1}}{d_2 d_1^3 - 2d_1 d_2 + 1} \tag{1.185}$$

$$p_E = \frac{2(d_1 - 1)d_2 - \sqrt{\frac{d_1^3 d_2^2 - 2d_1 d_2^2 + 3d_2^2 + (d_1^3 - 5d_1)d_2 + d_1 + 1}{d_1 + 1}}}{d_1^2 d_2 - d_1 d_2 - d_2 + 1}. \tag{1.186}$$

We skip the expression p_F for Fei criterion ($x = \sqrt{2/d_1}, y = \sqrt{2/d_2}$) p_F because is not short and simple. In the next section we prove that $p_E < p_R$. Let us calculate the minimum of the expression (1.182). One has

$$\partial_{\tilde{x}} p_{xy} = 0 \iff (1 + \gamma)\tilde{y} = \tilde{x} - \gamma. \tag{1.187}$$

This is a necessary condition for minimum. One can check, that substituting (1.187) to (1.182) a constant value $\Gamma/\sqrt{1 + \gamma}$ is obtained, hence we have the whole line $(1 + \gamma)\tilde{y} = \tilde{x} - \gamma$ (hyperbola in x,y) of minima of p_{xy}. One can summarize the above observations in the following:

Theorem 1.9.2 The minimum of p_{xy} is attained in points of the hyperbola:

$$\frac{x^2}{d_1 - 1} - (1 + \gamma)\frac{y^2}{d_2 - 1} = \gamma \tag{1.188}$$

and the value of the minimum is

$$p_{min} = \frac{\Gamma}{\sqrt{1 + \gamma}} = \sqrt{\frac{d_2 - 1}{d_2(d_1^2 + d_1 - 1) - 1}}. \tag{1.189}$$

The figure **??** illustrates the hyperbola of minima of p_{xy} (reducing to line if dimensions are equal) and four characteristic points representing the four criteria distinguished in the literature.

Comparison with Enhanced Realignment Criterion

From the enhanced realignment criterion in Eq. 1.118, we use as basis $\{|e_i\rangle\langle e_j|\}_{i,j=0}^{d_1 - 1} \subset \mathcal{B}(\mathbb{C}^{d_1})$ and $\{|f_i\rangle\langle f_j|\}_{i,j=0}^{d_2 - 1} \subset \mathcal{B}(\mathbb{C}^{d_2})$, then

$$\rho_p - \rho_1 \otimes \rho_2 = \frac{p}{d_1}\sum_{i,j=1}^{d_1} |e_i\rangle\langle e_j| \otimes |f_i\rangle\langle f_j| - \frac{p}{d_1^2}\mathbf{1}_{d_1} \otimes \mathbf{1}_{d_1} \tag{1.190}$$

and via vectorization of an operator we applied the realignment as in Eq.(1.165) having

$$C_{ER} \equiv C(\rho_p - \rho_1 \otimes \rho_2) = \frac{p}{d_1}\mathbf{1}_{d_1^2} - \frac{p}{d_1^2}|\mathbf{1}_{d_1}\rangle\langle\mathbf{1}_{d_1}|. \tag{1.191}$$

C_{ER} stands for enhanced realignment correlation matrix and the spectrum related to $C_{ER}C_{ER}^{\dagger}$ is

$$\sigma\left(C_{ER}C_{ER}^{\dagger}\right) = \left\{\frac{p^2}{d_1^2}\right\} \times (d_1^2 - 1) \cup \{0\}. \tag{1.192}$$

This brings to the condition

$$\frac{d_1^2 - 1}{d_1}p \leq \sqrt{\frac{d_1 - 1}{d_1}}\sqrt{\frac{d_2 - 1}{d_2} - p^2\left(\frac{d_2 - d_1}{d_1 d_2}\right)}. \tag{1.193}$$

The equality holds for

$$p_{\mathrm{ER}} = \sqrt{\frac{d_2 - 1}{d_2\left(d_1^2 + d_1 - 1\right) - 1}}. \tag{1.194}$$

This is exactly the value of p_{xy} along the hyperbola(1.188) of the minimal values. We have proven in the previous sectionr that Enhanced realignment criterion is equivalent to the family of *XY-criteria* for large value of x, y on a certain value of the ratio y/x. Here there exists a hyperbola which connects this optimal limit case in the infinity with the point: $x = \sqrt{(d_1 - 1)\gamma}$, $y = 0$. The function p_{xy} does not behave in this way for generic states.

Geometrical relations of the criteria

Now we can present the relation of the criteria. Analytically we can compare the criteria calling p_{dV}, p_R, p_F and p_E the thresholds which realized the equality in Eq. 1.170-1.173 respectively for Di Vincente, Realignment, Fei, ESIC criteria. Figure 1.5 show that the Gühne conjecture[43], namely $p_R - p_E \geq 0$ is always realized. The general trend is shown in Fig. 1.5, despite for $d_1 = 2$, $d_2 = 3$ Di Vincente criteria detect less than ESIC and Realignment. Also Fei detect more than Realignment for low d_1, d_2. According to numerics we support $p_{dV} \leq p_F$ and $p_E \leq p_F$ but we skip this check due to the lengthy of calculations. Overall, the lowest value among all d_1 and d_2 is always realized by p_{ER} (Enhanced Realignment). We show that for this state Günhe conjecture is true.

Proof of $p_E \leq p_R$

The thresholds p_E and p_R are defined as the lowest roots of the quadratic polynomials:

$$2(d_1^3 d_2 - 2d_1 d_2 + 1)p_R^2 - 4d_2(d_1^2 - 1)p_R$$
$$+ 2(d_1 d_2 - 1) \stackrel{df}{=} f_R(p_R) = 0 \tag{1.195}$$
$$(d_1^3 d_2 - 2d_1 d_2 + d_1 - d_2 + 1)p_E^2 - 4d_2(d_1^2 - 1)p_E$$
$$+ (3d_1 d_2 - d_1 - d_2 - 1) \stackrel{df}{=} f_E(p_E) = 0 \tag{1.196}$$

We will prove the relation between roots $p_E \leq p_R$ by showing that all roots of f_R and f_E are in a set: $\{x : f_E(x) < f_R(x)\}$. To show it let us calculate the difference $f_E - f_R$:

$$(f_E - f_R)(x) = -(d_1^3 d_2 - 2d_1 d_2 + d_2 - d_1 + 1)x^2$$
$$+ (d_1 - 1)(d_2 - 1) \tag{1.197}$$

It is positive in the range $[-x_0, x_0]$, where:

$$x_0 = \sqrt{\frac{d_2 - 1}{(d_1 + 1)d_1 d_2 - (d_2 + 1)}}. \tag{1.198}$$

We will show that f_R and f_E are positive in the above range, showing that
1. $f_R(x_0) = f_E(x_0)$,
2. f_R is descending in x_0.

One has

$$f_R(x_0) = f_E(x_0) = d_2 \frac{2d_1^3 d_2 + d_1^2 d_2 - 3d_1 d_2 - d_1^3 - d_1^2 + 2}{(d_1 + 1)d_1 d_2 - (d_2 + 1)}$$
$$- 2d_2(d_1^2 - 1)\sqrt{\frac{d_2 - 1}{(d_1 + 1)d_1 d_2 - (d_2 + 1)}}. \tag{1.199}$$

Hence, we want to prove that

$$2d_1^3 d_2 + d_1^2 d_2 - 3d_1 d_2 - d_1^3 - d_1^2 + 2$$
$$-2(d_1^2 - 1)\sqrt{(d_2 - 1)((d_1 + 1)d_1 d_2 - (d_2 + 1))} \geq 0. \qquad (1.200)$$

To do this, we will rewrite the above as:

$$(d_1^2 - 1) + d_1 d_- \frac{2d_1 + 3}{2d_1 + 2} \geq$$
$$\sqrt{d_-^2 (d_1^2 + d_1 - 1) + d_- d_1 (2d_1 + 3)(d_1 - 1) + (d_1^2 - 1)^2},$$

where $d_- = d_2 - d_1$. After squaring the latter simplifies to:

$$d_1^2 d_-^2 (2d_1 + 3)^2 \geq 4d_-^2 (d_1 + 1)^2 (d_1^2 + d_1 - 1),$$

what finally gives:

$$d_-^2 (d_1^2 + 4d_1 + 4) = (d_2 - d_1)^2 (d_1 + 2)^2 \geq 0.$$

We prove the second property showing, that the minimum of f_R is greater than x_0:

$$\frac{d_2(d_1^2 - 1)}{d_2 d_1^3 - 2d_1 d_2 + 1} > \sqrt{\frac{d_2 - 1}{d_1^2 d_2 + d_1 d_2 - d_2 - 1}}$$

While $d_1 \leq d_2$, we can estimate the RHS from above by $1/(d_1 + 1)$ and prove that the inequality holds for the estimation. The latter reduces to:

$$0 < d_2(d_1^2 - 1)(d_1 + 1) - (d_2 d_1^3 - 2d_1 d_2 + 1) = d_2 d_1^2 - d_2 - 1$$

and holds for $d_1, d_2 \geq 2$.

One has $f_E \geq f_R \geq 0$ in $[-x_0, x_0]$ and $f_E < f_R$ for $x > x_0$. The threshold p_E and p_R are roots on the left of the vertices of the parables f_E and f_R in Eq. (1.195) and (1.196) respectively. Both p_E and p_R are obviously greater than x_0 where $f_E < f_R$. It implies that f_E reaches 0 first and hence $p_E < p_R$. $\square$

It is worth to mention that the state detected by the four criteria are NPT. In order to prove that, notice that after partial transposition the elements along the diagonal are $(1 - p)/d_1 d_2$ and the off-diagonal terms are p/d_1. Moreover the matrix is Hermitian, then we applied the Sylvestre's criterion for the positivity on the following block

$$\text{Det} \begin{pmatrix} \frac{1-p}{d_1 d_2} & \frac{p}{d_1} \\ \frac{p}{d_1} & \frac{1-p}{d_1 d_2} \end{pmatrix} \geq 0. \qquad (1.201)$$

Therefore, ρ_p of Eq.(1.164) is separable if

$$p \leq \frac{1}{d_2 + 1}. \qquad (1.202)$$

Now from Eq. (1.194), since $d_2 > d_1$

$$p_{\text{ER}} = \sqrt{\frac{d_2 - 1}{d_2(d_1^2 + d_1^2 - 1) - 1}} \geq \sqrt{\frac{d_2 - 1}{d_2^3 + d_2^2 - d_2 - 1}} = \frac{1}{d_2 - 1},$$

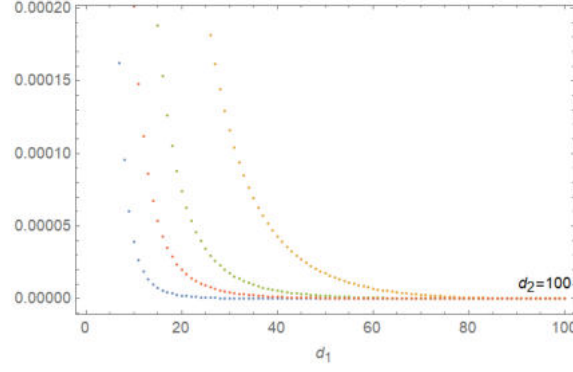which is equivalent to all the criteria for $d_1 = d_2$.

Figure 1.5: The difference of the thresholds which realize the equality in Eqs. 1.170-1.173 and 1.194 ($p_{dV} - p_{EH}$ in blue, $p_E - p_{EH}$ in red, $p_F - p_{EH}$ in green, $p_R - p_{EH}$ in orange) varying $d_1 = 2, \ldots, 100 = d_2$. This an asymptotic pattern for high values of d_1, d_2. For low value of d_1, d_2 the pattern is not respected. In particular for low values of d_1, d_2 $p_E \leq p_{dV}$ and $p_R \leq p_F$. For $d_1 = 2, d_2 = 3$ also $p_R \leq p_{dV}$.

1.10 Optimal witness for qubit-qubit

A particularly interesting necessary condition for the separability problem is given by the so called *range criterion* [62]. According to this criterion, if a state ρ acting on a finite dimensional Hilbert space is separable, then there must exist a set of product vectors $\{|e_k, f_k\rangle\}$ that span the range $R(\rho)$, such that the set of partial complex conjugated product states $\{|e_k, f_k^*\rangle\}$ span the range of the set of the partial transpose of ρ with respect to the second system, i.e., ρ^Γ. Among PPT entangled state (PPTES) that violate this criterion, there are particular states with the property that if one subtracts a projector onto a product vector from them, the resulting operator is no longer a PPTES [42, 63]. In this sense, these states lie in the edge between PPTES's and entangled states with nonpositive partial transposition, and therefore we will call them *edge* PPTES's. Despite this method is quite general and can be addressed on nondecomposable EW's, which are those that detect the presence of PPTES's here we show just an example of how to apply the spanning criterion to construct an optimal witnesses from Eq.1.137.

Definition 1.10.1 Given an EW, W we define the following set of quantum states detected by W

$$D_W = \{\rho \geq 0 : \mathrm{Tr} W\rho < 0\}. \tag{1.203}$$

Now, given two EW's, W_1 and W_2, we say that W_1 is *finer* than W_2 if $D_{W_2} \subseteq D_{W_1}$; that is, if all quantum states detected by W_2 are also detected by W_1. We say that W is an *optimal entanglement witness* if there exists no other EW which is finer. Let

$$\begin{aligned}\mathscr{P}_W &= \{|e, f\rangle \in \mathbb{C}^{d_A} \otimes \mathbb{C}^{d_B} : \langle e, f|W|e, f\rangle = 0\} \\ &= \{|e, f\rangle \in \mathbb{C}^{d_A} \otimes \mathbb{C}^{d_B} : |f\rangle \in \ker W_e, |e\rangle \in \ker W_f\} \end{aligned} \tag{1.204}$$

that is the set of the product state where W vanishes. where $W_e = \langle e|W|e\rangle$ and $W_f = \langle f|W|f\rangle$. Now, if we have a witness W which detect an entangled state ρ, then W detects also the following

state

$$\rho = \sum_k p_k |e_k, f_k\rangle \langle e_k, f_k|, \qquad p_k \geq 0, \tag{1.205}$$

and $|e_k, f_k\rangle \in \mathscr{P}_W$. Note the important role that the vectors in $\mathscr{P}_W$ play regarding entanglement. Indeed, this means that any quantum state from Eq. 1.205 is on the border between separable and nonseparable(entangled) set of states. In other words, if we add an arbitrary small amount of ρ it will be nonseparable state. Hence, the structure of $\mathscr{P}_W$ characterizes the hyperplane W tangent to the point of the set of convex separable state (see figure 1.1). Therefore, if span$\mathscr{P}_W = \mathbb{C}^{d_A} \otimes \mathbb{C}^{d_B}$, then W is optimal[42, 64, 65].

We want to find an optimal witness from the family of witness in Eq.1.137. This is non a simple problem neither in the simplest case, which has only a pedagogical worth because it considers $d_A = d_B = 2$. In the following we find the constrain which admit optimability, and we pave the way for its generalization. Then, the witnesses in Eq.1.137, for 2 by 2 case has the following form

$$W = diag\left\{ c + \eta s_\theta u_3 + \eta c_\theta v_3 + o_{33}, c + \eta s_\theta u_3 - \eta c_\theta v_3 - o_{33}, c - \eta s_\theta u_3 + \eta c_\theta v_3 - o_{33}, \right.$$

$$\left. c - \eta s_\theta u_3 - \eta c_\theta v_3 + o_{33} \right\} +$$

$$\begin{pmatrix} \cdot & \cdot & \cdot & \cdot \\ \eta c_\theta \tilde{v} + o_{31} + io_{32} & \cdot & \cdot & \cdot \\ \eta s_\theta \tilde{u} + o_{13} + io_{23} & o_{11} - io_{12} + io_{21} + o_{22} & \cdot & \cdot \\ o_{11} + io_{12} + io_{21} - o_{22} & \eta s_\theta \tilde{u} - o_{13} - io_{23} & \eta c_\theta \tilde{v} - o_{31} - io_{32} & \cdot \end{pmatrix} \tag{1.206}$$

with $\tilde{v} = (v_1 + iv_2)$, $c_\theta \equiv \cos\theta$, analogously for u and $\sin\theta$, o_{ij} are the entries of the orthogonal matrix O, the dots here replace the complex and conjugate since $W = W^\dagger$ and

$$c = \frac{1}{2}\left(\frac{d_A - 1}{d_A}\tan\theta + \frac{d_B - 1}{d_B}\cot\theta + \eta^2 \sin\theta\cos\theta\right). \tag{1.207}$$

We need to find $\{|f_\alpha\rangle\}_{\alpha=1}^{d_A} \in \ker W_e$ and $\{|e_\beta\rangle\}_{\beta=1}^{d_B} \in \ker W_f$ respectively linear independent. It is enough consider W_e, using the computational basis $|e_0\rangle = |0\rangle$ and $|e_1\rangle = |1\rangle$ for $\mathbb{C}^{d_A}$ and determine the basis

$$W_e = \left(\frac{1}{2}\left(\frac{d_A - 1}{d_A}\tan\theta + \frac{d_B - 1}{d_B}\cot\theta + \eta^2\sin\theta\cos\theta\right) + \eta\sin\theta\sum_{\alpha=1}^{d_A^2-1} u^\alpha\langle e|G_\alpha|e\rangle\right)\mathbf{1}_{d_B}$$

$$+ \sum_{\beta=1}^{d_B^2-1}\left(\eta v^\beta\cos\theta + \sum_{\alpha=1}^{d_A^2-1} O^{\alpha\beta}\langle e|G_\alpha|e\rangle\right)G_\beta^B \in \mathscr{B}(\mathbb{C}^{d_B}). \tag{1.208}$$

Then solving $W_e|f_1\rangle = 0$ and $W_e|f_2\rangle = 0$ we have respectively the following conditions

$$\frac{\left(\eta^2(\cos 4\theta - 1) + 4\cos 2\theta\right)^2}{\sin\theta\cos^2\theta} = 64\eta u_3\left(\sqrt{2}\cos 2\theta\tan\theta - 2\eta\sin^3\theta\left(\sqrt{2}\eta\cos\theta + u_3\right)\right) \tag{1.209}$$

$$\left(\eta^2 \sin 2\theta + \tan \theta + \cot \theta\right)^2 - 8\eta^2 \cos^2 \theta \left(u_3 \tan^2 \theta \left(\sqrt{2}\eta \cos \theta - u_3\right) + 1\right)$$
$$+ 8\sqrt{2}\eta u_3 \cos \theta - 4\sqrt{2}\eta u_3 \sec \theta = 4 \tag{1.210}$$

It is interesting that our family of witnesses include also the family of the witness discussed in [66, 67] for the case of qutrit-qutrit.

1.11 Multipartite linear entanglement witnesses

Our separability criterion (1.109) may be generalized for the multipartite scenario: consider N partite system living in $\mathscr{H}_1 \otimes \ldots \otimes \mathscr{H}_N$, and let $G^{(k)}_{\alpha_k}$ denotes an orthonormal basis in $\mathscr{B}(\mathscr{H}_k)$. Given a state ρ define a correlation (hyper)matrix

$$C^N_{\alpha_1 \ldots \alpha_N} = \left\langle G^{(1)}_{\alpha_1} \otimes \ldots \otimes G^{(N)}_{\alpha_N} \right\rangle_\rho .$$

In order to derive generalization of (1.109), let us reformulate the definition of the trace norm (1.6) inspired by proposition 1.3.1

$$\|X\|_{\mathrm{Tr}} = \sup_M \frac{|\langle M|X \rangle_{\mathrm{HS}}|}{\|M\|_\infty}, \tag{1.211}$$

where the supremum is taken over all matrices of appropriate size. It is well known that supremum is always realized by some isometry (as we used in the previous sections). Now, we generalize (1.211) to an arbitrary N-tensor $X^N_{i_1 \ldots i_N}$, where

$$\left\langle M^N | X^N \right\rangle_{\mathrm{HS}} = \sum_{i_1, \ldots, i_N} \left(M^N_{i_1 \ldots i_N}\right)^* X^N_{i_1 \ldots i_N}, \tag{1.212}$$

and the spectral (operator) norm is defined as follows

$$\|M^N\|_\infty := \sup_{|x^{(1)}|=\cdots=|x^{(N)}|=1} | \sum_{i_1, \ldots, i_N} M^N_{i_1 \ldots i_N} x^{(1)}_{i_1} \ldots x^{(N)}_{i_N}|. \tag{1.213}$$

The N-partite CCNR criterion reads

Theorem 1.11.1 If N-partite state is fully separable, then $\|C^N\|_{\mathrm{Tr}} \leq 1$.

Proof. again it is enough to check it for a product state $\rho^1 \otimes \ldots \otimes \rho^N$. Since the trace norm does not depend upon the basis let us take the canonical one. One finds for the correlation hypermatrix

$$C^N_{\alpha_1 \ldots \alpha_n} = R^1_{\alpha_1} \ldots R^N_{\alpha_N},$$

where the vector $R^k \in \mathbb{R}^{d_k}$ reads

$$R^k_{\alpha_k} = \left\langle G^{(k)}_{\alpha_k} \right\rangle_{\rho^k} = \mathrm{Tr}(\rho^k G^{(k)}_{\alpha_k}) = (1/\sqrt{d_k}, \mathbf{r}^k)$$

and $\mathbf{r}^k$ is a Bloch vector of ρ^k. One has:

$$\langle M^N | C^N \rangle_{\mathrm{HS}} \leq \|M^N\|_\infty |R^1_{\alpha_1}| \ldots |R^N_{\alpha_N}| \leq \|M^N\|_\infty$$

and hence $\|C^N\|_{\mathrm{Tr}} \leq 1$.   ∎

To generalize (1.109) let us define N diagonal $d_k^2 \times d_k^2$ matrices

$$D_{x_k}^k = \text{diag}\{x_k, 1, \ldots, 1\},$$

and $C^N(x_1, \ldots, x_N)$ defined as follows

$$C_{i_1 \ldots i_N}^N(x_1, \ldots, x_N) = C_{i_1 \ldots i_N}^N (D_{x_1}^1)_{i_1 i_1} \ldots (D_{x_N}^N)_{i_N i_N}.$$

One proves

Theorem 1.11.2 If ρ is fully separable, then

$$\|C^N(x_1, \ldots, x_N)\|_{\text{Tr}} \leq \mathcal{N}_1(x_1) \ldots \mathcal{N}_N(x_N), \qquad (1.214)$$

where for $k = 1, \ldots, N$

$$\mathcal{N}_k(x_k) = \sqrt{\frac{d_k - 1 + x_k^2}{d_k}}.$$

Proof. The proof is similar to that of Theorem 1.6.1. Indeed, taking again a product state $\rho^1 \otimes \ldots \otimes \rho^N$ one finds

$$\langle M^N | C^N(x_1, \ldots, x_N) \rangle_{\text{HS}} \leq \|M^N\|_\infty |R^1(x_1)| \ldots |R^N(x_N)|,$$

where $R^k(x_k) = (x_k/\sqrt{d_k}, \mathbf{r}^k)$, and hence

$$\|C^N(x_1, \ldots, x_N)\|_{\text{Tr}} \leq |R^1(x_1)| \ldots |R^N(x_N)|.$$

Finally, note that $|R^k(x_k)|^2 = x_k^2/d_k + |\mathbf{r}^k|^2 \leq \mathcal{N}_k(x_k)$ due to $|\mathbf{r}^k|^2 \leq (d_k - 1)/d_k$, which ends the proof. ∎

Actually, the trace-norm (or more generally Ky-Fan norm) was generalized for N-tensors using a procedure of so called *unfoldings* [68]: given an $X^N \in \mathbb{C}^{d_1} \otimes \ldots \otimes \mathbb{C}^{d_N}$ one defines an n-unfolding (or an n-mode matricization of X^N) $X_{(n)}$ which is a $d_n \times \bar{d}_n$ matrix with $\bar{d}_n = (d_1 d_2 \ldots d_N)/d_n$ (see [68] for a precise definition). Now, the Ky-Fan norm of X^N is defined as follows

$$\|X^N\|_{\widetilde{\text{Tr}}} := \max_n \|X_{(n)}^N\|_{\text{Tr}}. \qquad (1.215)$$

Using the same arguments one easily derives

Proposition 1.11.3 If ρ is fully separable, then

$$\|C^N(x_1, \ldots, x_N)\|_{\widetilde{\text{Tr}}} \leq \mathcal{N}_1(x_1) \ldots \mathcal{N}_N(x_N). \qquad (1.216)$$

Note, however that due to $\|X^N\|_{\text{Tr}} \leq \|X^N\|_{\widetilde{\text{Tr}}}$ the separability criterion based on (1.216) is weaker than (1.214). The procedure of unfolding gives rise to a family of matrices each of which only controls bipartite entanglement in $d_n \times \bar{d}_n$ system. Interestingly, criterion (1.216) for $x_k = 0$ ($k = 1, \ldots, N$) was already derived in [69], and for $x_k = \sqrt{2/d_k}$ ($k = 1, \ldots, N$) it was derived in [51]. It should be clear that if each $\mathscr{H}_k$ allows for the existence of SIC POVM, then for $x_k = \sqrt{d_k + 1}$ one obtains a multipartite generalization of ESIC criterion from [43]. However, as we already observed, the existence of SICs is not essential.

As final attempt in the next section 1.12 we would like to generalize the equivalence between XY–criterion with the enhanced realignment criterion in the multipartite scenario.

1.12 Generalization of XY–criterion

Here, the generalization of the criterion, is referred to the equivalent family of linear (state independent) witnesses with respect to the enhanced realignment criterion which is not possible to generalize. The appealing comes from the reformation of the definition of the trace norm in Eq. 1.211-1.212-1.213. We show that the norm $||\cdot||_\infty$ defined in 1.213, in the bipartite case corresponds to the usual operational norm as in Eq.1.217.

Proof. In the bipartite case, the definition of operational norm is

$$||O||_{op} = \sup_{|x^{(1)}|=1} ||Ox^{(1)}||_{HS}$$

$$= \sup_{|x^{(1)}|=1} \sqrt{\sum_{\alpha\beta'\beta} O_{\alpha\beta'} O_{\alpha\beta} x^{(1)}_{\beta'} x^{(1)}_{\beta}}. \tag{1.217}$$

Now we show that this definition correspond to the definition in 1.213 for $N = 2$. Indeed, we can rewrite

$$||O||_{op} = \sup_{|x^{(2)}|=1} ||Ox^{(2)}|| = \sup_{|x^{(1)}|=|x^{(2)}|=1} ||x^{(1)}|| ||Ox^{(2)}||$$

$$\geq \sup_{|x^{(1)}|=|x^{(2)}|=1} \left| \left\langle x^{(1)} | Ox^{(2)} \right\rangle \right|$$

$$= \sup_{|x^{(1)}|=|x^{(2)}|=1} \left| \sum_{i_1 i_2} O_{i_1 i_2} x^{(1)}_{i_1} x^{(2)}_{i_2} \right|.$$

On the right hand side of the Cauchy-Schwarz inequality, the supremum is reached when $x^{(1)} = Ox^{(2)}/||Ox^{(2)}||$, therefore

$$\sup_{|x^{(2)}|=1} \frac{\left\langle Ox^{(2)} | Ox^{(2)} \right\rangle}{||Ox^{(2)}||} = \sup_{|x^{(2)}|=1} ||Ox^{(2)}|| = ||O||_{op}. \tag{1.218}$$

This means that

$$||O||_{op} = \sup_{|x^{(1)}|=|x^{(2)}|=1} \left| \sum_{i_1 i_2} O_{i_1 i_2} x^{(1)}_{i_1} x^{(2)}_{i_2} \right| \equiv ||O||_\infty. \tag{1.219}$$

∎

In the bipartite case, as we shown previous, the isometry is based on an orthogonal $d_1^2 \times d_2^2$ matrix O. We have already presented in the section 1.7 in Eq. 1.139 that the matrix O naturally rises up in the definition of the trace norm with some constrains applied on its entries: the vertex O^{00}, the edges $O^{\alpha 0}, O^{0\beta}$, and the face $O^{\alpha\beta}$, for $\alpha, \beta > 0$. In the following we discuss the constrains for the entries of the tensor M based on the condition imposed by the definition of the norm $||\cdot||_\infty$. Let us start from the tripartite scenario.

Tripartite scenario

For the tripartite case, the *XY-criterion* says that if ρ is separable, then

$$||C^{N=3}(x_1, x_2, x_3)|| \leq \mathcal{N}_1(x_1) \mathcal{N}_2(x_2) \mathcal{N}_3(x_3) \tag{1.220}$$

where

$$||C^{N=3}(x_1,x_2,x_3)||_{\text{tr}} = \sup_M \frac{\langle M|C^N(x_1,x_2,x_3)\rangle}{||M||_\infty} \tag{1.221}$$

and

$$||M||_\infty = \sup_{|x^{(1)}|=|x^{(2)}|=|x^{(3)}|=1} \left|\left\langle x^{(1)} \otimes x^{(2)} \otimes x^{(3)}|M\right\rangle\right|$$

$$= \sup_{|x^{(1)}|=|x^{(2)}|=|x^{(3)}|=1} \left|\sum_{i_1 i_2 i_3} M_{i_1 i_2 i_3} x_{i_1}^{(1)} x_{i_2}^{(2)} x_{i_3}^{(3)}\right|. \tag{1.222}$$

For this case, the witnesses are

$$W(x_1,x_2,x_3) = a(x_1,x_2,x_3) G_0 \otimes G_0 \otimes G_0 +$$

$$+ x_1 x_2 \sum_{i_3>0} M_{00i_3} G_0 \otimes G_0 \otimes G_{i_3} + \ldots$$

$$+ x_1 \sum_{i_2,i_3>0} M_{0i_2i_3} G_0 \otimes G_{i_2} \otimes G_{i_3} + \ldots$$

$$+ \sum_{i_1,i_2,i_3>0} M_{i_1 i_2 i_3} G_{i_1} \otimes G_{i_2} \otimes G_{i_3}$$

with

$$a(x_1,x_2,x_3) = \sqrt{\prod_{i=1,2,3}(d_i - 1 + x_i^2)}||M||_\infty + x_1 x_2 x_3 M_{000}. \tag{1.223}$$

For avoid cumbersome notation, we consider the same basis and the same dimension for each subsystem. Our aim, now is to characterize the family of witnesses in the limit of large x_1, x_2, x_3. The generalization runs easily. According to the bipartite case, we razionalize $a(x_1,x_2,x_3)$ as follows

$$\frac{\prod_i(d_i - 1 + x_i^2)||M||_\infty^2 - (x_1 x_2 x_3 M_{000})^2}{\sqrt{\prod_i(d_i - 1 + x_i^2)}||M||_\infty - x_1 x_2 x_3 M_{000}} \sim \tag{1.224}$$

$$\frac{(d-1)||M||_\infty^2 f(\theta_1,\theta_2) r}{||M||_\infty - M_{000}} + \frac{(||M||_\infty^2 - M_{000}^2) g(\theta_1,\theta_2) r^3}{||M||_\infty - M_{000}}.$$

We neglected the smaller order term of r and writing x_1, x_2, x_3 in the spherical coordinates we defined the functions g and f as follows

$$g(\theta_1,\theta_2) = \sin^2\theta_1 \cos\theta_2 \sin\theta_2 \cos\theta_1, \tag{1.225}$$

$$f(\theta_1,\theta_2) = \frac{\sin^2\theta_1 \sin\theta_2 \cos\theta_2}{\cos\theta_1} + \cot\theta_2 \cos\theta_1 + \tan\theta_2 \cos\theta_1.$$

It is trivial to say that, the quantity of Eq. 1.224 diverges as r. This provides a pointless family of witnesses for detecting entanglement. However, each witness can be always re-scaled. In this case, we need to divide by r. Moreover, in this analysis we skip the choice to take such M independent from x_1, x_2, x_3 (for the bipartite case, for O independent on x, y we obtained the Di Vincente' s criterion ruled by the isometry of Eq. 1.131). Therefore, we should be careful re-scaling the witnesses according to the entries of M.

In order to have a finite coefficient proportional to the identity term of the witnesses, the asymptotic

behavior of a should run as r, this implies that $||M||_\infty^2 - (M_{000})^2 \sim r^{-2}$, and in the limit we have $M_{000} \to -||M||_\infty$. Notice that $||M||_\infty$ does not depend on the coordinates, and the sign minus is crucial, otherwise the denominator diverges. The asymptotic behavior of the entries of M is

$$
\begin{aligned}
W \sim r G_0 \otimes G_0 \otimes G_0 &+ r^2 \sum_{i_3>0} M_{00i_3} G_0 \otimes G_0 \otimes G_{i_3} + \ldots \\
&+ r \sum_{i_2,i_3>0} M_{0i_2i_3} G_0 \otimes G_{i_2} \otimes G_{i_3} + \ldots \\
&+ r^0 \sum_{i_1,i_2,i_3>0} M_{i_1i_2i_3} G_{i_1} \otimes G_{i_2} \otimes G_{i_3}.
\end{aligned}
$$

Therefore, the re-scaled family of witnesses is

$$
\begin{aligned}
\tilde{W}(\theta_1,\theta_2) =&\, \tilde{a}(\theta_1,\theta_2) G_0 \otimes G_0 \otimes G_0 + \\
&+ e \sin\theta_1 \sin\theta_2 \cos\theta_1 \sum_{i_1>0} u_{i_1} G_{i_1} \otimes G_0 \otimes G_0 + \ldots \\
&+ \cos\theta_1 \sum_{i_1,i_2>0} \pi_{i_1i_2} G_{i_1} \otimes G_{i_2} \otimes G_0 + \ldots
\end{aligned}
\tag{1.226}
$$

with

$$
M_{000} = -||M||_\infty \sqrt{1 - \frac{\eta^2}{r^2}},
\tag{1.227}
$$

$$
(M_{i_100}, M_{0i_20}, M_{00i_3}) = \left(\frac{e u_{i_1}}{r}, \frac{\varepsilon v_{i_2}}{r}, \frac{\xi w_{i_3}}{r} \right),
$$

$$
(M_{i_1i_20}, M_{i_10i_3}, M_{0i_2i_3}) = (\pi_{i_1i_2}, \sigma_{i_1i_3}, \tau_{i_2i_3}),
$$

$$
M_{i_1i_2i_3} = \boldsymbol{M}_{i_1i_2i_3}.
$$

We call the entries of the tensor M as the vertex M_{000}, the edges $M_{P[i_100]}$, the faces $M_{P[i_1i_20]}$ (P, here is a permutation) and the interior $M_{i_1i_2i_3}$ for $i_1,i_2,i_3 > 0$. Notice that, the interior $\boldsymbol{M}$ is vanishing in the witnesses because it cannot depend on r, since M is bounded (see Eq. 1.222). Moreover, from the Eq. 1.211 it easy to notice that the tensor M can be always re-normalized, such that $||M||_\infty = 1$. Then, the function $\tilde{a} = a/r$ results

$$
\tilde{a}(\theta_1,\theta_2,\eta) = \frac{(d-1) f(\theta_1,\theta_2) + g(\theta_1,\theta_2) \eta^2}{2}.
\tag{1.228}
$$

Proof. Let us expand Eq. 1.224

$$a(x_1, x_2, x_3) = \frac{(d_1 - 1 + x_1^2)(d_2 - 1 + x_2^2)(d_3 - 1 + x_3^2)||M||_\infty^2 - (x_1 x_2 x_3 M_{000})^2}{\sqrt{(d_1 - 1 + x_1^2)(d_2 - 1 + x_2^2)(d_3 - 1 + x_3^2)}||M||_\infty - x_1 x_2 x_3 M_{000}}$$

$$= ||M||_\infty^2 \frac{(d-1)^3 + (d_2 - 1)^2 (x_1^2 + x_2^2 + x_3^2) + (d_3 - 1)(x_1^2 x_2^2 + x_1^2 x_3^2 + x_2^2 x_3^2)}{x_1 x_2 x_3 \left[||M||_\infty \sqrt{\left(\frac{d-1}{x_1^2} + 1\right)\left(\frac{d-1}{x_2^2} + 1\right)\left(\frac{d-1}{x_3^2} + 1\right)} - M_{000}\right]}$$

$$+ \frac{(x_1 x_2 x_3)^2 \left[||M||_\infty^2 - (M_{000})^2\right]}{x_1 x_2 x_3 \left[||M||_\infty \sqrt{\left(\frac{d-1}{x_1^2} + 1\right)\left(\frac{d-1}{x_2^2} + 1\right)\left(\frac{d-1}{x_3^2} + 1\right)} - M_{000}\right]}$$

$$= \frac{(d-1)(x_1^2 x_2^2 + x_1^2 x_3^2 + x_2^2 x_3^2)||M||_\infty^2 + (x_1 x_2 x_3)^2 \left[||M||_\infty^2 - (M_{000})^2\right]}{x_1 x_2 x_3 \left[||M||_\infty - M_{000}\right]}$$

$$= \frac{(d-1)||M||_\infty^2 \left(\frac{x_1 x_2}{x_3} + \frac{x_1 x_3}{x_2} + \frac{x_2 x_3}{x_1}\right) + \left[||M||_\infty^2 - (M_{000})^2\right] x_1 x_2 x_3}{\left[||M||_\infty - M_{000}\right]}. \tag{1.229}$$

Then

$$\tilde{a}(\theta_1, \theta_2) = a/r$$

$$= \frac{(d-1)||M||_\infty^2 \left(\frac{\sin^2 \theta_1 \sin \theta_2 \cos \theta_2}{\cos \theta_1} + \frac{\sin \theta_1 \cos \theta_2 \cos \theta_1}{\sin \theta_1 \sin \theta_2} + \frac{\sin \theta_1 \sin \theta_2 \cos \theta_1}{\sin \theta_1 \cos \theta_2}\right)}{||M||_\infty - M_{000}}$$

$$+ \frac{\left[||M||_\infty^2 - (M_{000})^2\right] \sin^2 \theta_1 \cos \theta_2 \sin \theta_2 \cos \theta_1 r^2}{||M||_\infty - M_{000}}.$$

such that

$$M_{000} = -\sqrt{||M||_\infty^2 - \frac{\eta^2}{r^2}} \implies ||M||_\infty^2 - (M_{000})^2 = \frac{\eta^2}{r^2}. \tag{1.230}$$

It implies

$$||M||_\infty - M_{000} = ||M||_\infty + \sqrt{||M||_\infty^2 - \frac{\eta^2}{r^2}}$$

$$= ||M||_\infty + ||M||_\infty \sqrt{1 - \frac{\eta^2}{r^2 ||M||_\infty^2}} \to 2||M||_\infty$$

where

$$f(\theta_1, \theta_2) = \left(\frac{\sin^2 \theta_1 \sin \theta_2 \cos \theta_2}{\cos \theta_1} + \frac{\sin \theta_1 \cos \theta_2 \cos \theta_1}{\sin \theta_1 \sin \theta_2} + \frac{\sin \theta_1 \sin \theta_2 \cos \theta_1}{\sin \theta_1 \cos \theta_2}\right) \tag{1.231}$$

$$g(\theta_1, \theta_2) = \sin^2 \theta_1 \cos \theta_2 \sin \theta_2 \cos \theta_1. \tag{1.232}$$

Finally we have

$$\tilde{a}(\theta_1, \theta_2) = \frac{(d-1)||M||_\infty^2 f(\theta_1, \theta_2) + g(\theta_1, \theta_2)\eta^2}{2||M||_\infty}. \tag{1.233}$$

It is worth to notice that in this case $||M||_\infty$ does not depend by r after the limit, or at least $O(||M||_\infty) < O\left(\frac{\eta^2}{r^2}\right)$. In other words its limit cannot be neither infinity nor vanishing. ∎

Now we want to characterized the edges.

Proposition 1.12.1 All the entries of the edges, namely $M_{P[i_1 00]}$ is vanishing for $i_1 > 0$.

Proof. $M_{P[i_1 00]}$ are multiplied by r, then we must require that (u, v, w) go asymptotically as $1/r$ (the faces do not need any dependence on the coordinates). The characterization of the edges and faces is based on the unique condition of Eq. 1.222 that for $||M||_\infty = 1$ becomes

$$1 \geq \left| \sum_{i_1 i_2 i_3} M_{i_1 i_2 i_3} x_{i_1}^{(1)} x_{i_2}^{(2)} x_{i_3}^{(3)} \right|. \tag{1.234}$$

Since it holds for all $x^{(1)}, x^{(2)}, x^{(3)}$, let us consider the first column of the tensor, choosing opportunely $x^{(1)}, x^{(2)}, x^{(3)}$ in order to check if there exists one entries $\alpha \neq 0$ in the $(k-1)$-th position, as well as $M_{(k-1)00}$ different from zero.

$$x^{(1)} = (-1, 0, \dots \alpha, \dots, 0) / \sqrt{1 + \alpha^2}, \tag{1.235}$$
$$x^{(2)} = (1, 0, 0, \dots, 0), \tag{1.236}$$
$$x^{(3)} = (1, 0, 0, \dots, 0). \tag{1.237}$$

Notice that $x_0^{(1)} = -1$ because $M_{000} = -1$. The condition 1.234 yields

$$\sqrt{1 + \alpha^2} \geq \left| 1 + \alpha M_{(k-1)00} \right|. \tag{1.238}$$

Therefore

$$\begin{cases} -1 \leq M_{(k-1)00} \leq 0 & \alpha > 0 \\ 0 \leq M_{(k-1)00} \leq 1 & \alpha < 0. \end{cases} \tag{1.239}$$

This concludes the proof $M_{(k-1)00} \in [-1, 0] \cap [0, 1] = \{0\}$. You can see that $M_{P[0\alpha 0]}$ vanish in the limit. ∎

As regards the faces of the tensor connected to the vertex $M_{i_1 i_2 0}, M_{0 i_2 i_3}, M_{i_1 0 i_3}$, follows

Proposition 1.12.2 All the entries of the faces, namely $M_{P[i_1 i_2 0]}$, satisfied the condition $-1 < M_{P[i_1 i_2 0]} < 1$ for $i_1, i_2 > 0$.

Proof. Let us start from the first face $M_{i_1 i_2 0}$, thus we choose

$$x^{(1)} = (-1, 0, \dots \alpha, \dots, 0) / \sqrt{1 + \alpha^2}, \tag{1.240}$$
$$x^{(2)} = (1, 0, 0, \dots, \beta \dots, 0) / \sqrt{1 + \beta^2}, \tag{1.241}$$
$$x^{(3)} = (1, 0, 0, \dots, 0). \tag{1.242}$$

In limit $M_{000} \sim -1$ and $M_{P[\alpha 00]} \sim 0$, as we have found above, with α and β respectively in $(k-1)$-th and $(j-1)$-th position, the condition 1.234 gives

$$\sqrt{1 + \alpha^2} \sqrt{1 + \beta^2} \geq \left| 1 + \alpha \beta M_{(k-1)(j-1)0} \right|. \tag{1.243}$$

We found that $M_{(k-1)(j-1)0} \in [-1, 1]$, $\forall \alpha, \beta \in \mathbb{R}$. Therefore for all permutation P, we have $-1 < M_{P[\alpha \beta 0]} < 1$. ∎

Lemma 1.12.3 Notice that the interior is vanishing for our particular case of large x_1, x_2, x_3, however we can also consider the original witnesses which comes from the criterion and applied the same procedure. We would have

$$x^{(1)} = (-1, 0, \ldots \alpha, \ldots, 0) / \sqrt{1 + \alpha^2} \tag{1.244}$$

$$x^{(2)} = (1, 0, \ldots, \beta \ldots, 0) / \sqrt{1 + \beta^2} \tag{1.245}$$

$$x^{(3)} = (1, 0, \ldots, \gamma, \ldots, 0) / \sqrt{1 + \gamma^2} \tag{1.246}$$

which brings to

$$\sqrt{1 + \alpha^2} \sqrt{1 + \beta^2} \sqrt{1 + \gamma^2} \geq |1 + \alpha \beta M_{(k-1)(j-1)0}$$
$$+ \alpha \gamma M_{(k-1)0(l-1)} - \beta \gamma M_{0(j-1)(l-1)} + \alpha \beta \gamma M_{(k-1)(j-1)(l-1)}|. \tag{1.247}$$

The final witness for the tripartite scenario in the limit of large x_1, x_2, x_3 is, we call $W^\infty = \tilde{W}(\theta_1, \theta_2, \eta)$ such that

$$W^\infty = \frac{(d-1) f(\theta_1, \theta_2) + g(\theta_1, \theta_2) \eta^2}{2} \bigotimes_{i=1}^{3} G_0 + \cos \theta_1 \sum_{i_1, i_2 > 0} M_{i_1 i_2 0} G_{i_1} \otimes G_{i_2} \otimes G_0$$
$$+ \sin \theta_1 \sin \theta_2 \sum_{i_1, i_3 > 0} M_{i_1 0 i_3} G_{i_1} \otimes G_0 \otimes G_{i_3} + \sin \theta_1 \cos \theta_2 \sum_{i_2, i_3 > 0} M_{0 i_2 i_3} G_0 \otimes G_{i_2} \otimes G_{i_3}.$$

Now let us decompose the quantum state as follows (we consider the special case $d_i = d$, for $i = 1, 2, 3$, and in the same hermitian orthonormal basis $\left\langle G_k^\dagger | G_j \right\rangle = \delta_{kj}$)

$$\rho = \sum_{i_1 i_2 i_3} \left\langle G_{i_1} \otimes G_{i_2} \otimes G_{i_3} | \rho \right\rangle G_{i_1} \otimes G_{i_2} \otimes G_{i_3}$$
$$= \sum_{i_1 i_2 i_3} C_{i_1 i_2 i_3} G_{i_1} \otimes G_{i_2} \otimes G_{i_3}$$
$$= \frac{1}{d} \otimes \frac{1}{d} \otimes \frac{1}{d} + \sum_{i_1 > 0} r_{i_1}^{(1)} G_{i_1} \otimes \frac{1}{d} \otimes \frac{1}{d} + \ldots$$
$$+ \sum_{i_1 i_2 > 0} \pi_{i_1 i_2}^{(1)} G_{i_1} \otimes G_{i_2} \otimes \frac{1}{d} + \ldots$$
$$+ \sum_{i_1 i_2 i_3 > 0} t_{i_1 i_2 i_3} G_{i_1} \otimes G_{i_2} \otimes G_{i_3}$$

This brings to the condition $\mathrm{Tr}\rho W^\infty > 0$ where

$$\mathrm{Tr}\rho W^\infty = \frac{(d-1) f(\theta_1, \theta_2) + g(\theta_1, \theta_2) \eta^2}{2} + \cos \theta_1 \sum_{i_1, i_2 > 0} M_{i_1 i_2 0} \pi_{i_1 i_2}^{(1)}$$
$$+ \sin \theta_1 \sin \theta_2 \sum_{i_1, i_3 > 0} M_{i_1 0 i_3} \pi_{i_1 i_3}^{(2)} + \sin \theta_1 \cos \theta_2 \sum_{i_2, i_3 > 0} M_{0 i_2 i_3} \pi_{i_2 i_3}^{(3)}.$$

and $\pi_{i_1 i_2}^{(1)} = \mathrm{Tr}\rho G_{i_1} \otimes G_{i_2} \otimes G_0$ and analogously for the others.

A further development might be the optimization of this function finding the minimum as we have shown for the bipartite scenario. In the following we generalize such procedure for the N partite case.

N partite case

For this case the bound condition to characterize the entries of the N-rank tensor M from Eq. 1.213 is

$$||M||_\infty \geq \left| \sum_{i_1 \ldots i_N} M_{i_1 \ldots i_N} x_{i_1}^{(1)} \ldots x_{i_N}^{(N)} \right|. \tag{1.248}$$

. Notice that the modulus in such equation can be removed.

> **Theorem 1.12.4** The multipartite witnesses from the criterion 1.214 are
>
> $$W = ||M||_\infty \prod_{i=1,\ldots,N} \sqrt{(d_i - 1 + x_i^2)} \bigotimes_{k=1}^{N} G_0^{(k)} + \sum_{i_1,\ldots,i_N} M_{i_1,\ldots,i_N} \bigotimes_{k=1}^{N} G_{i_k}^{(k)} \left(D_{x_k}^k \right)_{i_k i_k} \tag{1.249}$$
>
> with
>
> $$\left(D_{x_k}^k \right)_{i_k i_k} = \operatorname{diag}\{x_k, 1, \ldots, 1\} \tag{1.250}$$

Proof. Let us writing again the n-partite correlation tensor

$$C_{i_1 \ldots i_N}^N = \left\langle G_{i_1}^{(1)} \otimes \cdots \otimes G_{i_N}^{(N)} \right\rangle_\rho = \operatorname{Tr}\left(G_{i_1}^{(1)} \otimes \cdots \otimes G_{i_N}^{(N)} \rho \right) \tag{1.251}$$

with $D_{x_1}^k = \operatorname{diag}\{x_k, 1, \ldots, 1\}$ such that

$$C^N(x_1, \ldots, x_N) = C_{i_1 \ldots i_N}^N \left(D_{x_1}^1 \right)_{i_1 i_1} \ldots \left(D_{x_N}^N \right)_{i_N i_N}. \tag{1.252}$$

Again the separability criterion holds for

$$||C^N(x_1, \ldots, x_N)|| \leq \mathcal{N}_1(x_1) \cdots \mathcal{N}_N(x_N) \tag{1.253}$$

where

$$||C^N(x_1, \ldots, x_N)||_{\mathrm{tr}} = \sup_M \frac{\left| \langle M | C^N(x_1, \ldots, x_N) \rangle \right|}{||M||_\infty}, \tag{1.254}$$

and

$$||M||_\infty = \sup_{|x^{(1)}| = \cdots = |x^{(N)}| = 1} \left| \left\langle x^{(1)} \otimes \cdots \otimes x^{(N)} | M \right\rangle \right|$$

$$= \sup_{|x^{(1)}| = \cdots = |x^{(N)}| = 1} \left| \sum_{i_1 \ldots i_N} M_{i_1 \ldots i_N} x_{i_1}^{(1)} \ldots x_{i_N}^{(N)} \right|. \tag{1.255}$$

The Eq. 1.253 can be also written as the following from

$$\operatorname{Tr}\rho \prod_{i=1,\ldots,N} \mathcal{N}_i(x_i) ||M||_\infty + \left| \langle M | C^N(x_1, \ldots, x_N) \rangle \right| \geq 0$$

$$\operatorname{Tr}\rho \prod_{i=1,\ldots,N} \mathcal{N}_i(x_i) ||M||_\infty + \sum_{i_1,\ldots,i_N} M_{i_1,\ldots,i_N} C_{i_1 \ldots i_N}^N \left(D_{x_1}^1 \right)_{i_1 i_1} \ldots \left(D_{x_N}^N \right)_{i_N i_N} \geq 0. \tag{1.256}$$

<div align="right">∎</div>

In the following we would like to characterize the witnesses in Eq. 1.249 in terms of vertex $(0-\text{rank}$ tensor), the N edges, which are the $1-\text{rank}$ tensors, the $\begin{pmatrix} N \\ 2 \end{pmatrix}$ faces $(2-\text{rank tensors})$ and so on. In general, we have $\begin{pmatrix} N \\ k \end{pmatrix}$ $k-\text{rank}$ tensors for $k = 0, \ldots, N$. We expand the summation of Eq. 1.249 is a very compact and useful notation as follows

$$
\begin{aligned}
W = & \left(\prod_{i=1}^{N} \sqrt{(d_i - 1 + x_i^2)} ||M||_\infty + \prod_{i=1}^{N} x_i M_{I_0} \right) \left(\bigotimes G \right)_{I_0} \\
& + \sum_{j_1=1}^{N} \left(\prod_{i=1, i \neq j_1}^{N} x_i \right) \sum_{i_{j_1}=1}^{d_{j_1}} M_{I_1(i_{j_1})} \left(\bigotimes G \right)_{I_1(i_{j_1})} \\
& + \sum_{j_1 < j_2} \left(\prod_{i=1, i \neq j_1, j_2}^{N} x_i \right) \sum_{i_{j_1}=1}^{d_{j_1}} \sum_{i_{j_2}=1}^{d_{j_2}} M_{I_2(i_{j_1}, i_{j_2})} \left(\bigotimes G \right)_{I_2(i_{j_1}, i_{j_2})} + \cdots \\
& + \sum_{j_1 < \cdots < j_k} \left(\prod_{i=1, i \neq j_1 \ldots j_k}^{N} x_i \right) \sum_{i_{j_1} \ldots i_{j_k}=1}^{d_{j_1} \ldots d_{j_k}} M_{I_k(i_{j_1} \ldots j_k)} \left(\bigotimes G \right)_{I_k(i_{j_1} \ldots j_k)} \\
& + \cdots + \sum_{i_1=1}^{d_1} \sum_{i_2=1}^{d_2} \cdots \sum_{i_N=1}^{d_N} M_{i_1, \ldots, i_N} \bigotimes_{k=1}^{N} G_{i_k}^{(d_k)}
\end{aligned}
\tag{1.257}
$$

where $I_k = (\ldots 0, i_{j_1}, 0, \ldots 0, i_{j_2}, 0, \ldots, 0, i_{j_k}, 0 \ldots)$ with $j_l = 1, \ldots d_l, \quad l = 1 \ldots k$ and

$$
\begin{aligned}
\left(\bigotimes G \right)_{I_k(i_{j_1}, i_{j_2}, \ldots, i_{j_k})} = & G_0^{(1)} \otimes \ldots \otimes G_0^{(j_1-1)} \otimes G_{i_{j_1}}^{(j_1)} \otimes G_0^{(j_1+1)} \ldots \\
& \otimes G_0^{(j_k-1)} \otimes G_{i_{j_k}}^{(j_k)} \otimes G_0^{(j_k+1)} \cdots \otimes G_0^{(N)}.
\end{aligned}
\tag{1.258}
$$

Here d_l is the dimension of $l-\text{th}$ Hilbert subspace and k is the rank of the tensor (the number of non zero indices).

■ **Example 1.2** To better understand the notation we show an example. Let $N = 5$, with $d_k = 3$, for $k = 1, \ldots, 5$, $I_0 = (0,0,0,0,0)$ and $I_1(3_4) = (0,0,0,3,0)$, $j_1 = 4$, $i_{j_1} = 3$. In particular, simple examples are $I_0 = (0, \ldots, 0)$, and $I_N = (i_{j_1}, i_{j_2}, \ldots, i_{j_N}) = (i_1, \ldots, i_N)$, because the sub-index j_l point out the j–th position for $j_l = 1, \ldots d_j$ of the j–th Hilbert space. The index $l = 1, \ldots, k$ means that in the list I_k there are k non vanish terms. Let me rewritten the formula 1.257 in a more suitable fashion for the next calculations, where $j_1, \ldots, j_k$ tell us the position of non vanishing index of $M_{I_k(i_{j_1}, i_{j_2}, \ldots, j_k)}$. Let us define the term which contain the vertex as

$$
W_0 = \prod_{i=1}^{N} \sqrt{(d_i - 1 + x_i^2)} ||M||_\infty + \prod_{i=1}^{N} x_i M_{I_0}
\tag{1.259}
$$

and $W_{i_{j_1}}^{j_1}$ the term proportional to the j_1–th edge as follows

$$
W_{i_{j_1}}^{j_1} = \left(\prod_{i=1, i \neq j_1}^{N} x_i \right) M_{I_1(i_{j_1})}, \qquad i_{j_1} = 1, \ldots, d_{j_1}.
\tag{1.260}
$$

Analogously for the $(i_{j_1}, i_{j_2})-\text{th}$ faces

$$
W_{i_{j_1}, i_{j_2}}^{j_1, j_2} = \left(\prod_{i=1, i \neq j_1, j_2}^{N} x_i \right) M_{I_2(i_{j_1}, i_{j_2})}, \quad i_{j_1} = 1, \ldots d_{j_1}, i_{j_2} = 1, \ldots, d_{j_2}
\tag{1.261}
$$

and so on. Finally the equation 1.249 becomes

$$
\begin{aligned}
W = & W_0 \left(\bigotimes G \right)_{I_0} + \sum_{j_1=1}^{N} \sum_{i_{j_1}=1}^{d_{j_1}} W_{i_{j_1}}^{j_1} \left(\bigotimes G \right)_{I_1\left(i_{j_1}\right)} \\
& + \sum_{j_1<j_2} \sum_{i_{j_1}=1}^{d_{j_1}} \sum_{i_{j_2}=1}^{d_{j_2}} W_{i_{j_1},i_{j_2}}^{j_1,j_2} \left(\bigotimes G \right)_{I_2\left(i_{j_1},i_{j_2}\right)} \\
& + \sum_{j_1<\cdots<j_k} \sum_{i_{j_1}\dots i_{j_k}=1}^{d_{j_1}\dots d_{j_k}} W_{i_{j_1}\dots i_{j_k}}^{i_{j_1}\dots i_{j_k}} \left(\bigotimes G \right)_{I_k\left(i_{j_1}\dots j_k\right)} \\
& + \dots + \sum_{i_1=1}^{d_1} \sum_{i_2=1}^{d_2} \cdots \sum_{i_N=1}^{d_N} M_{i_1,\dots,i_N} \bigotimes_{k=1}^{N} G_{i_k}^{(d_k)}.
\end{aligned}
\tag{1.262}
$$

Notice that the last term is $W_{i_{j_1},i_{j_2},\dots,i_{j_N}}^{j_1,j_2,\dots,j_N} = M_{i_1,\dots,i_N}$, because $j_1 < \cdots < j_N$, and we do not need anymore to specify which position has non zero index.

Let us start from the definition of W for the N partite case of Eq. 1.257. As in the tripartite case, we analyze the term proportional to $\bigotimes_i G_0^{(d_i)}$ which must be regularized via the re-scaling procedure.

$$
W_0 = \left(||M||_\infty \sqrt{\prod_{i=1}^{N} \left(d_i - 1 + x_i^2\right)} + M_{I_0} \prod_{i=1}^{N} x_i \right)
$$

$$
= \frac{\left(\prod_{i=1}^{N} \left(d_i - 1 + x_i^2\right) ||M||_\infty^2 - \prod_{i=1}^{N} x_i^2 M_{I_0}^2\right)}{\left(\prod_{i=1}^{N} x_i\right) \left(||M||_\infty \prod_{j=1}^{N} \sqrt{\left(\frac{d_i-1}{x_j^2} + 1\right)} - M_{I_0}\right)}
$$

$$
\sim \frac{\left(r^0 + r^2 + \cdots + r^{2N}\right) - r^{2N}}{r^N}
$$

namely   ∎

$$
\tilde{W}_0 = \frac{||M||_\infty^2 \sum_{j=1}^{N} \prod_{k\neq j}^{N} f_k^2 \left(d_j - 1\right) + \left(\prod_{k=1}^{N} f_k^2\right) ||M||_\infty^2 \eta^2}{\left(\prod_{i=1}^{N} f_i\right) \left(||M||_\infty \prod_{j=1}^{N} \sqrt{\left(\frac{d_i-1}{r^2 f_j^2} + 1\right)} + ||M||_\infty \sqrt{1 - \eta^2/r^2}\right)}.
\tag{1.263}
$$

We are forced to normalized by r^{N-2}, indeed

$$
\tilde{W} = \frac{W}{r^{N-2}} = \frac{\left(O\left(r^0\right) + O\left(r^2\right) + \cdots + O\left(r^{2N-2}\right) + O\left(r^{2N}\right)\right) - O\left(r^{2N}\right)}{O\left(r^{2N-2}\right)}.
\tag{1.264}
$$

For all N the re-normalization is always provided re-scaling by r^{N-2}. Indeed, this is consistent with the case $N = 2, 3$ that previously we found explicitly. In the following we study which are the relevant $k-$tensors in the expression of $\tilde{W}$ for large values of x_i $(i = 1,\dots,N)$ rewritten in $N-$spherical coordinates. Let us start from the vertex of M.

If $\left(||M||_\infty^2 - M_{I_0}^2\right) r^2 = O(1)$, we require

$$
M_{I_0} = -||M||_\infty \sqrt{1 - \eta^2/r^2}.
\tag{1.265}
$$

In fact $\left(||M||_\infty^2 - M_{I_0}^2 \right) r^2 = ||M||_\infty^2 \eta^2$ and

$$\tilde{W}_0^\infty = \frac{||M||_\infty}{2} \left(\sum_{j=1}^N (d_j - 1) \prod_{k \neq j}^N \frac{f_k}{f_j} + \eta^2 \prod_{k=1}^N f_k \right). \tag{1.266}$$

It corresponds, for $N = 3$, to the Eq. 1.228 and it is a finite term after the limit of large x_i's. Moreover, the functions f_i are the angular part of the spherical coordinates

$$f_i = \frac{x_i}{r} = \begin{cases} \prod_{j=1}^{N-1} \sin \theta_j \cos \theta_i & i = 1, \ldots, N - 1 \\ \prod_{j=1}^N \sin \theta_j & i = N \end{cases}. \tag{1.267}$$

In the following we proof this result in a more detailed version.

Proof. Expanding Eq. 1.259 and denoting

$$\mathrm{D} = ||M||_\infty \prod_{j=1}^N \sqrt{\left(\frac{d_j - 1}{x_j^2} + 1 \right)} - M_{I_0} \tag{1.268}$$

then we have

$$\frac{\prod_{i=1}^N \left(d_i - 1 + x_i^2 \right) ||M||_\infty^2 - \prod_{i=1}^N x_i^2 M_{I_0}^2}{r^{N-2} \mathrm{D} \prod_{i=1}^N x_i} = \frac{1}{\prod_{i=1}^N f_i \mathrm{D}}$$
$$\times \left(||M||_\infty^2 \sum_{j=1}^N \prod_{k \neq j}^N f_k^2 (d_j - 1) + r^2 \left(\prod_{k=1}^N f_k^2 \right) \left(||M||_\infty^2 - M_{I_0}^2 \right) \right)$$

If $\left(||M||_\infty^2 - M_{I_0}^2 \right) r^2 = O(1)$, we require

$$M_{I_0} = -||M||_\infty \sqrt{1 - \frac{\eta^2}{r^2}}. \tag{1.269}$$

Indeed $\left(||M||_\infty^2 - M_{I_0}^2 \right) r^2 = ||M||_\infty^2 \eta^2$ and

$$\frac{||M||_\infty^2 \sum_{j=1}^N \prod_{k \neq j}^N f_k^2 (d_j - 1) + \left(\prod_{k=1}^N f_k^2 \right) ||M||_\infty^2 \eta^2}{\left(\prod_{i=1}^N f_i \right) \left(||M||_\infty \prod_{j=1}^N \sqrt{\left(\frac{d_i - 1}{r^2 f_j^2} + 1 \right)} + ||M||_\infty \sqrt{1 - \eta^2/r^2} \right)}$$
$$\sim \frac{||M||_\infty}{2} \left(\sum_{j=1}^N (d_j - 1) \prod_{k \neq j}^N \frac{f_k}{f_j} + \eta^2 \prod_{k=1}^N f_k \right). \tag{1.270}$$

∎

As concern the $W_{i_{j_1}}^{j_1}$, the j_1–th edge defined in Eq. 1.260 we find $W_{i_{j_1}}^{j_1} \sim r^{N-1} M_{I_1\left(i_{j_1} \right)}$, and after the re-scaling by r^{N-2}, we have in spherical coordinates

$$\tilde{W}_{i_{j_1}}^{j_1} = r \left(\prod_{i=1, i \neq j_1}^N f_i \right) M_{I_1\left(i_{j_1} \right)}. \tag{1.271}$$

In order to have a finite limit, each edge $M_{I_1\left(i_{j_1} \right)}$ should goes like r^{-1}. We should apply the condition 1.265 on the convergence of W_0 fixing, as we have already done in the tripartite scenario,

$$||M||_\infty = \sup_{|x^{(1)}| = \cdots = |x^{(N)}| = 1} \left| \sum_{i_1 \ldots i_N} M_{i_1 \ldots i_N} x_{i_1}^{(1)} \cdots x_{i_N}^{(N)} \right| = 1. \tag{1.272}$$

Hence without the supremum the condition on the $N-$rank tensor M is

$$1 \geq \left| \sum_{i_1 \ldots i_N} M_{i_1 \ldots i_N} x_{i_1}^{(1)} \cdots x_{i_N}^{(N)} \right|. \tag{1.273}$$

To determine the condition on the edges, let us consider the j_1–th edge of the tensor, choosing opportunely $x^{(1)}, \ldots, x^{(N)}$. In this way we check if there exists one entry $\alpha \neq 0$ in the $(k-1)$–th position of $x^{(1)}$, where $k \in \{0, \ldots, d_1 - 1\}$

$$x^{(j_1)} = (-1, 0, \ldots \alpha, \ldots, 0) / \sqrt{1 + \alpha^2}, \tag{1.274}$$

$$x^{(k)} = (1, 0, 0, \ldots, 0), \ k = 1, \ldots, N, \ k \neq j_1. \tag{1.275}$$

In the following, we proof that this is not allowed. Notice that $x_0^{(1)} = -1$ because $M_{I_0} = -1$. The condition 1.273 yields

$$\left| \sum_{i_{j_1}} M_{0,\ldots i_{j_1},\ldots 0} x_{i_{j_1}}^{(j_1)} \right| = \left| \frac{1 + \alpha M_{0,\ldots k-1,\ldots 0}}{\sqrt{1 + \alpha^2}} \right| \leq 1 \tag{1.276}$$

$$\sqrt{1 + \alpha^2} \geq |1 + \alpha M_{0,\ldots k-1,\ldots 0}|. \tag{1.277}$$

Therefore, we obtain the same strategies of the three partite case. Hence this concludes the proof that all the edges goes at least like r^{-1}.

Notice that $W_{i_{j_1}, i_{j_2}, \ldots, i_{j_k}}^{j_1, j_2, \ldots, j_k} \sim r^{2-k}$ for $k > 2$, thus the only term which survive is $W_{i_{j_1}, i_{j_2}}^{j_1, j_2}$, which are the faces of the tensor M. Finally we have

$$W^\infty = \tilde{W}_0^\infty \left(\bigotimes G \right)_{I_0} + \sum_{j_1 < j_2} \left(\prod_{i=1, i \neq j_1, j_2}^{N} f_i \right) \sum_{i_{j_1}, i_{j_2}=1}^{d_{j_1}, d_{j_2}} M_{I_2(i_{j_1}, i_{j_2})} \left(\bigotimes G \right)_{I_2(i_{j_1}, i_{j_2})}.$$

We found an extremely interesting result: the most general witness parametrized by the $N-$rank tensor M, in the limit of large $x_i's$ depends only on terms proportional to the vertex M_{I_0} and the $2-$rank tensor $M_{I_2(i_{j_1}, i_{j_2})}$. This is a well candidate to be the $N-$partite family of witnesses of the Enhanced realignment criterion, the strongest effectively computable simplification of Correlation Matrix Criterion, because we proved that for $N = 2$ Enhanced realignment criterion and our *XY-criterion* are equivalent. Even more general, one can study the case without to consider the limit of large x's. Indeed, futher research in this line [70] would be the analysis of the hypercorrelation matrix C^N,

$$||C^N(x_1, \ldots, x_N)||_{\text{tr}} = \sup_M \frac{|\langle M | C^N(x_1, \ldots, x_N) \rangle|}{||M||_\infty}. \tag{1.278}$$

We are sure that the supremum is achieved when M is an isometry. In order to generalize we could start again for $N = 3$. In the following we provide the most abstract definition of isometry.

Definition 1.12.1 We say that M is an isometry iff it belongs to the extremal point of the following convex set of tridimensional tensors, $M \in \text{ext}.\mathscr{I}$, where

$$\mathscr{I} = \{M \in \mathbb{R} \otimes \mathbb{R} \otimes \mathbb{R} : ||M||_\infty \leq 1\}. \tag{1.279}$$

Then the discussion will regard on the characterization of tridimensional isometries $M_{i_1 i_2 i_3}$, in particular we are more interested at the special case of empty interior of $M_{i_1 i_2 i_3}$ (for $i_1, i_2, i_3 > 0$, $M_{i_1 i_2 i_3}$ are zero). Notice that $||M||_\infty = 1$ is not enough to be an isometry because only one singular value is 1, and we don't achieve the maximum number of singular values which is equal to 1. In the bipartite case, not only one singular values must be 1, but all of them. However we can also ask, what is the relation between the bidimensional isometries (e have already characterized) and tridimensional isometries? Are the faces of a tridimensional isometry bidimensional isometries? What is the relation between the edges (for the bipartite case we saw $u = Ov$ in Eq. 1.140)? A prominent insight to understand the extremal points behavior would be the study of three qubit case with M having empty interior, namely

$$||M||_\infty = \sup_{|x^{(i)}|} \left| \sum_{i_1, i_2, i_3}^{*} M_{i_1 i_2 i_3} x_{i_1}^{(1)} x_{i_2}^{(2)} x_{i_3}^{(3)} \right| \tag{1.280}$$

where $\sum_{i_1, i_2, i_3}^{*}$ means that there exists at least one vanishing index. For the future, we have to find if the extremal point of the set of such Mtensor are ruled by some conditions which relate the vertex, edges and faces choosing properly $x^{(i)}$.

1.13 Further studies

"To the uncertainty that rules certainly"

In this section we discuss other non classical resources of quantum mechanics beside the Entanglement, indeed there exists an example which show non locality without entanglement [1]. Moreover, with this research, not only we detect entanglement, but we will try to measure it quantitatively[71]. Then, in the first subsection, we briefly introduce the concept of *contextuality*, as a signature of quantum mechanics. We investigate how it captures the mystery of wave-particle duality in quantum theory and the comparison between local and realistic model, as well as any hidden variable model and a model which admits EPR states.

In the second subsection, we derive a generalization of CHSH scenario.

We start keeping in mind Feynman's words about double–slit experiment to introduce wave–particle duality.

1.13.1 Is wave-particle duality in quantum mechanics captured by Contextuality?

The non causal structure of Quantum Entanglement is administered for quantum technologies as a non classical resource and seems to be the cornerstone in the Young's double–slit experiment on an electron. This is eloquently explicated by Feynman in his third book of celebrated lectures [72]:

"In this chapter we shall tackle immediately the basic element of the mysterious behavior in its most strange form. We choose to examine a phenomenon which is impossible, absolutely impossible, to explain in any classical way, and which has in it the heart of quantum mechanics. In reality, it contains the only mystery. We cannot make the mystery go away by explaining" how it works. We will just tell you how it works. In telling you how it works we will have told you about the basic peculiarities of all quantum mechanics."

Although the double–slit experiment is extremely well-known, let us briefly resume its phenomenology. From Fig. 1.6, input an electron to a plate pierced with two parallel slits of appropriate dimensions and distance between them, then a screen. One performs the experiment many times and if he/she thinks the electron as a bullet, any interference pattern occurs, on the screen. But
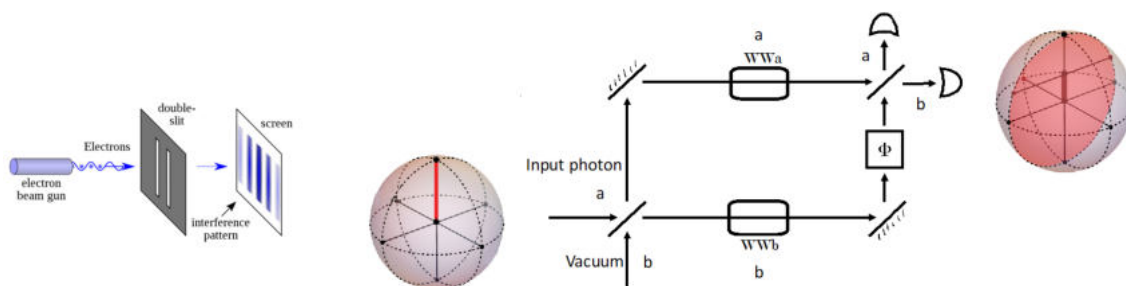
Figure 1.6: Recasting double–slit experiment on the left (Young version) via Mach–Zender interferometer (MZI) on the right. An example of an input quanton in the pure state $|0\rangle\langle 0|$ on the Bloch sphere show decoherence reducing the Bloch radius indicated by a red rod on the xz–plane at the output of the MZI. Along the path *a* and analogously on the path *b* where is placed according a classical statistic distribution a *"which way detector"* which acquires partial information regards from which way the quanton went.

if he/she thinks the electron as a wave, he/she will notice the same behavior of water wave. Surprisingly, the electron seems to show a non local behavior and draw an interference pattern. Even more incredibly, if you put a detector to know which way the particle goes you learn which slit the particle has gone through and you obtain the same pattern that a bullet would draw. This is a particle-like behavior. This aspect puts into question *"What is the true nature of quantum objects?"*, and it is better known as wave/particle duality.

Basically, the action of placing the detector on one of the slits seems to have an instantaneous (non local) influence on the particle, that changes its trajectory depending on the presence or absence of the detector. How can the particle passing through one of the two slits know if the other path has a detector or not? There must be some instantaneous influence from one path to the other. However the same phenomenology of the two slit experiment can be recast into a Mach–Zender interferometer (MZI). If you do not put any detector you see that all photons go to the top detector. You can imagine top detector as the bright fringes of the interference pattern (that get occupied) and the bottom as the dark fringes (that remain empty). This means interference, hence wave behavior. But if you insert a detector on one arm to acquire the which way information all fringes get occupied (particle behavior). In this scenario, we can still wonder how the photon going in one path can know about the detector being present or absent in the other path. It seems that it must know, as its behavior changes accordingly. The argument that we made previously about the non local influence between the two slits runs analogously in terms of the non local influence from one arm of the interferometer to the other.

This example rises up some philosophical implications of quantum mechanics. Perhaps, when philosophical ideas associated with science are dragged into another field, they are usually completely distorted. Therefore we shall confine our remarks as much as possible to physics itself.

In this example, concerning the double-slit experiment comes up the idea of the uncertainty principle (the noncommutativity of observables); the observer is forced into a sort of trade-off disturbance–information and in quantum mechanics there is no way to rearrange the apparatus to decrease the disturbance of the measurement.

However, if the basis of a science is its ability to predict, quantum mechanics fits very well with this task in two-slit experiment. In this sense it is an operational theory. Anyway operationalism is not enough. Still explanations are required in a ontological description of the nature. In this direction, the notion of *Quantum Contextuality* rises up the constrains for a realistic model which tries to explain the predictions of the experiments which involve quantum phenomena, as well as, the two-slit experiment[73].

Contextuality means that if you have two equivalent experimental procedures, there exist two different probability distribution in the hidden variable model (ontological model)

Quantum Contextuality is consider to be the leading notion of nonclassicality and in the following we explain how it captures the mistery of wave–particle duality in quantum mechanics. We need to find two equivalent experimental preparations for a quantum state which corresponds to write it in two different decompositions. Finally, the task is to prove that such decompositions are different in the hidden variable model, although they represent the same state.

Contextuality

Operational equivalence maps into ontological equivalence – noncontextuality or classical understanding requires Leibniz's indiscernible principle[74]: given two object x, y, if for every property F, x has F iff y has F, then x is ontological identical to y.

$$\forall F \quad (Fx \leftrightarrow Fy) \rightarrow x = y. \tag{1.281}$$

When the principle holds we are in the classical or noncontextual regime, when it fails we say that the model is contextual, e.g. quantum models. Nevertheless, contextuality emerges when one would describe an ontological reality via operationalism. If we will be able to show quantitatively the dependence of the context, then we can states to assist to a quantum signature. One of the early notion of noncontextual model comes from Bell-Kochen-Specker.

> **Definition 1.13.1** (Bell-Kochen-Specker) Given A, B, C Hermitian operators such that $[A, B] = [A, C] = 0$, but $[B, C] \neq 0$, in a noncontextual hidden variable model of quantum theory the value predicted to occur in a measurement of A does not depend on wheter B or C was measured simultaneously.

However we refer to Spekkens' notion[75]

> **Definition 1.13.2** A *noncontextual ontological model of an operational theory* is one wherein if two experimental procedures are operationally equivalent, then they have equivalent representation in the ontological model.

The role of an operational theory is merely to specify the probability $p(k|, P, T, M)$ of different outcomes k that may result from a measurement procedure M, given a particular preparation P and a particular transformation T.

> **Definition 1.13.3** Equivalence class of preparations, transformations, measurements and experimental procedure. The equivalence relation of the equivalence class is pointed out with this symbol $\sim$.

- $P \sim P' \Leftrightarrow p(k|, P, T, M) = p(k|, P', T, M) \qquad \forall T, M$
- $T \sim T' \Leftrightarrow p(k|, P, T, M) = p(k|, P, T', M) \qquad \forall P, M$
- $M \sim M' \Leftrightarrow p(k|, P, T, M) = p(k|, P, T, M') \qquad \forall P, T$
- $(P, T, M) \sim (P', T', M') \Leftrightarrow p(k|, P, T, M) = p(k|, P', T', M')$.

Then a *noncontextual ontological model of an operational theory* is an attempt to offer an explanation of the success by assuming that there exist physical systems that are the subject of the experiment. These systems are presumed to have attributes which describe the real state of affairs of the system. Thus, a specification of which instance of each attribute applies at a give time we call the *ontic state* λ of the system[2]

---

[2]Essentially, you reckon with the ontic, you understand the ontological: the ontic is something adequately grasped by something like counting, while the ontological is something grasped only adequately when it is seen and participated in as significant.

Now, we mathematically expose the ontological model for an operational theory. We shall denoted the complete set of the variables in an ontological model by $\lambda \in \Lambda$, and the space of values of λ by Ω. Given an ontological model we say that

- for an operational preparation P, the probability measurement $\mu_P(\lambda)$ on the ontic states is determined. $\mu_P : \Omega \mapsto [0,1]$, $\int_\Lambda \mu_P(\lambda)\,d\lambda = 1$.
- for an operational measurement M, the probability of obtaining the outcomes labelled by k are determined by a set of indicator function $\{\xi_{M,k}(\lambda)\}_k$ over the ontic states, $\xi_{M,k} : \Omega \mapsto [0,1]$ such that $\sum_k \xi_{M,k}(\lambda) = 1, \quad \forall \lambda$.
- for an operational transformation T, the transition from the ontic state λ to the ontic state λ' is determined by $\Gamma_T : \Omega \times \Omega \mapsto [0,1]$ such that $\forall \lambda : \int_\Lambda \Gamma(\lambda',\lambda)\,d\lambda' = 1$.

The predictions of the operational theory are reproduced exactly by the ontological model for all P, M, T

$$p(k|P,T,M) = \int_{\Lambda^2} \mu_P(\lambda) \Gamma_T(\lambda',\lambda) \xi_{M,k}(\lambda')\,d\lambda d\lambda'. \tag{1.282}$$

We say that two procedures are equivalent $(P,T,M) \sim (P,T,M)'$ because they prepare the ontic state of the system in precisely the same way. In the following, we will focus on the a preparation non contextual model. We naturally assume the following lemma[75].

Lemma 1.13.1 (distinguishability) If two preparation procedures P and P' are distinguishable in a single-shot measurement, then $\mu_P(\lambda)\mu_{P'}(\lambda) = 0 \,\forall \lambda \in \Lambda$ (nonoverlapping).

Lemma 1.13.2 (convex combination) Given two preparation procedures P and P', which respectively correspond on the ontological model the distribution $\mu_P(\lambda)$ and $\mu_{P'}(\lambda)$, we can build P'' tossing a coin uniformly random distributed which give P with probability p and P' with probability p'. The distribution on the ontological model for P'' is $\mu_{P''}(\lambda) = p\mu_P(\lambda) + (1-p)\mu_{P'}(\lambda)$. The convex sum for arbitrary preparation is an easy iteration.

Now, we apply such concepts to study of *wave-particle duality* in quantum mechanics on a quantum object called *"quanton"* in the Mach Zender interferometer MZI coupled with a which way detector. Both, the quanton and the detector are legitimate qubits with the initial density matrix respectively given by $\rho_Q^{(i)}$ and $\rho_D^{(i)}$. For a symmetric interferometer

$$\rho_Q^{(i)} = \frac{1}{2}\left(\mathbf{1} + \boldsymbol{s}^{(i)} \cdot \boldsymbol{\sigma}\right), \, s_x^{(i)} = 0, \, s_z^{(i)} + i s_y^{(i)} = e^{-i\theta}. \tag{1.283}$$

For simplicity we consider $\theta = 0$, hence $\rho_Q^{(i)}$ has Bloch vector $\boldsymbol{s}^{(i)} = (0,0,1)$ as in Fig 1.6. The interaction of the MZI is given by the action of two beam splitter, given by the unitary U_{BS} and a central transformation U_C as follows

$$U_{\mathrm{BS}} = e^{-i\frac{\pi}{4}\sigma_y} = \frac{1}{\sqrt{2}}\left(\mathbf{1}_2 + \sigma_y\right) \tag{1.284}$$

$$U_C = \frac{\mathbf{1}_2 + \sigma_z}{2} e^{i\phi_a/2\sigma_z} \otimes U_a + \frac{\mathbf{1}_2 - \sigma_z}{2} e^{-i\phi_b/2\sigma_z} \otimes U_b. \tag{1.285}$$

If we define $U_{\mathrm{MZI}} = U_{\mathrm{BS}} U_C U_{\mathrm{BS}}$, we have $\rho^{(f)} = U_{\mathrm{MZI}}\left(\rho_Q^{(i)} \otimes \rho_D^{(i)}\right) U_{\mathrm{MZI}}^\dagger$ which yields

$$\begin{aligned}
\rho^{(f)} = &\frac{1+\sigma_x}{4} \otimes U_a \rho_D^{(i)} U_a^\dagger + \frac{1-\sigma_x}{4} \otimes U_b \rho_D^{(i)} U_b^\dagger \\
&- \frac{\sigma_z - i\sigma_y}{4} \otimes e^{i\left(\frac{\phi_a+\phi_b}{2}+\theta\right)} U_a \rho_D^{(i)} U_b^\dagger - \frac{\sigma_z + i\sigma_y}{4} \otimes e^{-i\left(\frac{\phi_a+\phi_b}{2}+\theta\right)} U_b \rho_D^{(i)} U_a^\dagger.
\end{aligned} \tag{1.286}$$

Then, we have

$$\rho_Q^{(f)} = \mathrm{Tr}_D \rho^{(f)} = \frac{1}{2}\left(1 + \boldsymbol{s}^{(f)} \cdot \boldsymbol{\sigma}\right), \tag{1.287}$$

$$s_x^{(f)} = 0, s_z^{(f)} + i s_y^{(f)} = -e^{-i\left(\frac{\phi_a+\phi_b}{2}+\theta\right)}\mathrm{Tr}U_a \rho_D^{(i)} U_b^\dagger, \tag{1.288}$$

$$\rho_D^{(f)} = \mathrm{Tr}_Q \rho^{(f)} = \frac{1}{2}\left(U_b^\dagger \rho_D^{(i)} U_b + U_a^\dagger \rho_D^{(i)} U_a\right). \tag{1.289}$$

Notice that $\theta, \phi_a, \phi_b = 0$ implies $s_y = 0$ and the action of the MZI on the quanton reduces the Bloch ray of an amount of $\left|\boldsymbol{s}^{(f)}\right| = \left|s_z^{(f)}\right| = \mathrm{Tr}U_a^\dagger \rho_D^{(i)} U_b$ along the z–component and equally distribute the final state of the detector $\rho_D^{(f)}$ in two possible rotations according to the unitary matrices U_a and U_b. In quantum mechanics, we define the visibility of the interference fringes and the distinguishability of the which way as follows

$$\mathscr{V} = \left|\mathrm{Tr}U_a^\dagger \rho_D^{(i)} U_b\right|, \tag{1.290}$$

$$\mathscr{D} = \frac{1}{2}||U_b^\dagger \rho_D^{(i)} U_b - U_a^\dagger \rho_D^{(i)} U_a||_1. \tag{1.291}$$

Now we want to find a connection with the contextuality. Recall, the existence of a preparation noncontextual model for a single system $\rho_D^{(f)}$ implies the existence of a locally causal model for any bipartite scenario involving that system. In other words, any bipartite proof of Bell's theorem is a proof of preparation contextuality. The contrary is not guaranteed. Nevertheless, the existence of a preparation noncontextual model for four preparations and two tomographically complete binary measurements is equivalent to the existence of a Bell local model in the scenario considered by CHSH. Let us define the amout S concerning four preparation and two measurements

$$\begin{aligned} S = &p_1 P\left(0|\rho_1,X\right) + (1-p_1)P\left(1|\rho_3,X\right) + p_2 P\left(0|\rho_2,X\right) + (1-p_2)P\left(1|\rho_4,X\right) \\ &+ p_1 P\left(0|\rho_1,Z\right) + (1-p_1)P\left(1|\rho_3,Z\right) + p_2 P\left(1|\rho_2,Z\right) + (1-p_2)P\left(0|\rho_4,Z\right), \end{aligned}$$

> **Theorem 1.13.3** Quantitatively a preparation noncontextual model satisfies
>
> $$S \leq 3, \tag{1.292}$$
>
> therefore if $S > 3$ the notion of contextuality is required in the model.

Now, we know that a nonlocal and noncontextual ontological model satisfies the Englert inequality

$$\mathscr{D}^2 + \mathscr{V}^2 \leq 1. \tag{1.293}$$

but only for values of $(\mathscr{D}, \mathscr{V}) = (1,0) \wedge (0,1)$. If one consider, as in our case a pure state for the initial state of detector $\rho_D^{(i)} = |d\rangle\langle d|$ then $\mathscr{D}^2 + \mathscr{V}^2 = 1$.

Ⓡ   If $U_a = \pm U_b$ and the initial state is $\rho_Q^{(i)} = |0\rangle\langle 0|$, then the final bipartite state is respectively

$$|0\rangle \otimes U_b |d\rangle, \qquad |1\rangle \otimes U_b |d\rangle. \tag{1.294}$$

Notice that, the final state is separable and the concurrence is vanishing[76]. Moreover from the definition

$$\mathscr{V} = \left| \mathrm{Tr} U_a^\dagger |d\rangle \langle d| U_b \right| = 1 \tag{1.295}$$

$$\mathscr{D} = \frac{1}{2} ||U_b^\dagger |d\rangle \langle d| U_b - U_a^\dagger |d\rangle \langle d| U_a||_1 = 0. \tag{1.296}$$

On contrary, if $U_b U_a^\dagger = 0$ the final state must correspond to the maximally entangled state, $\mathscr{V} = 0$ and from the property that [77]

$$AB^\dagger = 0 \Longleftrightarrow ||A - B||_1 = ||A||_1 + ||B||_1 \tag{1.297}$$

we have

$$\mathscr{D} = \frac{1}{2} ||U_b^\dagger |d\rangle \langle d| U_b||_1 + ||U_a^\dagger |d\rangle \langle d| U_a||_1 = 1. \tag{1.298}$$

In the end, we have to find due decompositions which correspond to the intermediate stage $U_b U_a^\dagger \neq 0$ such that $\mathscr{D}, \mathscr{V} \in (0,1)$ and $\mathscr{D}^2 + \mathscr{V}^2 = 1$ and violate Pusey's inequality. Another possibility is to derive a proof of contextuality from the trade–off disturbance information as in [78]. Besides this tools, in order to prove contextuality, here we might apply another idea. We observe that the problem to distinguish the way of the quanton in the MZI can be a consequence of No-Cloning theorem [79], namely we cannot identify a given state drawn from a set of non-orthogonal states with certainty using a single copy. The Unambiguous Quantum State Discrimination (UQSD) deals with number of copies required so as to identify such a state drawn from a set of non-orthogonal states though not certainly but with some probability and express the visibility in terms of confusability as in Refs. [80, 81].

1.13.2 A new way to derive Bell inequalities

Bell inequalities in the bipartite case lead to a Bell witness to detect entanglement [37]. In this section, we would derive a general Bell inequality in order to construct a new family of multipartite entanglement witnesses. Indeed, the original Bell inequality which is based on the perfect anti-correlations of the so called singlet state, was extended by Clauser, Horne, Shimony and Holt to a more general inequality based on a local realistic model for two observers, each having the choice of two measurements settings with two outcomes. A violation of the inequality means there exist quantum predictions for correlation functions which describe the above situation which are not reproducible by local realistic models. Let us A_i and B_i $(i = 1, 2)$ two dichotomic measurements for Alice and for Bob respectively. Now if the physics can be described by a local and realistic model, or any *local hidden variable model* the following inequality must be satisfied

$$\langle A_1, B_1 \rangle + \langle A_1, B_2 \rangle + \langle A_2, B_1 \rangle - \langle A_2, B_2 \rangle \leq 2 \tag{1.299}$$

where $\langle A_i, B_j \rangle$ is the expectation value of the correlation experiment $A_i \otimes B_j$. For the two qubit case one introduce the following CHSH operator

$$B_{\mathrm{CHSH}} = \boldsymbol{a}_1 \boldsymbol{\sigma} \otimes (\boldsymbol{b}_1 + \boldsymbol{b}_2) \boldsymbol{\sigma} + \boldsymbol{a}_2 \boldsymbol{\sigma} \otimes (\boldsymbol{b}_1 - \boldsymbol{b}_2) \boldsymbol{\sigma} \tag{1.300}$$

with $\boldsymbol{a}_i, \boldsymbol{b}_i \in \mathbb{R}^3$ for $(i = 1, 2)$ and $\boldsymbol{\sigma} = (\sigma_1, \sigma_2, \sigma_3)$ is the vector of Pauli matrices. The CHSH inequality requires that

$$\mathrm{Tr}(B_{\mathrm{CHSH}} \rho_{\mathrm{LHV}}) \leq 2 \tag{1.301}$$

is fulfilled for all two qubit states ρ_{LHV} states and which can be constructed as follows

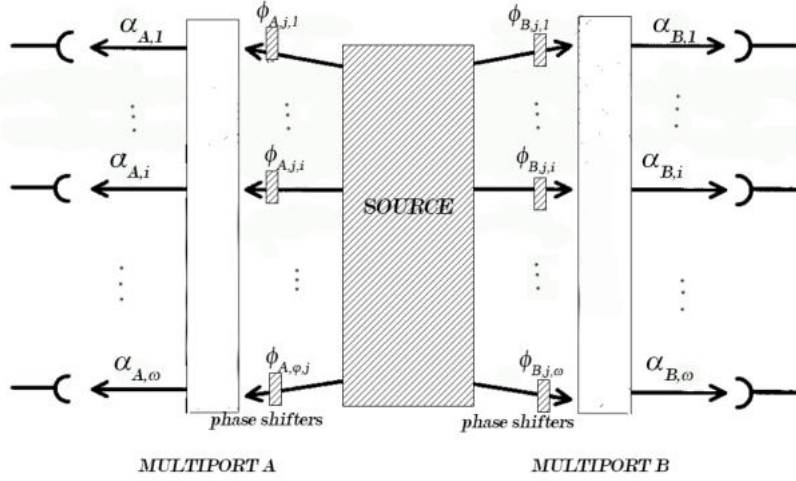$$W_{\mathrm{CHSH}} = 2\mathbf{1}_2 \otimes \mathbf{1}_2 - B_{\mathrm{CHSH}}. \tag{1.302}$$

Figure 1.7: An example with 2 multiports ($v = A, B$) with 2ω pins (input+output) and σ different settings. Even if there are ω pins as output, only one detector will give a click. (In the picture the counter starts from 1).

Properly W_{CHSH} is a "non-local witness", that is, if $\langle W_{\text{CHSH}}\rangle_\rho < 0$ then ρ cannot be relied to a LHV model. However if non-locality implies entanglement, then it is also an entanglement witness. Any bipartite Bell inequality may be in the following form

$$\sum_{i,j} \lambda_{ij} \langle A_i, B_j \rangle \leq c \tag{1.303}$$

for two family of local observables $A_i \in \mathscr{B}(\mathscr{H}_A)$ and $B_i \in \mathscr{B}(\mathscr{H}_B)$ and the corresponding witness may be

$$W = c\mathbf{1}_2 \otimes \mathbf{1}_2 - \sum_{i,j} \lambda_{ij} \langle A_i, B_j \rangle \tag{1.304}$$

It was conjectured by Peres that for a bipartite scenario a PPT state can not violate any Bell inequality. If the conjecture is true then all entangled witnesses constructed out of the Bell inequalities are decomposable [82, 36].

The key idea to generalize a CHSH scenario is based on the correlation function and on the conjugate basis. For the definition of correlation function of two outcomes situation we use original Bell's idea to use roots of unity to represent the results $\pm 1 = e^{-i\frac{2\pi}{2}x}$, with $x = 1, 2$. Notice that such are the functions used to get the discrete Fourier transforms

$$f(k) = \sum_{x=0}^{d-1} F(x)e^{i\frac{2\pi}{d}xk}. \tag{1.305}$$

In the most general Bell scenario we have v parties σ settings (a family of phase shifters), with ω phase shifters in the ω input ports $\left\{\vec{\phi}_{\mu,j}\right\}_{\mu=0,j=0}^{v-1,\sigma-1} = \left\{\phi_{\mu,j,i}\right\}_{\mu=0,j=0,i=0}^{v-1,\sigma-1,\omega-1}$ and ω possible outcomes $\left\{k_{\mu,i}\right\}_{\mu=0,i=0}^{v-1,\omega-1} \leftrightarrow \left\{\alpha_{\mu,i}\right\}_{\mu=0,i=0}^{v-1,\omega-1}$. Fixing $\phi_{\mu,j,i} \in [0, 2\pi]$ we choose μ-th multiport, the j-th setting and the i-th input port that rotates the state by the angle $\phi_{\mu,j,i}$. Each multiport has ω pins output and only one gives the click in the detector which records $k_{\mu,i}$ in 1-to-1 correspondence with the Bell numbers $\alpha_{\mu i}$ (see fig. 1.7). Therefore running many times the experiment we know *the a priori* distribution $P\left(k_{0,i_0}, \ldots, k_{v-1,i_{v-1}} | \phi_{0,j_0,i_0}, \ldots, \phi_{v-1,j_{v-1},i_{v-1}}\right)$ for $i_0, \ldots, i_{v-1} \in \{0, \ldots, \omega-1\}$ and $j_0, \ldots, j_{v-1} \in \{0, \ldots, \sigma-1\}$ which is the probability to get outcome k_{0,i_0} given the settings

$\vec{\phi}_{0,j_0}$ in the multiport 0-th;$\ldots$;$k_{v-1,i_{v-1}}$ given the settings $\vec{\phi}_{v-1,j_{v-1}}$ in the multiport $v-1$-th. The local hidden variable model in its correlation function $\mathscr{E}$ describes all possible already establish (real) possibilities without any nonlocal influence the assumption of realism. Therefore

$$
\mathscr{E}_{LR} = \underbrace{\sum_{i_{0,0}=0}^{\omega-1} \cdots \sum_{i_{0,\sigma-1}=0}^{\omega-1}}_{\sigma \text{ times}} ;\ldots \underbrace{\sum_{i_{v-1,0}=0}^{\omega-1} \cdots \sum_{i_{v-1,\sigma-1}=0}^{\omega-1}}_{\sigma \text{times}} p_{i_{0,0},\ldots i_{0,\sigma-1};\ldots;i_{v-1,0},\ldots i_{v-1,\sigma-1}}
$$

$$
\times \overbrace{\underbrace{\begin{pmatrix} \alpha^{i_{0,0}} \\ \vdots \\ \alpha^{i_{0,\sigma-1}} \end{pmatrix}}_{\sigma-\text{lenght}} \otimes \cdots \otimes \underbrace{\begin{pmatrix} \alpha^{i_{0,v-1}} \\ \vdots \\ \alpha^{i_{v-1,\sigma-1}} \end{pmatrix}}_{\sigma-\text{lenght}}}^{v-\text{length}} \tag{1.306}
$$

In a more fashionable form $P\left(k_0,\ldots,k_{v-1}\middle|\vec{\phi}_{0,j_0},\ldots,\vec{\phi}_{v-1,j_{v-1}}\right) = p_{i_{0,0}\ldots i_{0,\sigma-1};\ldots i_{v-1,0}\ldots i_{v-1,\sigma-1}} \equiv p_{i_{\mu,j}}$ which sum to 1 ($\sum_{\mu=0}^{v-1}\sum_{j=0}^{\sigma-1}\sum_{i_{j,\mu}=0}^{\omega-1} p_{i_{\mu,j}} = 1$). Notice that the notation $k_\mu \equiv k_{\mu,i_\mu}$ tell us the outcome k_μ among all possible k_{μ,i_μ}. The number of configurations are $\omega^{\sigma v}$. For example, in the case $(v=2, \sigma=4, \omega=4)$ we have

$$
\mathscr{E}_{LR}^{2,4,4} = \sum_{\mu=0}^{1}\sum_{j=0}^{3}\sum_{i_{j,\mu}=0}^{3} p_{i_{\mu,j}} \begin{pmatrix} \alpha^{i_{0,0}} \\ \alpha^{i_{0,1}} \\ \alpha^{i_{0,2}} \\ \alpha^{i_{0,3}} \end{pmatrix} \otimes \begin{pmatrix} \alpha^{i_{1,0}} \\ \alpha^{i_{1,1}} \\ \alpha^{i_{1,2}} \\ \alpha^{i_{1,3}} \end{pmatrix}
$$

$$
= \sum_{i_{0,0},i_{0,1},i_{0,2},i_{0,3}=0}^{3} \sum_{i_{1,0},i_{1,1},i_{1,2},i_{1,3}=0}^{3} p_{i_{0,0},i_{0,1},i_{0,2},i_{0,3};i_{1,0},i_{1,1},i_{1,2},i_{1,3}}
$$

$$
\times \begin{pmatrix} \alpha^{i_{0,0}} \\ \alpha^{i_{0,1}} \\ \alpha^{i_{0,2}} \\ \alpha^{i_{0,3}} \end{pmatrix} \otimes \begin{pmatrix} \alpha^{i_{1,0}} \\ \alpha^{i_{1,1}} \\ \alpha^{i_{1,2}} \\ \alpha^{i_{1,3}} \end{pmatrix} .
$$

We are interested to the distributions that realized only 1 configuration with weight of probability 1and all other configuration with probability weight equal to 0 to happen. This corresponds to achieve the upper and lower bound in the functional K, that we will introduce in a while. Let us see what happens for the EPR state in quantum mechanics, as in Ref. [83] we have

$$
|\psi\rangle = \frac{1}{\sqrt{\omega}} \sum_{i=0}^{\omega-1} \bigotimes_{\mu=0}^{v-1} |i\rangle \tag{1.307}
$$

after the action of the phase shifters we have

$$
|\psi'\rangle = \frac{1}{\sqrt{\omega}} \sum_{i=0}^{\omega-1} \bigotimes_{\mu=0}^{v-1} e^{i\phi_{\mu,j_\mu,i}} |i\rangle \tag{1.308}
$$

and

$$
U_{ij}^{\omega} = \frac{\gamma_{\omega}^{(i-1)(j-1)}}{\sqrt{\omega}}, \quad \gamma_{\omega} = e^{i\frac{2\pi}{\omega}} . \tag{1.309}
$$

Therefore

$$P\left(k_0,\ldots,k_{\nu-1}|\vec{\phi}_{0,j_0},\ldots,\vec{\phi}_{\nu-1,j_{\nu-1}}\right) = \left|\left\langle k_{0,i_0},\ldots,k_{\nu-1,i_{\nu-1}}|\underbrace{U\otimes\cdots\otimes U}_{\nu\ \text{times}}|\psi'_j\right\rangle\right|^2$$

$$= \frac{1}{\omega^{\nu+1}}\sum_{i=0}^{\omega-1}\sum_{i'=0}^{\omega-1}e^{i\Sigma_{\mu=0}^{\nu-1}\left(\phi_{\mu,j_\mu,i}-\phi_{\mu,j_\mu,i'}\right)}\prod_{\mu=0}^{\nu-1}\gamma_\omega^{(k_\mu-1)(i-i')} \tag{1.310}$$

From the definition

$$\mathscr{E}_{MQ}\left(\vec{\phi}_{0,j_0},\ldots,\vec{\phi}_{\nu-1,j_{\nu-1}}\right) = \sum_{k_0,\ldots k_{\nu-1}}\prod_{\mu=0}^{\nu-1}\gamma_\omega^{k_\mu-1}P\left(k_0,\ldots,k_{\nu-1}|\vec{\phi}_{0,j_0},\ldots,\vec{\phi}_{\nu-1,j_{\nu-1}}\right) \tag{1.311}$$

which leads to

$$\mathscr{E}_{MQ}\left(\vec{\phi}_{0,j_0},\ldots,\vec{\phi}_{\nu-1,j_{\nu-1}}\right) = \frac{1}{\omega}\sum_{i=0}^{\omega-1}e^{i\Sigma_{\mu=0}^{\nu-1}\phi_{\mu,j_\mu,(i,i+1)}} = \mathscr{E}_{MQj_0,\ldots j_{\nu-1}} \tag{1.312}$$

with $\phi_{\mu,j,(i,i+1)} = \phi_{\mu,j,i} - \phi_{\mu,j,i+1}$. In the case $(\nu=2,\sigma=4,\omega=4)$ we have

$$\mathscr{E}_{MQ} = \begin{pmatrix} E\left(\vec{\phi}_{0,0};\vec{\phi}_{1,0}\right) & E\left(\vec{\phi}_{0,0};\vec{\phi}_{1,1}\right) & E\left(\vec{\phi}_{0,0};\vec{\phi}_{1,2}\right) & E\left(\vec{\phi}_{0,0};\vec{\phi}_{1,3}\right) \\ E\left(\vec{\phi}_{0,1};\vec{\phi}_{1,0}\right) & E\left(\vec{\phi}_{0,1};\vec{\phi}_{1,1}\right) & E\left(\vec{\phi}_{0,1};\vec{\phi}_{1,2}\right) & E\left(\vec{\phi}_{0,1};\vec{\phi}_{1,3}\right) \\ E\left(\vec{\phi}_{0,2};\vec{\phi}_{1,0}\right) & E\left(\vec{\phi}_{0,2};\vec{\phi}_{1,1}\right) & E\left(\vec{\phi}_{0,2};\vec{\phi}_{1,2}\right) & E\left(\vec{\phi}_{0,2};\vec{\phi}_{1,3}\right) \\ E\left(\vec{\phi}_{0,3};\vec{\phi}_{1,0}\right) & E\left(\vec{\phi}_{0,3};\vec{\phi}_{1,1}\right) & E\left(\vec{\phi}_{0,3};\vec{\phi}_{1,2}\right) & E\left(\vec{\phi}_{0,3};\vec{\phi}_{1,3}\right) \end{pmatrix}$$

$$=\text{Map}\left[E,\begin{pmatrix} \vec{\phi}_{0,0} \\ \vec{\phi}_{0,1} \\ \vec{\phi}_{0,2} \\ \vec{\phi}_{0,3}=1 \end{pmatrix}\otimes\begin{pmatrix} \vec{\phi}_{1,0} \\ \vec{\phi}_{1,1} \\ \vec{\phi}_{1,2} \\ \vec{\phi}_{1,3}=1 \end{pmatrix}\right]\equiv\mathscr{E}_{MQ}^{2,4,4}\left(\phi_{\mu,j,i}\right).$$

Since we are interested only to relative phase for each multiport we can put $\vec{\phi}_{0,3} = \vec{\phi}_{1,3} = 1$. Let me define the functional

$$K:\mathscr{T}_{\nu,\sigma,\omega} \mapsto \mathbb{R}$$
$$\mathscr{E} \mapsto K[\mathscr{E}] = \text{Re}[\mathscr{E}\cdot\mathscr{S}] \tag{1.313}$$

where $\alpha = \gamma_\omega$

$$\mathscr{S}_{\nu,\sigma,\omega}(n,\tau) = e^{i\frac{2\pi n}{f}}\sum_{\mu_0\ldots\mu_{\nu-1}=0}^{\omega-1}\alpha_\omega^{t(\mu_0,\ldots,\mu_{\nu-1})}\bigotimes_{m=0}^{\mu}\begin{pmatrix} \alpha^{q(\{\mu\})} \\ \alpha^{q(\{\mu\})} \\ \vdots \\ \alpha^{q(\{\mu\})} \end{pmatrix} \tag{1.314}$$

with f is the *"finer"* since it splits the unit circle in regular polygonal with roofs of unity as vertex and $q\{\mu\}$ is a generic function. For the case of $\nu=2$, σ settings and ω outcomes, it reduces to the following expression

$$\mathscr{S}_{2,\sigma,\omega} = e^{i\frac{2\pi n}{f}}\sum_{\mu_0\ldots\mu_{\nu-1}=0}^{\omega-1}\alpha_\omega^{t(\mu_0,\ldots,\mu_{\nu-1})}\begin{pmatrix} \alpha^{0*\mu_m} \\ \alpha^{1*\mu_m} \\ \vdots \\ \alpha^{(\sigma-1)\mu_m} \end{pmatrix}\otimes\begin{pmatrix} \alpha^{-0*\mu_m} \\ \alpha^{-1*\mu_m} \\ \vdots \\ \alpha^{-(\sigma-1)\mu_m} \end{pmatrix}. \tag{1.315}$$

Our aim is to compare to maximize and minimize the functionals $K\left[\mathscr{E}_{MQ}^{\mu,\sigma,\omega}\right]$ and $K\left[\mathscr{E}_{LR}^{\mu,\sigma,\omega}\right]$ and to find the maximal violation of Bell inequality entails in the following number

$$\frac{K\left[\mathscr{E}_{MQ}^{\mu,\sigma,\omega}\right] - K\left[\mathscr{E}_{LR}^{\mu,\sigma,\omega}\right]}{K\left[\mathscr{E}_{LR}^{\mu,\sigma,\omega}\right]}. \tag{1.316}$$

Our final results are

$$\frac{K\left[\mathscr{E}_{MQ}^{2,3,3}\right] - K\left[\mathscr{E}_{LR}^{2,3,3}\right]}{K\left[\mathscr{E}_{LR}^{2,3,3}\right]} = 0.14075. \tag{1.317}$$

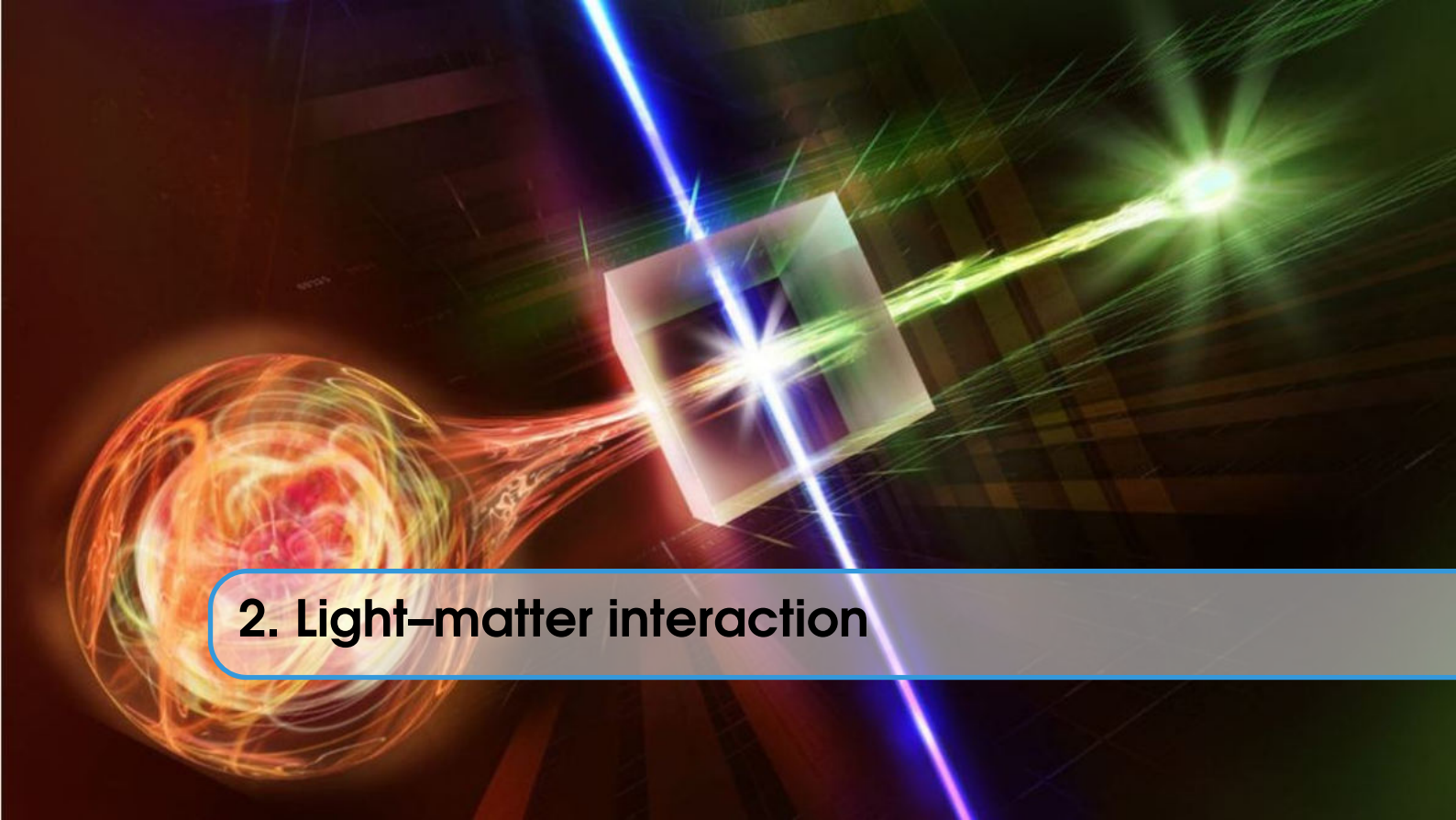$$\frac{K\left[\mathscr{E}_{MQ}^{2,4,4}\right] - K\left[\mathscr{E}_{LR}^{2,4,4}\right]}{K\left[\mathscr{E}_{LR}^{2,4,4}\right]} = \sqrt{2} - 1. \tag{1.318}$$

In conclusion we can pursue this direction obtaining a Bell operator in order to control the violation among all quantum pure states, rather than the only GHZ state (the maximal entangled state). A nice inset comes from the follow Ref. [84].

Part Two

2. Light–matter interaction

"If I were forced to sum up in one sentence what Copenhagen interpretation says to me, it would be – Shut up and calculate – ."(D. Mermin)

*S*pacetime is the ordinary environment for accommodating our scenarios. In this framework that we try to explain the entanglement, nonlocality, contextuality and all physical scenarios. Nothing else might be replace spacetime in its ordinary form. Unless we do not think deeper the notion of *tranquil nothingness*. The project of this chapter started with will to acquire knowledge on the fluctuating quantum vacuum and its fundamental processes which is based the quantum electrodynamics (QED). Then, we distinguish the vacuum electromagnetic field and the effective electromagnetic field in the presence of a dispersive environment which interacts with a quantum system.

Therefore, we study physical process involving QED vacuum effects, as well as, spontaneous emission, Lamb shift, van der Waals forces and the fundamental linewidth of a laser and the relation between vacuum and source fields[85].

We are also motivated to realize physical experiment to prepare quantum entanglement state that we showed in the previous chapter. Interestingly, when two quantum emitters are embedded in a taylored environment the pair can spontaneously relax towards an entangled state. However, in the following we construct the theory only for one emitter introducing a second emitter in future research for studying the entanglement in cavity systems.

Firstly, we expand the theory of light-matter interactions to include the spatial extension of the system, taken into account through its wavefunctions. We show that this ingredient enables us to overcome the divergence problem related to the Green tensor propagator and to develop a theory beyond the point-dipole approximation. In particular, the inclusion of the spatial structure of the atomic system involve also asymmetric quantum system with respect to spatial inversion and explain the role of this asymmetric effects in interaction with the host medium which acts on the system by *Van der Vaals forces*[86].
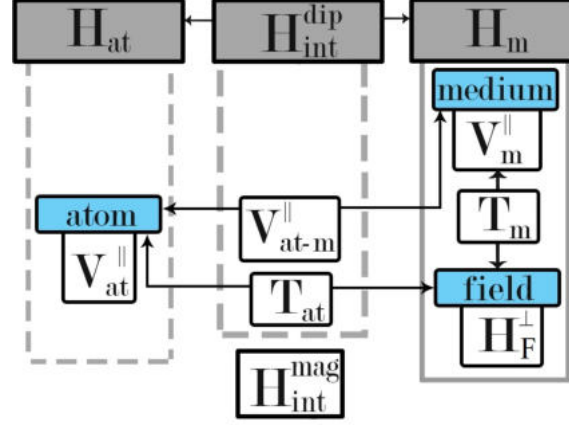
Figure 2.1: Graphic view of the total Hamiltonian. In blue, the atomic $V_{\mathrm{at}}^{\parallel}$, the medium $V_{\mathrm{m}}^{\parallel}$ [Eq. 2.2], and the field $H_{\mathrm{f}}^{\perp}$ [Eq. 2.5] Hamiltonians. The blue blocks are connected by the interaction blocks. Hence T_{m} and T_{at} connect the medium and the atom, respectively, with the field as in Eq. 2.4, and $V_{\mathrm{at\text{-}m}}^{\parallel}$ connects the atom and the medium, as in Eq. 2.3. These six terms appear in Eq. 2.1. The medium-assisted field H_{m} [Eq. 2.15] arises from the terms $V_{\mathrm{m}}^{\parallel}$, T_{m} and $H_{\mathrm{f}}^{\perp}$ (solid box on the right), and the atomic Hamiltonian becomes H_{at} via the PZW transformation [Eq. 2.11] (dashed box on the left). H_{at} interacts with H_{m} thru H_{int} as in Eq. 2.28. By neglecting the magnetic properties one obtains $H_{\mathrm{int}}^{\mathrm{dip}}$, which completes the model investigated.

2.1 Spontaneous emission in dispersive media

We start from a first-principle Hamiltonian where positive and negative charges of the atomic system and the medium are coupled with the electromagnetic field. If the focus is on the atomic dynamics, the system can be conveniently modeled by coupling the atom to a *medium-assisted* electromagnetic field, which is dressed by the interaction with the hosting medium (see Fig. 2.1). Let us consider the Coulomb-gauge Hamiltonian [87, 88], separating the longitudinal and transverse contributions

$$H = V_{\mathrm{at}}^{\parallel} + V_{\mathrm{m}}^{\parallel} + V_{\mathrm{at\text{-}m}}^{\parallel} + T_{\mathrm{at}} + T_{\mathrm{m}} + H_{\mathrm{F}}^{\perp}. \tag{2.1}$$

Atomic charges will be labelled by roman indices j, k and the charges of the medium by greek indices μ, ν. The terms

$$V_{\mathrm{at}}^{\parallel} = \frac{1}{8\pi\varepsilon_0} \sum_{j \neq k} \frac{Q_j Q_k}{|\boldsymbol{r}_j - \boldsymbol{r}_k|}, \qquad V_{\mathrm{m}}^{\parallel} = \frac{1}{8\pi\varepsilon_0} \sum_{\mu \neq \nu} \frac{Q_\mu Q_\nu}{|\boldsymbol{r}_\mu - \boldsymbol{r}_\nu|}, \tag{2.2}$$

represent the internal Coulomb interactions among the charges Q_k of the atomic system (placed at positions $\boldsymbol{r}_k$) and among the charges Q_μ of the medium (placed at positions $\boldsymbol{r}_\mu$), respectively. The atom-medium Coulomb interactions read

$$V_{\mathrm{at\text{-}m}}^{\parallel} = \frac{1}{4\pi\varepsilon_0} \sum_{j,\mu} \frac{Q_j Q_\mu}{|\boldsymbol{r}_j - \boldsymbol{r}_\mu|}. \tag{2.3}$$

The kinetic terms

$$T_{\mathrm{at}} = \sum_j \frac{\left(\boldsymbol{p}_j - Q_j \boldsymbol{A}(\boldsymbol{r}_j)\right)^2}{2m_j}, \qquad T_{\mathrm{m}} = \sum_\mu \frac{\left(\boldsymbol{p}_\mu - Q_\mu \boldsymbol{A}(\boldsymbol{r}_\mu)\right)^2}{2m_\mu}, \tag{2.4}$$

contain the minimal coupling between the charges (with canonical momenta $\boldsymbol{p}_j = -i\hbar\boldsymbol{\nabla}_{\boldsymbol{r}_j}$ and $\boldsymbol{p}_\mu = -i\hbar\boldsymbol{\nabla}_{\boldsymbol{r}_\mu}$, and masses m_j and m_μ, respectively) and the transverse part of the field, represented

by the Coulomb gauge vector potential $\boldsymbol{A}$ (purely transverse, $\boldsymbol{\nabla} \cdot \boldsymbol{A} = 0$). Finally,

$$H_{\mathrm{F}}^{\perp} = \frac{1}{2} \int \mathrm{d}^3 \boldsymbol{r} \left(\varepsilon_0 \dot{\boldsymbol{A}}^2(\boldsymbol{r}) + \frac{1}{\mu_0} [\boldsymbol{\nabla} \times \boldsymbol{A}(\boldsymbol{r})]^2 \right) \tag{2.5}$$

is the Hamiltonian of the free field in vacuum. If one considers a neutral atom, the charge density

$$\rho_{\mathrm{at}}(\boldsymbol{r}) = \sum_j Q_j \delta(\boldsymbol{r} - \boldsymbol{r}_j), \quad \text{with} \quad \sum_j Q_j = 0, \tag{2.6}$$

can be expressed as the divergence of a polarization density $\rho_{\mathrm{at}}(\boldsymbol{r}) = -\boldsymbol{\nabla} \cdot \boldsymbol{P}_{\mathrm{at}}(\boldsymbol{r})$. Here,

$$\boldsymbol{P}_{\mathrm{at}}(\boldsymbol{r}) = \sum_j q_j \int_0^1 \mathrm{d}s \, (\boldsymbol{r}_j - \boldsymbol{R}) \delta(\boldsymbol{r} - \boldsymbol{R} - s(\boldsymbol{r}_j - \boldsymbol{R})), \tag{2.7}$$

where $\boldsymbol{R}$ is the center-of-mass coordinate [88]. The atomic polarization density allows us to express the Coulomb interaction terms as follows

$$V_{\mathrm{at}}^{\|} = \frac{1}{2\varepsilon_0} \int \mathrm{d}^3 \boldsymbol{r} \left(\boldsymbol{P}_{\mathrm{at}}^{\|}(\boldsymbol{r}) \right)^2, \tag{2.8}$$

$$V_{\mathrm{at\text{-}m}}^{\|} = \frac{1}{\varepsilon_0} \int \mathrm{d}^3 \boldsymbol{r} \, \boldsymbol{P}_{\mathrm{at}}^{\|}(\boldsymbol{r}) \cdot \boldsymbol{\Pi}^{\|}(\boldsymbol{r}). \tag{2.9}$$

Here, $\boldsymbol{P}_{\mathrm{at}}^{\|}$ is the longitudinal part of the polarization, i.e. the only component that determines the atomic charge density, and $\boldsymbol{\Pi}^{\|}$ is the longitudinal displacement field of the medium, that satisfies

$$\boldsymbol{\nabla} \cdot \boldsymbol{\Pi}^{\|}(\boldsymbol{r}) = -\sum_\mu Q_\mu \delta(\boldsymbol{r} - \boldsymbol{r}_\mu). \tag{2.10}$$

The latter is proportional to the Coulomb field $\boldsymbol{E}^{\|} = -\boldsymbol{\Pi}^{\|}/\varepsilon_0$ generated by the medium charges.

2.1.1 Minimal coupling

We now analyze the coupling between the atom and the electromagnetic field, which is a consequence of the minimal coupling in the kinetic energy terms in Eq. (2.4). For an atom modeled as a point-like dipole, it is possible to shift from the "$\boldsymbol{p} \cdot \boldsymbol{A}$" to the "$\boldsymbol{r} \cdot \boldsymbol{E}$" coupling representation, through the unitary transformation $\exp(-\mathrm{i}Q\boldsymbol{r} \cdot \boldsymbol{A}/\hbar)$, where the vector potential is computed at the dipole center of mass [88]. The advantage of this transformation lies in the fact that, in the transformed picture, the canonical momentum of a particle coincides with its kinetic momentum and it is decoupled from the field variables (a thorough discussion of the implications of such a feature is given in Ref. [88]).

In the case of a finite-size dipole, the aforementioned unitary transformation generalizes to the Power-Zienau-Wolley (PZW) operator [88, 87]:

$$U_{\mathrm{PZW}} = \exp \left(-\frac{\mathrm{i}}{\hbar} \int \mathrm{d}^3 \boldsymbol{r} \, \boldsymbol{P}_{\mathrm{at}}(\boldsymbol{r}) \cdot \boldsymbol{A}(\boldsymbol{r}) \right) = \exp \left(-\frac{\mathrm{i}}{\hbar} \int \mathrm{d}^3 \boldsymbol{r} \, \boldsymbol{P}_{\mathrm{at}}^{\perp}(\boldsymbol{r}) \cdot \boldsymbol{A}^{\perp}(\boldsymbol{r}) \right). \tag{2.11}$$

The transformation property $U_{\mathrm{PZW}} \boldsymbol{\Pi}^{\perp}(\boldsymbol{r}) U_{\mathrm{PZW}}^{\dagger} = \boldsymbol{\Pi}^{\perp}(\boldsymbol{r}) + \boldsymbol{P}_{\mathrm{at}}^{\perp}(\boldsymbol{r})$ yields two transverse-field terms from Eq. (2.5)

$$V_{\mathrm{at}}^{\perp} = \frac{1}{2\varepsilon_0} \int \mathrm{d}^3 \boldsymbol{r} \left(\boldsymbol{P}_{\mathrm{at}}^{\perp}(\boldsymbol{r}) \right)^2, \qquad V_{\mathrm{at\text{-}m}}^{\perp} = \frac{1}{\varepsilon_0} \int \mathrm{d}^3 \boldsymbol{r} \, \boldsymbol{P}_{\mathrm{at}}^{\perp}(\boldsymbol{r}) \cdot \boldsymbol{\Pi}^{\perp}(\boldsymbol{r}). \tag{2.12}$$

These contributions are complementary to the ones in Eqs. (2.8-2.9). The latter, as well as the transverse part of the atomic polarization density, are instead left unchanged by the transformation. Although originally $\boldsymbol{\Pi}^{\perp} = -\varepsilon_0 \boldsymbol{E}^{\perp}$, the proportionality is lost after the transformation

$$\boldsymbol{\Pi}(\boldsymbol{r}) = -\varepsilon_0 U_{\mathrm{PZW}} \boldsymbol{E}(\boldsymbol{r}) U_{\mathrm{PZW}}^{\dagger} - U_{\mathrm{PZW}} \boldsymbol{P}_{\mathrm{at}}(\boldsymbol{r}) U_{\mathrm{PZW}}^{\dagger}, \tag{2.13}$$

which can be shown using Eq. 2.10. For a finite-size dipole, the equality between the kinetic and canonical momenta is not exactly realized in the transformed frame as in the case of a point-like dipole transformation. The reason is that the transformed kinetic momentum

$$U_{\text{PZW}}(\boldsymbol{p}_j + Q_j\boldsymbol{A}(\boldsymbol{r}_j))U_{\text{PZW}}^\dagger = \boldsymbol{p}_j + Q_j\int_0^1 \mathrm{d}s\, s(\boldsymbol{r}_j - \boldsymbol{R})\boldsymbol{B}(\boldsymbol{R} + s(\boldsymbol{r}_j - \boldsymbol{R})) \tag{2.14}$$

acquires an additional term, which generates a direct coupling between the charges and the magnetic field $\boldsymbol{B}$. Nevertheless, the difference between the two momenta in the transformed representation is suppressed with respect to the analogous difference in the Coulomb gauge as the ratio between the atomic size and the interacting light wavelength. Therefore, if one neglects the interaction with the magnetic field, it can be consistently assumed that $\boldsymbol{p}_j$ coincides with the j–th particle kinetic momentum in the transformed representation.

2.1.2 Medium-assisted electromagnetic field

The medium-assisted electromagnetic field is an effective model that conveniently describes, under certain approximations, the combination of the medium and the field degrees of freedom, as pictured in Fig. 2.1. The contributions to the medium-assisted Hamiltonian arise from the terms $V_{\text{m}}^\parallel$, T_{m} and $H_{\text{F}}^\perp$ in the Hamiltonian (2.1), as derived in detail in Refs. [89, 90, 91]. The resulting effective field Hamiltonian,

$$H_{\text{m}} = \int_0^\infty \mathrm{d}\omega \int \mathrm{d}^3\boldsymbol{r}\,\hbar\omega\boldsymbol{f}^\dagger(\boldsymbol{r},\omega)\cdot\boldsymbol{f}(\boldsymbol{r},\omega), \tag{2.15}$$

can be expanded in three-component mode operators $\boldsymbol{f}(\boldsymbol{r},\omega)$ and $\boldsymbol{f}^\dagger(\boldsymbol{r},\omega)$, satisfying canonical commutation relations

$$\left[f_k(\boldsymbol{r},\omega), f_{k'}^\dagger(\boldsymbol{r}',\omega')\right] = \delta_{kk'}\delta(\boldsymbol{r}-\boldsymbol{r}')\delta(\omega-\omega'), \tag{2.16}$$

$$\left[f_k(\boldsymbol{r},\omega), f_{k'}(\boldsymbol{r}',\omega')\right] = \left[f_k^\dagger(\boldsymbol{r},\omega), f_{k'}^\dagger(\boldsymbol{r}',\omega')\right] = 0,$$

with $k = 1, 2, 3$.

The displacement field $\boldsymbol{\Pi}$ and the vector potential $\boldsymbol{A}$ are related to the field variable $\boldsymbol{f}$ by

$$\Pi_j(\boldsymbol{r}) = \int_0^\infty \mathrm{d}\omega \int \mathrm{d}^3\boldsymbol{r}'\left[-\mathrm{i}\frac{\omega^2}{c^2}\sqrt{\frac{\hbar\varepsilon_0}{\pi}\varepsilon_I(\boldsymbol{r}',\omega)}G_{jk}(\boldsymbol{r},\boldsymbol{r}',\omega)f_k(\boldsymbol{r}',\omega) + \text{H.c.}\right], \tag{2.17}$$

$$A_j(\boldsymbol{r}) = \int_0^\infty \mathrm{d}\omega \int \mathrm{d}^3\boldsymbol{r}'\left[\frac{\omega}{c^2}\sqrt{\frac{\hbar}{\pi\varepsilon_0}\varepsilon_I(\boldsymbol{r}',\omega)}G_{jk}^\perp(\boldsymbol{r},\boldsymbol{r}',\omega)f_k(\boldsymbol{r}',\omega) + \text{H.c.}\right], \tag{2.18}$$

where ε_I is the imaginary part of the dielectric permittivity

$$\varepsilon(\boldsymbol{r},\omega) = \varepsilon_R(\boldsymbol{r},\omega) + \mathrm{i}\varepsilon_I(\boldsymbol{r},\omega). \tag{2.19}$$

We have assumed that the medium is isotropic, hence the permittivity is a scalar. The Green tensor G appearing in Eq. (2.17) is the solution of the equation [87]

$$\left[\partial_j\partial_\ell - \delta_{j\ell}\left(\nabla^2 + \frac{\omega^2}{c^2}\varepsilon(\boldsymbol{r},\omega)\right)\right]G_{\ell k}(\boldsymbol{r},\boldsymbol{r}',\omega) = \delta_{jk}\delta(\boldsymbol{r}-\boldsymbol{r}'), \tag{2.20}$$

and the term $G^\perp$ in Eq. (2.18) represents its transverse part, satisfying $\partial G^\perp_{\ell k}(\boldsymbol{r},\boldsymbol{r}',\omega)/\partial r_\ell = \partial G^\perp_{k\ell}(\boldsymbol{r}',\boldsymbol{r},\omega)/\partial r'_\ell = 0$. In the Coulomb gauge, the properties of the Green tensor and the analytic structure of $\varepsilon(\boldsymbol{r},\omega)$ in the complex frequency plane guarantee that the vector potential and the transverse part of the displacement field satisfy the canonical commutation relations

$$\left[A_j(\boldsymbol{r}),\Pi_k(\boldsymbol{r}')\right] = \mathrm{i}\hbar\delta^\perp_{jk}(\boldsymbol{r}-\boldsymbol{r}') = \mathrm{i}\hbar\int\frac{\mathrm{d}^3\boldsymbol{q}}{(2\pi)^3}\left(\delta_{j\ell}-\frac{q_jq_\ell}{|\boldsymbol{q}|^2}\right)\mathrm{e}^{\mathrm{i}\boldsymbol{q}\cdot(\boldsymbol{r}-\boldsymbol{r}')}. \tag{2.21}$$

For a translationally invariant medium, $\varepsilon(\boldsymbol{r},\omega)=\varepsilon(\omega)$, thus the Green tensor depends only on the coordinate difference, $G(\boldsymbol{r},\boldsymbol{r}',\omega)=G(\boldsymbol{r}-\boldsymbol{r}',\omega)$, and its Fourier transform

$$\tilde{G}_{jk}(\boldsymbol{q},\omega)=\int\mathrm{d}^3\boldsymbol{r}\,G_{jk}(\boldsymbol{r},\omega)\mathrm{e}^{-\mathrm{i}\boldsymbol{q}\cdot\boldsymbol{r}}, \tag{2.22}$$

reads

$$\begin{aligned}
\tilde{G}^\perp_{jk}(\boldsymbol{q},\omega)&=\left(\delta_{j\ell}-\frac{q_jq_\ell}{|\boldsymbol{q}|^2}\right)\tilde{G}_{\ell k}(\boldsymbol{q},\omega)=\frac{\delta_{jk}-q_jq_k/|\boldsymbol{q}|^2}{|\boldsymbol{q}|^2-\omega^2\varepsilon(\omega)/c^2},\\
\tilde{G}^\parallel_{jk}(\boldsymbol{q},\omega)&=\frac{q_jq_\ell}{|\boldsymbol{q}|^2}\tilde{G}_{\ell k}(\boldsymbol{q},\omega)=-\frac{q_jq_k}{|\boldsymbol{q}|^2}\frac{c^2}{\omega^2\varepsilon(\omega)}.
\end{aligned} \tag{2.23}$$

Hence, the displacement field reduces to

$$\Pi_j(\boldsymbol{r})=\int_0^\infty\mathrm{d}\omega\int\frac{\mathrm{d}^3\boldsymbol{q}}{(2\pi)^3}\left[-\mathrm{i}\frac{\omega^2}{c^2}\sqrt{\frac{\hbar\varepsilon_0}{\pi}\varepsilon_I(\omega)}\tilde{G}_{jk}(\boldsymbol{q},\omega)\tilde{f}_k(\boldsymbol{q},\omega)\mathrm{e}^{\mathrm{i}\boldsymbol{q}\cdot\boldsymbol{r}}+\mathrm{H.c.}\right], \tag{2.24}$$

where the operators

$$\tilde{\boldsymbol{f}}(\boldsymbol{q},\omega)=\int\mathrm{d}^3\boldsymbol{r}\,\boldsymbol{f}(\boldsymbol{r},\omega)\mathrm{e}^{-\mathrm{i}\boldsymbol{q}\cdot\boldsymbol{r}}, \tag{2.25}$$

satisfy

$$[\tilde{f}_j(\boldsymbol{q},\omega),\tilde{f}_k^\dagger(\boldsymbol{q}',\omega')]=(2\pi)^3\delta_{jk}\delta(\omega-\omega')\delta(\boldsymbol{q}-\boldsymbol{q}'). \tag{2.26}$$

For a point-like atomic system, singularities may arise in the interaction Hamiltonian due to the fact that the quantities $G^\parallel(\boldsymbol{r},\omega)$ and $G^\perp(\boldsymbol{r},\omega)$ diverge as $\boldsymbol{r}\to\boldsymbol{0}$. In fact, while

$$\mathrm{Im}G^\perp_{jk}(\boldsymbol{0},\omega)=\int\frac{\mathrm{d}^3\boldsymbol{q}}{(2\pi)^3}\mathrm{Im}\tilde{G}^\perp_{jk}(\boldsymbol{q},\omega)=\frac{\omega^2\varepsilon_I(\omega)}{c^2}\int\frac{\mathrm{d}^3\boldsymbol{q}}{(2\pi)^3}\frac{\delta_{jk}-q_jq_k/|\boldsymbol{q}|^2}{\left||\boldsymbol{q}|^2-\frac{\omega^2\varepsilon(\omega)}{c^2}\right|^2} \tag{2.27}$$

is finite and yields a well-defined transverse decay rate [89], $\mathrm{Im}G^\parallel(\boldsymbol{r},\omega)$ diverges as $\boldsymbol{r}\to\boldsymbol{0}$, due to the non integrability of $\mathrm{Im}\tilde{G}^\parallel_{jk}(\boldsymbol{q},\omega)\propto q_jq_k/|\boldsymbol{q}|^2$, and a consistent treatment of the longitudinal decay rate requires momentum regularization.

Techniques based on considering the source enclosed in an artificial cavity [92, 93, 94] have been developed to cope with such singularities. In the following, we will tackle the divergences of the longitudinal part with a less artificial approach, by considering the natural finite spatial extent of the atomic wavefunctions. This will allow us to unambiguously analyze the role of the asymmetry of the atomic states on the emission process.

2.1.3 Total Hamiltonian

From the previous parts of this section it follows that

$$H=H_{\mathrm{at}}+H^{\mathrm{el}}_{\mathrm{int}}+H^{\mathrm{mag}}_{\mathrm{int}}+H_{\mathrm{m}}. \tag{2.28}$$

Here,

$$H_{\text{at}} = H_{\text{at}}^0 + V_{\text{at}} = \sum_j \frac{\boldsymbol{p}_j^2}{2m_j} + \frac{1}{2\varepsilon_0} \int \mathrm{d}^3\boldsymbol{r} \left(\boldsymbol{P}_{\text{at}}(\boldsymbol{r})\right)^2 \tag{2.29}$$

is the atomic Hamiltonian,

$$H_{\text{int}}^{\text{el}} = \frac{1}{\varepsilon_0} \int \mathrm{d}^3\boldsymbol{r}\,\boldsymbol{P}_{\text{at}}(\boldsymbol{r}) \cdot \boldsymbol{\Pi}(\boldsymbol{r}) = \frac{1}{\varepsilon_0} \sum_j Q_j (\boldsymbol{r}_j - \boldsymbol{R}) \cdot \int \mathrm{d}s\, \boldsymbol{\Pi}(\boldsymbol{R} + s(\boldsymbol{r}_j - \boldsymbol{R}))$$

represents the interaction of the atomic system with the electric field, and

$$H_{\text{int}}^{\text{mag}} = \sum_j \left\{ \frac{Q_j}{m_j} \boldsymbol{p}_j \cdot \int_0^1 \mathrm{d}s\, s(\boldsymbol{r}_j - \boldsymbol{R}) \boldsymbol{B}(\boldsymbol{R} + s(\boldsymbol{r}_j - \boldsymbol{R})) \right.$$
$$\left. + \frac{Q_j^2}{2m_j} \left[\int_0^1 \mathrm{d}s\, s(\boldsymbol{r}_j - \boldsymbol{R}) \boldsymbol{B}(\boldsymbol{R} + s(\boldsymbol{r}_j - \boldsymbol{R})) \right]^2 \right\} \tag{2.30}$$

stands for the coupling with the magnetic field. The term H_{m} generally represents the Hamiltonian of the medium, that can be modeled in different ways, e.g. through the medium-assisted field Hamiltonian (2.15), as shown in Sect. 2.1.2. In the following part of this work we will neglect the magnetic contribution to the interaction. We will model the atom as a dipole of charge Q, with a heavy positive charge at the fixed position $\boldsymbol{R} = 0$ and a moving negative charge of coordinate $-\boldsymbol{r}$ and mass m. As a result, one finds the final form of the interaction Hamiltonian

$$H_{\text{int}}^{\text{dip}} = \frac{Q}{\varepsilon_0} \boldsymbol{r} \cdot \int_0^1 \mathrm{d}s\, \boldsymbol{\Pi}(-s\boldsymbol{r}), \tag{2.31}$$

representing the correct generalization of the "$\boldsymbol{r} \cdot \boldsymbol{E}$" Hamiltonian to an extended (non point-like) dipole. The expression 2.17 of the displacement field in terms of the Green tensor in the Hamiltonian $H_{\text{dip}}^{\text{int}}$ provides a new accurate and general approach. Exploiting the tensor allows one to consider different geometries of the host medium, in particular interfaces of different dimensions or photonic nanostructures, even though in the following examples we demonstrate the theory in the simple case of a homogeneous medium. However, the application of the Green's tensor leads to a divergent field at the position of the point-like quantum system. This divergence is usually removed in a somewhat artificial way by introducing virtual cavities or form factors. Here, the renormalization procedure is based on the physical size and orientation of the extended system represented with wavefunctions. It allows us to accurately describe the physics of the system without artifacts.
This is one of the main finding of this work, that arises as a connection between first-principle QED, represented through the canonical commutation relations, and the medium-assisted field ruled by Eq. (2.16).

2.1.4 Emission properties of a bound system of charges

According to the results of the previous section, each eigenstate of the internal atomic Hamiltonian is dressed by the surrounding medium. We now characterize the single-photon emission process and the Lamb shift of an atomic level in a medium-assisted photonic environment in a translationally invariant medium.

Consider an atom in an arbitrary environment, i.e. a dispersive medium of any geometry and material. Let $|a\rangle$ and $|b\rangle$ be two orthogonal eigenstates of the free atomic Hamiltonian H_{at}, characterized by

$$H_{\text{at}} |a\rangle = E_a |a\rangle, \quad H_{\text{at}} |b\rangle = E_b |b\rangle. \tag{2.32}$$

The atom-photon interaction is described by the matrix element

$$\mathscr{M}_j^{ab}(\boldsymbol{r}, \omega) = \langle a| H_{\text{int}}^{\text{dip}} f_j^\dagger(\boldsymbol{r}, \omega) |b\rangle, \tag{2.33}$$

which, for a translationally-invariant medium, can be expressed in the Fourier space through

$$\tilde{\mathscr{M}}_j^{ab}(\boldsymbol{q}, \omega) = \langle a| H_{\text{int}}^{\text{dip}} \tilde{f}_j^\dagger(\boldsymbol{q}, \omega) |b\rangle = -iC(\omega)\frac{\omega^2}{c^2}\tilde{G}_{jk}(\boldsymbol{q}, \omega) \langle a| r_k \int_0^1 ds\, e^{-is\boldsymbol{q}\cdot\boldsymbol{r}} |b\rangle, \tag{2.34}$$

where

$$C(\omega) = Q\sqrt{\frac{\hbar\varepsilon_I(\omega)}{8\pi^4\varepsilon_0}}.$$

If we insert the expression of $\tilde{G}_{jk}$ in Eq. (2.23) and exploit the orthogonality between longitudinal and transverse projectors, we obtain

$$\mathscr{T}_{ab}(\boldsymbol{q}, \omega) = \sum_{j=1}^3 \left|\tilde{\mathscr{M}}_j^{ab}(\boldsymbol{q}, \omega)\right|^2 \tag{2.35}$$

$$= \frac{C(\omega)^2}{|\varepsilon(\omega)|^2}\left[\mathscr{D}(|\boldsymbol{q}|, \omega)\mathscr{G}_{ab}(\boldsymbol{q}) + (1 - \mathscr{D}(|\boldsymbol{q}|, \omega))\frac{|\mathscr{F}_{ab}(\boldsymbol{q}) - \delta_{ab}|^2}{|\boldsymbol{q}|^2}\right], \tag{2.36}$$

where $\delta_{ab} = \langle a|b\rangle = 1$ if $|a\rangle$ and $|b\rangle$ coincide and 0 otherwise, with

$$\mathscr{D}(q, \omega) = \left|1 - \frac{q^2 c^2}{\omega^2\varepsilon(\omega)}\right|^{-2}, \tag{2.37}$$

$$\mathscr{F}_{ab}(\boldsymbol{q}) = \langle a| e^{-i\boldsymbol{q}\cdot\boldsymbol{r}} |b\rangle = \int d^3\boldsymbol{r}\, \psi_a^*(\boldsymbol{r})\psi_b(\boldsymbol{r}) e^{-i\boldsymbol{q}\cdot\boldsymbol{r}}, \tag{2.38}$$

$$\mathscr{G}_{ab}(\boldsymbol{q}) = \sum_{j=1}^3 \left|\langle a| r_j \frac{e^{-i\boldsymbol{q}\cdot\boldsymbol{r}} - 1}{\boldsymbol{q}\cdot\boldsymbol{r}} |b\rangle\right|^2. \tag{2.39}$$

The quantity defined in Eq. (2.36) determines both the total decay rate of the state $|a\rangle$ and its energy shift. The former can be evaluated according to the Fermi golden rule

$$\Gamma_a = \frac{2\pi}{\hbar}\sum_b \int_0^\infty d\omega\, \delta(\hbar\omega - \hbar\omega_{ab})T_{ab}(\omega) = \frac{2\pi}{\hbar^2}\sum_{b\neq a}\theta(\omega_{ab})T_{ab}(\omega_{ab}), \tag{2.40}$$

$$= \frac{2\pi}{\hbar}\sum_{b\neq a}\theta(\omega_{ab})\frac{C(\omega_{ab})^2}{|\varepsilon(\omega_{ab})|^2}\int\left[\mathscr{D}(|\boldsymbol{q}|, \omega_{ab})\mathscr{G}_{ab}(\boldsymbol{q}) + (1 - \mathscr{D}(|\boldsymbol{q}|, \omega))\frac{|\mathscr{F}_{ab}(\boldsymbol{q})|^2}{|\boldsymbol{q}|^2}\right]d^2\boldsymbol{q}$$

with

$$\omega_{ab} = \frac{E_a - E_b}{\hbar}, \qquad T_{ab}(\omega) = \int d^3\boldsymbol{q}\, \mathscr{T}_{ab}(\boldsymbol{q}, \omega), \tag{2.41}$$

and $\theta(x)$ being the Heaviside step function. The absence of a contribution from state $|a\rangle$ in the sum over states in the second equality of Eq. (2.40), albeit reasonable, is not a trivial result. Therefore, replacing Eq. 2.36 in the evaluation of the decay rate $\delta_{ab} = 0$ and the apparent divergence in the term proportional to $\mathscr{F}_{ab}$ is regularized by the wavefunctions spatial extension. Note that the two terms in Eq. (2.40) proportional to $\mathscr{D}(\boldsymbol{q}, \omega)$ correspond to the transverse contribution, while the remaining one is the longitudinal contribution responsible for non-radiative decay, because it is related to the absorption losses in the dielectric host medium.

In vacuum ($\varepsilon(\omega) = 1$), the decay rate in Eq. 2.40 becomes

$$\Gamma_a^{(\text{vac})} = \frac{Q^2 q^3}{8\pi^2\hbar\varepsilon_0}\int_{\mathbb{S}^2} d^2 S(\boldsymbol{n})\sum_{b\neq a}\left[\mathscr{G}_{ab}(q\boldsymbol{n}) - \frac{|\mathscr{F}_{ab}(q\boldsymbol{n})|^2}{q^2}\right], \tag{2.42}$$

where $q = \omega_{ab}/c$ and the integration is over the unit sphere $\boldsymbol{n} \in \mathbb{S}^2$. Note that in the point-dipole limit the quantity $\mathscr{F}_{ab}$ tends to δ_{ab}. In this way, we recover the familiar Weisskopf-Wigner result [95]. The frequency shifts of the atomic levels should be determined using Eqs. (2.36-2.41), through

$$\Delta_a = \frac{1}{\hbar^2} \sum_b \mathrm{P}\!\int_0^\infty \mathrm{d}\omega \frac{T_{ab}(\omega)}{\omega - \omega_{ab}}, \tag{2.43}$$

with $\mathrm{P}\!\int$ denoting principal value integration. For $a = b$ the function $\mathscr{T}_{ab}$ contains the state-independent, non-integrable term

$$\delta_{ab} C(\omega)^2 |\boldsymbol{q}|^{-2}(1 - \mathscr{D}(|\boldsymbol{q}|, \omega)) \sim |\boldsymbol{q}|^{-2} \quad \text{as } |\boldsymbol{q}| \to \infty, \tag{2.44}$$

which provides a divergent contribution to $T_{aa}(\omega)$. However, this contribution is also independent of the state, representing therefore the effect of a uniform energy shift. Physical quantities such as the perturbed transition frequency

$$\tilde{\omega}_{ab} = \omega_{ab} + \Delta_a - \Delta_b \qquad = \omega_{ab} + \frac{1}{\hbar^2} \mathrm{P}\!\int_0^\infty \mathrm{d}\omega \left[\frac{T_{aa}(\omega) - T_{bb}(\omega)}{\omega} \right.$$

$$\left. + 2\omega_{ab} \frac{T_{ab}(\omega)}{\omega^2 - \omega_{ab}^2} + \sum_{c \neq a,b} \left(\frac{T_{ac}(\omega)}{\omega - \omega_{ac}} - \frac{T_{bc}(\omega)}{\omega - \omega_{bc}} \right) \right] \tag{2.45}$$

are thus independent of the divergent term given in (2.44). Indeed, notice that, in the time domain the low-energy behavior of the dielectric permittivity is

$$\varepsilon(\omega) = 1 + \int_0^\infty \mathrm{d}t\, \chi(t) + \mathrm{i}\omega \int_0^\infty \mathrm{d}t\, t\, \chi(t) + O(\omega^2), \tag{2.46}$$

where $\chi(t)$ is the medium susceptibility with finite moments. This implies that $T_{ab}(\omega) \sim \omega$ close to the origin, and therefore the integration of the term $(T_{aa} - T_{bb})/\omega$ in Eq. (??) is well defined.

2.1.5 Asymmetric two-level atom

The parity asymmetry of the atomic Hamiltonian eigenstates, reflected by the presence of nonvanishing expectation values of one or more components of $\boldsymbol{r}$, affects the state-dependent quantities $\mathscr{F}_{ab}$ and $\mathscr{G}_{ab}$, which appear in the expression of $T_{ab}(\omega)$ and determine the decay rate Γ_a and the energy shift Δ_a. In a two-level atomic system, the three components of the Hermitian position operator $\boldsymbol{r}$ can be represented by spin operators [96, 95]

$$\boldsymbol{r} = \boldsymbol{\rho}\mathbf{1} + \boldsymbol{\delta}\sigma_z + \boldsymbol{r}_{ab}\sigma_x, \qquad \sigma_x = |a\rangle\langle b| + |b\rangle\langle a|, \qquad \sigma_z = |a\rangle\langle a| - |b\rangle\langle b| \tag{2.47}$$

acting on the two-dimensional space spanned by $|a\rangle, |b\rangle$, with

$$\boldsymbol{\rho} \quad = \frac{\langle a|\boldsymbol{r}|a\rangle + \langle b|\boldsymbol{r}|b\rangle}{2}, \tag{2.48}$$

$$\boldsymbol{\delta} \quad = \frac{\langle a|\boldsymbol{r}|a\rangle - \langle b|\boldsymbol{r}|b\rangle}{2}, \tag{2.49}$$

$$\boldsymbol{r}_{ab} \quad = \langle a|\boldsymbol{r}|b\rangle = \langle b|\boldsymbol{r}|a\rangle. \tag{2.50}$$

In the two-level case, the off-diagonal matrix element (2.50) can be made real and non-negative by absorbing a phase factor in the definition of one of the states.
The functions that determine the decay rate from $|a\rangle$ to $|b\rangle$ read

$$\mathscr{F}_{ab}(\boldsymbol{q}) \qquad = -\mathrm{i}\mathrm{e}^{-\mathrm{i}\boldsymbol{q}\cdot\boldsymbol{\rho}} \boldsymbol{q} \cdot \boldsymbol{r}_{ab} \operatorname{sinc}(A(\boldsymbol{q})), \tag{2.51}$$

$$\mathscr{G}_{ab}(\boldsymbol{q}) = \left| \nabla_{\boldsymbol{q}} \left[\boldsymbol{q} \cdot \boldsymbol{r}_{ab} \int_0^1 \operatorname{sinc}(sA(\boldsymbol{q}))\mathrm{e}^{-\mathrm{i}s\boldsymbol{q}\cdot\boldsymbol{\rho}}\mathrm{d}s \right] \right|^2,$$

with $\mathrm{sinc}(x) = \sin(x)/x$ and $A(\boldsymbol{q}) = \sqrt{(\boldsymbol{q} \cdot \boldsymbol{r}_{ab})^2 + (\boldsymbol{q} \cdot \boldsymbol{\delta})^2}$.

From these results, one can observe that the physical quantities computed from $\mathscr{G}_{ab}$ and from the square modulus of $\mathscr{F}_{ab}$ are invariant with respect to the inversions $\boldsymbol{\rho} \to -\boldsymbol{\rho}$ and $\boldsymbol{\delta} \to -\boldsymbol{\delta}$, but both depend on diagonal entries and which play the role of the asymmetric contributions.

To identify the lowest-order contributions to the decay rate, let us perform a small-$\boldsymbol{q}$ expansion of the functions appearing in the expression (2.36) of $\mathscr{T}_{ab}$ for $a \neq b$, namely

$$\frac{|\mathscr{F}_{ab}(\boldsymbol{q})|^2}{|\boldsymbol{q}|^2} \simeq \frac{(\boldsymbol{q} \cdot \boldsymbol{r}_{ab})^2}{|\boldsymbol{q}|^2} \left(1 - \frac{(\boldsymbol{q} \cdot \boldsymbol{r}_{ab})^2 + (\boldsymbol{q} \cdot \boldsymbol{\delta})^2}{6} \right), \tag{2.52}$$

and

$$\mathscr{G}_{ab}(\boldsymbol{q}) \simeq \quad |\boldsymbol{r}_{ab}|^2 \left(1 - \frac{(\boldsymbol{q} \cdot \boldsymbol{r}_{ab})^2}{3} + \frac{(\boldsymbol{q} \cdot \boldsymbol{\delta})^2}{9} + \frac{(\boldsymbol{q} \cdot \boldsymbol{\rho})^2}{12} \right)$$
$$+ \quad \frac{|\boldsymbol{\rho}|^2 (\boldsymbol{q} \cdot \boldsymbol{r}_{ab})^2}{4} + (\boldsymbol{q} \cdot \boldsymbol{r}_{ab}) \boldsymbol{r}_{ab} \cdot \left(\frac{(\boldsymbol{q} \cdot \boldsymbol{\rho}) \boldsymbol{\rho}}{2} - \frac{(\boldsymbol{q} \cdot \boldsymbol{\delta}) \boldsymbol{\delta}}{9} \right). \tag{2.53}$$

While the first-order contributions are regular, the second-order approximation in $\boldsymbol{q}$ of the functions in Eqs. (2.52-2.53) yield divergent integrals, that should be regularized by a cutoff $\Lambda_{\boldsymbol{q}}$, roughly corresponding to the inverse spatial size of the involved wavefunctions, that can range from 1 to 100 nm according to the considered system. Clearly, this cutoff is not needed if one uses the expressions in Eq. (2.51), that contains all orders in q. Based on the approximations 2.52 and 2.53 one can estimate that the corrections entailed by an asymmetry of the states $|a\rangle$ and $|b\rangle$ are of order $(\Lambda_{\boldsymbol{q}} |\boldsymbol{r}_{aa}|)^2$ and $(\Lambda_{\boldsymbol{q}} |\boldsymbol{r}_{bb}|)^2$. Notice that the asymmetry corrections compete with terms of order $(\Lambda_{\boldsymbol{q}} |\boldsymbol{r}_{ab}|)^2$, representing the first corrections to the point-dipole result, and are not characterized by a definite sign.

We have expressed a light-matter interaction Hamiltonian in terms of the Green tensor propagator, in a novel approach that avoids the usual divergence related to the approximation of a point-like atomic quantum system. The divergence was lifted via the inclusion of the wavefunctions, providing in this way a natural cutoff for the system investigated. The analysis focused on the determination of the decay rates and energy shifts of the bound states of an "atomic" system, which have been obtained under general assumptions. The most important among these assumptions is the hypothesis of homogeneous and isotropic media. We also discussed how to extend the theory to more general situations. In [[97]] the general result obtained are applied to the decay rate as a function of the asymmetry of the system and the absorption of the medium showing that asymmetry can yield small but detectable deviations with respect to the symmetric case. In the next section we introduce the effect of the asymmetry in the Rabi model.

2.2 Beyond the Rabi model: light interactions with polar atomic systems in a cavity

In quantum optics, the Rabi model accounts for a coupling of a single electromagnetic mode with a two-level atomic system characterized with inversion symmetry. The coupling occurs via two types of terms. The usually dominant resonant terms describe energy exchange between photonic and atomic excitations. The so-called counter-rotating terms are typically much weaker. They account for a simultaneous emission or absorption of a pair of excitations, one in the atomic system and one in the electromagnetic mode. In the electric-dipole approximation, these interaction terms arise from the coupling of the electric field with an *induced* transition dipole moment. If the inversion symmetry of the atomic system is broken, it becomes polar, which means that its eigenstates may acquire *permanent* electric dipole moments. As a consequence, a third type of terms describing light-matter interaction arises, related to the coupling of the permanent dipoles to the electric field. In this work, based on the time-independent perturbation theory, we compare light emission
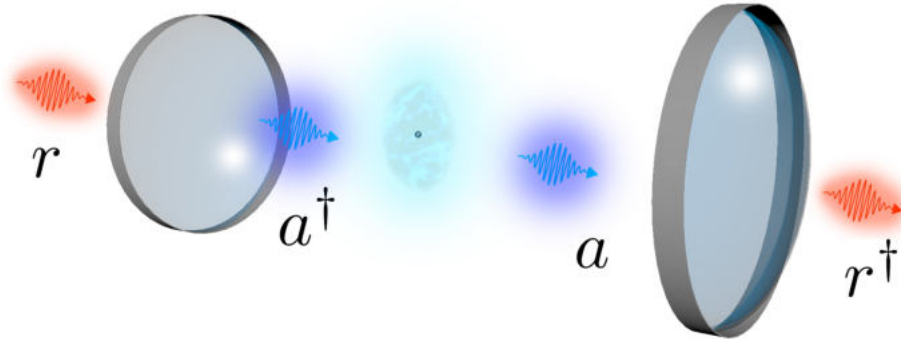
Figure 2.2: Artistic vision of the system under study: a two-level spatially asymmetric atomic system in a lossy cavity. The annihilation and creation operators a and $a^\dagger$ for the lossy cavity system, and analogously the annihilation and creation operators r and $r^\dagger$ for the reservoir. The decay rate Γ of the cavity system is ruled by Eq. 2.66.

intensities induced by the three types of terms. The analysis reveals that the emission strength related to the existence of permanent dipoles may surpass the one due to the counter-rotating interaction terms, but usually is much weaker than the emission due to the main, resonant coupling. This ratio can be modified in systems with a reduced dimensionality or through engineering of the density of electromagnetic states of the environment, as we demonstrate with a Lorentzian example.

2.2.1 Rabi model

The Rabi model is the fundamental model in quantum optics, which describes the coupling of a two-level system and a bosonic field mode [98]. The model extends beyond the simpler Jaynes-Cummings interaction, in which the energy is exchanged between the atomic excitation and a photon, such that creation of a photon is accompanied by annihilation of the atomic excitation and vice versa[99]. The Rabi model additionally accounts for the less intuitive processes of pairwise creation or annihilation of excitations in the atomic and photonic subsystems. The probability of these processes grows with the light-matter coupling constant and becomes significant in the so-called ultrastrong coupling regime, in which that coupling constant becomes comparable to the energy of the system [100]. Numerous experimental realizations include superconducting systems [101, 102] quantum wells [103, 104], photonic waveguide arrays [105], molecular ensembles [106], cold atoms [107], etc. In all these systems extension beyond the Jaynes-Cummings interaction may lead to considerable modification of the physics of the system: in particular, to a ground state with a nonvanishing number of excitations, squeezing dynamic, and a significant modification of the spectra [108, 109, 98]. Remarkably, analytical solutions of the Rabi model have been developed only in the last decade [108, 109].

The Rabi model describes the light - matter interaction scenario, where electromagnetic field induces transitions between the eigenstates of the two-level atomic system. A particular mechanism is related to a coupling of the electromagnetic radiation with a transition dipole moment element

induced between a pair of atomic eigenstates. However, simple two-level systems may sustain much richer physics, beyond the traditional Rabi model: a particular example is a coupling scenario where the electromagnetic field introduces energy shifts of the eigenstates rather than transitions between them [110, 111]. A simple realization exploits atomic systems with permanent dipole moments e.g. polar molecules or asymmetric quantum dots. Due to the interplay of permanent and induced electric dipole moments, polar systems are a playground where rich physics of light-matter interactions can be realized: polar quantum systems have been proposed for THz radiation sources [110] based on quantum dots [112] or molecular ensembles [113]. They can be exploited for squeezed light generation [114, 115] and they support nonlinear optical absorption [111]. Recently, the impact of spatial asymmetry of a quantum system on its spontaneous emission properties has been investigated [97].

Said works just sketch the plethora of possibilities provided by asymmetric quantum systems that simultaneously support light-matter interactions through three mechanisms. These correspond to the Jaynes - Cummings terms and the counter - rotating terms, both involving the transition dipole moments of the atomic system, and the scenario based on its permanent dipoles. For numerous applications given above it is essential to identify conditions in terms of experimentally tunable model parameters where different contributions make a significant influence on the system's optical response. This is our goal in this work. We study the relative impact of the three contributions and demonstrate with simple examples the possibility to tune it with density-of-states engineering. Our analysis follows the methodology introduced in Ref. [116], but extends it to include all the three interaction mechanisms.

2.2.2 Hamiltonian of the system

Let us consider a two level system with a ground and excited state denoted respectively as $|g\rangle$, $|e\rangle$, separated with energy $\hbar\omega_a$. The system is described by a set of Pauli operators $\sigma_- = |g\rangle\langle e|$, $\sigma_+ = |e\rangle\langle g|$ and $\sigma_z = |e\rangle\langle e| - |g\rangle\langle g|$. The two-level system interacts with a single electromagnetic mode with an annihilation operator a. The Hamiltonian H of the coupled system can be divided in two parts

$$H_{\text{int}} = H_{\text{JC}} + V. \tag{2.54}$$

The first term is the Jaynes-Cumming (JC) Hamiltonian [99]

$$H_{\text{JC}} = \hbar\omega_c a^\dagger a + \hbar\frac{\omega_a}{2}\sigma_z + \hbar g_R(\sigma_+ a + a^\dagger \sigma_-) \tag{2.55}$$

where g_R is the coupling strength between the parties of the system through the resonant JC channel. The following analysis could be performed without specification of the coupling mechanism. However, we will interpret the model for the physically important case of electric-dipole coupling in a rectangular cavity, for which $g_R = -\boldsymbol{d}_{\text{eg}} \cdot \boldsymbol{\varepsilon}\sqrt{\hbar\omega_c/2\varepsilon_0\mathscr{V}}$. Here, $\boldsymbol{d}_{\text{eg}} = -\langle e|\boldsymbol{d}|g\rangle$ stands for the off-diagonal element of the electric dipole operator $\boldsymbol{d}$ of the two-level system, $\boldsymbol{\varepsilon}$ is the polarization versor, ε_0 denotes vacuum electric permittivity and $\mathscr{V}$ is the quantization volume.

The term V of Eq. (2.54) accounts for the interaction of the two-level system and the electromagnetic mode through the counter-rotating (CR) mechanism and the diagonal-dipole mechanism

$$V = H_{\text{CR}} + H_{\text{diag}}, \tag{2.56}$$

$$H_{\text{CR}} = \hbar g_R \left(\sigma_+ a^\dagger + \sigma_- a\right), \qquad H_{\text{AS}} = \hbar g_S \left(\sigma_z + \mathbf{1}\right)\left(a + a^\dagger\right). \tag{2.57}$$

with $g_S = -\boldsymbol{d}_{\text{ee}} \cdot \boldsymbol{\varepsilon}\sqrt{\hbar\omega_c/8\varepsilon_0\mathscr{V}}$, proportional to the diagonal element of the dipole moment operator. Note that the expectation value of a dipole moment operator described only by off-diagonal elements $\boldsymbol{d}_{\text{eg}}|e\rangle\langle g| + \boldsymbol{d}_{\text{eg}}^*|g\rangle\langle e|$ may be nonzero only at presence of transitions between the eigenstates that

may be induced with external electric field. Therefore, these elements correspond to induced transition dipoles. Contrary, the diagonal element describes the permanent dipole moment of the excited state. Here, we have assumed for simplicity that the ground state does not sustain a dipole moment: $\left| \boldsymbol{d}_{\mathrm{gg}} \right| = 0$, but the analysis can be generalized in a straightforward manner to include this quantity and will not lead to qualitatively new effects. Notably, permanent dipole moments are sustained by polar systems, i.e. systems without inversion symmetry [110]. For this reason we will refer to the last Hamiltonian term as the "asymmetry term" and mark it with the AS subscript. Finally, note that while the Hamiltonian H_{JC} preserves the number of excitations, H_{AS} (H_{CR}) describes a modification of this number by 1 (by 2).

2.3 Perturbative analysis

In the following analysis we will treat V as a perturbation with respect to the system Hamiltonian H_{JC}. The eigenvalues of H_{JC} are

$$E_n^{s(0)} = \hbar \omega_c \left(n - \frac{1}{2} \right) + s\hbar \sqrt{ \frac{(\omega_c - \omega_a)^2}{4} + n g_R^2 } \tag{2.58}$$

for $s = \pm 1$, and the eigenstates are

$$\left| n_s^{(0)} \right\rangle = A_n^s \left| g; n \right\rangle + B_n^s \left| e, n-1 \right\rangle, \tag{2.59}$$

with

$$A_n^s = \frac{ E_n^{s(0)} - \hbar \omega_c (n-1) - \hbar \omega_a / 2 }{ \sqrt{ \left(E_n^{s(0)} - \hbar \omega_c (n-1) - \hbar \omega_a / 2 \right)^2 + \hbar^2 g_R^2 n } }, \tag{2.60}$$

$$B_n^s = \frac{ \hbar g_r \sqrt{n} }{ \sqrt{ \left(E_n^{s(0)} - \hbar \omega_c (n-1) - \hbar \omega_a / 2 \right)^2 + \hbar^2 g_R^2 n } }. \tag{2.61}$$

The pair $\left\{ \left| n_s^{(0)} \right\rangle \right\}_{s=\pm}$ defines a manifold $\mathscr{E}_{\mathrm{JC}}(n)$, which is the set of the states with the same number of the excitations (see Fig. 2.3). We denote it with the JC subscript, since the notion of the manifold will be generalized in the perturbed picture.

In the perturbation Hamiltonian V, the counter-rotating term H_{CR} is described by the same coupling constant g_R as the interaction term of the unperturbed Hamiltonian H_{JC}. However, the transition rates due to H_{CR} are much smaller since we assume to work far from the ultra-strong coupling regime $g_R \ll \omega$. Therefore, the perturbation theory approach is justified for up to moderate coupling strengths, as we show later on. We characterize the modified eigenstates with the time-independent perturbation theory up to the second order, with the wavefunction expansion given by $\left| n_s \right\rangle = \left| n_s^{(0)} \right\rangle + \left| n_s^{(1)} \right\rangle + \left| n_s^{(2)} \right\rangle$. The first-order correction reads

$$\left| n_s^{(1)} \right\rangle = \sum_{m \neq n} \sum_{\alpha = \pm} \frac{ V_{mn}^{\alpha s} }{ E_{nm}^{s\alpha} } \left| m_\alpha^{(0)} \right\rangle \equiv \frac{ V_{mn}^{\alpha s} }{ E_{nm}^{s\alpha} } \left| m_\alpha^{(0)} \right\rangle, \tag{2.62}$$

where $E_{n,m}^{s,\alpha} = E_n^{s(0)} - E_m^{\alpha(0)}$ and $V_{mn}^{\alpha s} = \left\langle m_\alpha^{(0)} | V | n_s^{(0)} \right\rangle$

$$V_{mn}^{\alpha s} = \hbar g_R \left(\sqrt{n-1} B_n^s A_{n-2}^\alpha \delta_{m,n-2} + \sqrt{n+1} A_n^s B_{n+2}^\alpha \delta_{m,n+2} \right)$$

$$+ 2\hbar g_S B_m^\alpha B_n^s \left(\sqrt{n-1} \delta_{m,n-1} + \sqrt{n} \delta_{m,n+1} \right). \tag{2.63}$$

The above equation shows that the perturbed eigenstates include admixtures of states with $m = n \pm 1$ coupled by g_S and of states with $m = n \pm 2$ coupled by g_R, which follows directly from the forms of the H_{diag} and H_{CR} Hamiltonians. Including the second-order correction leads to

$$|n_s\rangle = \left(1 - \frac{1}{2}\sum_k \sum_{\alpha=\pm} \left(\frac{V_{nk}^{s\alpha}}{\varepsilon_{nk}^{s\alpha}}\right)^2\right)\left|n_s^{(0)}\right\rangle + \sum_k \sum_{\alpha=\pm}\left(\frac{V_{kn}^{\alpha s}}{\varepsilon_{nk}^{s\alpha}} + \sum_l \sum_{\beta=\pm}\frac{V_{kl}^{\alpha\beta}V_{ln}^{\beta s}}{\varepsilon_{nk}^{s\alpha}\varepsilon_{nl}^{s\beta}}\right)\left|k_\alpha^{(0)}\right\rangle. \quad (2.64)$$

Based on the above result, we define generalized manifolds $\mathscr{E}(n)$ as the pairs $\{|n_s\rangle\}_{s=\pm}$. According to the 2nd order perturbation, the eigenstate $|n_s\rangle$ includes superposition components with different numbers of excitations $\{n, n \pm 1, \ldots, n \pm 4\}$, while the label n refers to the central component, which is by far the leading superposition component for weak enough coupling strengths $g_{R,S}$, for which the theory is applicable.

The correction V does not perturb the eigenvalues at the first order, because $V_{\text{nn}}^{s\sigma} = \langle n_s|V|n_\sigma\rangle = 0$. Up to the second order, the energy eigenvalues are $E_n^s = E_n^{s(0)} + E_n^{s(1)} + E_n^{s(2)}$, with $E_n^{s(1)} = 0$ and

$$E_n^{s(2)} = \sum_{k \neq n} \sum_{j=\pm} \frac{\left(V_{kn}^{js}\right)^2}{E_{nk}^{sj}}. \quad (2.65)$$

Inclusion of the second-order corrections provides us with a method to estimate the range of validity for the theory, as described related section.

2.3.1 Outcoupling

In this section, we assume the cavity mirrors to be semi-transparent, so that the cavity photons described by a may exchange energy with an external reservoir mode r at a rate Γ. This approach follows directly the reasoning in Ref.~[116].

$$H_{\text{ex}} = \hbar\Gamma(ar^\dagger + a^\dagger r). \quad (2.66)$$

This Hamiltonian effectively models losses, since we assume the reservoir mode to be in the vacuum state $|0\rangle_R$.

The Fermi golden rule allows us to find the emission spectrum into the reservoir mode,

$$S(\omega) = \sum_{\iota,\phi=\pm}\sum_{i_\iota,f_\phi} \left|\langle f_\phi, 1_R|H_{\text{ex}}|i_\iota, 0_R\rangle\right|^2 L_{\text{fi}}(\omega)\,\mathscr{P}(\omega), \quad (2.67)$$

$$L_{\text{fi}}(\omega) = \frac{1}{2\pi}\frac{\hbar\gamma}{(E_{\text{if}}^{\iota\phi} - \hbar\omega)^2 + \left(\frac{\hbar\gamma}{2}\right)^2}.$$

We include contributions from all $|i_\iota\rangle \to |f_\phi\rangle$ transitions such that $|i_\iota\rangle, |f_\phi\rangle \in \{|n_s\rangle\}$ and $E_i^{\iota(0)} > E_f^{\phi(0)}$. To evaluate the contribution from a given pair of states, the corresponding transition element $\left|\langle f_\phi, 1_R|H_{\text{ex}}|i_\iota, 0_R\rangle\right|^2$ must be weighted with the Lorentzian distribution $L_{\text{fi}}(\omega)$ which accounts for the emission linewidth γ due to the finite lifetime of the cavity photons. Here, $E_{if}^{\iota\phi} = E_i^\iota - E_f^\phi$ and $\mathscr{P}(\omega)$ stands for the density of reservoir states. Since we fix the initial and final states of the reservoir, we can simplify

$$\left|\langle f_\phi, 1_R|H_{\text{ex}}|i_\iota, 0_R\rangle\right|^2 \sim \left|\langle f_\phi|a|i_\iota\rangle\right|^2 = \left|a_{f,i}^{\phi\iota}\right|^2 \quad (2.68)$$

and obtain $\left|a_{f,i}^{\phi\iota}\right|^2$ as the relevant quantity that contributes to the emission rate.

We now define a transition rate $P_{f,i}^{\phi\iota}$ that accounts for the emission through a given transition in a certain spectral range $\delta\omega$, which covers the emission bandwidth γ

$$P_{f,i}^{\phi\iota} = \frac{2\pi}{\hbar} \int_{\delta\omega} \left| \langle f_\phi, 1_R | H_{\mathrm{ex}} | i_\iota, 0_R \rangle \right|^2 L_{fi}(\omega) \mathscr{P}(\omega) \, d\omega. \tag{2.69}$$

Next, we assume the density of states which corresponds to a free space $\mathscr{P}(\omega) = \left(\frac{L}{\pi c}\right)^{p+1} \omega^p$, where L is the quantization length and $p = 0, 1, 2$ is the Jacobian exponent related to the dimension $d = p + 1$ of the system. For a sufficiently narrow transition $\gamma \ll \omega$, which can be safely assumed for a great majority of systems, the density of states can be approximated as a constant value across the transition bandwidth γ and replaced by $\mathscr{P}(\omega) \sim (\hbar\omega)^p \approx \left(E_{if}^{\iota\phi}\right)^p$

$$P_{f,i}^{\phi\iota} \propto \int_{\delta\omega} \left| a_{f,i}^{\phi\iota} \right|^2 L_{fi}(\omega) (\hbar\omega)^p \, d\omega \approx \left| a_{f,i}^{\phi\iota} \right|^2 \left(E_{if}^{\iota\phi}\right)^p. \tag{2.70}$$

We now evaluate the transition amplitude $a_{f,i}^{\phi\iota}$. At the $0-$th order, we find directly from Eq. (2.59)

$$\left\langle f_\phi^{(0)} | a | i_\iota^{(0)} \right\rangle \equiv c_i^{\phi\iota} \delta_{f,i-1} = \left(\sqrt{i} A_i^\iota A_{i-1}^\phi + \sqrt{i-1} B_i^\iota B_{i-1}^\phi \right) \delta_{f,i-1}. \tag{2.71}$$

This equation shows that only transitions between two subsequent excitation manifolds $\mathscr{E}_{\mathrm{JC}}(i)$ and $\mathscr{E}_{\mathrm{JC}}(i-1)$ are allowed in the Jaynes-Cummings model, as expected. Our goal is to analyze the emission probability via Eq. (2.69) when the eigenstates are corrected by the perturbation term V in Eq. (2.56) and the spectrum is defined in Eq. (2.58). In the perturbed expression for $a_{f,i}^{\phi\iota} = \langle f_\phi | a | i_\iota \rangle$, that is in the eigenstates $|n_s\rangle$, we consider all the correction terms up to the second order in the coupling strengths g_R and g_S. Using $V_{\mathrm{nn}} = 0$, we find

$$\left| \langle f_\phi | a | i_\iota \rangle \right|^2 = \left| \frac{V_{f+1,i}^{\alpha\iota}}{\varepsilon_{i,f+1}^{\iota\alpha}} c_{f+1}^{\phi\alpha} + \frac{V_{i+1,f}^{\alpha\phi}}{\varepsilon_{f,i+1}^{\phi\alpha}} c_i^{\alpha\iota} \right|^2 + \delta_{f,i-1} \left\{ \left(1 - \left(\frac{V_{ik}^{\iota\alpha}}{\varepsilon_{ik}^{\iota\alpha}} \right)^2 - \left(\frac{V_{fk}^{\phi\alpha}}{\varepsilon_{fk}^{\phi\alpha}} \right)^2 \right) \left| c_i^{\phi\iota} \right|^2 \right.$$
$$\left. + 2 c_i^{\phi\iota} \left(\frac{V_{il}^{\alpha\beta} V_{li}^{\beta\iota}}{\varepsilon_{ii}^{\iota\alpha} \varepsilon_{il}^{\iota\beta}} c_i^{\phi\alpha} + \frac{V_{k-1,i-1}^{\alpha\phi} V_{ki}^{\alpha'\iota}}{\varepsilon_{i-1,k-1}^{\phi\alpha} \varepsilon_{ik}^{\iota\alpha'}} c_k^{\alpha\alpha'} + \frac{V_{i-1,l}^{\alpha\beta} V_{l,i-1}^{\beta\phi}}{\varepsilon_{i-1,i-1}^{\phi\alpha} \varepsilon_{i-1,l}^{\phi\beta}} c_i^{\alpha\iota} \right) \right\}. \tag{2.72}$$

Inclusion of the perturbation Hamiltonian allows transitions to new manifolds. A close inspection of the form the perturbation V in Eq. (2.63) combined with the above form of $\left| \langle f_\phi | a | i_\iota \rangle \right|^2$ reveals that transitions between $\mathscr{E}(i) \longrightarrow \mathscr{E}(f = i)$ and $\mathscr{E}(i) \longrightarrow \mathscr{E}(f = i - 2)$ are due to the asymmetric Hamiltonian H_{AS} and the transition between $\mathscr{E}(i) \longrightarrow \mathscr{E}(i-3)$ are due to H_{CR}. The latter would also give rise to $\mathscr{E}(i) \longrightarrow \mathscr{E}(i+1)$ transitions, which are suppressed in a vacuum reservoir mode r. One might argue that this fact suggests a stronger contribution comes from the diagonal coupling than the counter-rotating terms because the former involves closer manifolds, hence is energetically more favorite. On the other hand, the transitions at higher frequencies contribute with an higher intensity due to the increased density of states $\mathscr{P}$. Therefore, we need a quantitative comparison which evaluates the spectrum and highlights properly the behavior in different regimes.

2.3.2 Result

In this section we analyze the transitions showed in Fig. 2.3, with a special emphasis on the ones induced by the perturbation Hamiltonian H_{AS} and H_{CR}. We will investigate relative emission strengths of transitions that origin from different Hamiltonian contributions in function of the coupling constants $g_{R,S}$. We also estimate the range of applicability of the theory.
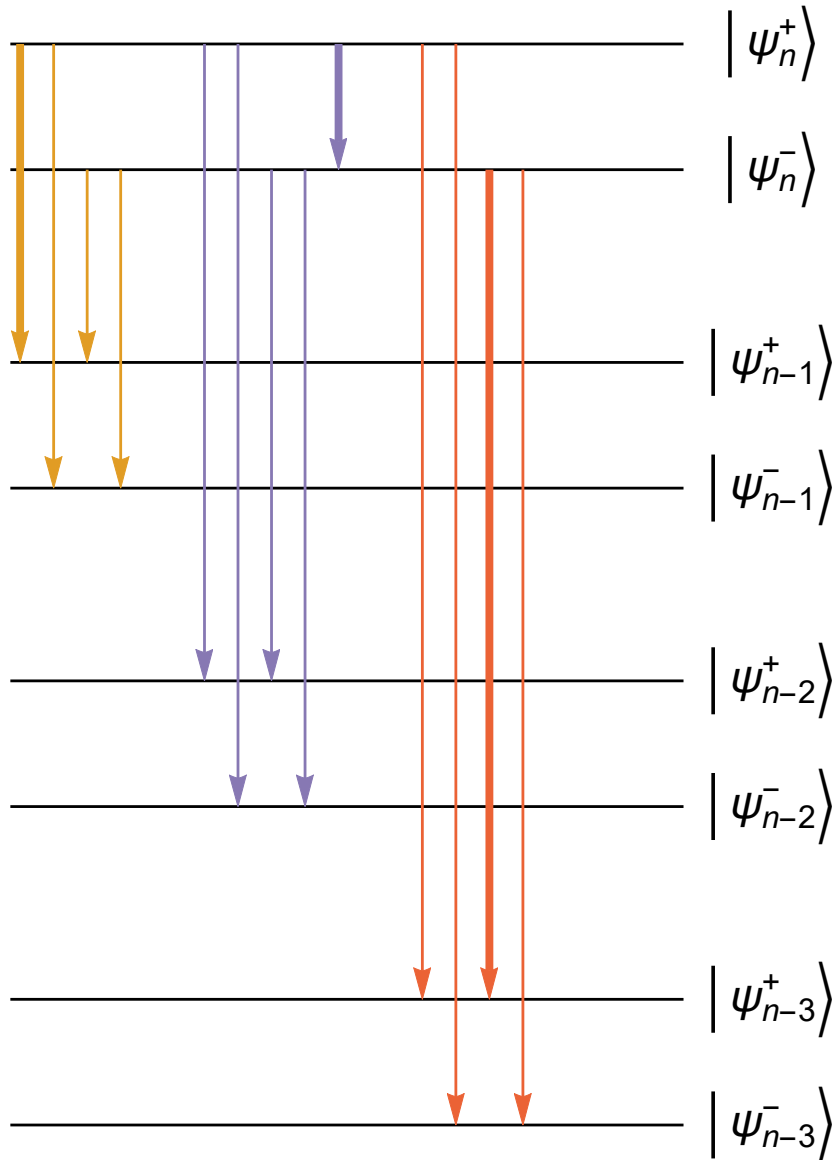
Figure 2.3: The first 4 bunch of transition are allowed by H_{JC}, as express in Eq. (2.71). Interestingly new 5 transitions are opened by H_S in violet. The 0-th order enable transition for $f = i - 1$, and symmetrically H_S enable new decay for $f = i, i - 2$. The transitions due to the counter rotating Hamiltonian H_R enable transitions for $f = i + 1, i - 3$. Of course f cannot be equal to $i + 1$ for the energy conservation, implicitly written in the Fermi golden rule. The three thicker lines will be studied in more details in the next subsection.

(a) resonant (left) and detuned (right)
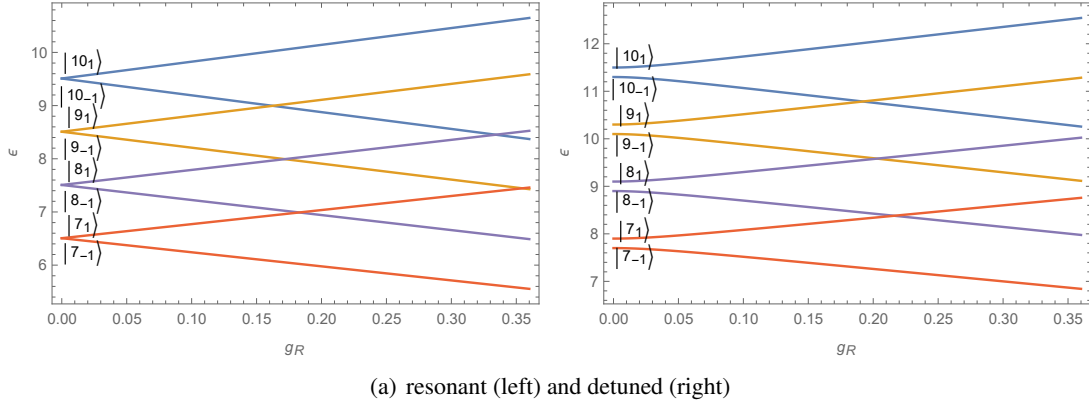
Figure 2.4: Energy spectrum from Eq. 2.58depends only on g_R/ω_c with $n = 10$, for the resonant case $\omega_a = \omega_c$ (a) and far from the resonance case $(\omega_c - \omega_a)/\omega_c = 0.2$ (b). Around $g_R = 0.16\omega_c$ on the left or $g_R = 0.19\omega_c$ on the right indicate the first energy crossings according to the JC model. For coupling constants beyond these values the structure of the energy ladder from Fig. (2.3) is not preserved.
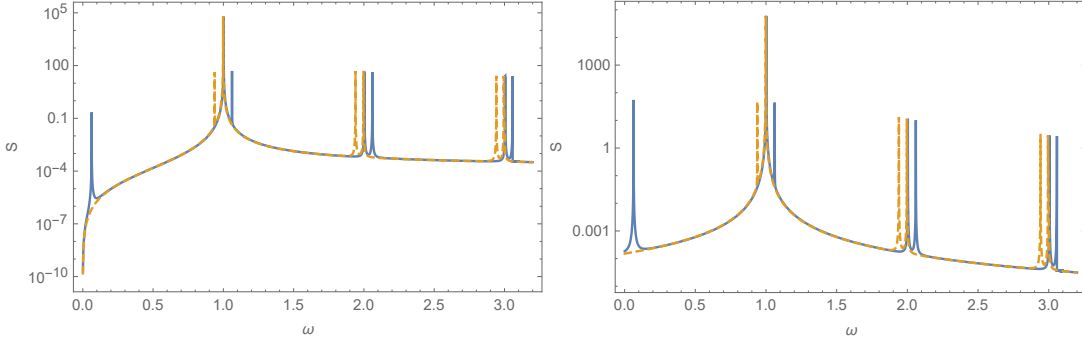

Figure 2.5: Emission spectra (arbitrary units) from the initial states $|10_+\rangle$ (blue) and $|10_-\rangle$ (orange) for the three- (a) and one-dimentional space (b), respectively sustaining densities of states ω^p with $p = 2$ (a) and $p = 0$ (b).

Fig. 2.3 depicts the thirteen allowed transitions from a selected manifold $\mathscr{E}(n)$, corresponding to different parts of the Hamiltonian, connecting respectively the $\mathscr{E}(n) \rightarrow \mathscr{E}(n-1)$ manifolds (the JC interaction term, green arrows), $\mathscr{E}(n) \rightarrow \mathscr{E}(n)$ and $\mathscr{E}(n) \rightarrow \mathscr{E}(n-2)$ manifolds (the AS Hamiltonian, purple arrows), $\mathscr{E}(n) \rightarrow \mathscr{E}(n-3)$ manifolds (the CR contribution, red arrows).

The transition frequencies will naturally depend on the coupling strength g_R, as already follows from the Jaynes-Cummings theory, and weakly on g_S through the second order perturbation [Eq. (2.65)]. The Jaynes-Cummings energy structure is shown in Fig. 2.4 for the states from $n = 7$ up to $n = 10$ manifolds, both in a resonant $\omega_c = \omega_a$ and detuned case $\omega_c - \omega_a = 0.2\omega_c$. In the Appendix, we argue that the range of applicability of the theory is limited by the first crossing of the states with energies below the initial state, which sets an upper limit on the coupling strength g_R. An even stronger limit is imposed by a normalization condition for the eigenstates (see the Appendix).

According to Eq. (2.67), the emission spectrum includes a set of approximately Lorentzian peaks. In Fig. 2.5 we separately plot spectra for the initial states $|10_+\rangle$ (solid blue line) and $|10_-\rangle$ (dashed orange line), for the resonant case $\omega_a = \omega_c$ and fixed coupling strengths $g_R = g_S = 0.1\omega_c$. The spectra are plotted for two different densities of states $\mathscr{P} \sim \omega^2$ [Fig. 2.5(a)] and $\mathscr{P} = \text{const.}$ [Fig. 2.5(b)]. The single low-energy peak around $\omega = 2\sqrt{10}g_R \approx 0.63\omega_c$ corresponds to the $|10_+\rangle \rightarrow |10_-\rangle$ transition induced by the inversion-symmetry breaking of the two-level system

and might unveil applications for low-frequency-sources. Therefore, its tunability is an important feature: the position of this peak depends on g_S, i.e. on the system's permanent dipole moment $\boldsymbol{d}_{ee}$ and on the field strength in the cavity related to the number of photons. In the classical limit, this provides the tuning possibility with the field amplitude [110]. Additionally, tuning could be achieved through orientation of the permanent dipole moment of the two-level system with an external DC electric field [113]. Around $\omega = \omega_c$ we recognize the Mollow triplet that arises from the JC interaction. Similar structures are repeated around $\omega = 2\omega_c$ and $\omega = 3\omega_c$, arising respectively from the AS and CR Hamiltonian perturbations. Note that the positions of sidebands of the Mollow-like triplet around $2\omega_c$ are related to the diagonal dipole moment and will accordingly be modified if g_S is tuned. We emphasize that all the peaks including the Mollow-like sidebands can be resolved in the spectra. In particular, even though the low-energy peak usually corresponds to the weakest transition intensities, it appears on top of a correspondingly suppressed background. In consequence, the signal-to-noise ratio is found comparable for all emission peaks. Below we analyze the intensity ratio of different peaks depending on the coupling strengths of the model.

We study three selected transitions representative for each Hamiltonian contribution, highlighted as thick arrows in Fig. 2.3: for the Jaynes-Cummings term we select the $|10_+\rangle \to |9_+\rangle$ transition, for the diagonal coupling term - the $|10_+\rangle \to |10_-\rangle$ transition, for the counter-rotating term - the $|10_+\rangle \to |7_-\rangle$ transition that corresponds to the highest frequency. In Fig. 2.6(a), we plot the squared amplitudes $|\langle f_\phi | a | i_\iota \rangle|^2$ which determine the transition probability in the one-dimentional case $p = 0$ [Eq. (2.70)]. The squared ampitudes are plotted separately for each of the considered transitions. As anticipated, the contribution due to the Jaynes-Cummings interaction is the leading term, overcoming other terms by several orders of magnitude for the investigated range of the coupling strengths g_R. The JC contribution itself weakly depends on g_R, though, which is also expected: the set of perturbed eigenstates $\{|n_\pm\rangle\}$ which are used as a basis closely corresponds to the Jaynes-Cummings basis $\left\{ |n_\pm^{(0)}\rangle \right\}$, from which it weakly deviates for large g_R. The purple (red) lines in Fig. 2.6 correspond to squared amplitudes for the selected transitions induced by the AS (CR) Hamiltonian, respectively. Results obtained for different values of $g_S = g_R, \frac{g_R}{10}, \frac{g_R}{100}$ are presented. We confirm the intuition suggested at the final paragraph of the previous section, that for equal coupling strengths $g_S = g_R$ the term induced by the diagonal coupling overcomes the counter-rotating contribution. Both terms share the same linear scaling with their respective coupling strengths g_S or g_R, so naturally as we decrease g_S, the squared transition amplitude $|a_{nn}^{+-}|^2$ is suppressed proportionally.

This simple linear scaling is slightly modified in the detuned case, in which the slopes change around $g_R \approx \frac{(\omega_c - \omega_a)}{2\sqrt{n}}$. An example for a strong detuning $\omega_a = 0.8\omega_c$ is shown in Fig. 2.6(b). We find that in this case the contribution of both perturbative terms is suppressed with respect to the resonant result. However, for relatively small coupling strengths $g_R < 4 \times 10^{-3}\omega_c$ the terms corresponding to the asymmetric contribution still dominate over the ones due to the counter-rotating Hamiltonian even for reduced $g_S \approx 0.01 g_R$.

For a wide range of the coupling strengths, the squared transition amplitudes induced by the part of the perturbation related to the asymmettry dominate over those originating from the counter-rotating term. However, the transition probability in a $p + 1$ dimensional space is rescaled by the density of states $\sim \left(E_i^\iota - E_f^\phi \right)^p$. Therefore, in 3D the low-energy transitions will be suppressed, while the high-energy component from the counter-rotating contribution to the Hamiltonian will be relatively increased. This rescaling is observed both in the resonant and off resonant case in Fig. 2.6(c,d). In the off-resonant case we note that the for equal coupling strengths $g_S = g_R$ the terms that origin at the diagonal-coupling still dominate over the counter-rotating ones, despite the latter are by far more energetically favorable.
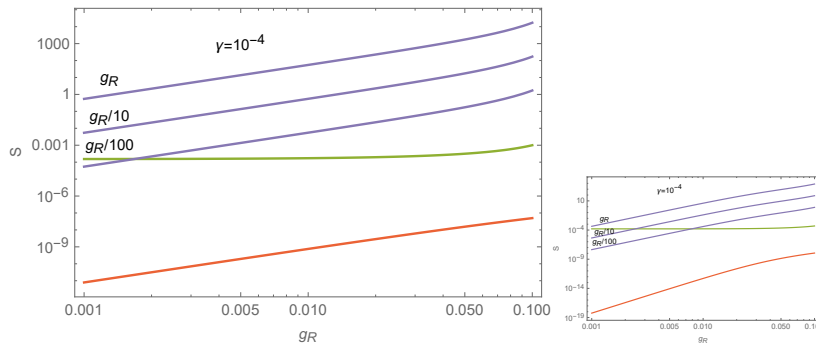
Rescaling of the transition probabilities between the one-dimentional [Fig. 2.6(a,b)] and three-
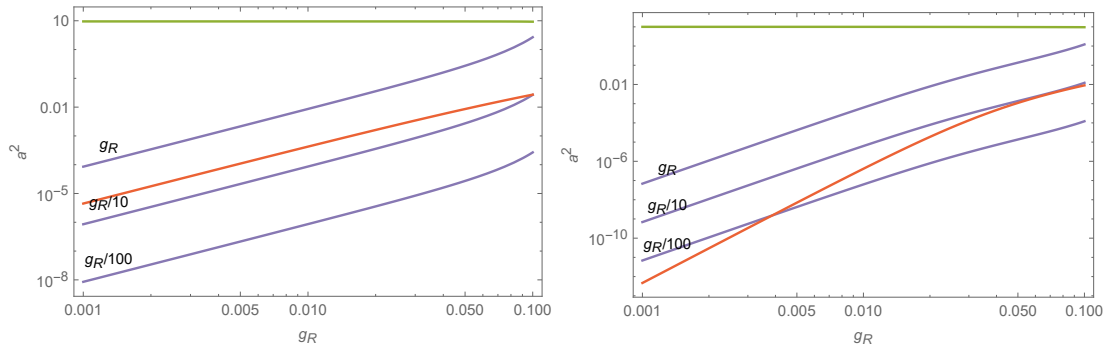
(a) 1D, resonant (on the left) detuned (on the right)
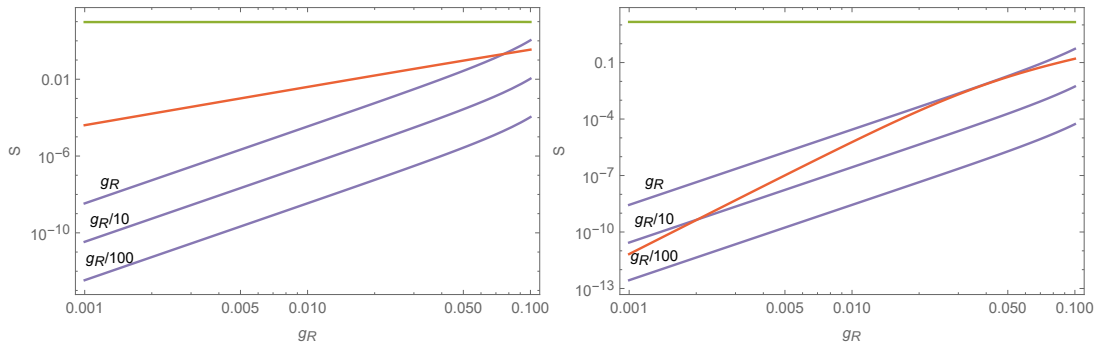
(b) 3D, resonant (on the left) detuned (on the right)

(c) Lorentzian, resonant (on the left) detuned (on the right)

Figure 2.6: Rescaled transition rates for densities of states corresponding to the 1D environment [$p = 0$, $\mathscr{P} = $ const., panels (a,b)], 3D [$p = 2$, $\mathscr{P} \sim \omega^{\in}$, panels (c,d)] case, as well as for a Lorentzian cavity resonant at $\hbar\omega_c = E_{ii}^{+-(0)}$ and with a quality factor $\gamma/\omega_c = 10^{-4}$ [panels (e,f)]. For $p = 0$, the result corresponds to the squared transition elements $\left| \langle f_\phi | a | i_\iota \rangle \right|^2$. Colors indicate different transition mechanisms: the Jaynes-Cummings transition $|10_+\rangle \to |9_+\rangle$ is shown in green, the counter-rotating term $|10_+\rangle \to |7_-\rangle$ in red, and the transition driven by the diagonal coupling $|10_+\rangle \to |10_-\rangle$ in violet for 3 values of the diagonal coupling strength $g_S = g_R, g_R/10, g_R/100$. Results are shown on resonance $\omega_c = \omega_a$ (a,c,e) and in a detuned case $(\omega_c - \omega_a)/\omega_c = 0.2$ (b,d,f).

dimentional cases [Fig. 2.6(c,d)] demonstrates the possibility of tailoring the output by density of states engineering. To highlight this point further, we insert the entire system in a single-mode cavity for which we assume a Lorentzian density of states, centered at the low-energy transition frequency $\omega_{\text{ext}} = E_{ii}^{+-(0)}$ and of full-width at half-maximum $\gamma_{\text{ext}} = 10^{-4}\omega_c$. A cavity with comparable parameters can be realized in photonic crystals [117] that provide 1D or 2D photonic environments, in whispering-gallery-mode resonators [118] or, with smaller quality factors, using metamaterials [119]. Here, the cavity is tailored to emphasize the strength of the low-energy transition $|n^+\rangle \to |n^-\rangle$ for the cost of suppressing other transitions. Indeed, as demonstrated in Fig. 2.6(e,f), this is successful both in the resonant case and for the strongly detuned one.

For the above analysis we have selected only one exemplary transition of the Jaynes-Cummings, diagonal-coupling and counter-rotating groups, corresponding to different-color arrows in Fig. 2.3. In Fig. 2.7, we demonstrate the total transition rates $\sum_{f,\phi} P_{f,10}^{\phi+}$ in each group, assuming a fixed initial state $|i_t\rangle = |10_+\rangle$. According to the notation in Eq. (2.69), the green line corresponds to the Jaynes-Cummings transitions $P_{9,10}^{++} + P_{9,10}^{-+}$, the purple line - to the diagonal coupling $P_{8,10}^{++} + P_{8,10}^{-+} + P_{10,10}^{-+}$, and the red line - to the counter-rotating contribution $P_{7,10}^{++} + P_{7,10}^{-+}$. We find that, as expected, the higher-energy contributions from the asymmetric Hamiltonian H_{AS} around $2\omega_a$ are strong enough to overcome the ones induced by the counter-rotating terms. This can be also seen from Fig. 2.7(c), in which we resolve different contributions induced by H_{AS} in the decay from the state $|10_+\rangle$. The difference between the two perturbative contributions becomes even smaller in the detuned case, in which all the perturbative terms are suppressed, as can be seen from panels (b,d) in Fig. 2.7.

2.3.3 Validity of the perturbative approach

In this section we verify the range of coupling strengths for which the perturbative approach applied in the main text is justified. Naturally, the condition is that the perturbation corrections to the energies are small with respect to the energy differences, and that the perturbation series converge both for the perturbed energies and the states. This is not the case around the energy crossings, where some of the series terms diverge. To identify the applicability range of the approach, we therefore perform two tests: we verify 1) preservation of the energy structure and 2) the normalization of the states.

Preservation of the energy structure

The structure of energy levels is preserved if the coupling strength g_R is small enough to avoid energy level crossings. Otherwise, a level crossing gives rise to divergent resonances which are not physical but they are artifacts of the theory: the energy differences in the denominators in Eq. (2.64) vanish and the expression diverges. The positions of the energy crossings depend on the initial state: in the following examples we choose $|10^+\rangle$ as the initial state, for which the first relevant crossing appears between the energies of states $|10^-\rangle$ and $|9^+\rangle$. Its position depends on the atom-cavity detuning: on resonance $\omega_a = \omega_c$ the crossing appears around $g_R/\omega_a = 0.15$, and blue-shifts as the cavity red-shifts from the atomic transition. That dependence is visualized in Fig. 2.8. Note that for a strong blue detuning of the cavity $\frac{\omega_a}{\omega_c} \leq 0.5$, the level ordering in the ladder structure from Fig. 2.3 is reshuffled and the analysis in this regime would have to be done independently.

Preservation of the ladder structure is just the necessary condition for the following analysis. In practice, the denominators in the coefficients in Eq. (2.64) can get arbitrarily large in close proximity of the crossing point, i.e. for $g_{R,\text{crossing}} - g_R < \delta$. This condition defines the parameter region for which the ladder structure is correctly represented in Fig. 2.4, and yields that the coupling strength must be strictly smaller than a threshold value $g_{R,\text{crossing}} - \delta$. We deem the distance δ to be safe if the energy difference of the states responsible for the first crossing (in the illustrated

(a) 1D, resonant (left) and detuned (right)

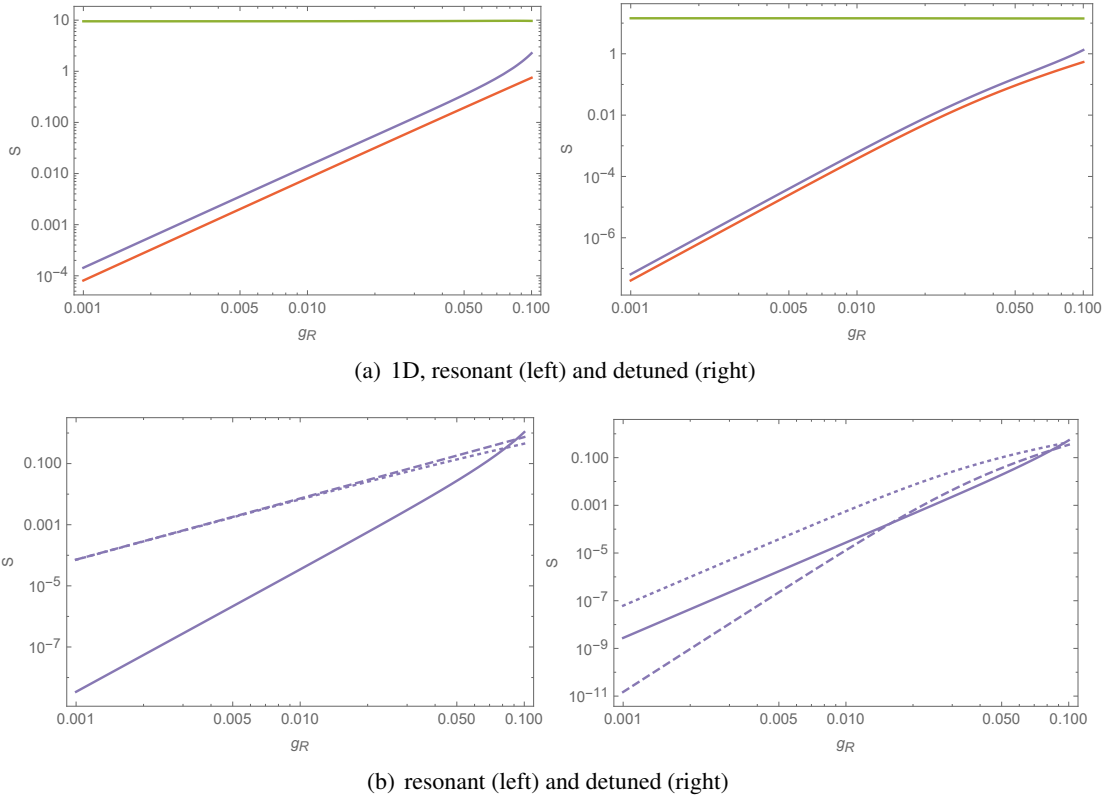(b) resonant (left) and detuned (right)

Figure 2.7: Total transition rates for each Hamiltonian contribution and for a fixed initial state $|10^+\rangle$: rate of the Jaynes-Cummings transitions $P_{9,10}^{++} + P_{9,10}^{-+}$ (green), diagonal coupling mechanism $P_{8,10}^{++} + P_{8,10}^{-+} + P_{10,10}^{-+}$ (violet), and the counter-rotating transitions $P_{7,10}^{++} + P_{7,10}^{-+}$ (red) on resonance (a) or for the detuned case (b). Individual contributions to the diagonal coupling are resolved in panels (c) - for the resonant, and (d) - the detuned cases, where the solid line represents the low-energy transition rate $P_{10,10}^{-+}$, while the dashed ($P_{8,10}^{++}$) and dotted ($P_{8,10}^{-+}$) lines correspond to the transitions around $2\omega_a$.
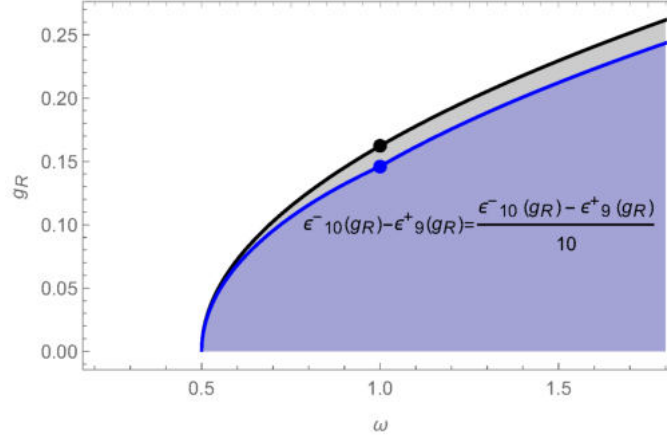
Figure 2.8: The black line corresponds to the position of the first level crossing in function of the relative energy of the atomic system and the cavity mode. The figure corresponds to the initial state $|10^+\rangle$. The black point corresponds to the first crossing in the left panel of Fig. 2.4. The structure of Fig. 2.3 is preserved in the part of parameter space shaded in grey. and the validity of our model is a subarea in blue where we consider the 10% of the energy difference without any coupling ($g_R = 0$). This analysis does not depend on g_S.

example: $E_{10}^{-(0)} - E_9^{+(0)}$) for a given coupling strength g_R is larger than 10% of its value for $g_R = 0$:

$$E_{10}^{-(0)}(g_R) - E_9^{+(0)}(g_R) \leq \frac{E_{10}^{-(0)}(0) - E_9^{+(0)}(0)}{10},$$

and the equality is achieved for $g_R = g_{R,\text{crossing}} - \delta$. Safe parameter space defined in this way is shaded in blue in Fig. 2.8.

Preservation of state normalization

The state norm is approximately preserved for a set of model parameters sufficiently away from an energy crossing. For the cases investigated in the main manuscript, the first energy crossing among the investigated states appears for those corresponding to the highest manifold. In Fig. 2.9, we plot the norm of the state $|10_+\rangle$ in function of $g_S = g_R$. A clear divergence appears for the coupling strengths approaching $0.14\omega_c$, which results from a crossing involving higher manifolds, in this case up to $\mathscr{E}(14)$. The vertical line in the figure indicates the limit for the coupling strengths considered in the main text.

In conclusion we have applied the 2nd order perturbation theory to investigate the emission properties of a two-level system coupled to a single-mode electromagnetic field, including interaction channels based on the Jaynes-Cummings, counter-rotating and asymmetry-related contributions. In the electric-dipole interaction mechanism, the first two arise from the coupling of the field mode with the induced transition dipole moment, the latter requires a permanent dipole characterizing the system's eigenstates. Light-matter coupling with permanent dipoles gives birth to additional emission peaks. We have demonstrated that even though at some frequencies the asymmetry-related contribution is weak in relative terms, the signal-to-noise ratio is comparable for all emission peaks. Moreover, the relative strengths of the emission peaks can be modified with a suitable photonic environment, as we have discussed for 1D systems and for a Lorentzian cavity. In the latter example we have shown that for cavity parameters that lie well within the range of experimental capabilities, the asymmetry-related emission channel may even dominate in absolute terms.
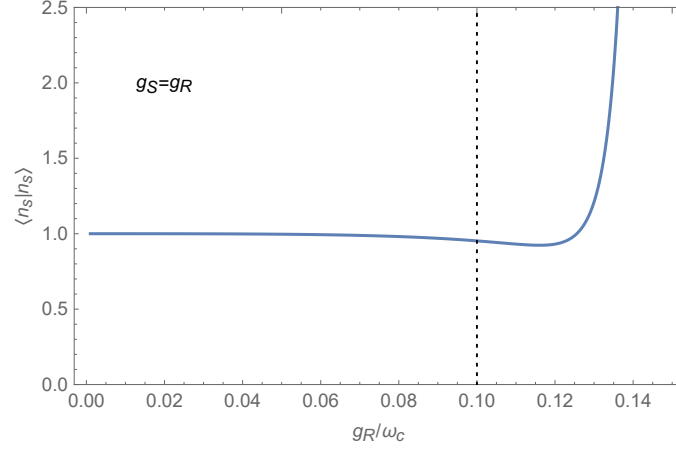
Figure 2.9: Norm of the state $|10_+\rangle$. For coupling strengths around and above $g_R > 0.1\omega_c$ the norm deviates from 1, which is an indication of breakdown of the perturbation theory.

2.4 Future research: the role of the environment and canonical derivation

In the analysis of section 2.1 we solve the problem of the divergence in the longitudinal component of the Green tensor propagator as discussed after Eq. 2.27, using the spatial extension of the wavefunctions which provide a natural regularization of the integral momenta of the quantum system surrounded by a continuum dispersive medium. However we can also solve the problem considering a point-like quantum system and regularize the continuum dispersive medium such that at higher frequencies the coupling with the quantum system is vanishing. Indeed, at this regime the theory doesn't work because the discretization of the atoms in the medium becomes relevant. In the following, we suggest how to implement this idea.

We implemented the phenomenological effective Hamiltonian in Eq. 2.15. However, starting from first principles of QED we can rewrite the creation and annihilation operators $\boldsymbol{f}^\dagger$ and $\boldsymbol{f}$ in terms of the noise polarization[87, 120], as follows

$$\boldsymbol{P}_N(\boldsymbol{r},\omega) = i\sqrt{\frac{\hbar\varepsilon_0}{\pi}\varepsilon_I(\boldsymbol{r},\omega)}\,\boldsymbol{f}(\boldsymbol{r},\omega), \tag{2.73}$$

where $\varepsilon_I(\boldsymbol{r},\omega) = \mathrm{Im}\varepsilon(\boldsymbol{r},\omega)$. The quantity rise up in the expression of the polarization due to the presence of the *bound* charge in the macroscopic treatment of Maxwell equation, in the expression of the polarization as a transfer function of the medium in the presence of an electric field[121]

$$\boldsymbol{P}_b(\boldsymbol{r},t) = \varepsilon_0 \int \int_0^\infty \chi(\boldsymbol{s},t)\boldsymbol{E}(\boldsymbol{r}-\boldsymbol{s},t-\tau)\,d\tau d^3 s + \boldsymbol{P}_N(\boldsymbol{r},t) \tag{2.74}$$

$$\tilde{\boldsymbol{P}}_b(\boldsymbol{k},\omega) = \varepsilon_0\varepsilon(\boldsymbol{k},\omega)\left(\tilde{\boldsymbol{E}}(\boldsymbol{k},\omega)-1\right) + \boldsymbol{P}_N(\boldsymbol{k},\omega), \tag{2.75}$$

with $\varepsilon(\boldsymbol{k},\omega) = 1 + \chi(\boldsymbol{k},\omega)$ and the latter equation is the Fourier transform of the former. The susceptibility χ of the medium is the *response function*, and it is convoluted in space and time with the electric field $\boldsymbol{E}$. Notice that there not exists an analogous term $\boldsymbol{P}_N$, in classical physics where we do not applied the same concept of vacuum. Nonetheless, according to fluctuation–dissipation theorem of classical statistical physics [2, 3], the fluctuation spectrum of a physical quantity $\boldsymbol{f}$ can be related to the imaginary part of the susceptibility. Denoting classical fluctuations by $\Delta\boldsymbol{P}_N = \boldsymbol{P}_N - \langle\boldsymbol{P}_N\rangle_{\mathrm{cl}}$ (the noise terms vanish on the classical average $\langle\boldsymbol{P}_N\rangle_{\mathrm{cl}}$[121]) the fluctuation and dissipation theorem (Fourier transform only in time) reads

$$\langle\Delta\boldsymbol{P}_N(\boldsymbol{r},\omega)\Delta\boldsymbol{P}_N^*(\boldsymbol{r}',\omega')\rangle_{\mathrm{cl}} = \frac{k_B T}{\pi\omega}\varepsilon_0\mathrm{Im}\chi(\boldsymbol{r},\omega)\delta(\boldsymbol{r}-\boldsymbol{r}')\delta(\omega-\omega') \tag{2.76}$$

with (k_B: Boltzmann constant; T: temperature). The imaginary parts of the response functions determine whether the medium is absorbing or amplifying. We only consider absorbing media for which $\chi(\boldsymbol{r}, \omega)$ has a positive imaginary part. The above equations thus reveal the intrinsic connection between fluctuations and absorption: fluctuations are necessarily present in any absorbing system at non-zero temperature. Note that the classical fluctuations vanish in the zero-temperature limit.

On the other hands, for a system prepare in a quantum state $|\psi\rangle$ of an appropriate Hilbert space, the quantum average observable is given by $\langle \boldsymbol{P}_N \rangle = \langle \psi | \boldsymbol{P}_N | \psi \rangle$, where now $\boldsymbol{P}_N$ is an operator acting on such Hilbert space. Its quantum fluctuations can be calculated according to $\left\langle (\Delta \boldsymbol{P}_N)^2 \right\rangle = \left\langle \boldsymbol{P}_N^2 \right\rangle - \left\langle \boldsymbol{P}_N \right\rangle^2$, with $\Delta \boldsymbol{P}_N = \boldsymbol{P}_N - \langle \boldsymbol{P}_N \rangle$. Then we have that the noise polarization vanishes on its grounds state average $\langle \boldsymbol{P}_N \rangle = 0$ and its fluctuations ruled by the fluctuation-dissipation theorem is

$$\left\langle \mathscr{S}\left(\Delta \boldsymbol{P}_N(\boldsymbol{r}, \omega) \Delta \boldsymbol{P}_N^\dagger(\boldsymbol{r}', \omega') \right) \right\rangle = \frac{\hbar}{2\pi} \varepsilon_0 \mathrm{Im}\chi(\boldsymbol{r}, \omega) \delta(\boldsymbol{r} - \boldsymbol{r}') \delta(\omega - \omega') \tag{2.77}$$

with $\mathscr{S}(ab) = \frac{1}{2}(ab + ba)$ denotes a symmetrised operator product. Note that the average thermal energy $k_B T$ appearing in the classical fluctuation-dissipation theorem has been replaced with the quantum ground-state energy $\frac{1}{2}\hbar\omega$ of a bosonic system. The use of a noise polarisation with a spectrum governed by (2.77) is known as Rytov theory [122], it lies at the heart of Lifshitz' s famous calculation of the Casimir force [123].

The imaginary part of the longitudinal Green tensor propagator for a non local susceptibility in Eq. 2.23 becomes

$$\mathrm{Im}\tilde{G}_{jk}^{\parallel}(\boldsymbol{q}, \omega) = \frac{c^2}{\omega^2} \frac{q_j q_k}{|\boldsymbol{q}|^2} \frac{\varepsilon_I(\boldsymbol{q}, \omega)}{|\varepsilon(\boldsymbol{q}, \omega)|^2} \tag{2.78}$$

In the relation of the permittivity we propose our model of suscptibility χ_0

$$\varepsilon(\boldsymbol{k}, \omega) = 1 + \chi(\boldsymbol{k}, \omega) = 1 + \chi_0(\boldsymbol{k}, \omega) \tag{2.79}$$

such that

$$\chi_0(\boldsymbol{k}, \omega) = (\chi_{0,R} + i\chi_{0,I}) \exp\left(-\frac{k^2}{k_M^2} \right). \tag{2.80}$$

This provide a convergent integral of with a cut-off paramenter k_M, as follows

$$\mathrm{Im}\tilde{G}_{jk}^{\parallel}(\boldsymbol{\rho}, \omega) = \frac{2\pi c^2}{(2\pi\omega)^2} \frac{\Im\chi_0(0, \omega)}{|1 + \chi_0(0, \omega)|^2} \frac{2k_M^3}{3\sqrt{\pi}} \delta_{ij} \left(1 + O(\rho^4) \right). \tag{2.81}$$

Here $\boldsymbol{\rho}$ is the relative distance between the positive charge at the origin and the relative negative charge.

In the end, one should be rigorous to derive the commutation relation of $\boldsymbol{f}$ and $\boldsymbol{f}^\dagger$ starting from the Lagrangian and applied the Fano diagonalization on the Hamiltonian obtained by the Legendre transform similarly to Ref [90].

Part Three

3. Second–order interferometry

"Building imaging setups via imagination: noise (fluctuation of source) becomes a resource"

(Watchmen)

In this chapter we introduce the basis of optical coherence theory which, deeply involves correlation functions to establish new methods for imaging. In particular, we discuss the working principle of the imagine technique called *Correlation Plenoptic Imaging* (CPI), focusing our attention on the case based on classical correlations between intensity fluctuations. The approach originates from the principles of ghost imaging with chaotic light and entangled photons. We will show that, in CPI, intensity correlation measurements between two spatially-resolving detectors provide the imaging capabilities typical of a plenoptic device, namely, multi-perspective imaging and refocusing. We characterize the signal–to–noise ratio for three experimental configurations based on the CPI method. We also show an application for remote distance sensing. In the end we discuss future research which has still a great unveil potential for the applications,as well as, turbulence-free imaging and fundamental insights for Quantum Optics.

3.1 History and state of the art

In 1954, Robert Hanbury Brown and Richard Q. Twiss introduced the intensity interferometer, applying an idea from the radio astronomy to the visible light range [124, 125]. The measurement of correlations of light intensity, leading to counter–intuitive interference effects in absence of field coherence [126, 127], has fostered the development of quantum optics [128]. In particular, the second-order correlation measurement at the heart of HBT effect has been the working tool of all entanglement-based protocols, from Bell's inequality tests [16] to quantum-enhanced technologies such as quantum imaging and lithography [129, 130], information [131, 132, 133, 134, 135], and teleportation [136]. Even more astonishing, starting from the new millennium, many of these effects have been replicated by exploiting the correlations of chaotic light [137, 138, 139, 140, 141, 142, 143]. Recently, novel schemes where second-order interference occurs effectively between light propagating through two pairs of paths. The light beams are mutually incoherent.

For more details, the theoretical suggestions are in Refs [144, 145, 146] and experimentally realized in [147, 148, 149, 150] for both the temporal and spatial domain. The physics behind this *"second-order interference beyond coherence"* phenomenon is very counter–intuitive and requires a deeper understanding of second-order coherence with thermal light with respect to the standard HBT paradigm [146]. On the other hand, this effect enables both sensing applications [144, 145, 146, 147, 148, 149, 150] and the simulation of a C-NOT gate with a single chaotic source [144, 145, 148]. In particular, in the spatial domain, it can be used for plenoptic imaging, a recent established optical imaging technique, based on the idea of recording both the spatial distribution and propagation direction of light in a single exposure, or to infer the feature of an object, namely a distant double-slit mask, with respect to a reference double-slit mask [145, 147]. Future developments are going toward the experimental setup in turbulence regime. In particular, interference was also tested in the presence of turbulence for a single mask [150].

3.2 Optical coherence theory

We discuss the properties of fluctuating electromagnetic fields, paying attention mainly to the optical region of the electromagnetic spectrum. It seems hardly necessary to stress that every electromagnetic field found in nature has some fluctuations associated with it. Even though these fluctuations are usually much too rapid to be observed directly at optical frequency, one can deduce their existence from suitable experiments that provide information about correlations between the fluctuations at two or more space-time points. The simplest manifestations of correlations in optical fields are the well-known interference effects that arise when two light beams that originate from the same source are superposed at appropriate distance and controlled parameters to be visible. With the availability of modern light detectors and electronic circuitry of very short resolving time, other types of correlations in optical fields began to be studied in more recent times. These investigations led to a systematic classification of optical correlation phenomena and the complete statistical description of optical fields. The area of optics concerned with such questions is now generally known as *optical coherence theory*[151].

Let us start from the description of the electromagnetic wave in the free space. Despite the electromagnetic field has a vector structure and it should generally described with two perpendicular polarization terms, for our purposes we assume that the polarization is not relevant and we consider a complex scalar V

$$\boldsymbol{\nabla} V\left(\boldsymbol{r},t\right) = \frac{1}{c^2}\frac{\partial^2}{\partial t}V\left(\boldsymbol{r},t\right). \tag{3.1}$$

Physically, the scalar field is a fluctuation function of space and time that can be described via a stationary appropriate ensemble. Since different frequency components of a stationary ensemble are not correlated, it is sufficient to deal with one frequency component at a time, thus we can assume that our ensemble consists of quasi–monochromatic components centered at the frequency v with the spatial and temporal dependence factorized, i.e. $V\left(\boldsymbol{r},t\right) = v\left(\boldsymbol{r}\right)\mathrm{e}^{\mathrm{i}2\pi vt}$, where v contains the amplitude and the phase of the wave at the point $\boldsymbol{r}$. Due to the value of optical frequencies, V cannot be measured as a function of time, since optical periods are of the order of 10^{15}s, whereas photoelectric detectors have typically resolving times of the order of 10^{11}s. Mathematically speaking, with the nowadays devices $\langle V\left(\boldsymbol{r},t\right)\rangle = 0$. However, although one cannot study the rapid time variations of the field, one can make measurements of the slowly–varying correlations of the field at two or more space-time points, related the cross correlation function W or the Glauber function Γ that will be introduced later on (more details in [151]).

The statistical implementation of this average will be applied for the wavefield V on the source of the light, as well as, on the emitters, because its propagation is deterministic and it comes from

Eq. 3.1. Hence, for monochromatic field with the dependence on the time factorized in a phase, the Eq. 3.1 becomes

$$\nabla^2 V(\boldsymbol{r}) + k^2 V(\boldsymbol{r}) = 0, \tag{3.2}$$

with $k = 2\pi\nu/c$, named the free-space wave number and c, the speed of light. We consider a field that propagates along the z–axis and under the paraxial approximation, namely the field is measured only for small angles around the z–axis. By replacing $V(\boldsymbol{r}) = v(\boldsymbol{r})\,\mathrm{e}^{ikz}$ and neglecting the second derivative of v with respect to z we obtain the paraxial equation

$$\left(2ik\frac{\partial}{\partial z} + \frac{\partial^2}{\partial y^2} + \frac{\partial^2}{\partial x^2}\right) V(\boldsymbol{r}) = 0. \tag{3.3}$$

Knowing the field in $V(\boldsymbol{\rho}_0, 0)$, the value propagated at a distance z from Eq. 3.3 is determined by the optical deterministic transfer function $\mathscr{G}$ as follows

$$V(\boldsymbol{\rho}, z) = \int V(\boldsymbol{\rho}_0, 0)\mathscr{G}(\boldsymbol{\rho} - \boldsymbol{\rho}_0)\,\mathrm{d}^2\rho_0, \qquad \mathscr{G}(\boldsymbol{\rho} - \boldsymbol{\rho}_0) = \frac{k\mathrm{e}^{ikz}}{2\pi iz}\mathrm{e}^{i\frac{k}{2z}(\boldsymbol{\rho} - \boldsymbol{\rho}_0)^2}. \tag{3.4}$$

However, to describe the propagation of the field emitted by chaotic sources, the result 3.4 can be generalized to the case of a quasi-monochromatic random field $V(\boldsymbol{\rho}_0, 0)$.

Now we know how the field is propagated. In the following we see what is the proper observable for the second-order interference function.

As we have mentioned in the introduction of this chapter, interference is a measurement of correlation, which is the key concept to achieve the characterization of the source. As a phenomena related to the correlation, in the following we briefly recall what is the interference. Let V the field at the coordinate $(\boldsymbol{r}, t)$ as a sum of two fields emitted from sources placed in the points $\boldsymbol{r}_1$ and $\boldsymbol{r}_2$ at time t_1 and t_2, respectively

$$V(\boldsymbol{r}, t) = \sum_{i=1,2} V(\boldsymbol{r}_i, t - t_i), \text{ with } t_i = |\boldsymbol{r} - \boldsymbol{r}_i|/c. \tag{3.5}$$

The instantaneous intensity is $i(\boldsymbol{r}, t) = V(\boldsymbol{r}, t)V^*(\boldsymbol{r}, t)$ and the intensity that we measure $I(\boldsymbol{r}, t) = \langle i(\boldsymbol{r}, t)\rangle$ gives the *law of interference*

$$I(\boldsymbol{r}, t) = I_1(\boldsymbol{r}, t - t_1) + I_2(\boldsymbol{r}, t - t_2) + 2\mathrm{Re}[\langle V(\boldsymbol{r}_1, t - t_1)V^*(\boldsymbol{r}_2, t - t_2)\rangle]. \tag{3.6}$$

The *cross-correlation function* of the random processes $V(\boldsymbol{r}_1, t)$ and $V(\boldsymbol{r}_2, t)$ is

$$W^{(t)}(\boldsymbol{r}_1, t_1; \boldsymbol{r}_2, t_2) = \langle V(\boldsymbol{r}_1, t - t_1)V^*(\boldsymbol{r}_2, t - t_2)\rangle \tag{3.7}$$

which is a modulation of the averaged intensity $I_1(\boldsymbol{r}, t)$ and $I_2(\boldsymbol{r}, t)$ rising up an energy redistribution process.

The function $W^{(t)}(\boldsymbol{r}_1, t_1; \boldsymbol{r}_2; t_2)$ is the main quantity of the elementary *theory of optical coherence*, where the superscript points out the temporal dependence. Assuming that the optical field is stationary, at least in the wide sense, and ergodic, then we can define also the *cross-spectral correlation density function* as

$$\langle \tilde{V}^*(\boldsymbol{r}_1)\tilde{V}(\boldsymbol{r}_2)\rangle = \tilde{W}(\boldsymbol{r}_1, \boldsymbol{r}_2, \nu)\,\delta(\nu' - \nu), \tag{3.8}$$

which comes from the Fourier transform of 3.7. Temporal and spectral spatial coherence are characterized in terms of $W^{(t)}$ and $W^{(\nu)}$, respectively. In the first case, the dependence of the correlation on the parameter t or ν is crucial, with the points in $\boldsymbol{r}_1$ and in $\boldsymbol{r}_2$ being coincident and kept fixed; in the second case the dependence on the position of the two points is crucial, while, the
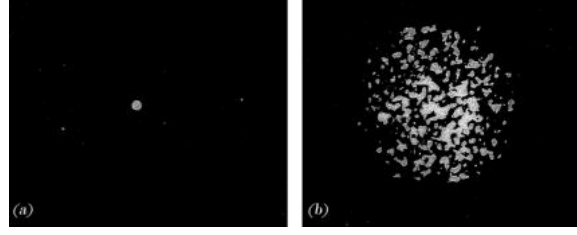
Figure 3.1: Intensity distribution narrow and coherent typical of a laser beam (a), and broaden and partially coherent source typical of pseudothermal light (b). Intensity distribution is a frame and a speckle is intuitively defined as a part of the frame where the coherence light is uniformly bright.

time delay t is kept essentially fixed. In other words, the correlation is restricted to a range that is short compared to $1/\Delta\nu$. However, only in very simple cases one can sharply distinguish between temporal and spatial coherence, whereas generally these two types of coherence are coupled (more details in Ch.4 of [151]).

However, for our purposes, we consider only Eq. 3.7 at equal time $t_1 = t_2$. The (ensemble) average on the left-hand side is taken on the set of the different realizations of the field. More precisely, a realization of the field is defined as a frame pattern which preserves its longitudinal coherence along its path from the source to the detector (see Fig. 3.1). Actually, we identify V as the appropriate field variable such that the detector performs an average over a time interval that is long compared to the time scales of the fluctuating field, i.e. long compared to the mean period and to the coherence time of the light. Alternatively, the ensemble average of the intensity may be found from a succession of measurements, whether the measurement times are long or short.

Considering a monochromatic planar source S to be $z = 0$ for convenience and defining $\boldsymbol{\rho} = (x, y)$ as the two-dimensional transverse coordinate, the cross-correlation functions from Eq. 3.7 is

$$W_S(\boldsymbol{\rho}_1, \boldsymbol{\rho}_2) = \langle V(\boldsymbol{\rho}_1, 0) V^*(\boldsymbol{\rho}_2, 0) \rangle = \langle V_S(\boldsymbol{\rho}_1) V_S^*(\boldsymbol{\rho}_2) \rangle. \tag{3.9}$$

We can always think W_S like the geometric average of the intensities from the points $\boldsymbol{\rho}_1$ and $\boldsymbol{\rho}_2$ weighted by an adimensional function g which depends on the difference between $\boldsymbol{\rho}_1$ and $\boldsymbol{\rho}_2$, therefore we write

$$W_S(\boldsymbol{\rho}_1, \boldsymbol{\rho}_2) = \sqrt{I_S(\boldsymbol{\rho}_1) I_S(\boldsymbol{\rho}_2)} g(\boldsymbol{\rho}_1, \boldsymbol{\rho}_2). \tag{3.10}$$

The intensity $I_S(\boldsymbol{\rho}) = \langle V_S(\boldsymbol{\rho}_1) V_S^*(\boldsymbol{\rho}_2) \rangle$ is the average value of the distribution $i_S(\boldsymbol{\rho}) = V_S(\boldsymbol{\rho}_1) V_S^*(\boldsymbol{\rho}_2)$ represented in Fig. 3.1 and g, the complex degree of spatial coherence of the field across the source satisfying $g(0) = 1$. Here, we make the hypothesis that $V(\boldsymbol{r}, t) = v(\boldsymbol{r}) e^{i\varphi(\boldsymbol{r})}$, namely the amplitude of field is deterministic with a random phase, and that g depends only on the distance of the transverse coordinates $\boldsymbol{\rho}_1$ and $\boldsymbol{\rho}_2$, it can be expressed as

$$g(\boldsymbol{\rho}_1 - \boldsymbol{\rho}_2) = \left\langle e^{i(\varphi(\boldsymbol{\rho}_2) - \varphi(\boldsymbol{\rho}_1))} \right\rangle. \tag{3.11}$$

The phase φ is a complex function. With the dependence on the difference we are saying that only in a neighborhood of $\boldsymbol{\rho}_1$ there is correlation. For a lighter notation let us call $\phi \equiv \varphi(\boldsymbol{\rho}_2) - \varphi(\boldsymbol{\rho}_1)$.

Therefore, the expansion in series centered at $\boldsymbol{\rho}_1$ yields

$$
\begin{aligned}
\langle \mathrm{e}^{\mathrm{i}\phi} \rangle = 1 + \mathrm{i} \sum_{i=x,y} & \left\langle \partial_i \phi \Big|_{\boldsymbol{\rho}_2=\boldsymbol{\rho}_1} \right\rangle (\boldsymbol{\rho}_2 - \boldsymbol{\rho}_1)_i \\
& - \frac{1}{2} \sum_{i,j} \left\langle \partial_j \phi \partial_i \phi \Big|_{\boldsymbol{\rho}_2=\boldsymbol{\rho}_1} \right\rangle (\boldsymbol{\rho}_2 - \boldsymbol{\rho}_1)_i (\boldsymbol{\rho}_2 - \boldsymbol{\rho}_1)_j \\
& + \frac{\mathrm{i}}{2} \sum_{i,j} \left\langle \partial_j \partial_i \phi \Big|_{\boldsymbol{\rho}_2=\boldsymbol{\rho}_1} \right\rangle (\boldsymbol{\rho}_2 - \boldsymbol{\rho}_1)_i (\boldsymbol{\rho}_2 - \boldsymbol{\rho}_1)_j + o\left((\boldsymbol{\rho}_2 - \boldsymbol{\rho}_1)^2\right),
\end{aligned}
\tag{3.12}
$$

here the summation is assumed on the planar component of $\boldsymbol{\rho}_1, \boldsymbol{\rho}_2$. Now, we assume that φ has a random phase, and also its variation is random, then the second term

$$
\left\langle \partial_i \phi \Big|_{\boldsymbol{\rho}_2=\boldsymbol{\rho}_1} \right\rangle = 0.
\tag{3.13}
$$

We also assume that the phase is homogeneously random, therefore also the last term is vanishing. The remain terms can be rewritten as follows

$$
\begin{aligned}
\langle \mathrm{e}^{\mathrm{i}\phi} \rangle = 1 - \frac{1}{2} & \left\langle (\partial_x \phi)^2 \Big|_{\boldsymbol{\rho}_2=\boldsymbol{\rho}_1} (x_2 - x_1)^2 + (\partial_y \phi)^2 \Big|_{\boldsymbol{\rho}_2=\boldsymbol{\rho}_1} (y_2 - y_1)^2 \right\rangle \\
& - \left\langle \partial_x \phi \partial_y \phi \Big|_{\boldsymbol{\rho}_2=\boldsymbol{\rho}_1} \right\rangle (x_2 - x_1)(y_2 - y_1) + o\left((\boldsymbol{\rho}_2 - \boldsymbol{\rho}_1)^2\right)
\end{aligned}
$$

Now, an isotropic hypothesis implies $\left\langle (\partial_x \phi)^2 \right\rangle = \left\langle (\partial_y \phi)^2 \right\rangle = \sigma_g^{-2}$, and the hypothesis of independence of variation along orthogonal direction gives us $\langle \partial_x \phi \partial_y \phi \rangle = \langle \partial_x \phi \rangle \langle \partial_y \phi \rangle = 0$. Finally, neglecting higher order terms we have

$$
g(\boldsymbol{\rho}_1 - \boldsymbol{\rho}_2) = 1 - \frac{(\boldsymbol{\rho}_2 - \boldsymbol{\rho}_1)^2}{2\sigma_g^2} + o\left((\boldsymbol{\rho}_2 - \boldsymbol{\rho}_1)^2\right) \simeq \exp\left(-\frac{(\boldsymbol{\rho}_2 - \boldsymbol{\rho}_1)^2}{2\sigma_g^2}\right).
\tag{3.14}
$$

Here, the expression of g reflects the idea that close emitters on the source have non-vanishing relative phase. In addition, from Eq. 3.10 we take Gaussian source profile

$$
I_S(\boldsymbol{\rho}_S) = I_S \frac{\mathrm{e}^{-\frac{\boldsymbol{\rho}_S^2}{2\sigma_i^2}}}{2\pi\sigma_i^2}, \qquad g(\boldsymbol{\rho}) = \mathrm{e}^{-\frac{\boldsymbol{\rho}^2}{2\sigma_g^2}}.
\tag{3.15}
$$

This is known as *Gaussian-Schell model* (see details in[152]). Here, $I_S := I_S(\mathbf{0})$ is the intensity peak, σ_i defines the effective width of the intensity profile and σ_g, the transverse coherence length of the relative distance $\boldsymbol{\rho}$ between two points. Combining Eqs. (3.9,3.10,3.15) the field $V_S(\boldsymbol{\rho}_s)$ at a point $\boldsymbol{\rho}_S$ on the source, Eq. 3.10 assume the following fashion

$$
W_S(\boldsymbol{\rho}_S, \boldsymbol{\rho}_S') = \langle V_S(\boldsymbol{\rho}_s) V_S^*(\boldsymbol{\rho}_s) \rangle = I_S \mathrm{e}^{-\frac{\rho_S^2}{4\sigma_i^2}} \mathrm{e}^{-\frac{\rho_S'^2}{4\sigma_i^2}} \mathrm{e}^{-\frac{(\rho_S - \rho_S')^2}{2\sigma_g^2}}.
\tag{3.16}
$$

The equation (3.16) fully entails the characterization of the statistical model of the source, and since the propagation is deterministic, of the entire following treatment. Moreover, the choice of the Gaussian profile source is particularly useful, because it is preserved also for the observable that we measure by means of the detectors through Eq (3.4). In particular, more than the mutual coherence

function W, we are interested to measure on the detector the correlation intensity fluctuation Γ that is defined as follows

$$\Gamma(\boldsymbol{r}_1, \boldsymbol{r}_2) = \langle \Delta i(\boldsymbol{r}_1) \Delta i(\boldsymbol{r}_2) \rangle. \tag{3.17}$$

where $\Delta i(\boldsymbol{r}) = i(\boldsymbol{r}) - I(\boldsymbol{r})$. In our scenario we assume that the full statistics of the fields $V(\boldsymbol{\rho})$ depends only on the second order moment. It can be proven that the only random variable in agreement with such statistics must be a Gaussian probabilistic distribution. In order to evaluate Γ in Eq. 3.17 we define a random vector $\mathbb{V} = (V^*(\boldsymbol{r}_1), V(\boldsymbol{r}_1), V^*(\boldsymbol{r}_2), V(\boldsymbol{r}_2))$ such that it follows a Gaussian probabilistic distribution. We write

$$\mathbb{V} \sim \mathcal{N}(\boldsymbol{\mu}, \Sigma) = \exp\left[-\frac{1}{2}(\boldsymbol{V} - \boldsymbol{\mu})^\dagger \Sigma (\boldsymbol{V} - \boldsymbol{\mu})\right] \tag{3.18}$$

where $\boldsymbol{\mu}$ is the mean vector and Σ is the covariance matrix. Under this conditions we can apply the Isserlis-Wick's theorem [153], where all even order moment can we written in terms of second order moments.

$$\begin{aligned}
\Gamma(\boldsymbol{r}_1, \boldsymbol{r}_2) &= \langle (i(\boldsymbol{r}_1) - I(\boldsymbol{r}_1))(i(\boldsymbol{r}_2) - I(\boldsymbol{r}_2)) \rangle \\
&= \langle V^*(\boldsymbol{r}_1) V(\boldsymbol{r}_1) V^*(\boldsymbol{r}_2) V(\boldsymbol{r}_2) \rangle \\
&\quad - \langle V^*(\boldsymbol{r}_1) V(\boldsymbol{r}_1) \rangle \langle V^*(\boldsymbol{r}_2) V(\boldsymbol{r}_2) \rangle \\
&= \langle V^*(\boldsymbol{r}_1) V(\boldsymbol{r}_2) \rangle \langle V^*(\boldsymbol{r}_2) V(\boldsymbol{r}_1) \rangle \\
&\quad + \langle V^*(\boldsymbol{r}_1) V^*(\boldsymbol{r}_2) \rangle \langle V(\boldsymbol{r}_1) V(\boldsymbol{r}_2) \rangle \\
&= |W(\boldsymbol{r}_1, \boldsymbol{r}_2)|^2 + \langle V^*(\boldsymbol{r}_1) V^*(\boldsymbol{r}_2) \rangle \langle V(\boldsymbol{r}_1) V(\boldsymbol{r}_2) \rangle.
\end{aligned}$$

Here, $W(\boldsymbol{r}_1, \boldsymbol{r}_2) = \langle V^*(\boldsymbol{r}_1) V(\boldsymbol{r}_2) \rangle$; $\langle V^*(\boldsymbol{r}_1) V^*(\boldsymbol{r}_2) \rangle$ and $\langle V(\boldsymbol{r}_1) V(\boldsymbol{r}_2) \rangle$ are vanishing under the assumption of Gaussian distribution function on the field, because for those functions the respective phases are not in the difference. It is a straightforward calculation that here we only explain with the intuition that for $\boldsymbol{r}_2$ closer and closer to $\boldsymbol{\rho}_1$ the degree of coherence g in Eq. 3.15 must increase. But for these case we have $\langle e^{\pm i(\varphi(\boldsymbol{r}_2) + \varphi(\boldsymbol{r}_1))} \rangle \sim \langle e^{\pm i2\varphi(\boldsymbol{r}_1)} \rangle = 0$, because any notion of distance between the emitters makes sense. This is also know as *random phase assumption*. Therefore Γ becomes

$$\Gamma(\boldsymbol{r}_1, \boldsymbol{r}_2) = |W(\boldsymbol{r}_1, \boldsymbol{r}_2)|^2. \tag{3.19}$$

Applying the correlator on two different points A and B on the detectors D_a and D_b, respectively, together with the assumption used for deriving the propagator in Eq. 3.4 along z direction, the deterministic part goes out the average, which yields in the limit of completely incoherent source $\sigma_g \to 0$

$$\Gamma(\boldsymbol{\rho}_A, \boldsymbol{\rho}_B) = I(\boldsymbol{\rho}_A) I(\boldsymbol{\rho}_B) e^{-\frac{(\boldsymbol{\rho}_A - \boldsymbol{\rho}_B)^2}{\sigma^2}}, \tag{3.20}$$

where $\sigma = \lambda z / 2\pi \sigma_i$ is the coherence area at a distance $z = z_1 = z_2$ from the source (an explicitly derivation can be found in [154]). This relation entails the typical point–to–point correspondence of an imaging setup. Basically, each point on the plane object as a corresponding transfer function to the image plane as one can see in Fig. 3.2. This equation is the key concept of second-order imaging [1] The function Γ at a given $\boldsymbol{\rho}_a$ is significantly different from zero in a neighborhood of the corresponding point $\boldsymbol{\rho}_b$ on the other sensor. This is at the basis of the possibility to retrieve a

---

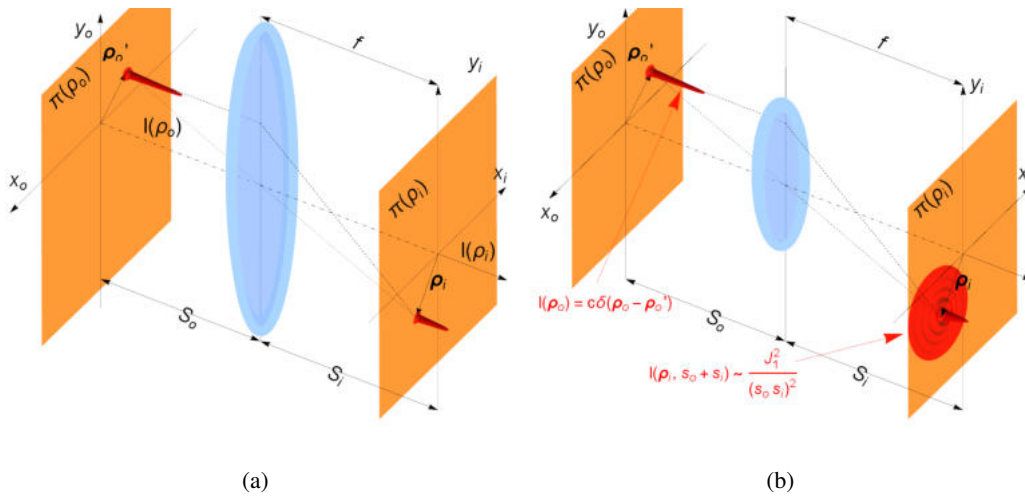[1]Second order is referred to the correlations between intensity, and it will be at the forth order in the wavefields.

Figure 3.2: In the simplest imaging setup, a point with coordinate $\boldsymbol{\rho}'_o$ in the object plane (visualized as a chaotic source) is mapped by a lens into a point with coordinate $\boldsymbol{\rho}_i$ for the ideal case of infinite lens (a), and in more realistic configuration to a Point Spread Function (PSF), proportional to the Bessel function J_1 as in the example on the right (b). Interestingly, Eq. 3.20 enable a similar correspondence, hence is useful for experimental imaging configurations. This is the kernel of the second-order imaging.

"ghost" image. Let us consider Fig. 3.5-a where two holes are placed respectively in $\boldsymbol{\rho}_{b1}$ and $\boldsymbol{\rho}_{b2}$. Therefore

$$\Gamma(\boldsymbol{\rho}_A, \boldsymbol{\rho}_B) = I(\boldsymbol{\rho}_A) I(\boldsymbol{\rho}_B) e^{-\frac{(\boldsymbol{\rho}_A - \boldsymbol{\rho}_B)^2}{\sigma^2}} \sim \begin{cases} 0 & \boldsymbol{\rho}_B \neq \{\boldsymbol{\rho}_{b1}, \boldsymbol{\rho}_{b2}\}, \\ 0 & \boldsymbol{\rho}_A - \boldsymbol{\rho}_B \gg \sigma^2, \\ I(\boldsymbol{\rho}_A) I(\boldsymbol{\rho}_B) & \boldsymbol{\rho}_A \sim \boldsymbol{\rho}_{b1} \vee \boldsymbol{\rho}_{b2}. \end{cases} \quad (3.21)$$

The above equation clearly shows that the function Γ is large in correspondence of the positions of points where the light passes through the object mask[155, 156, 157, 158, 147]. Let us observe that integration over the whole sensor D_b, at fixed $\boldsymbol{\rho}_a$, yields an incoherent image of the object, which sets a quasi one-to-one correspondence between points $\boldsymbol{\rho}_a$ and $\boldsymbol{\rho}_b$.

As an example, to better highlight the correspondence properties between the point $\boldsymbol{\rho}_A$ and $\boldsymbol{\rho}_O$ of an object described by its object transmission function $A(\boldsymbol{\rho}_O)$ we consider Fig. 3.5-a and define $\Sigma_{z_a}(\boldsymbol{\rho}_A)$, the *signal* observable [156]

$$\Sigma_{z_a}(\boldsymbol{\rho}_A) = \int_{D_b} \Gamma(\boldsymbol{\rho}_A, \boldsymbol{\rho}_B) \, d^2\rho_B \sim \int |A(\boldsymbol{\rho}_O)|^2 \left| \tilde{I}\left(\frac{\omega_0}{c z_a}(\boldsymbol{\rho}_O - \boldsymbol{\rho}_A) \right) \right|^2 d^2\rho_B. \quad (3.22)$$

Here $\tilde{I}$ is the Fourier transform of the Gaussian intensity profile. Up to an intensity-rescaling factor Eq. 3.22 sets a quasi one-to-one correspondence between points of the plan of the objects $\boldsymbol{\rho}_O$ and the pixel of the sensor D_a at $\boldsymbol{\rho}_A$ with a spread uncertainty $\Delta\boldsymbol{\rho}_A \simeq 2\pi c z_a / (\omega_0 D_s)$, defined by the effective diameter $D_s \simeq 2\pi\sigma_i^2$ of the source in Eq. 3.15.

Up to now we provided a model of a statistical source of the light and the expression of a suitable observable Γ, and it integration on the bucket to better visualize the features of the point spread function of a simplest scenario of Fig. 3.5-a) (more details in [156]). This analysis showed how to overpass the problem of rapidly fluctuation of the field and enable us to applying the second-order interferometry properties for imaging setups. Let us close the section with a remark on the definition of Γ in Eq. (3.17) depending on the intensity fluctuations.
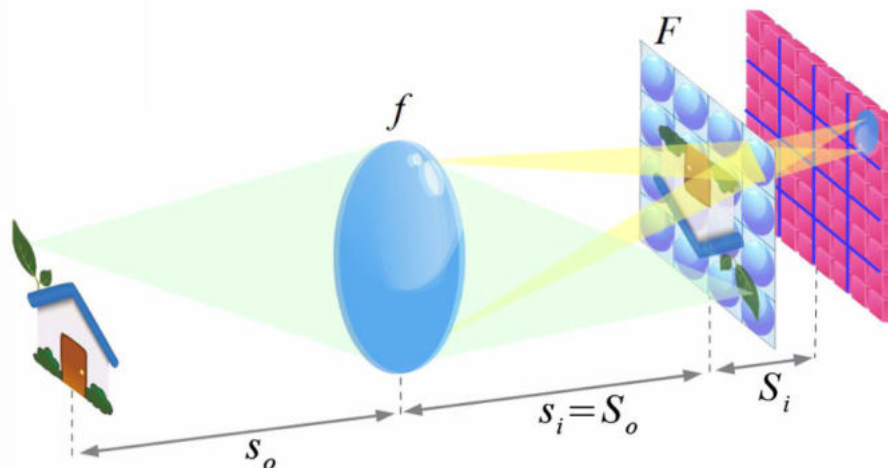
Figure 3.3: The lens focuses the object on a lenslet array. Each micro–lens focuses the main lens on a macro–pixel (blue lines) of the sensor to provide directional information.

Commonly, the fluctuations of an observable are considered noise, but here such noise is properly the resource that we will use to implement the well-know Correlation Plenoptic Imaging, and studying its typical Signal-to-Noise ratio [159].

3.3 Correlation Plenoptic Imaging

Ordinary cameras record the total amount of light at each point on the photo–sensor. The goal of a plenoptic camera is to acquire also the amount of light traveling along each ray that intersects the sensor. One can also think of this as capturing the directional lighting distribution arriving at each location on the sensor. The purpose of capturing the additional directional data is to allow us to apply ray-tracing techniques to compute synthetic photographs flexibly from the acquired light, namely refocusing out-of-focus parts of the scene, extending the depth of field, and performing three-dimensional reconstruction [160]. The key feature of a plenoptic imaging device is a micro–lens array inserted in the native image plane, between the imaging lens and the sensor. The micro–lenses act as imaging pixels to collect spatial information of the scene. Moreover, each one of them reproduces an image of the main lens on the sensor array (see Fig. (3.3)), thus providing the angular information associated with each imaging pixel [160]. Despite being very useful for extending the depth of field (DOF), the structure of plenoptic imaging devices entails a strong trade-off between spatial and angular resolution, in the form of an inverse proportionality. Correlation plenoptic imaging (CPI), a novel imaging technique that exploits the correlations between the intensity fluctuations of light is proposed for overcoming this fundamental limit [161]. Therefore the leading idea comes from the evaluation of the second-order spatial–temporal correlation properties of light to perform spatial and directional detection on two distinct sensors: using correlated beams, high-resolution ghost imaging is performed on one sensor while simultaneously obtaining the angular information on the second sensor[162, 163, 164, 130]. Since two separate sensors are used, the image resolution can reach the diffraction limit (see Fig. (3.5).

CPI takes inspiration from Ghost Imaging (GI), a quantum imaging technique experimentally proved in 1995 [166, 167]. The first GI experiment used a source of entangled "twin" photon pairs as a light source, characterized by strong momentum and position correlation. Such correlations enabled to retrieve the image of an object by means of a spatially resolving detector that did not measure photons that had propagated through the object; the photons interacting with the object, in fact, were propagating in a "twin" beam and were collected by a bucket detector, i.e. not endowed
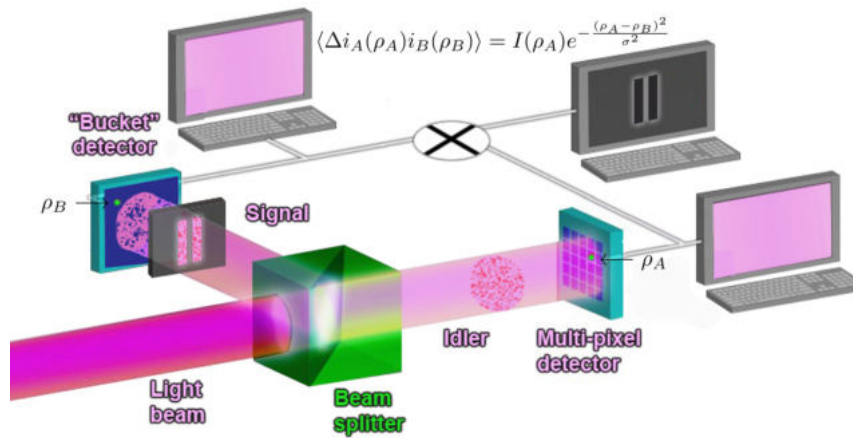
Figure 3.4: Ghost Imaging work's principle: many twin frames from a chaotic source are obtained by a beam splitter. Each frame contains speckles that impinge on the high resolution detector D_a and the bucket detector if such speckle is transmitted through the object mask and records only the click. This happens for each speckle of a frame with an average effective coherence length ($\sigma = \lambda z / 2\pi \sigma_i$ Eq. 3.20) comparable with a side of the pixels. Running many statistically independent twin frames obviously the screens are uniform behind each detectors, but apply point-to-point correlations the screen show the restored image of the object.
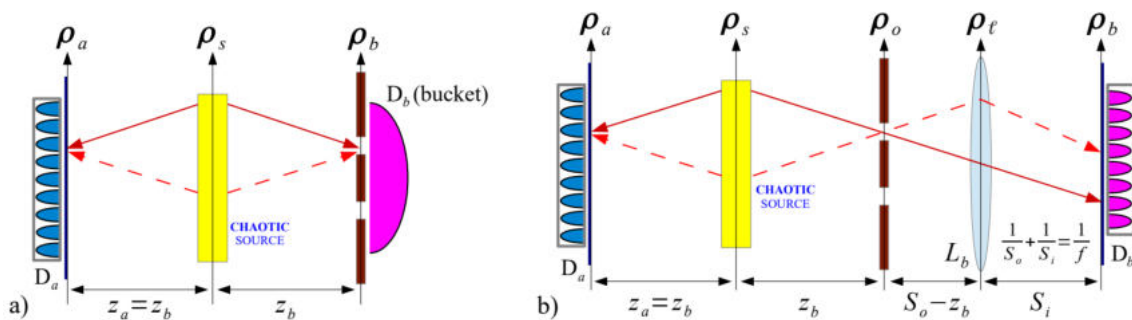

Figure 3.5: Klyshko's pictures respectively of ghost image in Fig.(3.3) in (a) and of CPI SETUP1 in Fig. (3.6(a)) in (b) (at focus $z_a = z_b$). (Picture from [165]) In ghost imaging, a bucket detector collects light transmitted by the object, with neither spatial nor directional resolution. In CPI, the high-resolution detector D_b enables measuring point-by-point intensity correlations between the two sensors and simultaneously reconstruct both the transmission profile of the object and the propagation direction of light from the source (focusing element) to the object.
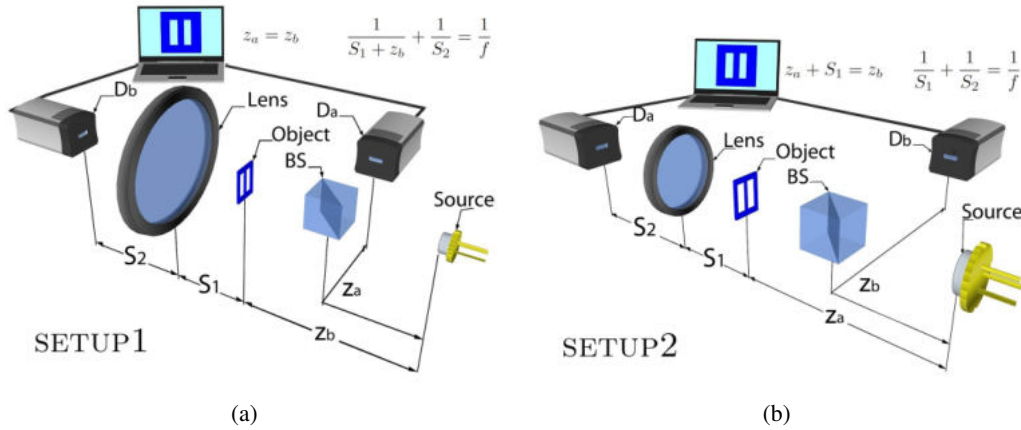
Figure 3.6: CPI configurations: in (a) chaotic source is focused by the lens on detector D_b, while the "ghost" image of the object rises up from the correlations in Eq 3.17; in (b) the object is focused by the lens as standard commercial cameras in D_a (high resolution detector), in addition the "ghost" image of the lens is achieved computing correlations between D_a (in this case plays as "bucket detector") and D_b (high resolution detector.

with spatial resolution. Shortly after the first experiments, it was shown that GI could be carried over without entangled photons, but through correlation of the speckle patterns [168][169] typical of chaotic light sources. It is using chaotic light, in fact, that CPI has been firstly implemented. Nevertheless, the advantages that quantum imaging with entangled photons provide over imaging with chaotic illumination, such as less noisy imaging at lower intensities and sub-shot noise imaging [170], have led to the generalization of CPI to illumination with entangled photons [157]. Entangled pairs can be easily produced by Spontaneous Parametric Down-Conversion (SPDC), a process in which photons belonging to a laser beam interacting with a non-linear crystal are converted into correlated pairs [171]. As concerns entangled photons the image of the object is retrieved because the law rate of photons enable a coincidence process point-to-point.

Thanks to this overview of CPI, now, as a pilot in the maneuver dive with his air force aircraft, we deeply studied two different CPI schemes based on chaotic light. Both the schemes employed ghost imaging: for the object (SETUP1) and for the focusing element (SETUP2). Then, we characterize their noise reduction properties in terms of the signal-to-noise ratio (SNR) and compare their performances.

Partially spoilering, we will find that the SNR can be significantly easier to control in SETUP2 involving standard imaging of the object; under adequate conditions, this scheme enables the number of frames for achieving the same SNR to be reduced by 1 order of magnitude [159].

3.3.1 Correlation plenoptic imaging setups

We compute the signal-to-noise ratio SNR of the setups (SETUP1 and SETUP2) represented in Fig. 3.6. These configurations have been proposed in [155] and [172], respectively, and an experimental proof of principle of plenoptic imaging and refocusing in SETUP1 has been performed [161].

The two schemes essentially differ by the way ghost imaging is employed to obtain an image of either the object plane (SETUP1) or the focusing element, as well as a lens (SETUP2). The common feature of the two setups is the fact that light emitted by a chaotic source is split in two paths a and b by a beam splitter (BS) and is recorded at the end of each path by the high–resolution detectors D_a and D_b. An object is always placed in one of the two paths. More specifically, intensity patterns $i_A(\boldsymbol{\rho}_a)$ and $i_B(\boldsymbol{\rho}_b)$, with $\boldsymbol{\rho}_{a,b}$ the coordinate on each detector plane, are recorded in time to reconstruct the correlation of intensity fluctuations Γ of Eq. 3.17 which encodes the images of

the object plane (SETUP1) and of the focusing element aperture (SETUP2).

In SETUP1, an image of the object can be obtained only by measuring intensity correlations between D_a and D_b. Along path a (the reflected path in the figure), light directly impinges on detector D_a, placed at an optical distance z_a from the source. On the other side, in path b (the transmitted path in the figure), a transmissive object lies at a distance z_b from the source. A thin lens of focal length f is placed between the object and the detector D_b at a distance S_1 from the former and S_2 from the latter. Such distances are chosen in order to focus the source on D_b with magnification $M = S_2/(S_1 + z_b)$; hence, they satisfy the thin-lens equation $1/S_2 + 1/(S_1 + z_b) = 1/f$. In the case $z_b = z_a$, measurement of the correlation function $\Gamma_{AB}(\boldsymbol{\rho}_a, \boldsymbol{\rho}_b)$ and direct integration over $\boldsymbol{\rho}_b$ provides the focused ghost image of the object [143].

In SETUP2, the image of the lens is recovered from intensity correlations between D_a and D_b. Along path b (the reflected path in figure), light directly impinges on the detector D_b, placed at an optical distance z_b from the source. In path a (the transmitted path in figure), the transmissive object is placed at a distance z_a from the source. The thin lens of focal length f lies between the object and the detector D_a, at a distance S_1 from the former and S_2 from the latter. In this case, the setup is designed to obtain a focused ghost image of the lens on the detector D_b. Therefore, distances are fixed in order to satisfy $z_b = z_a + S_1$. The object-to-lens and lens-to-D_a distances are arbitrary. However, it is intuitive that, if $S_2 = S_2^f$ such that $1/S_1 + 1/S_2^f = 1/f$, the image of the object will be sharply focused on D_a.

The refocusing capability of both setups is determined by the fact that the correlation function Γ encodes multiple coherent images of the object, one for each point $\boldsymbol{\rho}_b$ on D_b. The images corresponding to different pixels on D_b are generally displaced with respect to each other unless a focusing condition is satisfied. In the focused case, integration over detector D_b yields an incoherent image. In the out-of-focus cases, the collected coherent images need to be realigned *before* integrating over D_b, following

$$\Sigma_{\text{ref}}(\boldsymbol{\rho}_a) = \langle \mathscr{S}_{(\alpha,\beta)}(\boldsymbol{\rho}_a) \rangle, \qquad \mathscr{S}_{(\alpha,\beta)}(\boldsymbol{\rho}_a) = \int_{D_b} \Delta i_A(\alpha\boldsymbol{\rho}_a + \beta\boldsymbol{\rho}_b)\Delta i_B(\boldsymbol{\rho}_b)\,\mathrm{d}^2\rho_b \qquad (3.23)$$

where the parameter (α, β) that approach $(1, 0)$ at focus, are properly chosen to realign the coherent images depending on the setup [159]. When the focusing conditions are satisfied, any shift and rescaling is required in the first argument of Γ, and the high resolution of detector D_b becomes pointless. In all other cases, the spatial resolution of D_b is crucial to reconstruct the image of an out-of-focus object, which, by straightforward integration over D_b, without realignment algorithm, would be blurred.

Its fluctuations function $\mathscr{F}$ is

$$\mathscr{F}(\boldsymbol{\rho}_a) = \left\langle \mathscr{S}_{(\alpha,\beta)}(\boldsymbol{\rho}_a)^2 \right\rangle - \left\langle \mathscr{S}_{(\alpha,\beta)}(\boldsymbol{\rho}_a) \right\rangle^2. \qquad (3.24)$$

Let N_f the number of frames collected in time to evaluate the expectation values in Eqs. 3.23 3.24 statistically independence each other we can define the signal–to–noise ratio as

$$R(\boldsymbol{\rho}_a) = \frac{\Sigma_{\text{ref}}(\boldsymbol{\rho}_a)}{\sqrt{\mathscr{F}(\boldsymbol{\rho}_a)/N_f}}, \qquad (3.25)$$

where $\sqrt{\mathscr{F}(\boldsymbol{\rho}_a)/N_f}$ identifies the noise since it is the root–mean–square error affecting the evaluation of Σ_{ref}. The average are based on the previous statistical model of the source which provides an effective description of a chaotic, named pseudothermal light source in the semiclassical regime $\sigma_g \to 0$ (the quantum corrections to the derived quantities will scale like the inverse number of photons per mode), hence from Eq. 3.16 one gets

$$W_S(\boldsymbol{\rho}_S, \boldsymbol{\rho}_S') = 2\pi\sigma_g^2 I_S e^{-\frac{\boldsymbol{\rho}_S^2}{2\sigma_i^2}} \delta^{(2)}(\boldsymbol{\rho}_S - \boldsymbol{\rho}_S') \qquad (3.26)$$

under the integrals. Notice that the propagation is deterministic and to evaluation of Σ and $\mathscr{F}$ consists of eight-point field correlators on the source. Using the Gaussian approximation, we can apply again the Wick-Isserlis theorem as we have done in Eq. 3.19 and insert the generalized function in Eq. 3.16 to compute the two-point field correlator. Look that, according to distribution theory the limit of $\sigma_g \to 0$ is performed under the integral. Mathematically speaking, the correlator that involve an equal number of V's and V^*'s is

$$\left\langle \prod_{j=1}^{n} V_S(\boldsymbol{\rho}_j) V_S^*(\boldsymbol{\rho}'_j) \right\rangle = \sum_{\mathrm{P}} \prod_{j=1}^{n} \left\langle V_S(\boldsymbol{\rho}_j) V_S^*(\mathrm{P}\boldsymbol{\rho}'_j) \right\rangle, \tag{3.27}$$

with P a permutation of the primed indexes, while all other expectation values, including $\langle V \rangle$ and $\langle V^* \rangle$, vanish. Propagation from the source to the detectors along the two paths a and b is deterministic, and depends on the transmission functions of the object and the lens.

In both setups, $\mathscr{F}(\boldsymbol{\rho}_a)$ is determined with good approximation by the contribution that features only the autocorrelations

$$\mathscr{F}_0(\boldsymbol{\rho}_a) := \int \Gamma_{AA}(\alpha\boldsymbol{\rho}_a + \beta\boldsymbol{\rho}_{b1}, \alpha\boldsymbol{\rho}_a + \beta\boldsymbol{\rho}_{b2}) \Gamma_{BB}(\boldsymbol{\rho}_{b1}, \boldsymbol{\rho}_{b2}) \, \mathrm{d}^2\boldsymbol{\rho}_{b1}\mathrm{d}^2\boldsymbol{\rho}_{b2} \tag{3.28}$$

where

$$\Gamma_{DD}(\boldsymbol{\rho}_1, \boldsymbol{\rho}_2) = \langle \Delta I_D(\boldsymbol{\rho}_1) \Delta I_D(\boldsymbol{\rho}_2) \rangle = |\langle V_D(\boldsymbol{\rho}_1) V_D^*(\boldsymbol{\rho}_2) \rangle|^2, \tag{3.29}$$

with $D = A, B$. Other contributions are typically suppressed as

$$\frac{|\mathscr{F} - \mathscr{F}_0|}{\mathscr{F}_0} \sim \frac{1}{\mathscr{N}_b}, \tag{3.30}$$

with $\mathscr{N}_b$ the number of transverse modes that propagate towards the detector D_b. Since this quantity determines the number of spatial (in SETUP1) or directional (in SETUP2) resolution cells, it is typically large in a plenoptic imaging setup, therefore, in the following, we shall approximate $\mathscr{F} \simeq \mathscr{F}_0$ when computing the SNR.

In Ref. [159] are shown all the details and the calculations. Here, we provide an useful estimation of $R(\boldsymbol{\rho}_a)$ in Eq. 3.25 given by the geometrical-optics approximation, as well as, a method of steepest descent, for both the setups.

SETUP 1

As concerns the SETUP1, Eq.3.25 gives in the geometric limit

$$R^{(g)}(\boldsymbol{\rho}_a) = \sqrt{2}\pi\sigma_B\sigma_i \left| 1 - \frac{z_b}{z_a} \right| |A(\boldsymbol{\rho}_a)|^2 \sqrt{\frac{N_f}{J^{(g)}}}, \tag{3.31}$$

with

$$J^{(g)} = \int \mathrm{d}^2\boldsymbol{\rho}_1 \mathrm{d}^2\boldsymbol{\rho}_2 |A(\boldsymbol{\rho}_1)A(\boldsymbol{\rho}_2)|^2 e^{-\frac{(\boldsymbol{\rho}_1 - \boldsymbol{\rho}_2)^2}{2\sigma_i^2(1 - z_a/z_b)^2}}. \tag{3.32}$$

Let us first discuss this result in the focused case, in which $z_a = z_b = z$ and $\sigma_A = \sigma_B = z/k\sigma_i$, which are the coherence area at distance z. The integrand of (3.32) becomes localized around $\boldsymbol{\rho}_1 = \boldsymbol{\rho}_2$, and Eq. 3.31 reduces to

$$R^{(g)}(\boldsymbol{\rho}_a)\Big|_{z_b = z_a} = \sqrt{N_f \frac{\pi\sigma_B^2}{\int \mathrm{d}^2\boldsymbol{\rho}|A(\boldsymbol{\rho})|^4}} |A(\boldsymbol{\rho}_a)|^2. \tag{3.33}$$

It is evident in Eq. 3.33 the ratio between the coherence area $\sim \sigma_B$ on the object and an "effective area" of the object itself, given by the integral of the $|A|^4$ factor, which is equal to the actual area in the case of binary transmission function. Since the same coherence area determines the resolution through

$$\Sigma_{\text{ref}}^{(g)}(\boldsymbol{\rho}_a) = I_s^2 \frac{\pi \sigma_g^4}{\sigma_A^2} |A(\boldsymbol{\rho}_a)|^2, \tag{3.34}$$

Eq. 3.33 entails the well-known trade–off between resolution and SNR typical of ghost imaging [173, 174, 175, 176].

Deep in the out-of-focus regime, when $\sigma_i|1 - z_b/z_a|$ becomes larger than the typical size of the object yields

$$R^{(g)}(\boldsymbol{\rho}_a) \simeq \sqrt{\frac{N_f}{2}} \lambda z_b \left| 1 - \frac{z_b}{z_a} \right| \frac{|A(\boldsymbol{\rho}_a)|^2}{\int d^2\boldsymbol{\rho} |A(\boldsymbol{\rho})|^2}, \tag{3.35}$$

with $\lambda = 2\pi/k$ the light wavelength. This expression shows a less trivial dependence on the longitudinal position z_b of the refocused plane, but can still be interpreted in terms of the resolution–SNR trade-off. Actually, as discussed in [155], a good estimate of the resolution of the refocused image is given by $\Delta x = (\lambda z_b/a)|1 - z_b/z_a|$, where a is the typical linear size of the smallest transmissive parts of the object. Notice, however, that the inverse dependence on the effective area of the object has changed with respect to the focused case(3.33). As a rule of thumb, we can estimate the SNR of refocused images as

$$\frac{R^{(g)}(\boldsymbol{\rho}_a)}{\sqrt{N_f}} \sim \sqrt{\frac{a^2}{A_{\text{obj}}}} \sqrt{\frac{(\Delta x)^2}{A_{\text{obj}}}} |A(\boldsymbol{\rho}_a)|^2, \tag{3.36}$$

a result that depends on the product of the ratios (resolution cell)/(total area) and (smallest detail area)/(total area). In Fig. 3.7, we show the behavior of the SNR in SETUP1 as a function of the source-to-object distance z_b, comparing the result with the case of a focused ghost image taken with $z_a = z_b$ [Eq. (3.33)]. The higher SNR of correlation plenoptic imaging is related to the lower resolution of the refocused image with respect to the focused ghost image.

SETUP2

In the analysis of SETUP2, the estimate of the SNR based on Eq. (3.25) is less trivial than in SETUP1, since the denominator depends on $\boldsymbol{\rho}_a$ and shows different spatial behaviors with varying defocusing. The geometrical-optics expression of the SNR reads

$$R^{(g)}(\boldsymbol{\rho}_a) = 2\sigma_B \sqrt{N_f \frac{\pi}{A_{D_b} J^{(g)}(\boldsymbol{\rho}_a)}} \left(\frac{1 - S_2/S_2^f}{S_2/S_1} \right)^2 \left| A\left(-\frac{\boldsymbol{\rho}_a}{\mu} \right) \right|^2 \int d^2\boldsymbol{\rho} |P(\boldsymbol{\rho})|^2. \tag{3.37}$$

In the focused case, the above quantity reduces to the simple expression

$$R^{(g)}(\boldsymbol{\rho}_a) \Big|_{S_2 = S_2^f} = 2\sigma_B \sqrt{N_f \frac{\pi}{A_{D_b}}}. \tag{3.38}$$

A result that does not depend on $\boldsymbol{\rho}_a$, since noise is proportional to the signal. The constant SNR in (3.38) is essentially the square root of the ratio of the coherence area $\sim \sigma_B^2$ on D_b and the area A_{D_b} of the same detector, which can also be interpreted as (coherence area on the lens)/(area of the lens), in perfect analogy with Eq. (3.33), after replacing the object with the lens. The SNR thus coincides with the one expected for the ghost image of the lens.
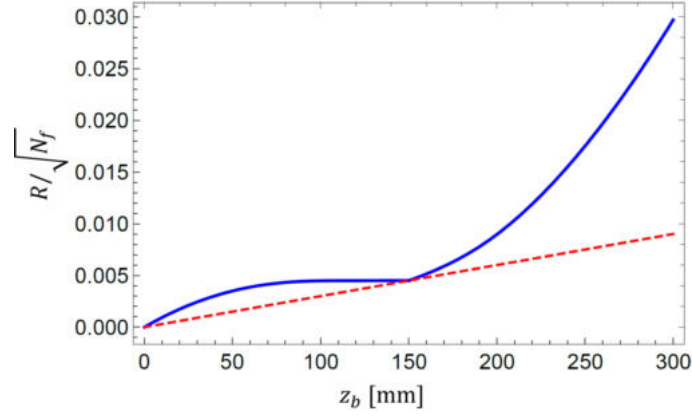
Figure 3.7: Signal-to-noise ratio, normalized to the square root of the number of frames, for the refocused image (3.34) obtained in SETUP1 (solid blue line). The source is characterized by wavelength $\lambda = 532\,\text{nm}$ and a Gaussian intensity profile of width $\sigma_i = 2.5\,\text{mm}$, and is placed at a fixed distance $z_a = 150\,\text{mm}$ from detector D_a. The focused image, obtained at $z_a = z_b$, is characterized by resolution $\Delta x = 10\,\mu\text{m}$. The values are computed in correspondence of a totally transmissive point ($A = 1$) of a binary object with transmissive area $A_{\text{obj}} = 4\,\text{mm}^2$. The SNR for a ghost image taken at $z_a = z_b$, as a function of z_b (red dashed line), is shown for comparison.

In the deep out-of-focus case, a background noise emerges, and the SNR becomes similar in form to (3.35), yielding

$$R(\boldsymbol{\rho}_a)^{(g)} \simeq 2\sigma_B \sqrt{N_f \frac{\pi}{A_{D_b}}} \left(\frac{1 - S_2/S_2^f}{S_2/S_1} \right)^2 \frac{\int d^2\boldsymbol{\rho}\,|P(\boldsymbol{\rho})|^2}{\int d^2\boldsymbol{\rho}\,|A(\boldsymbol{\rho})|^2} |P(0)|^2 \left| A\left(-\frac{\boldsymbol{\rho}_a}{\mu} \right) \right|^2. \tag{3.39}$$

The ratio between the area of the lens and the area of the object is generally large for image magnification $\mu \gtrsim 1$, and the SNR also increases quadratically with defocusing, providing a generally more favorable picture compared to SETUP1. A good rule to estimate the order of magnitude of the refocused image SNR thus reads

$$\frac{R^{(g)}(\boldsymbol{\rho}_a)}{\sqrt{N_f}} \sim \left(\frac{S_2/S_1}{1 - S_2/S_2^f} \right)^2 \sqrt{\frac{\sigma_B^2}{A_{\text{lens}}} \frac{A_{\text{lens}}}{A_{\text{obj}}}} \left| A\left(-\frac{\boldsymbol{\rho}_a}{\mu} \right) \right|^2, \tag{3.40}$$

where we have assumed that the area of the detector is matched to the area of the lens. In Fig. 3.8, we represent the behavior of the SNR in SETUP2 as a function of the object-to-lens distance S_1, and compare the result with the case of a focused image taken with $S_2^f = S_2$ (notice that S_2^f is a function of S_1).

Advantage of the schemes

The results obtained provide to the experimenter to determine the scaling of the SNR with the number of frames, and consequently to fix the number of frames needed for a fast and accurate imaging of the scene. The problem of optimizing the acquisition time is particularly relevant both in view of real-time imaging and in all those cases in which additional difficulties in retrieving intensity correlations are present, as it happens when considering unconventional sources like X rays [177, 178] to perform CPI.

The results obtained for the SETUP2 are generally more advantageous than the SETUP1. In the focused case, SETUP2 is characterized by the suppression of background noise, that, on the other hand, is a typical feature affecting the ghost image obtained in SETUP1. Moreover, noise in SETUP1
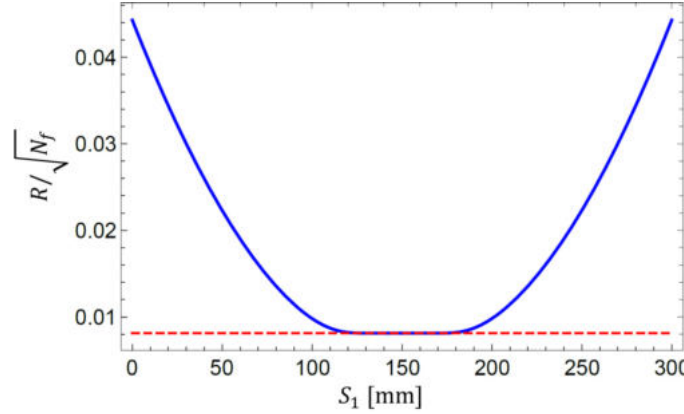
Figure 3.8: Signal-to-noise ratio, normalized to the square root of the number of frames, for the refocused image (3.38) obtained in SETUP2 (solid blue line). The source is characterized by a wavelength $\lambda = 532$ nm and a Gaussian intensity profile of width $\sigma_i = 2.5$ mm, and is placed at a fixed distance $z_b = z_a + S_1 = 300$ mm from the detector D_b. The lens has a focal length $f = 75$ mm and a Gaussian pupil function of width $\sigma_p = 2.5$ mm. Fixing the value $S_2 = 2f = 150$ mm, the focused image, obtained at $S_1 = S_2$, is characterized by the same resolution, depth of field and magnification as in the case shown in Fig. 3.7. The values are computed in correspondence of a totally transmissive point ($A = 1$) of a binary object with transmissive area $A_{obj} = 4$ mm^2. The SNR for a ghost image taken at $S_2 = S_2^f = (1/f - 1/S_1)^{-1}$ as a function of S_1 (red dashed line) is shown for comparison.

increases with improving resolution on the object, thus entailing a trade-off between resolution and SNR trade-off. In the out-of-focus case, background noise is present in both configurations. However, in SETUP1 it depends on small quantities, namely the ratios $(\Delta x)^2/A_{obj}$ between the area of an effective resolution cell and the total area of the object, and a^2/A_{obj}, where the numerator is the area corresponding to the size a of the finest details of the object. In SETUP2, instead, we find that the SNR depends also on the ratio A_{lens}/A_{obj}, a quantity that is not necessarily small. Therefore, we expect that a smaller number of frames is needed to achieve the same resolution in SETUP2 compared to SETUP1.

To get a quantitative hint of the SNR improvement in SETUP2, we compare the results shown in Figs. 3.7-3.8, which are referred to two cases that are as homogeneous as possible in terms of resolution, depth of field and magnification of the focused image. We find that he ratio between the SNR in SETUP2 and SETUP1 at fixed N_f is consistently larger than one: when such a ratio reaches values around 3.2, for an object placed at $z_b = S_1 = 80$ mm, one tenth of the frames is needed in SETUP2 to reach the same SNR as in SETUP1. Notice that, by considering the expressions (3.35)-(3.39), the ratio of the SNRs for out-of-focus images is very weakly dependent of the light wavelength and the area of the object, provided the conditions for the validity of geometrical optics approximation are satisfied.

3.4 Correlation Plenoptic Microscope

In this section, we compare the CPI protocol with the configuration of the SETUP2 of the previous section based on ghost imaging with a novel scheme named *Correlation plenoptics Microscope* (CMP) in SETUP3 in Fig. (3.9), which is not based on the ghost imaging. Analogously to Eqs. 3.35 and 3.39 respectively for (SETUP1) and (SETUP2), also for this scheme (SETUP3) we calculate the
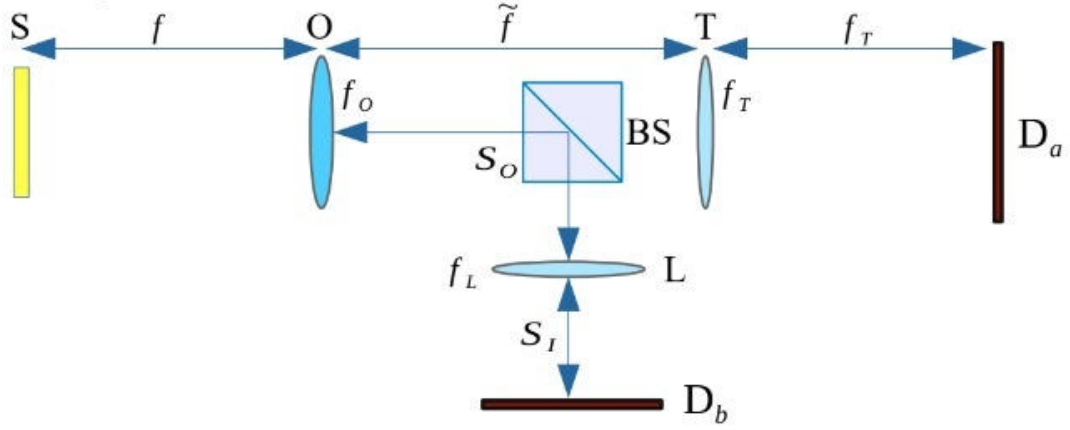
Figure 3.9: CPM: The setup is arranged so that $\tilde{f} = f_O + f_T$, and $f \neq f_O$ in the most general (out of focus) case. Lens L images lens O on detector D_b, so that $1/s_O + 1/s_I = 1/f$ is satisfied.

SNR out-of-focus in the geometric approximation, which is

$$R_\Sigma^{(g)}(\rho_a) = \frac{f}{k}\left(1 - \frac{f}{f_o}\right)^2 \frac{|A(\rho_a)|^4 |P_o(0)|^2 \int |P_o(\rho)|^2 d\rho}{\left|P_o\left(\frac{f_o}{f_o-f}\rho_a\right)\right|^2 T(f)\int |A(\rho)|^2 d\rho}, \tag{3.41}$$

with

$$T(f) = \sqrt{\int d\rho d\kappa |A(\rho)|^2 \left|A\left(\rho + \frac{f}{k}\kappa\right)\right|^2 |\mathscr{P}(\kappa)|^2}. \tag{3.42}$$

At focus $f = f_o$ supposing an infinitesimal point spread function (PSF)[2] we get

$$R_\Sigma^\infty(\rho_a) = \frac{\lambda f_o}{\sqrt{\int |A(\rho)|^4 d\rho}\sqrt{\int P_o(\rho) d\rho}} \frac{\left|A\left(-\frac{f_o}{f_t}\rho_a\right)\right|^4}{\left|A\left(-\frac{f_o}{f_t}\rho_a\right)\right|^2}. \tag{3.43}$$

This expression must be compared to Eqs. 3.33-3.38 respectively for (SETUP1) and (SETUP2). If we call $\sigma_o = \lambda f_o / \sqrt{\int |A(\rho)|^4 d\rho}$ considered as the effective coherence length on the objective lens, Eq. 3.43 ultimately depends on the ratio between σ_o and the radius of the objective lens $\sqrt{\int P_o(\rho) d\rho} \sim \sqrt{\int \exp\left(-\rho^2/\sigma_L^2\right) d\rho} \sim \sigma_L$.

For 3D–imaging applications is more useful a comparison in terms of the intensity fluctuations Γ, rather than Σ. Therefore the corresponding fluctuation function of Γ is $\mathscr{F}_\Gamma$ which is

$$\mathscr{F}_\Gamma(\boldsymbol{\rho}_a, \boldsymbol{\rho}_b) = \left\langle(\Delta i_A(\boldsymbol{\rho}_a)\Delta i_B(\boldsymbol{\rho}_b))^2\right\rangle - \left\langle\Delta i_A(\boldsymbol{\rho}_a)\Delta i_B(\boldsymbol{\rho}_b)\right\rangle^2$$
$$= (I_A(\boldsymbol{\rho}_a)I_B(\boldsymbol{\rho}_b) + 2\Gamma(\boldsymbol{\rho}_a, \boldsymbol{\rho}_b))^2 - \Gamma(\boldsymbol{\rho}_a, \boldsymbol{\rho}_b)^2. \tag{3.44}$$

---

[2]The point spread function describes the response of an imaging system to a point source (see Fig. (3.2)).

The signal-to-noise ratio over the average value 3.17, estimated by collecting N_f statistically independent frames, can be evaluated as

$$\mathrm{SNR}_\Gamma(\boldsymbol{\rho}_a, \boldsymbol{\rho}_b) = \frac{\Gamma(\boldsymbol{\rho}_a, \boldsymbol{\rho}_b)}{\sqrt{N_f \mathscr{F}_\Gamma(\boldsymbol{\rho}_a, \boldsymbol{\rho}_b)}} = \frac{1}{\sqrt{N_f \left[\left(\frac{I_A(\boldsymbol{\rho}_a) I_B(\boldsymbol{\rho}_b)}{\Gamma(\boldsymbol{\rho}_a, \boldsymbol{\rho}_b)} + 2 \right)^2 - 1 \right]}}. \tag{3.45}$$

Since CMP is a promising scheme for 3D-application, we also define a "signal-to-background ratio", meant as the ratio between the signal evaluated at a generic point pair $(\boldsymbol{\rho}_a, \boldsymbol{\rho}_b)$ and the "background" noise evaluated at a reference point $(\boldsymbol{\rho}_a', \boldsymbol{\rho}_b)$ of the same point-of-view image in which the signal is practically vanishing:

$$\mathrm{SBR}(\boldsymbol{\rho}_a, \boldsymbol{\rho}_b; \boldsymbol{\rho}_a') = \left. \frac{\Gamma(\boldsymbol{\rho}_a, \boldsymbol{\rho}_b)}{\sqrt{N_f \mathscr{F}_\Gamma(\boldsymbol{\rho}_a', \boldsymbol{\rho}_b)}} \right|_{\Gamma(\boldsymbol{\rho}_a', \boldsymbol{\rho}_b) \simeq 0} = \frac{\Gamma(\boldsymbol{\rho}_a, \boldsymbol{\rho}_b)}{I_A(\boldsymbol{\rho}_a') I_B(\boldsymbol{\rho}_b)}, \tag{3.46}$$

where it is evident that both quantities are fixed a ratio of the form $\Gamma / i_A i_B$. In order to estimate this ratio, we consider the cases of focused and out-of-focus image in the geometrical approximation. In the case of CPI (SETUP2), the correlation $\Gamma(\boldsymbol{\rho}_a, \boldsymbol{\rho}_b)$ encodes the image with unitary magnification of the object transmission function A, while intensity on the detector D_a is uniform. Taking $\boldsymbol{\rho}_b = 0$ for definiteness, at the focused case

$$\Gamma(\boldsymbol{\rho}_a, 0) \sim |A(\boldsymbol{\rho}_a)|^2, \qquad i_A(\boldsymbol{\rho}_a) \sim \mathrm{const.} \tag{3.47}$$

It implies

$$\mathrm{SNR}(\boldsymbol{\rho}_a, 0) \simeq \frac{1}{\sqrt{N_f \left[\left(\frac{\alpha^{(\mathrm{CPI})}}{|A(\boldsymbol{\rho}_a)|^2} + 2 \right)^2 - 1 \right]}}, \qquad \mathrm{SBR}(\boldsymbol{\rho}_a, 0; \boldsymbol{\rho}_a') \simeq \frac{|A(\boldsymbol{\rho}_a)|^2}{\alpha^{(\mathrm{CPI})}}. \tag{3.48}$$

Therefore, both quantities vanish if the signal is small.
For focused CPM, both Γ and the intensity on D_a encode an image of the object intensity profile $\mathscr{A}$,

$$\Gamma(\boldsymbol{\rho}_a, 0) \sim \mathscr{A}\left(-\frac{f_O}{f_T} \boldsymbol{\rho}_a \right)^2, \qquad I_A(\boldsymbol{\rho}_a) \sim \mathscr{A}\left(-\frac{f_O}{f_T} \boldsymbol{\rho}_a \right), \tag{3.49}$$

where f_O is the objective focal length and f_T the tube lens focal length. Therefore, the SNR is approximately independent of the spatial modulation of the signal

$$\mathrm{SNR}(\boldsymbol{\rho}_a, 0) \simeq \frac{1}{\sqrt{N_f \left[\left(\frac{\alpha^{(\mathrm{CPM})}}{\mathscr{A}(\boldsymbol{\rho}_a)} + 2 \right)^2 - 1 \right]}}; \tag{3.50}$$

and since the intensity I_A vanishes out of the object profile,

$$\mathrm{SBR}(\boldsymbol{\rho}_a, 0; \boldsymbol{\rho}_a') \to \infty \quad \text{if } \mathscr{A}(\boldsymbol{\rho}_a) > 0. \tag{3.51}$$

In the out-of-focus case, intensity on the spatial sensor remains uniform in the case of CPI

$$\Gamma(\boldsymbol{\rho}_a, 0) \sim \left| A\left(\frac{z_b}{z_a} \boldsymbol{\rho}_a \right) \right|^2, \qquad i_A(\boldsymbol{\rho}_a) \sim \mathrm{const.} \tag{3.52}$$
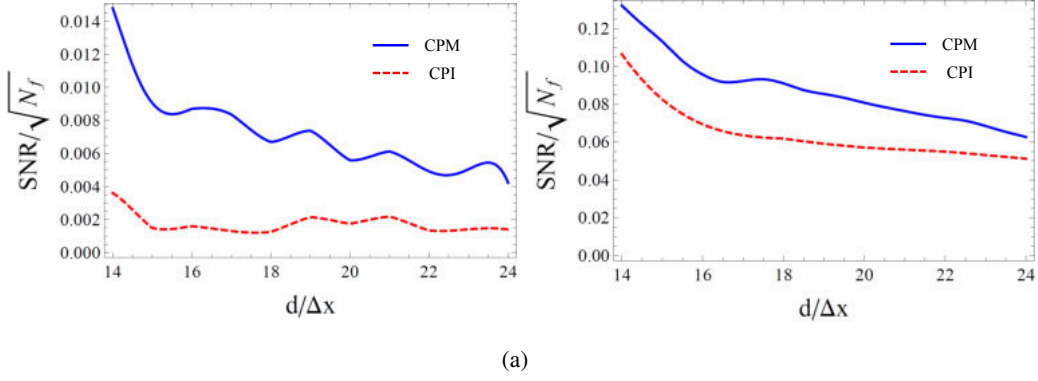
(a)

Figure 3.10: SNR for a triple-slit image (mediated over the central parts of the slits) for CPI and CPM systems with $\Delta x = 3\mu$m resolution, illuminated by light of wavelength $\lambda = 550$nm. The parameter d represents the center-to-center distance of neighboring slits.

with z_a the source-to-D_a distance and z_b the source-to-object distance, but tends to become uniform even in the case of CPM

$$\Gamma(\boldsymbol{\rho}_a, 0) \sim \mathscr{A}\left(-\frac{z_s}{f_T}\boldsymbol{\rho}_a\right)^2, \qquad i_A(\boldsymbol{\rho}_a) \sim \text{const.} \tag{3.53}$$

with z_s the distance of the sample from the objective first principal plane. Therefore, one obtains formally similar results in one case

$$\text{SNR}(\boldsymbol{\rho}_a, 0) \simeq \frac{1}{\sqrt{N_f\left[\left(\frac{\beta^{(\text{CPI})}}{|A(z_b\boldsymbol{\rho}_a/z_a)|^2} + 2\right)^2 - 1\right]}}, \qquad \text{SBR}(\boldsymbol{\rho}_a, 0; \boldsymbol{\rho}_a') \simeq \frac{|A(z_b\boldsymbol{\rho}_a/z_a)|^2}{\beta^{(\text{CPI})}}, \tag{3.54}$$

and in the other

$$\text{SNR}(\boldsymbol{\rho}_a, 0) \simeq \frac{1}{\sqrt{N_f\left[\left(\frac{\beta^{(\text{CPM})}}{\mathscr{A}(-z_s\boldsymbol{\rho}_a/f_T)^2} + 2\right)^2 - 1\right]}}, \qquad \text{SBR}(\boldsymbol{\rho}_a, 0; \boldsymbol{\rho}_a') \simeq \frac{\mathscr{A}(-z_s\boldsymbol{\rho}_a/f_T)^2}{\beta^{(\text{CPM})}}. \tag{3.55}$$

Out-of-focus, the advantage of CPM depends on the detailed structure of the intensities and the correlation function.

In Fig. 3.10 is show a comparison (Here table of all outcomes talk with Francesco).

3.5 Distance sensing

In this section, we discuss a second application also based on the second-order interference with pseudothermal light which pretend to estimate and provide the distances in the space of the object in remote mode. Again we evaluate the correlation between intensity fluctuations on two detectors. We applied the simplest non trivial application concerning two double slit mask: one is the control mask and the other is the target mask that we want to measure the distance z_T and the distance between the pinholes as in Fig. 3.11. This enables us to be sensitive to arbitrary distances between an incoherent, i.e. pseudothermal source and an object and between an object and a detector, even when first-order interference provides no information on such parameters.

The obtained results lay the foundations of novel protocols for distance sensing, that can integrate and improve state-of-the-art applications, such as those based on pulsed light (e.g., time-of-flight
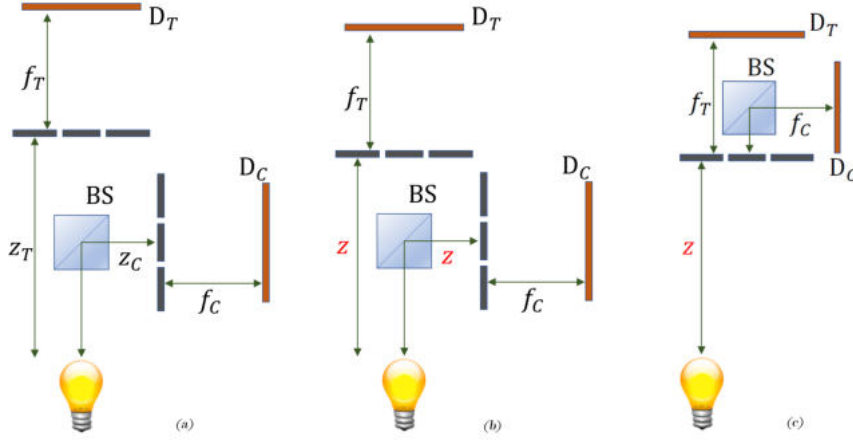
Figure 3.11: Panel (a): Distance sensing interferometric scheme to measure either the distance f_T or z_T, when both the reference distances f_C and z_C are controlled; the source emits narrow-bandwidth thermal light; the double-slit masks are followed by two spatially resolving detectors, enabling spatial correlation measurements. Panel (b): Case of identical distances between source and masks ($z_T = z_C = z$), ideal to measure only the distance f_T. Panel (c): Configuration with a single mask and the beam splitter placed after the mask, equivalent in the outcome of the correlation measurements to the case (b) when the two masks are identical.

cameras [179]) or first-order interference (e.g., coherent LIDAR [180]), tasks in metrology and information processing [181, 140, 182, 183, 133, 184], as well as optical algorithms [185, 186, 187, 188, 189].

Here, we shall consider the transmission function of double-slits masks of negligible thickness a, approximated as

$$A_J(x_o) = a \left[\delta \left(x_o - X_J + \frac{d_J}{2} \right) + \delta \left(x_o - X_J - \frac{d_J}{2} \right) \right], \tag{3.56}$$

with $\delta(x)$ the one-dimensional Dirac delta distribution, where we assume the slit distances to satisfy the far-field condition $d_J \ll \lambda f_J$, where $J = C, T$ is the distance between the pinholes and X_J the middle point.

In general, the correlation of intensity fluctuations in Eq. (3.17) can be expressed as a finite Fourier series:

$$\Gamma(x_C, x_T) = 1 + \text{Re} \left[\sum_{J=C,T} F_{1J}(z_T) \exp \left(-i \frac{k d_J x_J}{f_J} \right) \right.$$
$$\left. + \sum_{s=\pm} F_2^{(s)}(z_T) \exp \left[-i \left(s \frac{k d_T x_T}{f_T} + \frac{k d_C x_C}{f_C} \right) \right] \right], \tag{3.57}$$

apart from an overall constant factor given by the zero-spatial-frequency component. Henceforth, we will assume the case in which the two masks are centered on the respective optical axes $X_T = X_C = 0$, and a source with a Gaussian average intensity profile $\mathscr{S}(x_s) = \mathscr{S}_0 \exp \left(-x_s^2 / 2\sigma^2 \right)$, with the coherence length assuming the values

$$\sigma_T = \frac{z_T}{k\sigma}, \quad \sigma_C = \frac{z_C}{k\sigma}, \tag{3.58}$$

at the two mask planes at distances z_T and z_C, respectively. In this case, the Fourier coefficients in

(a) $\alpha = 9.77 \cdot 10^2$, $\beta = 0$ (b) $\alpha = 2.29$, $\beta = 14.3$ (c) $\alpha = 1.05$, $\beta = 18.0$ (d) $\alpha = 0.50$, $\beta = 21.2$
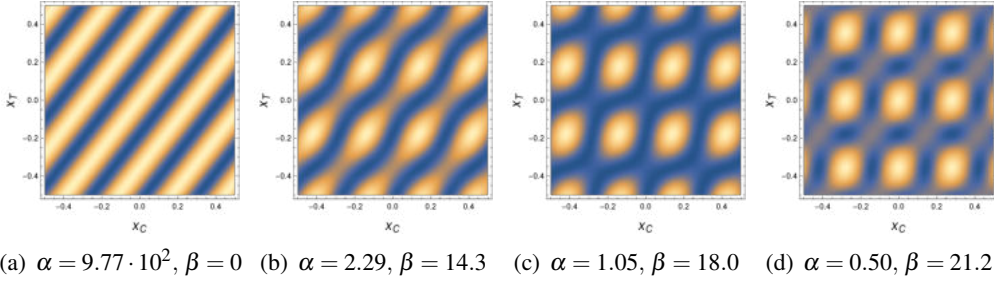
Figure 3.12: Density plots of the correlation function $\Gamma(x_C, x_T)$ in Eq. (3.57), measured at different values of the target distance z_T at the output of the setup in Fig. 3.11(a), with color scale ranges from blue ($\Gamma = 0$) to white (Γ equal to its maximum). The values of the relevant parameters α and β in Eq. (3.61) are reported in captions. The case in panel (a) is obtained for $z_T = z_C = z$, as in Fig. 3.11(b). The simple periodical behavior of the correlation function in this case allows to estimate easily the length of a remote path from the detector D_T to the corresponding mask for $d_C d_T \gg \ell_c^2$. The results in panels (b), (c), (d) are obtained for $z_T/z_C = 2.07, 2.86, 4.29$, respectively, and show intermediate range not particularly favorable for estimating z_T. The constant parameters are $\lambda = 980$ nm, $d_C = 0.70$ mm, $d_T = 0.55$ mm, $\sigma = 0.55$ mm, $z_C = 70$ mm, $f_T = f_C = 200$ mm.

Eq.(3.57)

$$F_{1C}(z_T) = F_{1T}(z_T) = \frac{\cos(\alpha\beta/2)}{\cosh(\alpha/2)} \equiv F_1(z_T), \tag{3.59}$$

$$F_2^{(+)}(z_T) = 1 - F_2^{(-)}(z_T) = \frac{1}{1 + \exp(\alpha)}, \tag{3.60}$$

depending on the absolute difference of the coherence areas in Eq. 3.58 through two dimensionless critical parameters

$$\alpha = \frac{d_C d_T}{\ell_c^2}, \quad \beta = \sigma \left| \frac{1}{\sigma_T} - \frac{1}{\sigma_C} \right| = k\sigma^2 \frac{|z_T - z_C|}{z_T z_C}. \tag{3.61}$$

with the rst one dened by the eective second-order correlation length

$$\ell_c = \sqrt{(1 + \beta^2)\, \sigma_C \sigma_T} \tag{3.62}$$

at the transverse planes at distances z_C and z_T from the source. In particular, for $z_T = z_C = z$, such second-order correlation length reduces to the first-order coherence length: $\ell_c = z/k\sigma$. Notice also that the Fourier coefficients in the correlation function Γ in Eq.3.57 depend on the slit distances only through their product, since the masks are both centered transverse with respect to the optical axis. Interestingly, the terms in Eq.3.57 manifesting a correlation between the two masks, particularly between slits on opposite sides of the optical axis ($F_2^{(+)}$) and between slits on the same side ($F_2^{(-)}$), fully depend on the ratio α between such a product and the squared second-order correlation length ℓ_c.

Remarkably, the measurement of the spatial frequencies in the correlation function (3.57) allows to infer the distance of the length f_T of the target path from the detector D_T to the corresponding mask. Furthermore, an analysis of the Fourier coefficients allows us to extrapolate the value of the distance z_T from the source to the target mask. In Fig. 3.12, we show the behavior of the correlation function in the (x_C, x_T) plane with varying z_T. We emphasize that the intensity at the detector D_T

$$I(x_T) = 1 + \exp\left(-\frac{d_T^2}{2\sigma_T^2}\right) \cos\left(\frac{k d_T x_T}{f_T}\right). \tag{3.63}$$

is highly sensitive to f_T only if $d_T \ll \sigma_T$, and to z_T (through the coherence length σ_T) only if $d_T \sim \sigma_T$. Remarkable, we show now how second-order correlation measurement allows us to retrieve this sensitivity in arbitrary ranges of σ_T by a proper tuning of the parameters related to the mask C from Eq. 3.57, 3.59, 3.60 and 3.61.

1. *Factorized limit*—The correlation function Γ is factorized with respect to its two detectors position variables iff $F_1 = 2F_2^{(+)} = 2F_2^{(-)}$ $\alpha \ll 1$, $\alpha\beta \ll 1$, basically when $d_C d_T \ll \ell_c^2$. and $z_C \sim z_T$

$$\Gamma(x_C, x_T) = \Gamma_{\mathrm{f}}(x_C, x_T) = 4\cos^2\left(\frac{kd_T x_T}{2f_T}\right)\cos^2\left(\frac{kd_C x_C}{2f_C}\right) \tag{3.64}$$

By considering the first order contribution in α to the Fourier coefficients

$$F_1 = 1 + O(\alpha^2), \quad F_2^{(\pm)} = \frac{1}{2}\left(1 \mp \frac{\alpha}{2}\right) + O(\alpha^2), \tag{3.65}$$

one obtains

$$\Gamma(x_C, x_T) \simeq \Gamma_{\mathrm{f}}(x_C, x_T) + \frac{\alpha}{2}\sin\left(\frac{kd_T x_T}{f_T}\right)\sin\left(\frac{kd_C x_C}{f_C}\right). \tag{3.66}$$

Thus, the presence of the additional modulation in Eq. (3.66) is, at the lowest order in α, the only indicator by which the value of z_T can be deduced.

2. *The limit of highly correlated interference pattern: higher sensitivity to f_T* — The correlation function Γ takes the form of a correlated interference pattern when $\alpha \gg 1$, namely $d_C d_T \gg \ell_c^2$, hence $F_1 = F_2^{(+)} = 0$ and $F_2^{(-)} = 1$,

$$\Gamma(x_C, x_T) = \Gamma_{\mathrm{cp}}(x_C, x_T) = 2\cos^2\left[\frac{k}{2}\left(\frac{d_T x_T}{f_T} - \frac{d_C x_C}{f_C}\right)\right], \tag{3.67}$$

where the orientation of the interference fringes is fixed by a specific linear combination of the two detector variables [see Fig. 3.12(a)]. This condition is opposed to the factorized case (3.64) and is optimal to detect the distance f_T. It is sufficient to characterize the oscillation period along any of the directions $x_T = \mu x_C + \nu$, with $\mu \neq 0$ and $\mu \neq (d_C/d_T)(f_T/f_C)x_C$, and ν arbitrary, in order to determine f_T. In particular, the frequency of the second-order interference pattern in the case $x_T = -(d_C/d_T)(f_T/f_C)x_C + \nu$ is *twice* the frequency of the pattern generated at first order by coherent light impinging the double slit mask (see also [145, 147]). The first-order corrections in $e^{-\alpha/2}$

$$F_1 = 2e^{-\frac{\alpha}{2}}\cos(\alpha\beta)[1 + O(e^{-\alpha})], \tag{3.68}$$

$$F_2^{(+)} = 1 - F_2^{(-)} = O(e^{-\alpha}) \tag{3.69}$$

enable one to infer (though not uniquely) the value of z_T from the amplitude of additional uncorrelated oscillations:

$$\Gamma(x_C, x_T) \simeq \Gamma_{\mathrm{cp}}(x_C, x_T) + 2e^{-\frac{\alpha}{2}}\cos(\alpha\beta)\sum_{J=C,T}\cos\frac{kd_J x_J}{f_J}. \tag{3.70}$$

However, this condition is not the most favorable for measuring z_T, since the additional terms by which it should be detected are very small; the discussed behavior is related to the presence of plateaus around $z_T = z_C$ in both F_1 and $F_2^{(-)}$, observed in Fig. 3.13(a)-(b). Let us stress, also in this case, that in order to reach $\alpha \gg 1$ it is not necessary that first-order interference is not visible on both detectors; the behavior approximately described by Eq. (3.67) can occur present even when the slits of *one* mask fall within the coherence length on their plane.
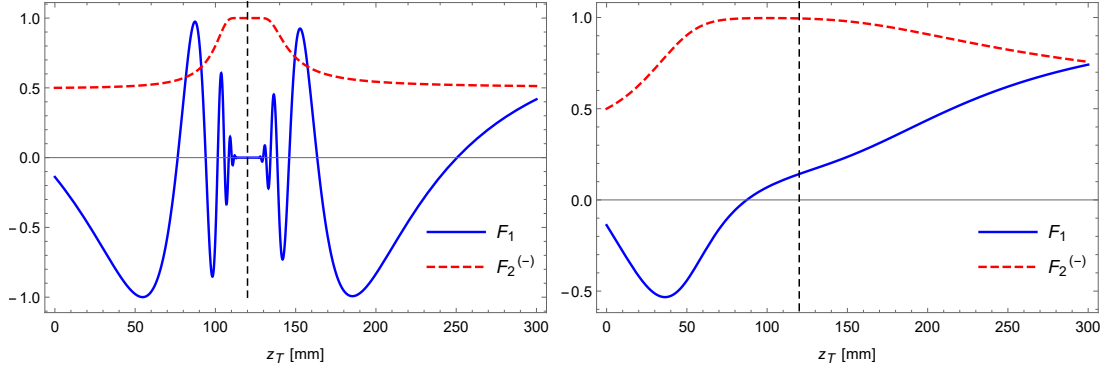
Figure 3.13: Plots of the Fourier coefficients $F_1(z_T)$ (solid blue line) and $F_2^{(-)}(z_T)$ (dashed red line), defined in Eqs. (3.59)-(3.60), as functions of the distance z_T between source and target mask T, at fixed $z_C = 120\,\text{mm}$, $\lambda = 980\,\text{nm}$ $d_T = 0.08\,\text{mm}$, $d_C = 0.8\,\text{mm}$, for two different values of the source width σ. The plateau around $z_C = z_T$ in panel (a) corresponds to a range in which $\alpha \gg 1$, producing correlated interference patterns analogous to the one in Fig. 3.12(a). Notice that, in the case $z_T = z_C$ of panel (b), $\alpha \simeq 5$ is not small, providing still a non-factorized pattern despite the two slits of mask C fall within the coherence area at a distance z_C.

3. *The intermediate range: higher sensitivity to z_T.*— The situations considered in the previous subsections represent extremal cases. These cases are not particularly favorable for measuring the distance z_T between the target mask and the detector D_T, since the asymptotic patterns (3.64) and (3.67) are robust with respect to small variations of z_T, especially in the case $\alpha \gg 1$, where deviations from the asymptotic pattern are exponentially suppressed. In the case of $\alpha \ll 1$ and $\alpha\beta \gtrsim 1$, occurring when $d_C d_T \gtrsim \sigma\,|\sigma_T - \sigma_C| \gg \sigma_C\sigma_T$, $F_2^{(\pm)}$ behave as in Eq. (3.65), while $F_1 \simeq \cos(\alpha\beta/2)$ is not small. Provided one knows *a priori* that $\alpha\beta \in (2n\pi, (2n+1)\pi)$, with $n \in \mathbb{N}$, measuring F_1 can yield an unambiguous estimate to the distance z_T between the source and the mask T. In the case in which $\alpha \sim 1$ and $\beta \gtrsim 1$, namely $d_C d_T \sim \ell_c^2$, $\sigma\,|\sigma_T - \sigma_C| \gtrsim \sigma_C\sigma_T$, both the independent coefficients are sensitive to changes in the distance z_T. The detection of F_1 and $F_2^{(+)}$ therefore enables a combined estimate of z_T. As one can observe from Fig. 3.13, the coefficient F_1 is typically more sensitive than F_2 to small variations of z_T; however, it is disadvantaged by being strongly non-monotonous, as opposed to $F_2^{(\pm)}$, with monotonicity intervals typically centered around the cosine zeros $\alpha\beta = (2n+1)\pi$, with $n \in \mathbb{N}$. An effective strategy for the estimation of a completely unknown z_T can include a two-step process, in which one first performs a rougher estimate of the range of distance through the parameter F_2, less sensitive but characterized by only two monotonic ranges, and then proceeds to a more precise estimate through F_1. Finally, notice that both cases discussed in this subsection cannot occur when z_T is too close to z_C, since in this case $1/\sigma_{\text{eq}}$ tends to vanish.

This analysis also shed new light in the understanding of the emergence of second-order coherence with thermal light and its connection to the degree of correlation of the measured second-order interference pattern. The results in the opposite regimes show that correlations in the interference pattern become more relevant when the product of slit widths in the two masks (or the squared width in the single-mask scenario) goes beyond the squared critical coherence length ℓ_c, which represents a novel critical parameter in second order correlations with thermal light. These findings provide the basis for a convenient protocol to measure, even in presence of turbulence, the distance of reflective objects, placed either on the optical path between source and mask, or on the path between mask and detector. This works paves the way to interesting future research devoted to an

accurate evaluation of the error affecting the remote-mask distance estimate and of the ultimate precision bounds of the described measurement scheme [190], and the least possible error given the state of the field, quantified by the Quantum Fisher information [191]. Moreover in the following we show in Fig. 3.14, three results on the behavior of the coefficients F_1 and $F_2^{(-)}$ in the case $X_C = X_T = 0$, with varying distance of the remote slit. The three cases are referred to fixed values of z_C and σ, with two masks whose slit distances are, compared to the coherence length at z_C, (a) both smaller, (b) one larger and one smaller, and (c) both larger.
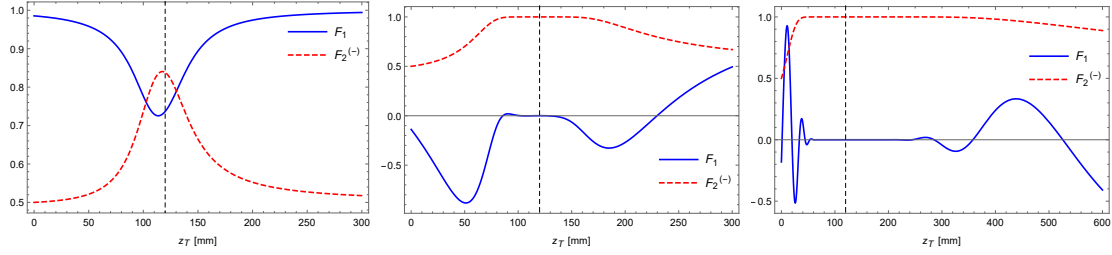

Figure 3.14: Plots of the two coefficients F_1 and $F_2^{(-)}$ as functions of z_T, at fixed $z_C = 120\,\text{mm}$, $\sigma = 0.3\,\text{mm}$ and $\lambda = 980\,\text{nm}$, for different values of the slit separations d_T and d_C. (a) When both slits are smaller than the coherence length at a distance z_C, there is no plateau around $z_T \simeq z_C$ and no oscillations in F_1. (b) If only the slit separation is smaller than the coherence length only for mask T, slight oscillations in F_1 and a plateau in both coefficients appear. On the other hand. (c) If both slit separations are beyond the coherence length at z_C, the presence of plateaus and oscillations in F_1 becomes more relevant.

3.6 Further studies: Quantum approach and Turbulence-free

In the above sections we studied four setups (SETUP1 and SETUP1 for CPI, SETUP3 for CMP and SETUPS4 for distance sensing) where we used the chaotic pseudothermal light source as model. It is interesting show that the same analysis can be applied for other kind of light models in order to answer fundamental questions, as well as, *"What is the true nature of the light?"* and to invent new paradigma for new imaging applications, and it is worth to notice that a huge variety of experiments in Physics end up with detectors sensitive to the light. Therefore analogous computation can be performed when working with low photon fluxes or whenever quantum features of a system are of interest. A quantum mechanical approach to photodetection is inevitable, and classical wavefields V need to be replaced with (hermitian) quantum operators; i.e., the electric field is $\hat{E} = \hat{E}^+ + \hat{E}^-$, where

$$\hat{E}_J^+ (\boldsymbol{\rho}_J, t_J) = C \int \hat{a}_{\boldsymbol{\kappa}} e^{-i\omega t_J} \mathscr{G}(\boldsymbol{\rho}_J, \boldsymbol{\kappa})\, d^2\kappa d\omega, \ \hat{E}_J^- (\boldsymbol{\rho}_J, t_J) = \left(\hat{E}_J^+ (\boldsymbol{\rho}_J, t_J)\right)^\dagger. \tag{3.71}$$

A scalar approximation is assumed for $\hat{E}_J^{(\pm)}$ which are the positive and negative frequency components of the electric wavefield at each planar detector D_J with each point defined by $\boldsymbol{\rho}_J$ (with $J = A, B$), t_J is the corresponding detection time. C is a normalization constant, ω is the frequency, $\boldsymbol{\kappa}$ is the transverse momentum, $\hat{a}_{\boldsymbol{\kappa}}$ is the canonical field operator, associated with the mode $\boldsymbol{\kappa}$, which satisfies the commutation relation: $\left[\hat{a}_{\boldsymbol{\kappa}}, \hat{a}_{\boldsymbol{\kappa}'}^\dagger\right] = \delta_{\boldsymbol{\kappa}, \boldsymbol{\kappa}'}$. The three dimensional wave vector $\boldsymbol{k} = (\boldsymbol{\kappa}, k_z)$ is such that $k_z \simeq \omega/c$. The second-order correlation measurement between each pixel of the sensors D_A and D_B is described by the Glauber correlation function

$$G^{(2)} (\boldsymbol{\rho}_A, t_A; \boldsymbol{\rho}_B, t_B) = \left\langle : \hat{i}_A (\boldsymbol{\rho}_A, t_A)\, \hat{i}_B (\boldsymbol{\rho}_B, t_B) : \right\rangle, \tag{3.72}$$

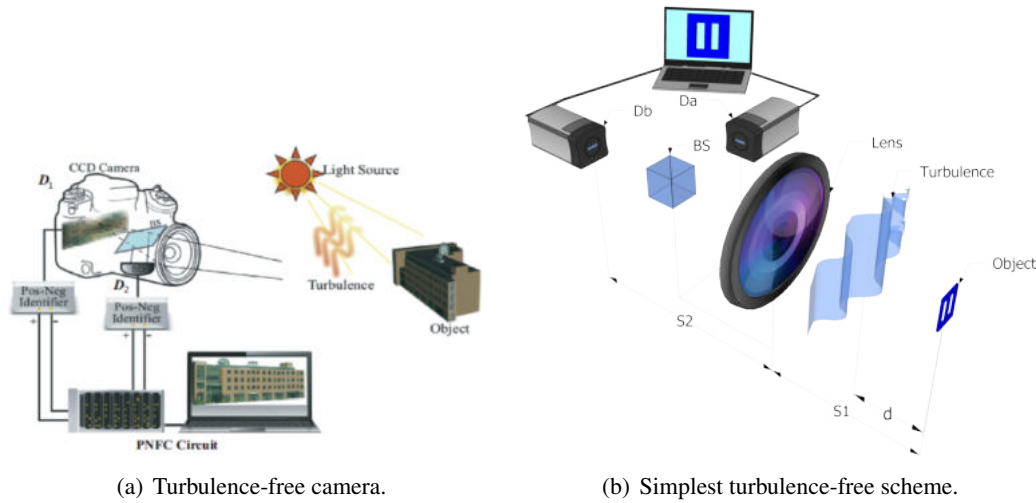(a) Turbulence-free camera.   (b) Simplest turbulence-free scheme.

Figure 3.15: In 3.15(a) the light from the building across the turbulence which perturbs the phase of the wavefield, but at the second order it goes away.[193]. In 3.15(b) a point with coordinate $\boldsymbol{\rho}'_o$ in the object plane (visualized as a chaotic source) is mapped by a lens into a point with coordinate $\boldsymbol{\rho}_i$. Interestingly, Eq. 3.20 is not affected by the turbulence in particular experimental regimes.

with

$$\hat{i}_J\left(\boldsymbol{\rho}_J, t_J\right) = \hat{E}_J^{(-)}\left(\boldsymbol{\rho}_J, t_J\right)\hat{E}_J^{(+)}\left(\boldsymbol{\rho}_J, t_J\right), \, J = A, B. \tag{3.73}$$

The expectation value $\langle\mathscr{O}\rangle = \mathrm{Tr}\left(\rho\mathscr{O}\right)$ in Eq 3.72 is evaluated by considering the quantum state ρ of the source with normal ordered wavefield operators. This expression can be interpreted as the probability of jointly detecting two photons at positions $\boldsymbol{\rho}_A$ at time t_A and $\boldsymbol{\rho}_B$ and time t_B, neglecting all their possible polarization states. The same evaluation of the expectation values of the previous section might be performed carried on an opportunely biphoton state ρ.

Beside the quantum approach, another extension of such outcomes goes in the direction of adding turbulence in the setup which should reduce the seeing, as astronomers well known for terrestrial astronomical imaging. Preliminaries and prominent works promise that the second-order theory can be applied for high sensitivity and stability observations such as for gravitational-wave detection [150, 192, 193] building turbulence–free setups. Roughly speaking these configurations are not sensible to the refraction index fluctuations which usually introduce such noise in the images. Nonetheless, just specific setups satisfied these properties as it is summarized in the Fig.3.15(a). However a theoretical description based on a mathematical model of the turbulence is required in order to unveil the fundamental principle that allow to avoid such noise in the optical systems. A possible model could describe the transmission turbulence function introduce a phase variation due to the Reyleigh scatter of the light with the atmosphere

$$T\left(\boldsymbol{\rho}\right) = e^{i\phi(\boldsymbol{\rho})} = 1 + i\phi\left(\boldsymbol{\rho}\right) - \frac{1}{2}\phi^2\left(\boldsymbol{\rho}\right) + o\left(\phi^2\right),$$

it is modeled upon a plan with coordinate $\boldsymbol{\rho} = (x, y)$ ruled by the following correlation phase function in two points of the turbulence plan

$$\langle\phi\left(\boldsymbol{\rho}_1\right)\phi\left(\boldsymbol{\rho}_2\right)\rangle_T = \sigma_\phi^2 e^{-\frac{(\boldsymbol{\rho}_1-\boldsymbol{\rho}_2)^2}{2\sigma_T^2}},$$

with σ_ϕ represents the intensity of the correlation and σ_T the correlation length of the two considered points. Since the scattering is isotropic, the mean value of difference processes at any point $\boldsymbol{\rho}$ is

$\langle \phi(\boldsymbol{\rho}) \rangle_T = 0$. Therefore up to the second order we have $T(\boldsymbol{\rho}) = 1 + i\langle \phi(\boldsymbol{\rho}) \rangle_T - \frac{1}{2}\langle \phi^2(\boldsymbol{\rho}) \rangle_T = 1 - \frac{\sigma_\phi^2}{2}$ and the correlation of two point in the transmission function, which is the crucial term in the second order imaging reads

$$
\begin{aligned}
\langle T^*(\boldsymbol{\rho}_1) T(\boldsymbol{\rho}_2) \rangle_T &= \langle e^{i(\phi(\boldsymbol{\rho}_1) - \phi(\boldsymbol{\rho}_2))} \rangle_T \\
&= 1 - \sigma_\phi^2 + \langle \phi(\boldsymbol{\rho}_2) \phi(\boldsymbol{\rho}_1) \rangle_T \\
&= 1 - \sigma_\phi^2 + \sigma_\phi^2 e^{-\frac{(\boldsymbol{\rho}_1 - \boldsymbol{\rho}_2)^2}{2\sigma_T^2}}.
\end{aligned}
$$

However an interesting model which characterize the turbulence can be found in [194].
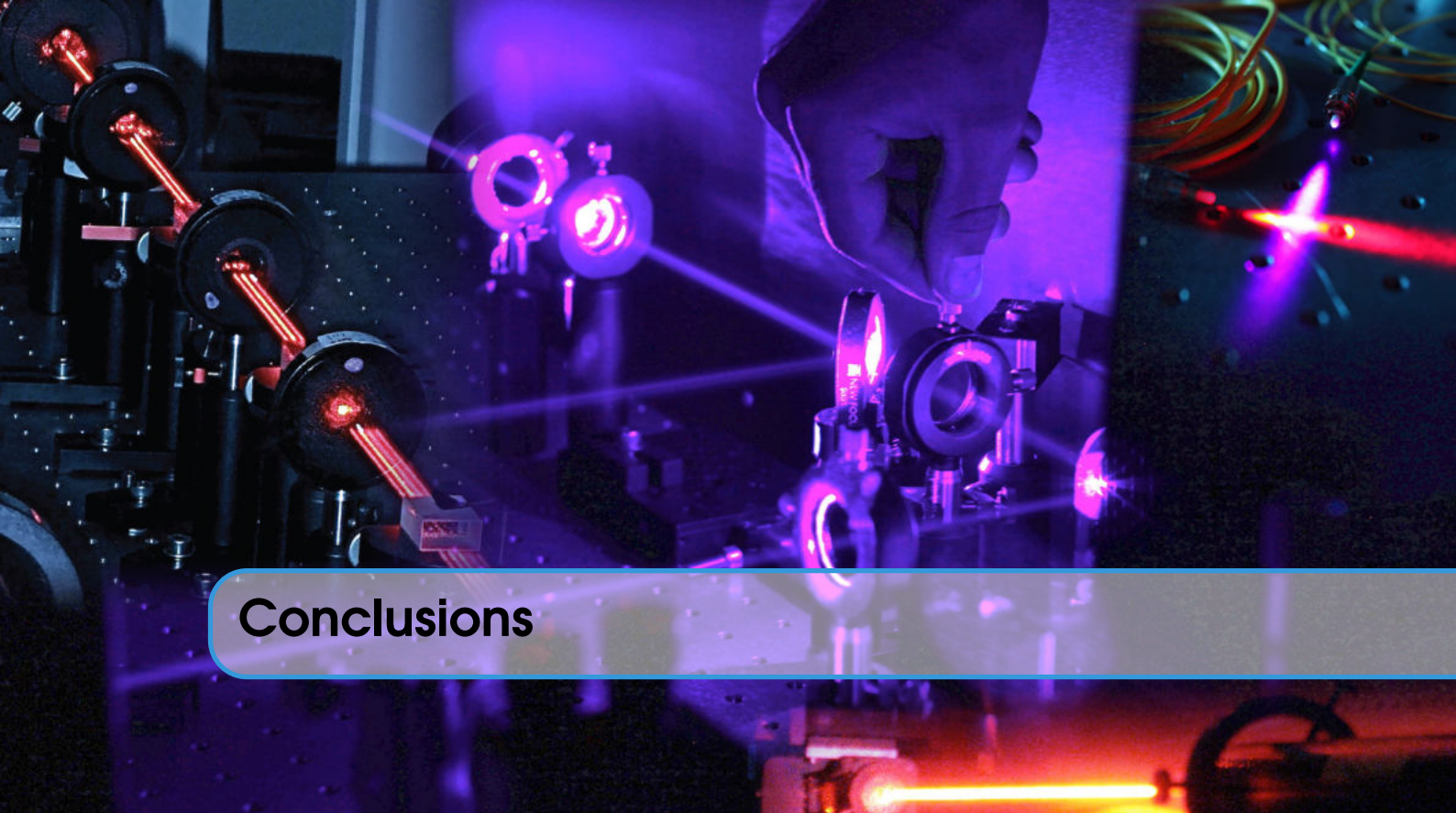
Conclusions

*A*s we have seen, a new method for the detection of entanglement have been proposed which unifies several criteria known before like, e.g., CCNR or realignment criterion, de Vicente criterion, and derived recently separability criterion based on SIC POVMs. All these criteria are based on the universal object—correlation matrix defined in terms of Hermitian orthonormal basis in the operator space. It should be stressed that, unlike the well-known CMC or LUR, these criteria are linear in the density operator. This property enables us to provide other classes of entanglement witnesses and positive maps. Interestingly, there is a natural generalization to a multipartite scenario using multipartite correlation matrix and multipartite generalizations of matrix norms. Moreover, we show that our criterion is equivalent to the enhanced realignment criterion via an educated limit which rises to a novel class of entanglement witnesses. In spite of the enhanced realignment criterion, our results call also for a multipartite generalization where details are postponed for a future research.

Other related quantum resources have been investigated as non locality and non contextuality. The former suggests a way to derive a new class of Bell's inequalities driving the question if it shows a stronger violation than the one currently in literature. The latter show that $\mathscr{D}^2 + \mathscr{V}^2 = 1$ achieve such bound if and only if the ontological model is contextual. In order to prove it we presented some methods of investigation and how the constrains in the ontological model rise up from the operational description of an experiment.

In the second part of the thesis we studied the dynamics of a charged system coupled to a medium-assisted electric field, beyond the point-dipole approximation, highlighting the role played by the finite size of the system, the dispersion and absorption by the medium and the spatial asymmetries. The analysis focused on the determination of the decay rates and energy shifts of the bound states of an atomic system, which have been obtained under general assumptions. The most important among these assumptions is based on homogeneous and isotropic media. We also discussed how to extend the theory to more general situations. The role of the asymmetry has been compared with respect to the counter-rotating terms in a cavity system coupled with a reservoir. The analysis shows in which regimes one can takes into account the asymmetry in perturbation theory neglecting the counter-rotating terms. Hints for further developments are lightly presented as key–idea rather than a detailed description.

In the third part we have shown that performing plenoptic imaging by correlation measurements has the potential to improve 3D imaging and microscopy, since it combines high resolution with the possibility to gain directional information. The results obtained provide the experimenter with rules to determine the scaling of the SNR with the number of frames, and consequently to fix the number of frames needed for a fast and accurate imaging of the scene. We provide an outline for our future research, where we plan to extend our analysis to the case in which CPI is performed with entangled photons. Moreover we compare CPI systems based on ghost–imaging with CPM protocol implemented for the microscope prototype showing pros and cons. In this part we also show how this physics of second-order interference can estimate remote distance sheding new light in the understanding of the emergence of second-order coherence with chaotic light and its connection to the degree of correlation of the measured second-order interference pattern.

"Ideas are like bundles of trajectories undergoing complicated evolution."
(G. Sudarshan)

Bibliography

[1] Charles H. Bennett, David P. DiVincenzo, Christopher A. Fuchs, Tal Mor, Eric Rains, Peter W. Shor, John A. Smolin, and William K. Wootters. Quantum nonlocality without entanglement. *Phys. Rev. A*, 59:1070–1091, Feb 1999.

[2] A. Einstein, B. Podolsky, and N. Rosen. Can quantum-mechanical description of physical reality be considered complete? *Physical Review*, 47(10):777–780, may 1935.

[3] Schrodinger. The present status of quantum mechanics. *Die Naturwissenschaften 23, 807.*, 23(48), 1935.

[4] J. S. Bell. On the einstein podolsky rosen paradox. *Physics Physique Fizika*, 1(3):195–200, nov 1964.

[5] John Conway and Simon Kochen. The free will theorem. *Foundations of Physics*, 36(10):1441–1473, jul 2006.

[6] Daniel M. Greenberger, Michael A. Horne, and Anton Zeilinger. Going beyond bell's theorem. In *Bell's Theorem, Quantum Theory and Conceptions of the Universe*, pages 69–72. Springer Netherlands, 1989.

[7] Simon Gröblacher, Tomasz Paterek, Rainer Kaltenbaek, Časlav Brukner, Marek Żukowski, Markus Aspelmeyer, and Anton Zeilinger. An experimental test of non-local realism. *Nature*, 446(7138):871–875, apr 2007.

[8] Stuart J. Freedman and John F. Clauser. Experimental test of local hidden-variable theories. *Physical Review Letters*, 28(14):938–941, apr 1972.

[9] Carl A. Kocher and Eugene D. Commins. Polarization correlation of photons emitted in an atomic cascade. *Physical Review Letters*, 18(15):575–577, apr 1967.

[10] Alain Aspect, Jean Dalibard, and Grard Roger. Experimental test of bell's inequalities using time- varying analyzers. *Physical Review Letters*, 49(25):1804–1807, dec 1982.

[11] Fabio A. Bovino, Giuseppe Castagnoli, Adán Cabello, and Antía Lamas-Linares. Experimental noise-resistant bell-inequality violations for polarization-entangled photons. *Physical Review A*, 73(6), jun 2006.

[12] Yuji Hasegawa, Rudolf Loidl, Gerald Badurek, Matthias Baron, and Helmut Rauch. Violation of a bell-like inequality in neutron-interferometer experiments. *Journal of the Physical Society of Japan*, 72(Suppl.C):42–45, jan 2003.

[13] Paul G. Kwiat, Klaus Mattle, Harald Weinfurter, Anton Zeilinger, Alexander V. Sergienko, and Yanhua Shih. New high-intensity source of polarization-entangled photon pairs. *Physical Review Letters*, 75(24):4337–4341, dec 1995.

[14] Z. Y. Ou and L. Mandel. Violation of bell's inequality and classical probability in a two-photon correlation experiment. *Physical Review Letters*, 61(1):50–53, jul 1988.

[15] M. A. Rowe, D. Kielpinski, V. Meyer, C. A. Sackett, W. M. Itano, C. Monroe, and D. J. Wineland. Experimental violation of a bell's inequality with efficient detection. *Nature*, 409(6822):791–794, feb 2001.

[16] W. Tittel, J. Brendel, H. Zbinden, and N. Gisin. Violation of bell inequalities by photons more than 10 km apart. *Physical Review Letters*, 81(17):3563–3566, oct 1998.

[17] Artur K. Ekert. Quantum cryptography based on bell's theorem. *Physical Review Letters*, 67(6):661–663, aug 1991.

[18] Ryszard Horodecki, Paweĺ Horodecki, Michaĺ Horodecki, and Karol Horodecki. Quantum entanglement. *Reviews of Modern Physics*, 81(2):865–942, jun 2009.

[19] Michael A Nielsen and Isaac L Chuang. Quantum computation and quantum information cambridge univ. 2000.

[20] Jonathan Barrett. Nonsequential positive-operator-valued measurements on entangled mixed states do not always violate a bell inequality. *Physical Review A*, 65(4), mar 2002.

[21] M. Żukowski, A. Zeilinger, M. A. Horne, and A. K. Ekert. "event-ready-detectors" bell experiment via entanglement swapping. *Physical Review Letters*, 71(26):4287–4290, dec 1993.

[22] Charles H. Bennett, Gilles Brassard, Claude Crépeau, Richard Jozsa, Asher Peres, and William K. Wootters. Teleporting an unknown quantum state via dual classical and einstein-podolsky-rosen channels. *Physical Review Letters*, 70(13):1895–1899, mar 1993.

[23] Reinhard F. Werner. Quantum states with einstein-podolsky-rosen correlations admitting a hidden-variable model. *Physical Review A*, 40(8):4277–4281, oct 1989.

[24] Sandu Popescu. Bell's inequalities and density matrices: Revealing hidden nonlocality. *Physical Review Letters*, 74(14):2619–2622, apr 1995.

[25] L. Gurvits. In proceedings of the 35th acm symposium on theory of computing, p.10-19. In *ACMPress, New York,*, 2003.

[26] Asher Peres. Separability criterion for density matrices. *Physical Review Letters*, 77(8):1413–1415, aug 1996.

[27] Kai Chen and Ling-An Wu. Test for entanglement using physically observable witness operators and positive maps. *Physical Review A*, 69(2), feb 2004.

[28] Oliver Rudolph. Further results on the cross norm criterion for separability. *Quantum Information Processing*, 4(3):219–239, aug 2005.

[29] Kai Chen and Ling-An Wu. A matrix realignment method for recognizing entanglement. *Quantum Inf. Comput.*, 3(3):193–202, 2003.

[30] Holger F. Hofmann and Shigeki Takeuchi. Violation of local uncertainty relations as a signature of entanglement. *Physical Review A*, 68(3), sep 2003.

[31] Cheng-Jie Zhang, Yong-Sheng Zhang, Shun Zhang, and Guang-Can Guo. Entanglement detection beyond the computable cross-norm or realignment criterion. *Physical Review A*, 77(6), jun 2008.

[32] O. Guhne, P. Hyllus, O. Gittsovich, and J. Eisert. Covariance matrices and the separability problem. *Phys Rev Lett*, 99(13), sep 2007.

[33] Oleg Gittsovich and Otfried Guhne. Quantifying entanglement with covariance matrices. *Physical Review A*, 81(3), mar 2010.

[34] Li Ming, Fei Shao-Ming, and Li-Jost Xianqing. Concurrence, tangle and fully entangled fraction. *Chinese Physics B*, 19(9):090315, sep 2010.

[35] Barbara M. Terhal. Detecting quantum entanglement. *Theoretical Computer Science*, 287(1):313–335, sep 2002.

[36] Barbara M. Terhal. Bell inequalities and the separability criterion. *Physics Letters A*, 271(5-6):319–326, jul 2000.

[37] Dariusz Chruściński and Gniewomir Sarbicki. Entanglement witnesses: construction, analysis and classification. *Journal of Physics A: Mathematical and Theoretical*, 47(48):483001, nov 2014.

[38] Otfried Gühne and Geza Tóth. Entanglement detection. *Physics Reports*, 474(1-6):1–75, apr 2009.

[39] Rudolf Haag. *Local Quantum Physics*. Springer Berlin Heidelberg, 1996.

[40] Anna Sanpera, Rolf Tarrach, and Guifré Vidal. Local description of quantum inseparability. *Physical Review A*, 58(2):826–830, aug 1998.

[41] Julio I. De Vicente. Separability criteria based on the bloch representation of density matrices. *Quantum Info. Comput.*, 2007.

[42] M. Lewenstein, B. Kraus, J. I. Cirac, and P. Horodecki. Optimization of entanglement witnesses. *Physical Review A*, 62(5), oct 2000.

[43] Jiangwei Shang, Ali Asadian, Huangjun Zhu, and Otfried Gühne. Enhanced entanglement criterion via symmetric informationally complete measurements. *Physical Review A*, 98(2), aug 2018.

[44] GERHARD ZAUNER. Quantum designs: Foundations of a noncommutative design theory. *International Journal of Quantum Information*, 09(01):445–507, feb 2011.

[45] Joseph M. Renes, Robin Blume-Kohout, A. J. Scott, and Carlton M. Caves. Symmetric informationally complete quantum measurements. *Journal of Mathematical Physics*, 45(6):2171–2180, jun 2004.

[46] Christopher Fuchs, Michael Hoang, and Blake Stacey. The sic question: History and state of play. *Axioms*, 6(4):21, jul 2017.

[47] D Marcus Appleby. Symmetric informationally complete–positive operator valued measures and the extended clifford group. *Journal of Mathematical Physics*, 46(5):052107, 2005.

[48] A. J. Scott and M. Grassl. Symmetric informationally complete positive-operator-valued measures: A new computer study. *Journal of Mathematical Physics*, 51(4):042203, apr 2010.

[49] Hermann Weyl. *The theory of groups and quantum mechanics*. Courier Corporation, 1950.

[50] J. Schwinger. UNITARY OPERATOR BASES. *Proceedings of the National Academy of Sciences*, 46(4):570–579, apr 1960.

[51] Ming Li, Jing Wang, Shao-Ming Fei, and Xianqing Li-Jost. Quantum separability criteria for arbitrary-dimensional multipartite states. *Physical Review A*, 89(2), feb 2014.

[52] Gniewomir Sarbicki, Giovanni Scala, and Dariusz Chruściński. Family of multipartite separability criteria based on a correlation tensor. *Physical Review A*, 101(1), jan 2020.

[53] Gniewomir Sarbicki, Giovanni Scala, and Dariusz Chruściński. Enhanced realignment criterion vs linear entanglement witnesses. *Journal of Physics A: Mathematical and Theoretical*, 53(45):455302, oct 2020.

[54] Ming Li, Shao-Ming Fei, and Zhi-Xi Wang. Separability and entanglement of quantum states based on covariance matrices. *Journal of Physics A: Mathematical and Theoretical*, 41(20):202002, apr 2008.

[55] Cosmo Lupo, Paolo Aniello, and Antonello Scardicchio. Bipartite quantum systems: on the realignment criterion and beyond. *Journal of Physics A: Mathematical and Theoretical*, 41(41):415301, sep 2008.

[56] Paolo Aniello and Cosmo Lupo. A class of inequalities inducing new separability criteria for bipartite quantum systems. *Journal of Physics A: Mathematical and Theoretical*, 41(35):355303, jul 2008.

[57] Otfried Gühne, Mátyás Mechler, Géza Tóth, and Peter Adam. Entanglement criteria based on local uncertainty relations are strictly stronger than the computable cross norm criterion. *Physical Review A*, 74(1), jul 2006.

[58] Cheng-Jie Zhang, Yong-Sheng Zhang, Shun Zhang, and Guang-Can Guo. Optimal entanglement witnesses based on local orthogonal observables. *Physical Review A*, 76(1), jul 2007.

[59] Charles H. Bennett, David P. DiVincenzo, Tal Mor, Peter W. Shor, John A. Smolin, and Barbara M. Terhal. Unextendible product bases and bound entanglement. *Physical Review Letters*, 82(26):5385–5388, jun 1999.

[60] David P. Di Vincenzo, Tal Mor, Peter W. Shor, John A. Smolin, and Barbara M. Terhal. Unextendible product bases, uncompletable product bases and bound entanglement. *Communications in Mathematical Physics*, 238(3):379–410, jul 2003.

[61] Dagmar Bruss and Asher Peres. Construction of quantum states with bound entanglement. *Physical Review A*, 61(3), feb 2000.

[62] Pawel Horodecki. Separability criterion and inseparable mixed states with positive partial transposition. *Physics Letters A*, 232(5):333–339, aug 1997.

[63] Paweł Horodecki, Maciej Lewenstein, Guifré Vidal, and Ignacio Cirac. Operational criterion and constructive checks for the separability of low-rank density matrices. *Physical Review A*, 62(3), aug 2000.

[64] Reinhold A. Bertlmann, Katharina Durstberger, Beatrix C. Hiesmayr, and Philipp Krammer. Optimal entanglement witnesses for qubits and qutrits. *Physical Review A*, 72(5), nov 2005.

[65] Alberto Riccardi, Dariusz Chruściński, and Chiara Macchiavello. Optimal entanglement witnesses from limited local measurements. *Physical Review A*, 101(6), jun 2020.

[66] Kil-Chan Ha and Seung-Hyeok Kye. One-parameter family of indecomposable optimal entanglement witnesses arising from generalized choi maps. *Physical Review A*, 84(2), aug 2011.

[67] Dariusz Chruściński and Gniewomir Sarbicki. Optimal entanglement witnesses for two qutrits. *Open Systems & Information Dynamics*, 20(02):1350006, jun 2013.

[68] Lieven De Lathauwer, Bart De Moor, and Joos Vandewalle. A multilinear singular value decomposition. *SIAM Journal on Matrix Analysis and Applications*, 21(4):1253–1278, jan 2000.

[69] Ali Saif M Hassan, Behzad Lari, and Pramod S Joag. Thermal quantum and classical correlations in a two-qubit xx model in a nonuniform external magnetic field. *Journal of Physics A: Mathematical and Theoretical*, 43(48):485302, nov 2010.

[70] Maria Anastasia Jivulescu, Cécilia Lancien, and Ion Nechita. Multipartite entanglement detection via projective tensor norms.

[71] Florian Mintert and Andreas Buchleitner. Observable entanglement measure for mixed quantum states. *Physical Review Letters*, 98(14), apr 2007.

[72] Richard P. Feynman, Robert B. Leighton, Matthew Sands, and R. Bruce Lindsay. The feynman lectures on physics, vol. 3: Quantum mechanics. *Physics Today*, 19(11):80–83, nov 1966.

[73] Lucien Hardy and Robert Spekkens. Why physics needs quantum foundations. *La Physique au Canada*, 66(2), 2010.

[74] Peter Forrest. The identity of indiscernibles. In Edward N. Zalta, editor, *The Stanford Encyclopedia of Philosophy*. Metaphysics Research Lab, Stanford University, winter 2016 edition, 2016.

[75] R. W. Spekkens. Contextuality for preparations, transformations, and unsharp measurements. *Physical Review A*, 71(5), may 2005.

[76] Matthias Jakob and János A. Bergou. Quantitative complementarity relations in bipartite systems: Entanglement as a physical reality. *Optics Communications*, 283(5):827–830, mar 2010.

[77] Yuan Li and Yu-E Li. Some characterizations of the trace norm triangle equality. *Linear Algebra and its Applications*, 484:396–408, nov 2015.

[78] Matthew F. Pusey. Anomalous weak values are proofs of contextuality. *Physical Review Letters*, 113(20), nov 2014.

[79] W. K. Wootters and W. H. Zurek. A single quantum cannot be cloned. *Nature*, 299(5886):802–803, oct 1982.

[80] M. S. Leifer and O. J. E. Maroney. Maximally epistemic interpretations of the quantum state and contextuality. *Physical Review Letters*, 110(12), mar 2013.

[81] David Schmid and Robert W. Spekkens. Contextual advantage for state discrimination. *Physical Review X*, 8(1), feb 2018.

[82] Philipp Hyllus, Otfried Gühne, Dagmar Bruß, and Maciej Lewenstein. Relations between entanglement witnesses and bell inequalities. *Physical Review A*, 72(1), jul 2005.

[83] Dagomir Kaszlikowski and Marek Żukowski. Greenberger-horne-zeilinger paradoxes forNN-dimensional systems. *Physical Review A*, 66(4), oct 2002.

[84] Daniel Alsina, Alba Cervera, Dardo Goyeneche, José I. Latorre, and Karol Życzkowski. Operational approach to bell inequalities: Application to qutrits. *Physical Review A*, 94(3), sep 2016.

[85] Peter W. Milonni. *The Quantum Vacuum: An Introduction to Quantum Electrodynamics*. Academic Press, Boston, 1994.

[86] A A Abrikosov, I Dzyaloshinskii, L P Gorkov, and Richard A Silverman. *Methods of quantum field theory in statistical physics*. Dover, New York, NY, 1975.

[87] Werner Vogel and Dirk-Gunnar Welsch. *Quantum Optics*. John Wiley & Sons, may 2006.

[88] C. Cohen-Tannoudji, J. Dupont-Roc, and G. Grynberg. *Photons and atoms: introduction to quantum electrodynamics*. John Wiley & Sons, 1997.

[89] Stephen M Barnett, Bruno Huttner, Rodney Loudon, and Reza Matloob. Decay of excited atoms in absorbing dielectrics. *J. Phys. B*, 29(16):3763, 1996.

[90] Bruno Huttner and Stephen M. Barnett. Quantization of the electromagnetic field in dielectrics. *Phys. Rev. A*, 46(7):4306–4322, oct 1992.

[91] Ho Trung Dung, Ludwig Knöll, and Dirk-Gunnar Welsch. Spontaneous decay in the presence of dispersing and absorbing bodies: General theory and application to a spherical cavity. *Phys. Rev. A*, 62(5):053804, 2000.

[92] G. Juzeliūnas. Spontaneous emission in absorbing dielectrics: A microscopic approach. *Phys. Rev. A*, 55(6):R4015, 1997.

[93] S. Scheel, L. Knöll, and D. G. Welsch. Spontaneous decay of an excited atom in an absorbing dielectric. *Phys. Rev. A*, 60(5):4094–4104, nov 1999.

[94] Stefan Scheel, Ludwig Knöll, Dirk-Gunnar Welsch, and Stephen M Barnett. Quantum local-field corrections and spontaneous decay. *Phys. Rev. A*, 60(2):1590, 1999.

[95] C. Cohen-Tannoudji, J. Dupont-Roc, and G. Grynberg. *Atom-photon interactions: basic processes and applications*. John Wiley & Sons, 1998.

[96] R. P. Feynman, R. B. Leighton, and M. Sands. *The Feynman Lectures on Physics*. Addison-Wesley, 1964.

[97] Giovanni Scala, Francesco Vincenzo Pepe, Paolo Facchi, Saverio Pascazio, and Karolina Slowik. Light interaction with extended quantum systems in dispersive media. *New Journal of Physics*, dec 2020.

[98] Qiongtao Xie, Honghua Zhong, Murray T Batchelor, and Chaohong Lee. The quantum rabi model: solution and dynamics. *Journal of Physics A: Mathematical and Theoretical*, 50(11):113001, 2017.

[99] Bruce W Shore and Peter L Knight. The jaynes-cummings model. *Journal of Modern Optics*, 40(7):1195–1238, 1993.

[100] P Forn-Díaz, L Lamata, E Rico, J Kono, and E Solano. Ultrastrong coupling regimes of light-matter interaction. *Reviews of Modern Physics*, 91(2):025005, 2019.

[101] Jérôme Bourassa, Jay M Gambetta, Abdufarrukh A Abdumalikov Jr, Oleg Astafiev, Y Nakamura, and A Blais. Ultrastrong coupling regime of cavity qed with phase-biased flux qubits. *Physical Review A*, 80(3):032109, 2009.

[102] Thomas Niemczyk, F Deppe, H Huebl, EP Menzel, F Hocke, MJ Schwarz, JJ Garcia-Ripoll, D Zueco, T Hümmer, E Solano, et al. Circuit quantum electrodynamics in the ultrastrong-coupling regime. *Nature Physics*, 6(10):772–776, 2010.

[103] G Günter, Aji A Anappara, J Hees, Alexander Sell, Giorgio Biasiol, Lucia Sorba, S De Liberato, Cristiano Ciuti, Alessandro Tredicucci, Alfred Leitenstorfer, et al. Sub-cycle switch-on of ultrastrong light–matter interaction. *Nature*, 458(7235):178–181, 2009.

[104] Qi Zhang, Minhan Lou, Xinwei Li, John L Reno, Wei Pan, John D Watson, Michael J Manfra, and Junichiro Kono. Collective non-perturbative coupling of 2d electrons with high-quality-factor terahertz cavity photons. *Nature Physics*, 12(11):1005–1011, 2016.

[105] Andrea Crespi, Stefano Longhi, and Roberto Osellame. Photonic realization of the quantum rabi model. *Physical review letters*, 108(16):163601, 2012.

[106] Jino George, Thibault Chervy, Atef Shalabney, Eloïse Devaux, Hidefumi Hiura, Cyriaque Genet, and Thomas W Ebbesen. Multiple rabi splittings under ultrastrong vibrational coupling. *Physical review letters*, 117(15):153601, 2016.

[107] P Schneeweiss, A Dareau, and C Sayrin. Cold-atom-based implementation of the quantum rabi model. *Physical Review A*, 98(2):021801, 2018.

[108] Daniel Braak. Integrability of the rabi model. *Physical Review Letters*, 107(10):100401, 2011.

[109] Qing-Hu Chen, Chen Wang, Shu He, Tao Liu, and Ke-Lin Wang. Exact solvability of the quantum rabi model using bogoliubov operators. *Physical Review A*, 86(2):023822, 2012.

[110] O. V. Kibis, G. Ya. Slepyan, S. A. Maksimenko, and A. Hoffmann. Matter coupling to strong electromagnetic fields in two-level quantum systems with broken inversion symmetry. *Phys. Rev. Lett.*, 102:023601, 2009.

[111] Emmanuel Paspalakis, John Boviatsis, and Sotirios Baskoutas. Effects of probe field intensity in nonlinear optical processes in asymmetric semiconductor quantum dots. *J. Appl. Phys.*, 114(15):153107, oct 2013.

[112] Igor Yu. Chestnov, Vanik A. Shahnazaryan, Alexander P. Alodjants, and Ivan A. Shelykh. Terahertz Lasing in Ensemble of Asymmetric Quantum Dots. *ACS Photonics*, 4(11):2726–2737, oct 2017.

[113] Piotr Gładysz, Piotr Wcisło, and Karolina Słowik. Propagation of optically tunable coherent radiation in a gas of polar molecules. *Scientific reports*, 10(1):1–11, 2020.

[114] Martin Koppenhöfer and Michael Marthaler. Creation of a squeezed photon distribution using artificial atoms with broken inversion symmetry. *Phys. Rev. A*, 93(2):023831, 2016.

[115] MA Antón, S Maede-Razavi, F Carreno, Ioannis Thanopulos, and Emmanuel Paspalakis. Optical and microwave control of resonance fluorescence and squeezing spectra in a polar molecule. *Physical Review A*, 96(6):063812, 2017.

[116] IG Savenko, OV Kibis, and Ivan A Shelykh. Asymmetric quantum dot in a microcavity as a nonlinear optical element. *Physical Review A*, 85(5):053818, 2012.

[117] Qijing Lu, Xiaogang Chen, Chang-Ling Zou, and Shusen Xie. Extreme terahertz electric-field enhancement in high-q photonic crystal slab cavity with nanoholes. *Optics Express*, 26(23):30851–30861, 2018.

[118] Dominik Walter Vogt and Rainer Leonhardt. Ultra-high q terahertz whispering-gallery modes in a silicon resonator. *APL Photonics*, 3(5):051702, 2018.

[119] Dimitrios C Zografopoulos and Romeo Beccherelli. Tunable terahertz fishnet metamaterials based on thin nematic liquid crystal layers for fast switching. *Scientific Reports*, 5:13137, 2015.

[120] Antonín Luk and Vlasta Perinová. *Quantum Aspects of Light Propagation*. Springer, Boston, MA, 2009.

[121] Stefan Yoshi Buhmann. *Dispersion Forces I*. Springer Berlin Heidelberg, 2012.

[122] Sergei M. Rytov, Yurii A. Kravtsov, and Valeryan I. Tatarskii. *Principles of Statistical Radiophysics 3*. Springer-Verlag Berlin Heidelberg, 1989.

[123] Evgenni Mikhailovich Lifshitz, M Hamermesh, et al. The theory of molecular attractive forces between solids. In *Perspectives in Theoretical Physics*, pages 329–349. Elsevier, 1992.

[124] R Hanbury Brown and Richard Q Twiss. Correlation between photons in two coherent beams of light. *Nature*, 177(4497):27–29, 1956.

[125] R Hanbury Brown and R Q Twiss. A test of a new type of stellar interferometer on sirius. *Nature*, 178(4541):1046–1048, 1956.

[126] Eric Brannen and HIS Ferguson. The question of correlation between photons in coherent light rays. *Nature*, 178:481–482, 1956.

[127] EM Purcell. The question of correlation between photons in coherent light rays. *Nature*, 178:1449–1450, 1956.

[128] Roy J Glauber. Photon correlations. *Physical Review Letters*, 10(3):84, 1963.

[129] Agedi N. Boto, Pieter Kok, Daniel S. Abrams, Samuel L. Braunstein, Colin P. Williams, and Jonathan P. Dowling. Quantum interferometric optical lithography: Exploiting entanglement to beat the diffraction limit. *Physical Review Letters*, 85:2733, 2000.

[130] I. N. Agafonov, M. V. Chekhova, T. Sh. Iskhakov, and L.-A. Wu. High-visibility intensity interference and ghost imaging with pseudo-thermal light. *Journal of Modern Optics*, 56:422–431, 2009.

[131] Jian-Wei Pan, Zeng-Bing Chen, Chao-Yang Lu, Harald Weinfurter, Anton Zeilinger, and Marek Zukowski. Multiphoton entanglement and interferometry. *Reviews of Modern Physics*, 84:777, 2012.

[132] E. Knill, R. Laflamme, and G. J. Milburn. A scheme for efficient quantum computation with linear optics. *Nature*, 409:46–52, 2000.

[133] Vincenzo Tamma and Simon Laibacher. Multiboson correlation interferometry with arbitrary single-photon pure states. *Physical Review Letters*, 114(24):243601, 2015.

[134] Simon Laibacher and Vincenzo Tamma. From the physics to the computational complexity of multiboson correlation interference. *Physical Review Letters*, 115(24):243605, 2015.

[135] Vincenzo Tamma. Sampling of bosonic qubits. *International Journal of Quantum Information*, 12(07n08):1560017, 2014.

[136] Yoon-Ho Kim, Sergei P. Kulik, and Yanhua Shih. Quantum teleportation of a polarization state with a complete bell state measurement. *Physical Review Letters*, 86:1370, 2001.

[137] Ryan S. Bennink, Sean J. Bentley, and Robert W. Boyd. "two-photon" coincidence imaging with a classical source. *Physical Review Letters*, 89:113601, 2002.

[138] Vincenzo Tamma and Simon Laibacher. Multiboson correlation interferometry with multimode thermal sources. *Phys. Rev. A*, 90:063836, Dec 2014.

[139] KF Lee and JE Thomas. Experimental simulation of two-particle quantum entanglement using classical fields. *Physical Review Letters*, 88(9):097902, 2002.

[140] Mark E Pearce, Thomas Mehringer, J Von Zanthier, and Pieter Kok. Precision estimation of source dimensions from higher-order intensity correlations. *Physical Review A*, 92(4):043831, 2015.

[141] G. Scarcelli, A. Valencia, and Y. Shih. Two-photon interference with thermal light. *EPL (Europhysics Letters)*, 68(5):618, 2004.

[142] Steffen Oppel, Thomas Büttner, Pieter Kok, and Joachim von Zanthier. Superresolving multiphoton interferences with independent light sources. *Physical review letters*, 109(23):233603, 2012.

[143] Giuliano Scarcelli, Vincenzo Berardi, and Yanhua Shih. Can two-photon correlation of chaotic light be considered as correlation of intensity fluctuations? *Phys. Rev. Lett.*, 96:063602, Feb 2006.

[144] Vincenzo Tamma and Johannes Seiler. Multipath correlation interference and controlled-not gate simulation with a thermal source. *New Journal of Physics*, 18(3):032002, 2016.

[145] Michele Cassano, Milena D'Angelo, Augusto Garuccio, Tao Peng, Yanhua Shih, and Vincenzo Tamma. Spatial interference between pairs of disjoint optical paths with a chaotic source. *Optics Express*, 25(6):6589–6603, 2016.

[146] Vincenzo Tamma. The physics of thermal light second-order interference beyond coherence. *Phys. Scr.*, 93:124010, 2018.

[147] M. D'Angelo, F. V. Pepe, A. Garuccio, and G. Scarcelli. Characterization of two distant double-slits by chaotic light second order interference. *Sci. Rep.*, 7:2247, 2017.

[148] Tao Peng, Vincenzo Tamma, and Yanhua Shih. Experimental controlled-not gate simulation with thermal light. *Scientific Reports*, 6:30152, 2016.

[149] Yong Sup Ihn, Yosep Kim, Vincenzo Tamma, and Yoon-Ho Kim. Second-order temporal interference with thermal light: Interference beyond the coherence time. *Phys. Rev. Lett.*, 119:263603, 2017.

[150] Thomas A. Smith and Yanhua Shih. Turbulence-free double-slit interferometer. *Phys. Rev. Lett.*, 120:063606, 2018.

[151] Leonard Mandel and Emil Wolf. *Optical coherence and quantum optics*. Cambridge University Press, 1995.

[152] Foley John and Zubairy M. S. The directionality of gaussian schell model beams. *Optics Communications*, 26(3), 1978.

[153] L. Isserlis. On a formula for the product-moment coefficient of any order of a normal frequency distribution in any number of variables. *Biometrika*, 12(134), 1918.

[154] G. Scala. master thesis: Quantum correlation and plenoptic imaging. *(private communication)*, 2017.

[155] Milena D'Angelo, Francesco V Pepe, Augusto Garuccio, and Giuliano Scarcelli. Correlation plenoptic imaging. *Physical Review Letters*, 116(22):223602, 2016.

[156] Francesco V Pepe, Giuliano Scarcelli, Augusto Garuccio, and Milena D'Angelo. Plenoptic imaging with second-order correlations of light. *Quantum Measurements and Quantum Metrology*, 3(1):20–26, 2016.

[157] Francesco V Pepe, Francesco Di Lena, Augusto Garuccio, Giuliano Scarcelli, and Milena D'Angelo. Correlation plenoptic imaging with entangled photons. *Technologies*, 4(2):17, 2016.

[158] Milena D'Angelo and YH Shih. Quantum imaging. *Laser Physics Letters*, 2(12):567–596, 2005.

[159] Giovanni Scala, Milena D'Angelo, Augusto Garuccio, Saverio Pascazio, and Francesco V. Pepe. Signal-to-noise properties of correlation plenoptic imaging with chaotic light. *Phys. Rev. A*, 99:053808, May 2019.

[160] Brédif M., Duval G., Horowitz M., Ng R., Levoy M., and Hanrahan P. Light field photography with a hand-held plenoptic camera. *Tech. Rep. CSTR 2005-02,Stanford Computer Science*, 2005.

[161] Francesco V. Pepe, Francesco Di Lena, Aldo Mazzilli, Eitan Edrei, Augusto Garuccio, Giuliano Scarcelli, and Milena D'Angelo. Diffraction-limited plenoptic imaging with correlated light. *Phys. Rev. Lett.*, 119:243602, Dec 2017.

[162] Jing Cheng. Transfer functions in lensless ghost-imaging systems. *Physical Review A*, 78(4):043823, 2008.

[163] Cheng Jing, Han Shen-Sheng, and Yan Yi-Jing. Resolution and noise in ghost imaging with classical thermal light. *Chinese Physics*, 15(9):2002, 2006.

[164] F Ferri, D Magatti, A Gatti, M Bache, E Brambilla, and LA Lugiato. High-resolution ghost image and ghost diffraction experiments with thermal light. *Physical Review Letters*, 94(18):183602, 2005.

[165] Francesco Di Lena, Francesco Pepe, Augusto Garuccio, and Milena D'Angelo. Correlation plenoptic imaging: An overview. *Applied Sciences*, 8(10):1958, oct 2018.

[166] TB Pittman, YH Shih, DV Strekalov, and AV Sergienko. Optical imaging by means of two-photon quantum entanglement. *Physical Review A*, 52(5):R3429, 1995.

[167] TB Pittman, MJ Fitch, BC Jacobs, and JD Franson. Experimental controlled-not logic gate for single photons in the coincidence basis. *Physical Review A*, 68(3):032316, 2003.

[168] Toshimitsu Asakura. Spatial coherence of laser light passed through rotating ground glass. *Opto-electronics*, 2(3):115–123, aug 1970.

[169] Alejandra Valencia, Giuliano Scarcelli, Milena D'Angelo, and Yanhua Shih. Two-photon imaging with thermal light. *Physical Review Letters*, 94(6):063601, 2005.

[170] G Brida, M Genovese, and I Ruo Berchera. Experimental realization of sub-shot-noise quantum imaging. *Nature Photonics*, 4(4):227–230, 2010.

[171] Morton H Rubin. Transverse correlation in optical spontaneous parametric down-conversion. *Physical Review A*, 54(6):5349, 1996.

[172] Francesco V Pepe, Ornella Vaccarelli, Augusto Garuccio, Giuliano Scarcelli, and Milena D'Angelo. Exploring plenoptic properties of correlation imaging with chaotic light. *Journal of Optics*, 19(11):114001, oct 2017.

[173] A. Gatti, M. Bache, D. Magatti, E. Brambilla, F. Ferri, and L. A. Lugiato. Coherent imaging with pseudo-thermal incoherent light. *Journal of Modern Optics*, 53(5-6):739–760, mar 2006.

[174] Baris I. Erkmen and Jeffrey H. Shapiro. Signal-to-noise ratio of gaussian-state ghost imaging. *Phys. Rev. A*, 79:023833, Feb 2009.

[175] Malcolm N. O'Sullivan, Kam Wai Clifford Chan, and Robert W. Boyd. Comparison of the signal-to-noise characteristics of quantum versus thermal ghost imaging. *Physical Review A*, 82:053803, 2010.

[176] G. Brida, M. V. Chekhova, G. A. Fornaro, M. Genovese, E. D. Lopaeva, and I. Ruo Berchera. Systematic analysis of signal-to-noise ratio in bipartite ghost imaging with classical and quantum light. *Phys. Rev. A*, 83:063807, Jun 2011.

[177] Daniele Pelliccia, Alexander Rack, Mario Scheel, Valentina Cantelli, and David M. Paganin. Experimental x-ray ghost imaging. *Phys. Rev. Lett.*, 117:113902, Sep 2016.

[178] Raimund Schneider, Thomas Mehringer, Giuseppe Mercurio, Lukas Wenthaus, Anton Classen, Günter Brenner, Oleg Gorobtsov, Adrian Benz, Daniel Bhatti, Lars Bocklage, Birgit Fischer, Sergey Lazarev, Yuri Obukhov, Kai Schlage, Petr Skopintsev, Jochen Wagner, Felix Waldmann, Svenja Willing, Ivan Zaluzhnyy, Wilfried Wurth, Ivan A. Vartanyants, Ralf Röhlsberger, and Joachim von Zanthier. Quantum imaging with incoherently scattered light from a free-electron laser. *Nature Physics*, 14(2):126–129, oct 2017.

[179] Fabio Remondino and David Stoppa. *TOF range-imaging cameras*, volume 68121. Springer, 2016.

[180] R. T. Menzies. Coherent and Incoherent Lidar – an Overview. In R. L. Byer, Gustafson E. K., and Trebino R., editors, *Tunable Solid State Lasers for Remote Sensing*, volume 51, pages 17–21. Springer, Berlin, Heidelberg, 1985.

[181] KF Lee and JE Thomas. Experimental simulation of two-particle quantum entanglement using classical fields. *Phys. Rev. Lett.*, 88(9):097902, 2002.

[182] Alejandra Valencia, Giuliano Scarcelli, Milena D'Angelo, and Yanhua Shih. Two-photon imaging with thermal light. *Phys. Rev. Lett.*, 94(6):063601, 2005.

[183] S. Oppel, T. Büttner, P. Kok, and J. von Zanthier. Superresolving multiphoton interferences with independent light sources. *Phys. Rev. Lett.*, 109:233603, Dec 2012.

[184] NJ Cerf, C Adami, and PG Kwiat. Optical simulation of quantum logic. *Physical Review A*, 57(3):R1477, 1998.

[185] Vincenzo Tamma. Analogue algorithm for parallel factorization of an exponential number of large integers: I. Theoretical description. *Quantum Inf. Process.*, pages 1–22, 2015.

[186] Vincenzo Tamma. Analogue algorithm for parallel factorization of an exponential number of large integers: Ii. optical implementation. *Quantum Information Processing*, pages 1–15, 2015.

[187] Vincenzo Tamma, Heyi Zhang, Xuehua He, Augusto Garuccio, Wolfgang P Schleich, and Yanhua Shih. Factoring numbers with a single interferogram. *Phys. Rev. A*, 83(2):020304, 2011.

[188] V Tamma, CO Alley, WP Schleich, and YH Shih. Prime number decomposition, the hyperbolic function and multi-path michelson interferometers. *Foundations of physics*, 42(1):111–121, 2012.

[189] Sabine Woelk, Wolfgang Merkel, WP Schleich, I Sh Averbukh, and Bertrand Girard. Factorization of numbers with gauss sums: I. mathematical background. *New Journal of Physics*, 13(10):103007, 2011.

[190] L. Motka, B. Stoklasa, M. D'Angelo, P. Facchi, A. Garuccio, Z. Hradil, S. Pascazio, F. V. Pepe, Y. S. Teo, J. Rehacek, and L. L. Sanchez-Soto. Optical resolution from fisher information. *Eur. Phys. J. Plus*, 131:130, 2016.

[191] Carmine Napoli, Samanta Piano, Richard Leach, Gerardo Adesso, and Tommaso Tufarelli. Towards superresolution surface metrology: Quantum estimation of angular and axial separations. *Phys. Rev. Lett.*, 122:140505, 2019.

[192] Eitan Edrei and Giuliano Scarcelli. Optical imaging through dynamic turbid media using the fourier-domain shower-curtain effect. *Optica*, 3(1):71–74, 2016.

[193] Yanhua Shih. The physics of turbulence-free ghost imaging. *Technologies*, 4:39, 12 2016.

[194] Ronald L. Fante. VI wave propagation in random media: A system approach. In *Progress in Optics*, pages 341–398. Elsevier, 1985.

4. Acknowledgments

I would like to express my profound gratitude to prof. S. Pascazio and dr. Pepe, for their overwhelming dedition, patience and support; nothing would have been possible without their effort. I am also thankful to prof. Facchi, D. Chruściński, prof. G. Sarbicki, and prof. K. Słowik for their precious comments and humanity and my fellow colleagues and friends D. Lonigro, L. N. Carenza, G. Gramegna, G. Angelone, R. Maggi, A. Konderak, M. Malitesta, Z. Kordi and all my Indians friends for enriching my academic journey.

I am highly grateful to my brothers Samanta, Lucia and Matteo, as well as to my parents and grandparents, for their moral support and affection during these years.

Many thanks to my friend Gianluca, Saguero and Fabio for their willingness and availability in any situation.

This work has benefited a lot from discussions and collaborations with many different people, in particular I cannot skip to thank to the best attack trident ever *el Chino–Ronnie–Bobo* who motivate me to do better. Finally, I am grateful to Tony Stark to give me the opportunity to be part in his galaxy, *Marvel Studios* where I found the possibility to think beyond my abilities even without any superhero costume.

From *"Spider-Man: Homecoming"* is coming the time of *"Spider-Man: Far from Home"*.

Declare of Originality

I hereby declare that the following thesis is composed of my own original work, developed during my PhD studies at University of Bari in QUANTUM group and at the University of Toruń. All published and unpublished work of others has been appropriately referenced and acknowledged.